Design, synthesis and properties of receptors incorporating acridinium and porphyrin units

Amy Edo-Osagie

UNIVERSITÉ DE STRASBOURG

ÉCOLE DOCTORALE DES SCIENCES CHIMIQUES

Institut de Chimie de Strasbourg - UMR7177

Laboratoire de Synthèse des Assemblages

Moléculaires Multifonctionnels (LSAMM)

THÈSE présentée par :

Amy EDO-OSAGIE

soutenue le : **28 avril 2022**

pour obtenir le grade de : **Docteur de l'université de Strasbourg**

Discipline/ Spécialité : Chimie moléculaire / Chimie supramoléculaire

Conception, synthèse et propriétés de récepteurs incorporant des unités acridiniums et porphyrines

THÈSE dirigée par :

Mme HEITZ Valérie Professeur, Université de Strasbourg

RAPPORTEURS :

M. BALLESTER Pablo Professeur, Institut de recherche chimique de Catalogne

M. BUCHER Christophe Directeur de recherches, Ecole normale supérieure de Lyon

---

AUTRES MEMBRES DU JURY :

M. WEISS Jean Directeur de recherches, Université de Strasbourg

M. JACQUOT DE ROUVILLE Henri-Pierre Chargé de Recherche au CNRS, Université de Strasbourg

Acknowledgements

Firstly, I would like to thank the members of the jury for agreeing to be a part of my thesis defense and taking the time to read and evaluate this work. Your joint understanding and cooperation in the organisation of the defense was and is very much appreciated.

It is perhaps redundant to say, but this work could of course not have been possible without the supervision and direction of my thesis supervisor: Prof. Valérie Heitz, and my secondary mentor: Dr. Henri-Pierre Jacquot de Rouville. Thanks to your joint expertise we were able to access a world of new compounds! We encountered many roadblocks along the way, and there were times where I felt as if these blocks were unsurmountable, but your support and advice kept the work going. Thank you for your guidance, your influence on my development as a researcher, and for the experience of being an LSAMM member, it's not one I shall soon forget!

To the past (Sebastien, Ryan, Alexis, Charly, Etienne) and present (Stéphanie, Johnny, Sonia and Nahid) members of the LSAMM group: thank you for welcoming me to the group and to Strasbourg! When I first came to France, I did not speak much French. Now, I will leave…still not speaking much French, but with plenty of francophone friends. Thanks for all the discussions, the pastries, the drinks, the pots, and the general comradery and warmth. And to the CLAC and IFM group members, thanks for helping make the 8th floor feel like a home from home. Thanks also and especially to Geneviève, who has been so kind in my time here and has been a massive help with all the administrative quirks of this project.

To the PIs and industrial partners that make up the NOAH-ITN: thank you all for your part in the development of NOAH, and for the many discussions and opportunities to further develop. Even with the unexpected force majeure that came in the form of COVID, you all managed to make sure that we, the ESRs, got as much from the project as possible. Thanks also to my NOAH secondment supervisors: Dr. Arno Wiehe, and Prof. Mike Ward, for accepting me into your groups, designing the secondment projects and being so helpful when COVID lockdowns struck during the secondments. Even with the circumstances, it was a true treat to be in Berlin and to return to Warwick. Thanks especially to Gemma, our project

coordinator who kept NOAH running through it all. To the ESRs of NOAH: thank you all for the support both in and outside of science. We have been in a unique situation for the past 3.5 years and being able to share and discuss with you has made a heavy project lighter.

To our collaborators (Dr. Christophe Gourlaouen, Dr. Barbara Ventura, Daniel Sanchez-Resá, Prof. Xavier Barril and Dr. Dylan Serillon): thank you all for your input in this work, which truly formed the basis of our understanding of these compounds. Many thanks also to the people of the NMR service (Bruno, Maurice and Lionel), the MS service (Stéphanie and Hélène), and the X-Ray service (Lydia, Nathalie and Corrine), for all your help in the characterisations of these compounds.

To all of my friends, from the TMV crowd (who I've known for over a decade), to my Warwick friends (from Westwood, chemistry and WWRFC): thank you all for your support, and the many ways you all have helped me. You lent a listening ear, you arranged video call meet ups when I couldn't attend get-togethers in-person, you offered me accommodation when I came back to Warwick, and some of you even came to visit in my first year in Strasbourg when I was feeling most out of place. I am so grateful for all of you.

To my family, my brothers Aaron and Alex, and my mum Olubunmi: I am most grateful for the three of you. You have been the biggest support throughout this all, my first point of call for comfort, my go-to for gist. I would not have made it through this PhD without you. I didn't fully anticipate it, but the hardest part of this experience has been being away from you all. To my mum especially, your words of comfort and prayer held me up when I most needed it. Uruẹse!

To my dad, Augustin: my only sadness at the end of this all is that you won't be there to see it. A few years ago, I came to the realisation that your only true hopes for your children were that we took every opportunity that came our way; that we not only dreamed but pursued those dreams; and that we didn't let life pass us by. This is something I've tried to do ever since. I hope you're proud of me wherever you are.

List of Abbreviations

[O]	Oxidant
[R]	Reductant
A.U.	Arbitrary Units
aq.	aqueous
BArF	tetrakis[3,5-bis(trifluoromethyl)phenyl]borate
$BF_3{\cdot}OEt_2$	boron trifluoride diethyl etherate
c	Concentration
CE	Counter Electrode
DABCO	1,4-diazabicyclo[2.2.2]octane
DDQ	2,3-dichloro-5,6-dicyano-p-benzoquinone
DFT	Density Functional Theory
DMF	dimethyl formamide
DOSY	Diffusion Ordered SpectroscopY
ESI	ElectroSpray Ionisation
Et_2O	diethyl ether
EtOAc	Ethyl acetate
Hex.	hexanes
l	optical path length of cuvette
M	Moles per litre
mM	Millimoles per litre
MMFF	Merck Molecular Force Field
MS	Mass Spectrometry
n-BuLi	n-butyllithium

NMR	Nuclear Magnetic Resonance
NOESY	Nuclear Overhauser Effect SpectroscopY
RE	Reference Electrode
RT	Room Temperature
SCE	Saturated Calomel Electrode
TBAOH	tetrabutylammonium hydroxide
$TBAPF_6$	tetrabutylammonium hexafluorophosphate
tBu	tertiary-butyl
TFA	trifluoro acetic acid
THF	tetrahydrofuran
UV-Vis	Ultraviolet Visible
WE	Working Electrode
XRD	X-Ray Diffraction
μM	Micromoles per litre

Table of Contents

Chapter 2: Synthesis and study of porphyrin-acridinium conjugates

Chapter 3: Synthesis and study of a porphyrin-acridinium tweezer

1

INTRODUCTION

Introduction

The importance of non-covalent interactions in holding together key structures in nature was not a fact well accepted until the mid-1900's, with the discovery of the impact of hydrogen bonding in DNA.[1,2] Since then, non-covalent interactions have been implicated in multiple key biological structures and processes. In the synthetic world, design and synthesis of molecules (hosts) capable of forming non-covalent interactions with other molecules (guests) to give host-guest complexes began in the 1960's, eventually birthing a new field: Supramolecular chemistry. The term supramolecular was coined by Jean-Marie Lehn, with the work of Pedersen (crown ethers),[3,4] Lehn (cryptands),[5–7] and Cram (spherands)[8,9] in molecular encapsulation forming the foundation of the field (Figure 1). Non-covalent interactions and molecular encapsulation were later extended to the self-assembly of molecular containers,[10,11] and further implicated in the efficient synthesis of mechanically interlocked molecules such as rotaxanes and catenanes.[12,13]

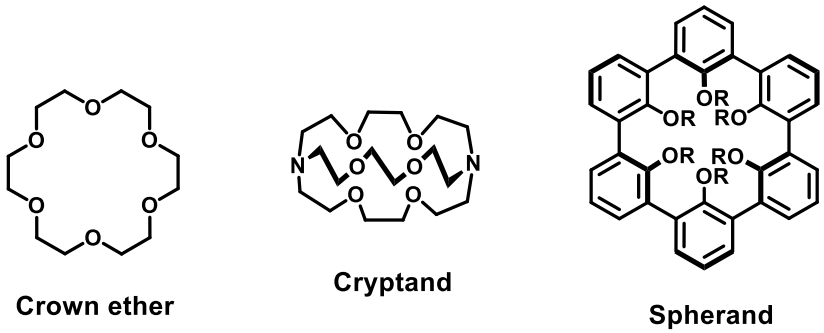

Figure 1. *Structures of the molecular containers first synthesised by Pedersen,* [3,4] *Lehn,* [5–7] *and Cram* [8,9] *respectively.*

As the field has developed, and the toolkit of available recognition units expanded, focus has shifted from the synthesis and characterisation of host-guest complexes. Instead, research has become more focused on the encoding of advanced functions into hosts, such as controlled motion, catalysis, switchable physical properties etc. These advanced functions allow the application of such systems in areas such as molecular sensing and separation, controlled catalysis, and drug delivery among others.[14–17] Of prime importance to the development of these functional host systems, is their ability to respond to stimuli. The use of various stimuli such as light, redox, and chemical, brings about a change in properties for

the host, which can sometimes be translated into a controlled change in properties for the guest. This can be a change in complexation (controlled uptake and/or release), catalysis of the guest, or further change in the electronic state or conformation of the guest.

In order to afford a responsive host, stimuli-responsive motifs must be incorporated into the host structure, either in conjunction with or *as* a recognition unit. Many stimuli-responsive motifs have been explored, including use of redox-responsive units such as viologen,[18] and TTF;[19–21] photo-responsive units such as azobenzene,[22,23] and diarylethene;[24,25] and chemically-responsive units such as hydrazone and amine/ammonium.[26] An often-used building block for functional hosts is that of the porphyrin, a fact not wholly surprising, given its properties.

The porphyrin and its derivatives (Figure 2), defined as an aromatic tetra-pyrrolic macrocycle with 18 delocalised π-electrons, is a recognition motif prolific in nature. Famed for their photophysical properties, namely their intense absorption and emission, porphyrins have been used in development of dyes, photodynamic therapeutic agents, and artificial photosynthetic systems,[27–30] harking back to cytochrome P_{450} and chlorophyll.[31,32]As well as originating its photophysical properties, the large π-conjugated system affords aromatic stability and robustness and the ability to form π–π interactions. In addition, the ability to coordinate different metals allows for further ligand coordination, as well as imbuing the molecule with its own metal specific properties.[33] As such, porphyrin units have been used to synthesise host molecules in differing architectures including tweezers, capsules, macrocycles, and cages.[34–38]

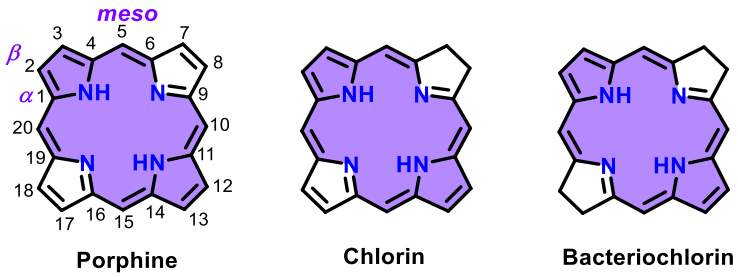

Figure 2. *Skeletal structures of the simplest porphyrin and two of its related derivatives, with an 18π pathway highlighted in purple (names for the carbon/proton positions are given).*

The porphyrin unit is known to be electro and photo active, with unique spectroscopic signatures with regards to UV-Vis spectroscopy, fluorescence spectroscopy and voltammetry (Figure 3).[39] As such, it can be used as a photo and/or redox switch in stimuli responsive systems. Additionally, metalated porphyrin species are responsive to pH stimulus, allowing their exploitation as chemically responsive units. Furthermore, the presence of multiple points of functionalisation (namely the β and *meso* positions) allows for the appendage of other stimuli-responsive motifs, to form responsive supramolecular receptors.

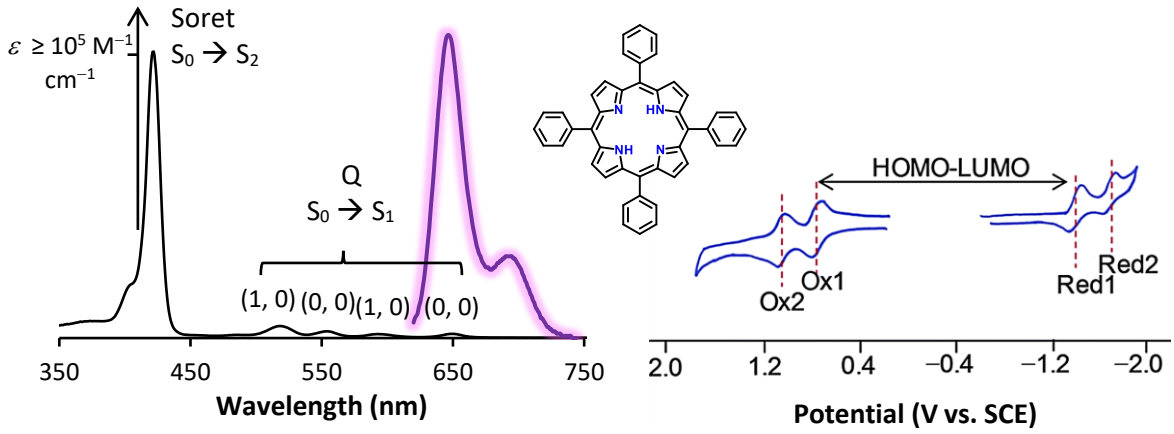

Figure 3. *Absorbance (in black) & fluorescence (in purple) spectra and cyclic voltammogram for a free base meso tetrakisphenyl porphyrin in CH_2Cl_2.*[39]

This introductory chapter will give an overview of key works in the development of stimuli-responsive porphyrin-based hosts, highlighting their structural design and how it translates to their function. Specifically, host-guest systems where application of external stimuli to the host thereby affects the host-guest interaction or the state (conformational or electronic) of the guest will be explored. Therefore, systems without the presence of a guest will be regarded strictly as molecular switches and hence excluded from this bibliography, unless explicitly linked to a relevant system. Furthermore, the host and the guest will be herein defined as separate entities, that are only linked via non-covalent interactions. As such, stimuli-responsive self-locking systems will be mostly excluded, except in the case where a separate guest is present.

1. Responsive porphyrin hosts

1.1. Light stimulus to control the function of porphyrin hosts

Use of light stimulus has been well explored in molecular encapsulation, with the attachment of photo-switchable motifs to recognition units commonly exploited to afford controlled guest uptake and/or release.[22,23,40,41] In such cases, the photo-switchable unit is covalently appended to the recognition unit in a way that leads to conformational change in the host upon irradiation, impacting the host-guest interaction. An exemplary case is that of Aida *et al.* who explored how light stimulus could be used to control the conformation of a freely rotating guest. The group first reported on a porphyrin-less photo-switchable molecular scissor (**1**) consisting of a ferrocene hinge with attached azobenzene groups (acting as the switch) and additional opposing phenyl "blades" (Figure 4).[42] Via irradiation at 350 nm, the azobenzene group could be switched from the *trans* to the *cis* isomer at a ratio of 11:89. This change in conformation was then conferred to the ferrocene hinge, pivoting the opposing phenyl blades.

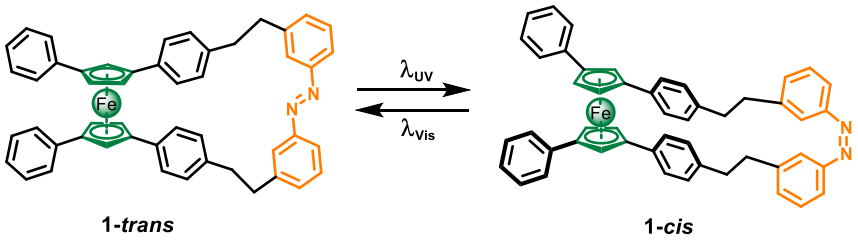

Figure 4. *Skeletal diagram of **1**. The photo-active unit (azobenzene) is highlighted in orange.*[42]

Based on this work, the Aida group then proposed a Zn(II)-porphyrin tweezer (**2**), [43] featuring the same scissor component, with the switching of the azobenzene groups, leading to a change in the orientation of the Zn(II)-porphyrin units (Figure 5). Control of the orientation of the porphyrin units could then be transferred to a ditopic rotor molecule upon its complexation to the two Zn(II)-porphyrin units of **2**. Similarly to **1**, the azobenzene group could be photo-induced to switch from the *trans* to the *cis* isomer via irradiation at 350 nm, at a slightly lower ratio of 22:77, as assessed spectroscopically. Back isomerisation could then be achieved via irradiation using visible light (> 420 nm). UV-Vis titrations of the *trans* and *cis*-

enriched **2** in CH_2Cl_2 showed binding constants of 1.3 and 2.6 × 10^6 M^{-1}, forming 1:1 complexes in both cases. Using CD spectroscopic experiments, Aida and co-workers were able to show that due to hindered free rotation the guest became optically active after complexation, with its conformation switching upon irradiation of **2** (Figure 4). Additionally, the CD activity of **2** was seen to increase due to restriction in the host flexibility upon complexation of the guest.

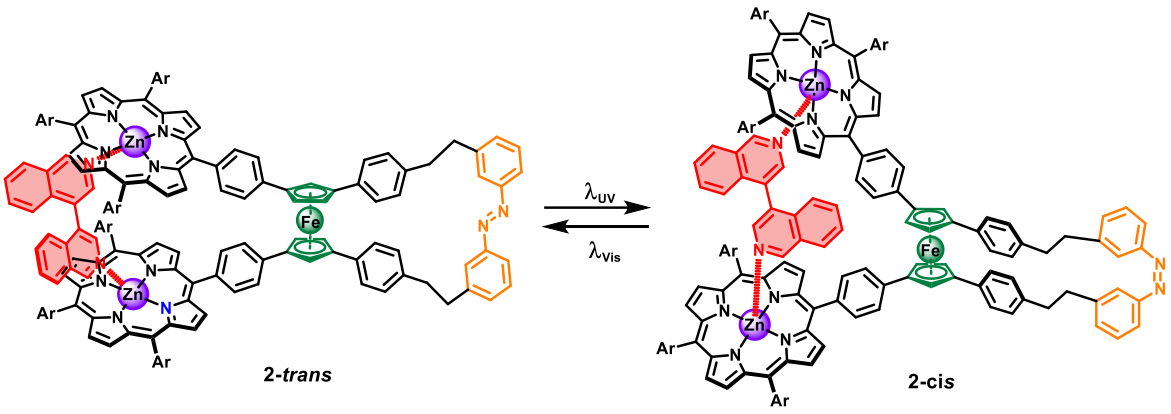

Figure 5. *Complexation of the freely rotating diamine (in red), and control of its conformation upon irradiation of* ***2****.* [43]

In a similar vein, the Nolte group have recently reported a Zn(II)-porphyrin-glycoluril cage (**3**),[44] featuring Feringa-type light switchable motors.[45] Due to the multiple points of chirality (point, planar and axial) **3** was obtained as three isolatable enantiomer pairs (Figure 6), with one pair featuring the two motors facing outward (away from the cage, Figure 6a), another having one inward-facing and one outward-facing motor (Figure 6b), and the third featuring the two motors facing inward (towards the cage, Figure 6c).

For the in-in and out-out forms of **3**, a stark difference in their affinities toward viologens could be seen, with the out-out cage having a binding constant 4.8 times larger than the in-in cage for the guest benzyl viologen (K_a = 3 × 10^5 vs. 6.3 × 10^4 M^{-1} in $CHCl_3/CH_3CN$ (1:1)). Via irradiation of the motors at 365 nm, the in-in and out-out cages could be isomerised to metastable pseudo-identical versions of each other (≈ 75% conversion), with inversion of the helicity of the motor. This feature was exploited to afford light-controlled tuning of the guest complexation. Using time resolved fluorescence quenching spectroscopy, they were able to

show that upon irradiation of a 1:1 [host-guest]:[host] solution ([**3**@viologen]:**3**), the fluorescence of the host changed. Since binding of the guest led to fluorescence quenching of the host, this amounted to a change in the affinity for the guest. In the case of the in-in cage, irradiation led to isomerisation to an out-out form. Thus, decrease in the **3** band was seen, in line with increased affinity for the guest. In contrast for the out-out cage, irradiation led to isomerisation to an in-in form. As such, the fluorescence band for **3** increased, in line with decreased affinity for the guest.

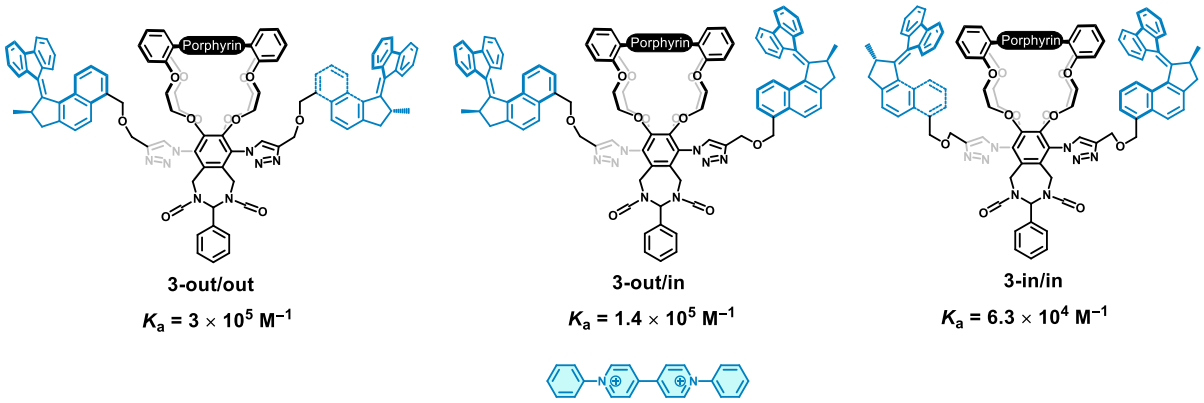

Figure 6. *A side-on representation of the three enantiomeric pairs of **3**, with the variation in the motor positioning for the three general forms (a) out/out, b) out/in and c) in/in) shown and the binding constants for the respective structures in binding of benzyl viologen stated.*[44]

1.2. Redox and electrochemical stimulus to control the function of porphyrin hosts

Redox-switchable hosts can be afforded via appendage of redox-active motifs to recognition sites, or indeed via the use of redox-active motifs as recognition sites.[46–48] In terms of porphyrinic hosts examples include the work of Bucher *et al.* of a porphyrin tweezer (**4**) featuring a short 3-carbon linker which utilises viologen groups as a redox-switch (Figure 7).[49] Due to the short length of the linker, coulombic repulsion between the viologen groups in $\mathbf{4}^{4+}$disfavoured a closed conformation. This was most apparent in the tetracationic tweezer's unwillingness to internally ditopically bind DABCO to form the 1:1 complex. However, reduction of the viologen units allowed for the formation of the π-dimer, causing $\mathbf{4}^{2+}$ to assume the closed u-conformation, with eclipsed porphyrin units (Figure 7). As such, upon

reduction of the viologens, the tweezer readily internally bound DABCO forming the 1:1 complex in dimethyl formamide, with a binding constant of 8.2×10^4 M^{-1} as assessed via UV-Vis titrations.

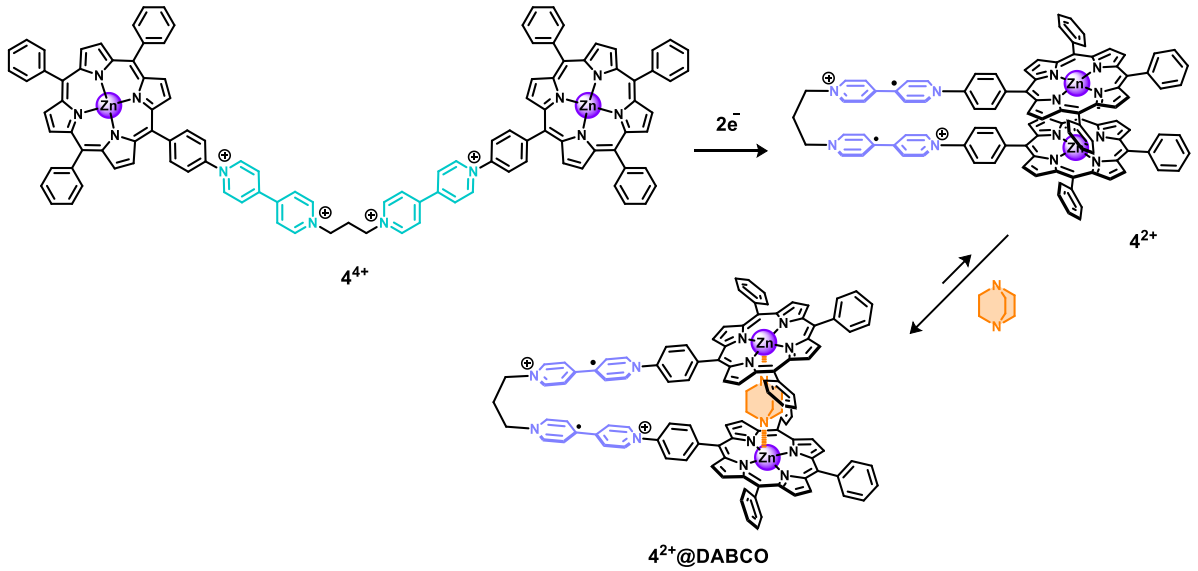

Figure 7. *Chemical structures of* ***4⁴⁺****,* ***4²⁺****, and the internal complexation of DABCO to form* ***4²⁺@DABCO⁺****.*[49]

Additionally, as redox-active recognition units, porphyrins can also be used directly as redox switches. The Weiss group reported a porphyrin pac-man type tweezer **5** (Figure 8), featuring a semi-flexible calixarene linker connecting two Zn(II)-porphyrin units.[50] The tweezer was shown to be able to bind ditopic ligands, with a binding constant of 1.6×10^8 M^{-1} (via UV-Vis spectroscopy in $CHCl_3$) found for binding of DABCO by **5** forming the macrocyclic complex **5@DABCO**. Furthermore, the ditopic nature of the binding of the guest was evidenced via UV-Visible and NMR spectroscopy.

In voltametric studies, the porphyrin units of **5** were shown to be reversibly oxidised at the same potential (E_{ox} = 0.31 V) to form a bis(radical cation), with slight broadening of the oxidation wave due to the weak exitonic coupling between the two porphyrin units. However, upon addition of an equivalent of DABCO, the two porphyrin units were found to be oxidised at two distinct potentials, with one significantly cathodically shifted oxidation to form a single radical cation (at E_{ox} = 0.14 V), and a second less shifted oxidation (at E_{ox} = 0.29 V) to form the bis(radical cation). The different oxidation potentials were assigned to decoordination of

DABCO from the second porphyrin upon oxidation of the first porphyrin, leading to a redox-induced change from a ditopic binding of DABCO to a monotopic binding of DABCO. Thus, the group were able to show a "chewing" action in the binding of DABCO when applying electrochemical stimulus.

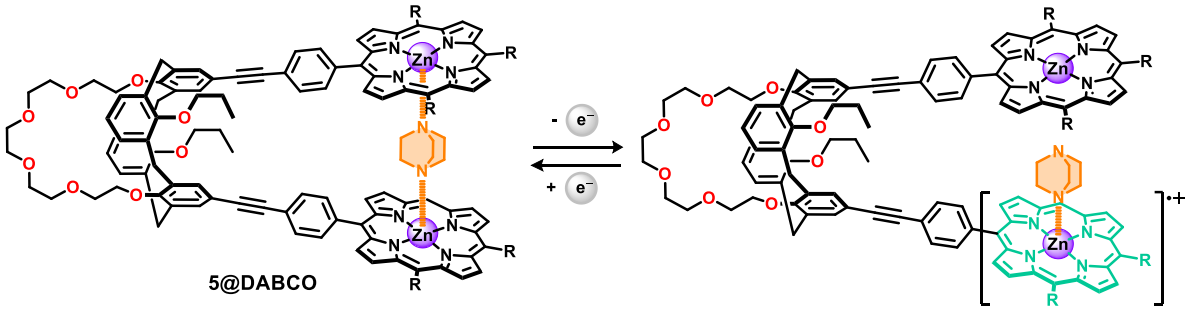

Figure 8. *Structure of the Weiss group's Pacman tweezer* ***5*** *and the change in coordination upon oxidation of the porphyrin units.* [50]

More recently, the Lipke group reported the trigonal nanoprism **6**.(Figure 9), with porphyrin walls, featuring $(PtL_2)^{2+}$ at its apexes where L is either 2,2'-bipyridine (biPy, **6a**) or Tetramethylethylenediamine (TMEDA, **6b**).[51] Electrochemical characterisation of the nanoprism via cyclic voltammetry, showed that the dodecacationic host could be reversibly reduced to a zwitterionic species with total charges of 9+, 6+, 3+ or 0, via single electron reductions of the biPy ligands (in the case of **6a**) and/or successive single electron reductions of the porphyrin walls (in the case of **6a** and **6b**).

As Cp_2Co was able to reduce the units, this was later exploited in the encapsulation of cationic $Cp^*_2Co^+$ in acetonitrile.[52] Addition of 12 equivalents of Cp^*_2Co to $\mathbf{6a^{12+}}$ led to reduction of the host forming $\mathbf{6a^0}$, and oxidation of Cp^*_2Co to form the cationic guest $Cp^*_2Co^+$. $\mathbf{6a^0}$ was able to encapsulate $Cp^*_2Co^+$ to form the host-guest complex $\mathbf{6a^0@Cp^*_2Co^+}$**.** Upon reoxidation of the host via addition of 12.5 equivalents of $AgBF_4$ or $AgPF_6$, the kinetic product $\mathbf{6a^{12+}@Cp^*_2Co^+}$was formed at a yield of 90% as assessed via NMR, with the cationic charges (localised at the apertures of the nanoprism) impeding dissociation of the cation-in-cation host-guest species. Accordingly, $\mathbf{6a^{12+}@Cp^*_2Co^+}$ was shown to have a half-life of 17 days in solution (CH_3CN, at 298 K), decomposing to the thermodynamic products: the free guest $Cp^*_2Co^+$ and the free host $\mathbf{6a^{12+}}$, but a persistent stability as a solid. Using the yield, the group was able to estimate

a binding constant of 1.3×10^3 M^{-1}, for the **6a^0** species. Interestingly, even in cases where **6a** was only partially reduced, complexation of the guest could still be seen, albeit with reduced estimated binding constants compared to **6a^0**, at 10 and 50 times smaller for **6a^{3+}** and **6a^{9+}** respectively. In contrast, direct addition of $Cp^*_2Co^+$ to a solution of **6a^{12+}** was not observed to lead to uptake of the guest, showing that the uptake was indeed redox induced. Studies via VT NMR, comparing the BF_4 and PF_6 salts of **6a^{12+}@Cp*$_2$Co$^+$**, coupled with computational analysis showed that the cation-in-cation species was in part stabilised by interaction with the counterions.

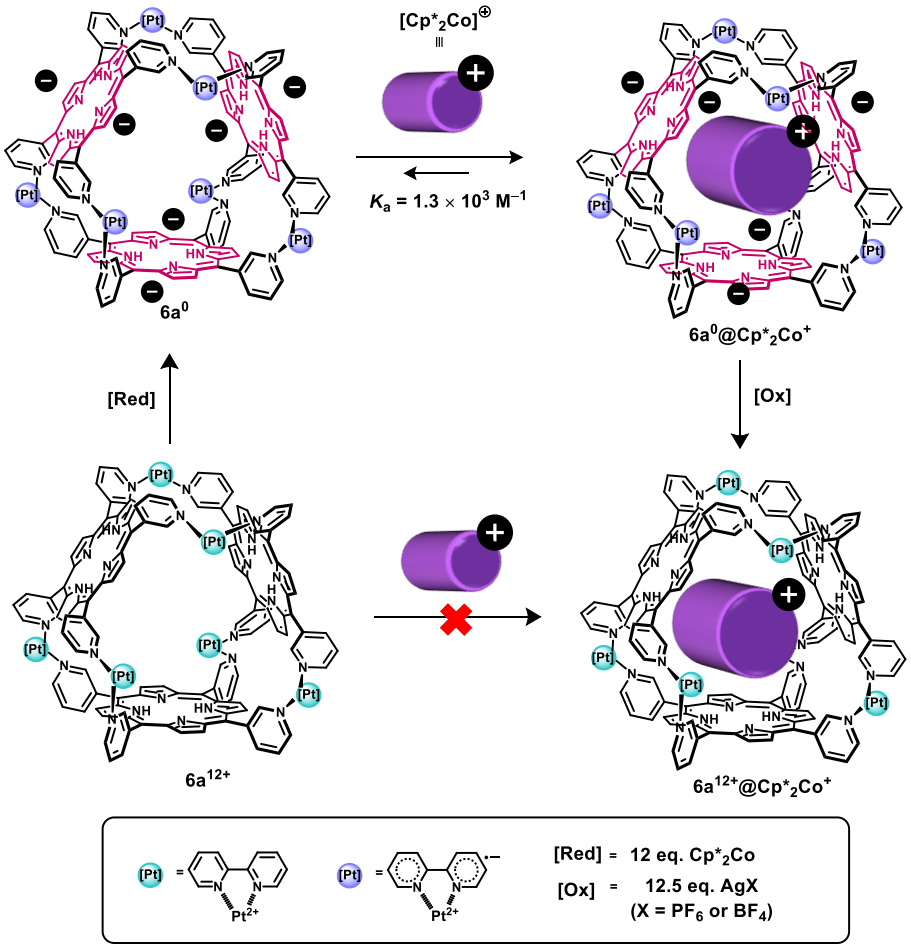

***Figure 9**. The redox-induced process by which **6a** is able to encapsulate $Cp^*_2Co^+$.* [52]

1.3. Chemical stimulus to control the function of porphyrin hosts

In the case of chemical stimuli, unsurprisingly, there are many different types of species that can be employed and different mechanisms by which control can occur. As with photo and electrochemical stimuli, a major mark of delineation is whether stimulus directly affects/alters the recognition site, or whether change is created in the recognition site via activation at a remote site. The direct alteration of a recognition site is dependent on the chemical species which the recognition site is sensitive to. Commonly, pH stimulus is used or in the case of metal-organic cages, change in the ligand:metal stoichiometries.

Shionoya *et al.*, presented a multi-chemical stimuli responsive receptor **7**, comprised of tris bipyridyl porphyrin fragments linked via coordination of Zn(II) at the apexes (Figure 10).[53] The receptor could be switched between a bowl (with a formula of $Zn_4Porphyrin_3X_6$, where X is a solvent ligand) or a capsule (with a formula of $Zn_4Porphyrin_4$). It was found that two guests, adamantane and an aryl sulfonamide derivative, preferentially bound to the capsule and bowl complex respectively. Furthermore, when in the presence of the opposite conformation, an induced fit would occur upon heating (at 70°C, in CH_3CN), with partial switching to the preferred conformation. As such, when adamantane was added to the bowl, a partial change to the capsule would occur giving a ratio of 41:59 (bowl:capsule). Further addition of aryl sulfonamide to this solution led to a reversion to the bowl (at a ratio of 89:11 bowl:capsule), with adamantane being released.

Upon heating (at 70°C, in CH_3CN) in the presence of different chemical stimuli, control of the conformation and hence further control of the guest encapsulated could be afforded. For example, due to the different ligand-metal ratios of the two forms, addition of metal could be used to trigger switching. Addition of 0.4 eq. of $ZnOTf_2$ to the bowl was shown to allow formation of the capsule, while addition of a further 0.56 eq. led to reformation of the bowl. Additionally, base/acid addition was used, with the bowl to capsule (1:9) transformation occurring upon addition of base due to the formation of the stable $Zn(OH)_2$ complex, and the capsule to bowl (21:79) upon addition of acid (via reaction with $Zn(OH)_2$ to form a more reactive complex, allowing reformation of the bowl).

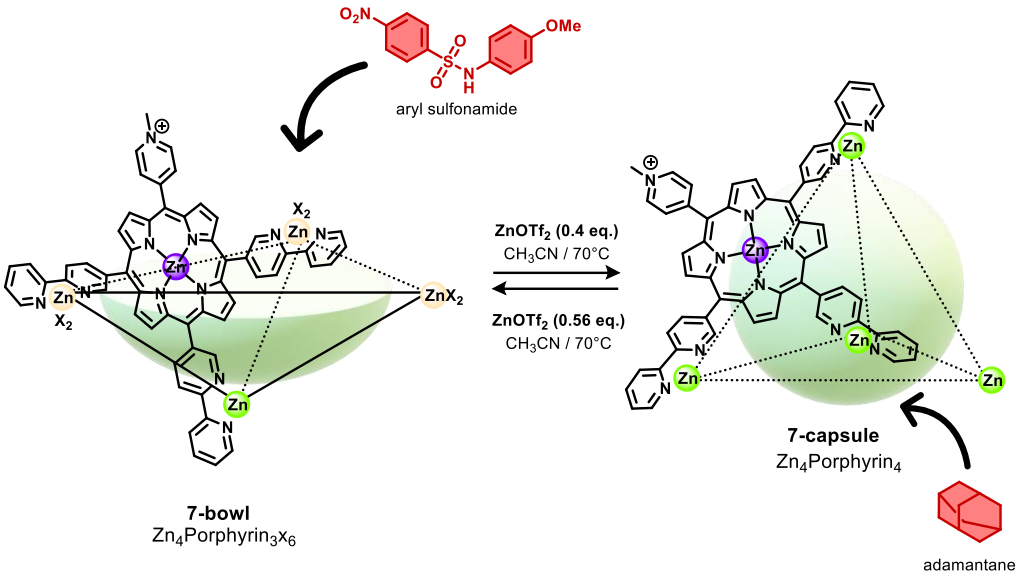

Figure 10. *The induced switch between the two states (bowl and capsule) upon addition of $Zn(OTf)_2$ to the Shionoya group's porphyrinic host* ***7****, and the preferentially bound guests.*[53]

Although there exist many ways to chemically alter and thereby impact the activity of a recognition site, chemical stimulus as a remote-control in guest uptake is a more prominently employed mechanism, similarly reflected in the prominence of a specific remote-control process in nature: Allosteric regulation.

2. Allosteric Regulation

Taken from the Greek "allos stereos" meaning different objects, the term is commonly defined as conformational changes in a macromolecule brought about by binding of a molecule (an effector, so called due to its role of triggering change as a chemical stimulus). These conformational changes lead to alterations in the binding ability/activity of/for a guest at a separate and distinct site. The process was first proposed in 1961 by Monod, Jacob and Changeux,[54,55] in response to several observations in biology where biosynthetic pathways were regulated by their end-product, despite the end products being stereochemically different from their preceding substrates.[56] These observations, in addition to the non-Michaelis-Menten kinetics observed, were used as the first signifiers of the presence of different stereospecific binding sites on enzymes and proteins.

Further development of this model led to the publishing of a paper in 1965 which has become the foundation of this field,[57] the so-called Monod-Wyman-Changeux (MWC) or concerted model (Figure 11), which stipulated that several proteins and enzymes displayed allosteric regulation and that this process was achieved via the following key features:

1. The ability of the macromolecule to assume two conformations, a relaxed (R) and tense (T) state, which exist in equilibrium.
2. The ligand/effector preferentially binding to one state over the other, stabilising the preferred state and shifting the equilibrium.

In addition, the various ways allosteric regulation/control could appear in nature were described, based on:

1. The relationship between the effector and substrate

Homotropic	Effector and guest are the same chemical species
Heterotropic	Effector and guest are different chemical species

2. The observed effect brought about by binding of the effector:

Positive	Binding of the effector leads to conformational changes which increases affinity/activity at secondary site
Negative	Binding of the effector leads to a conformational change which decreases affinity/activity at the secondary site

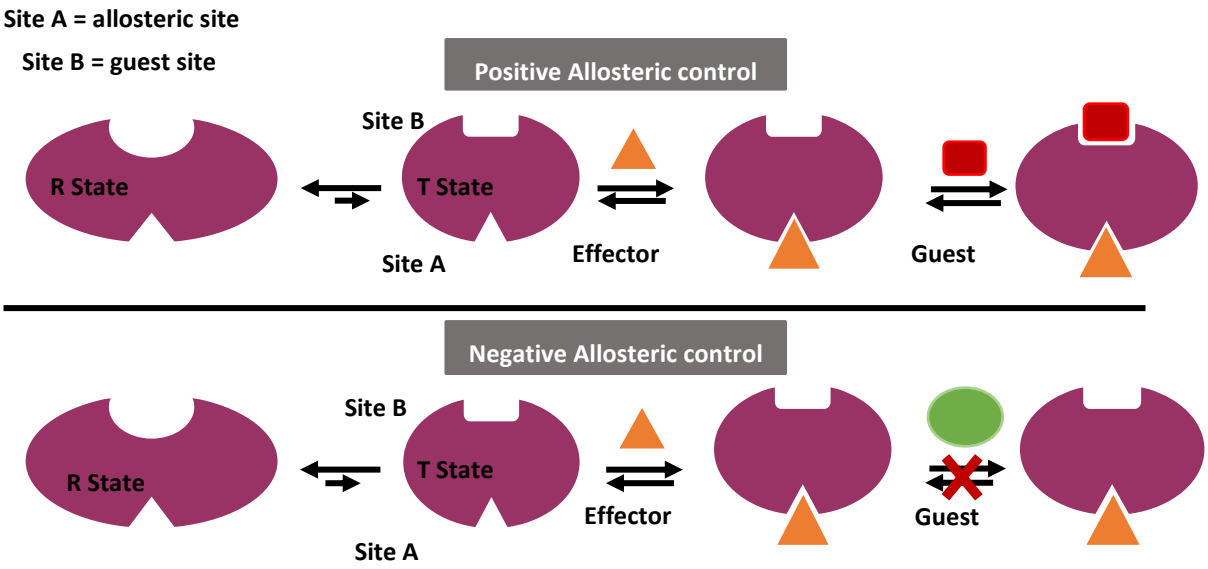

Figure 11. *Illustration of the MWC model of heterotropic allosteric regulation.*

An alternative theory in contrast to the MWC model, is that of the Koshland-Nemethy-Filmer (KNF) model published a year later (Figure 12). This model postulated a stepwise induced-fit mechanism for positive allosteric control, where the secondary state was assumed upon binding of the effector, rather than due to preferential binding.[58] Hence, in opposition to the MWC model, the "tensed" state cannot be assumed without the presence and binding of the effector.

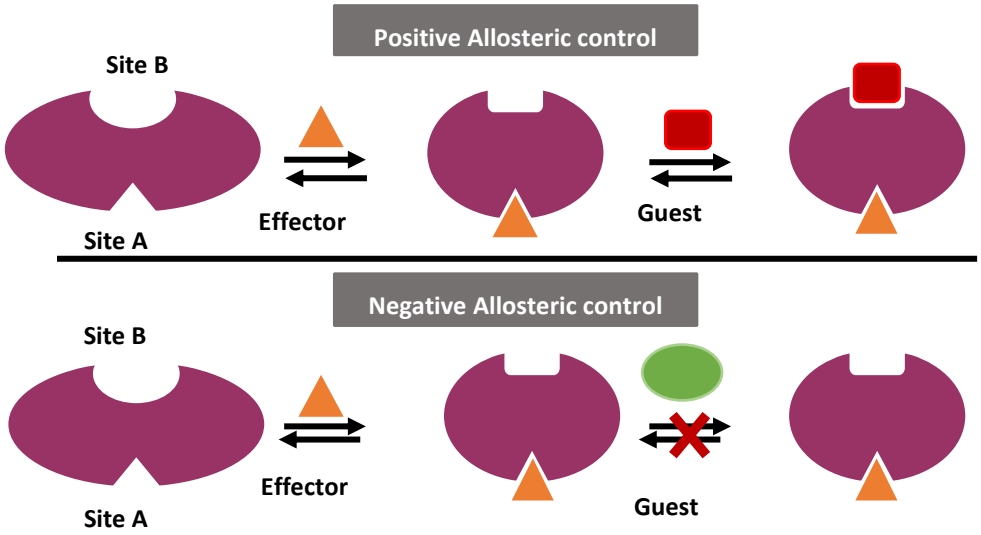

Figure 12. *Illustration of the KNF model of heterotropic allosteric control.*

In the over 50 years since the publication of the 1965 paper, many proteins and enzymes have been shown to exhibit allosteric behaviour, being implicated in many key biological processes:

2.1. Allosteric regulation in nature

2.1.1. O_2 Binding and transport

The transport of oxygen by the blood is a long-studied process, and the action of the central protein "haemoglobin" is a well examined example of allosteric regulation which was central to the development of the MWC model. Haemoglobin is comprised of four subunits (two *alpha* and two *beta*) arranged in a globular quaternary structure with a heme molecule embedded in each subunit (Figure 13). The heme molecules (Fe(II) coordinated porphyrin) act as binding sites for oxygen molecules (as well as for the inhibitors: CO and NO).

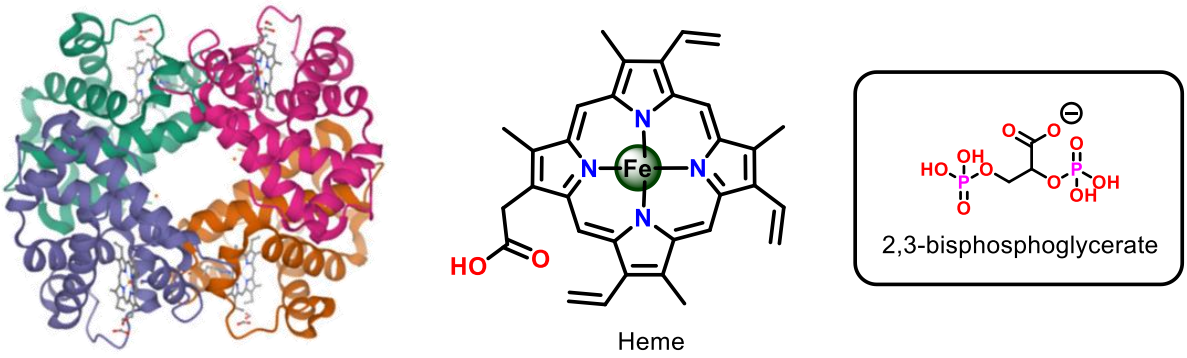

***Figure 13**. Crystal structure of deoxyhaemoglobin,[59] and skeletal structures of the oxygen binding unit: heme, and the heterotropic effector 2,3-bisphosphoglycerate.*

Haemoglobin is known to exhibit multiple allosteric pathways.[60] Homotropic positive allosteric regulation is shown where oxygen acts as both the effector and the guest. Binding of one oxygen molecule to a heme molecule leads to increased binding affinity at the remaining heme sites, with release of the oxygen molecules triggered in response to acidic pH stimulus. Additionally, heterotropic effects are also seen in the binding of oxygen via 2,3-Bisphosphoglycerate, which upon complexation increases the oxygen affinity of deoxyhemoglobin.

2.1.2. Enzyme regulation

Allosteric regulation has also been implicated in energy metabolism such as, in the synthesis of glucose-phosphate from glycogen,[61] which is controlled via the enzyme Glycogen phosphorylase (Figure 14). Two key forms of the enzyme (a and b) exist in the liver and in muscles with the presence or lack of phosphorylation at a serine residue leading to different allosteric expressions.[62] In particular, the Liver Glycogen Phosphorylase in its phosphorylated form (Liver Glycogen Phosphorylase a) is known to exhibit negative heterotropic allosteric regulation, with binding of glucose inhibiting the enzyme and preventing formation of glucose-phosphate, thereby regulating the formation and concentration of glucose in the liver.

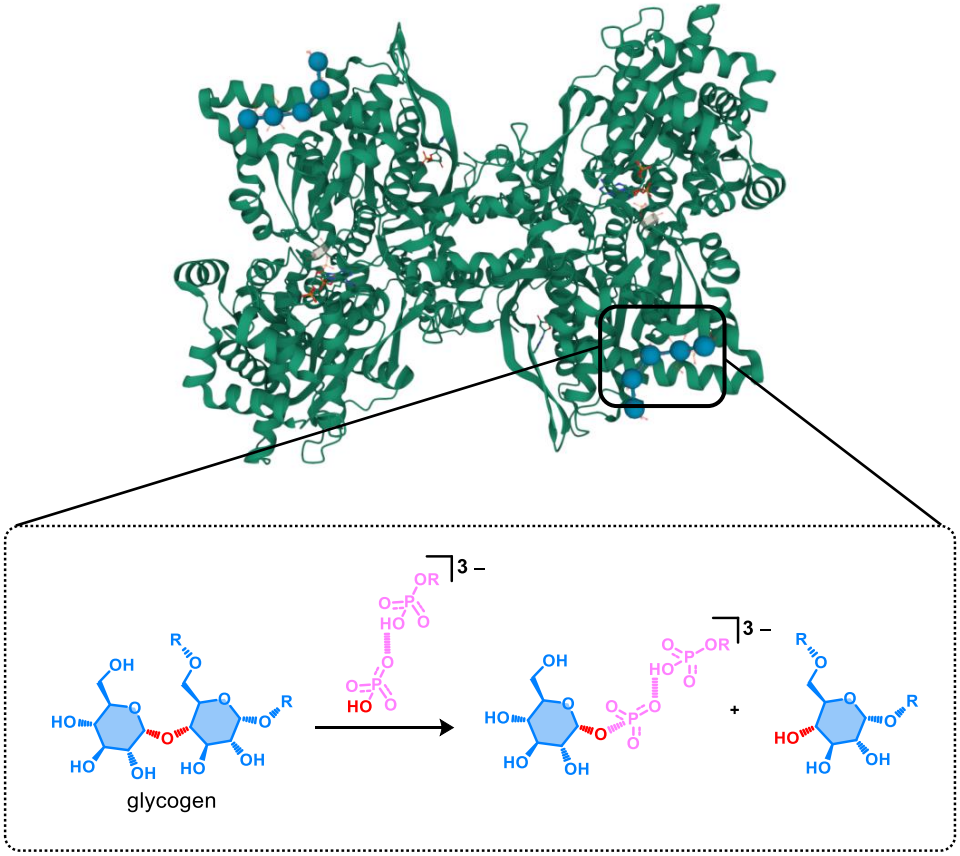

Figure 14. *Crystal structure of a glycogen phosphorylase enzyme with bound carbohydrates (represented in blue),[63] and illustration of the phosphorylation of glycogen to form glucose phosphate.*

2.2. Artificial allosteric Receptors

As can be seen in the presented biological examples, and as is intrinsic to the MWC and KNF model, the ability of the receptor to assume more than one conformational state i.e., the presence of some form of flexibility in the receptor structure, is needed in order to have an allosteric effect. Additionally, the ability to control the conformation via binding of guests is also required. Rebek named the basic requirements for the synthesis of an allosteric receptor as being the presence of an allosteric site, an active site, and a mechanism by which the two sites are coupled.[64]

The group of Rebek published in 1979 the first artificial allosteric receptor, in the synthesis of a two-dimensional receptor **8** featuring two recognition sites: a 2,2'-bipyridyl unit linked at its 3,3'-carbons to a crown ether motif (Figure 15).[64] Using out of plane effects brought about by binding at either site, **8** was able to show negative allosteric control. Binding of transition metals (namely $W(CO)_4$) by the bipyridyl, contorts the crown ether, thereby hindering binding of cations (such as Na^+ and K^+) and vice versa. The following year, Rebek and co-workers showed the ability of **8** to regulate the selectivity of ion-transport across a liquid membrane, with the ability to decrease the transport of K^+ ions across the membrane upon complexation of $W(CO)_4$ by a factor of 5 compared to the transport of Na^+. This presented an early example of an artificial receptor being used to model the functions of systems seen in nature.

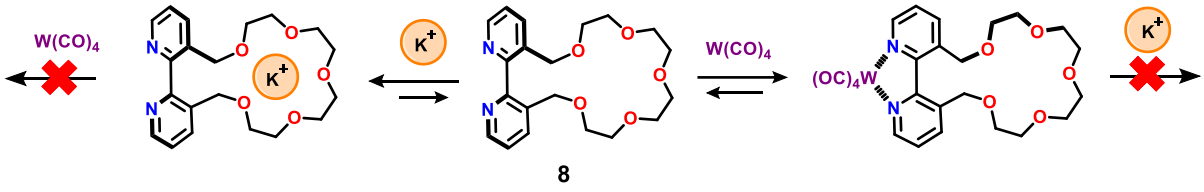

Figure 15. *Allosteric mechanism of the 1st allosteric receptor **8** reported by Rebek and co-workers in 1979.* [64]

The work of the Rebek group, was followed by the development of three-dimensional structures, with a number of motifs explored,[65–67] displaying key features important to the efficiency of biological allosteric receptors, and hence important to the development of sophisticated/advanced synthetic allosteric systems: 1) Large amplitude allosteric effects, 2) multiple pathways, 3) multi-dimensional translation of binding events, 4) catalysis and 5)

further control using other external stimuli . The use of porphyrin units as recognition sites was also considered, with the group of Kubo reporting the first heterotropic allosteric porphyrinic receptor in 1999 using a bis-porphyrin system connected by a biphenyl crown ether.[68]

2.2.1. Large amplitude allosteric effects in controlled encapsulation

The ability to use allosteric control as a true on/off switch in the encapsulation of guests or tune the binding affinity for guests by more than 2 orders of magnitude is of great importance in the development of high efficiency host-guest systems. Such large amplitude binding effects have been seen in the work of Shinkai *et al.* who reported a C_3 capsule (**9**) featuring three porphyrin units capped with two calixarene motifs (Figure 16).[69] Via coordination to the three Zn(II)-porphyrin sites, the capsule was able to bind tris(2-aminoethyl)amine (TREN) forming a 1:1 host:guest complex at a binding constant of 1.72×10^5 M^{-1} in $CHCl_3$. However, in the presence of $NaClO_4$ the binding constant was shown to increase by almost 3 orders of magnitude (1.5×10^8 M^{-1}). This was proposed to be due to binding of Na^+ ions by the calixarene caps leading to assumption of a more open conformation, presumably by interrupting intramolecular hydrogen bonding. The assertion was further supported by the effects of MeOH addition, where it was seen that titrations of TREN to **9** conducted in $CHCl_3$/MeOH (9:1) gave a higher binding constant (2.63×10^6 M^{-1}), instead of decreasing as typical in competitively coordinating solvents. In contrast, return to typical behaviour was seen for **9@Na$^+$** with the binding constant for TREN being lower in $CHCl_3$/MeOH (1.11×10^7 M^{-1}) compared to in $CHCl_3$ (1.5×10^8 M^{-1}).

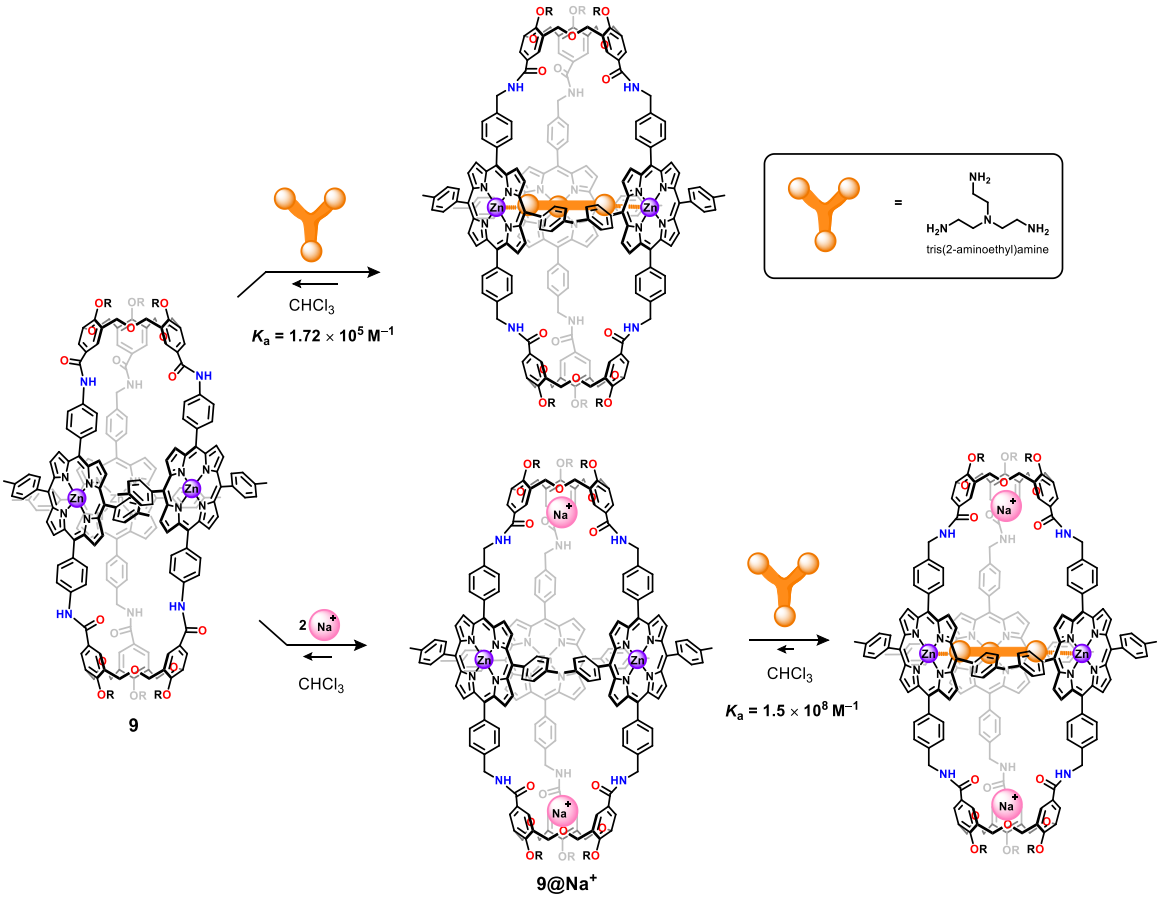

Figure 16. *Structure of the Shinkai group's capsule* ***9*** *featuring three Zn(II)-porphyrins and two terminal calixarene units, and illustration of the binding of the effector and guest.* [69]

Additionally, Ballester and co-workers were able to show on/off allosteric switching of guest uptake in a porphyrinic system. The group reported a Zn(II)-trisporphyrin featuring a central benzene tricarboxamide unit (**10**) able to bind up to three DABCO molecules (K_{13} = 2.2 × 10^{15} M^{-3} in $CHCl_3$, Figure 17).[70] When exposed to 1.5 equivalents of DABCO at millimolar concentrations, **10** formed a self-assembled molecular cage (**10**$_2$@$(DABCO)_3$), with a stability constant of K_{23} = 8 × 10^{27} M^{-4} found for the structure via UV-Visible titrations.

Using molecular modelling, the group found the cage had a binding cavity with a flexible height of up to 7 Å. As the upper end of the cavity height would allow binding of aromatic molecules, and the amide functional groups allowed formation of hydrogen bonds, the group investigated the ability of the cage to bind benzene-1,3,5-tricarboxamide guests. Conducting ITC measurements, an averaged binding constant of 1.4 × 10^4 M^{-1} was found for the guest tripentyl benzene carboxamide when titrated with **10**$_2$@$(DABCO)_3$. In contrast, in the absence

of DABCO, **10** was not seen to bind the guest. ITC dilution measurements indicated dimerization of **10** at millimolar concentrations with a dissociation constant of 1.1×10^{-3} M, but no uptake of the guest by the dimer was seen. Thus, **10** was shown to be able to form an allosteric supramolecular cage.

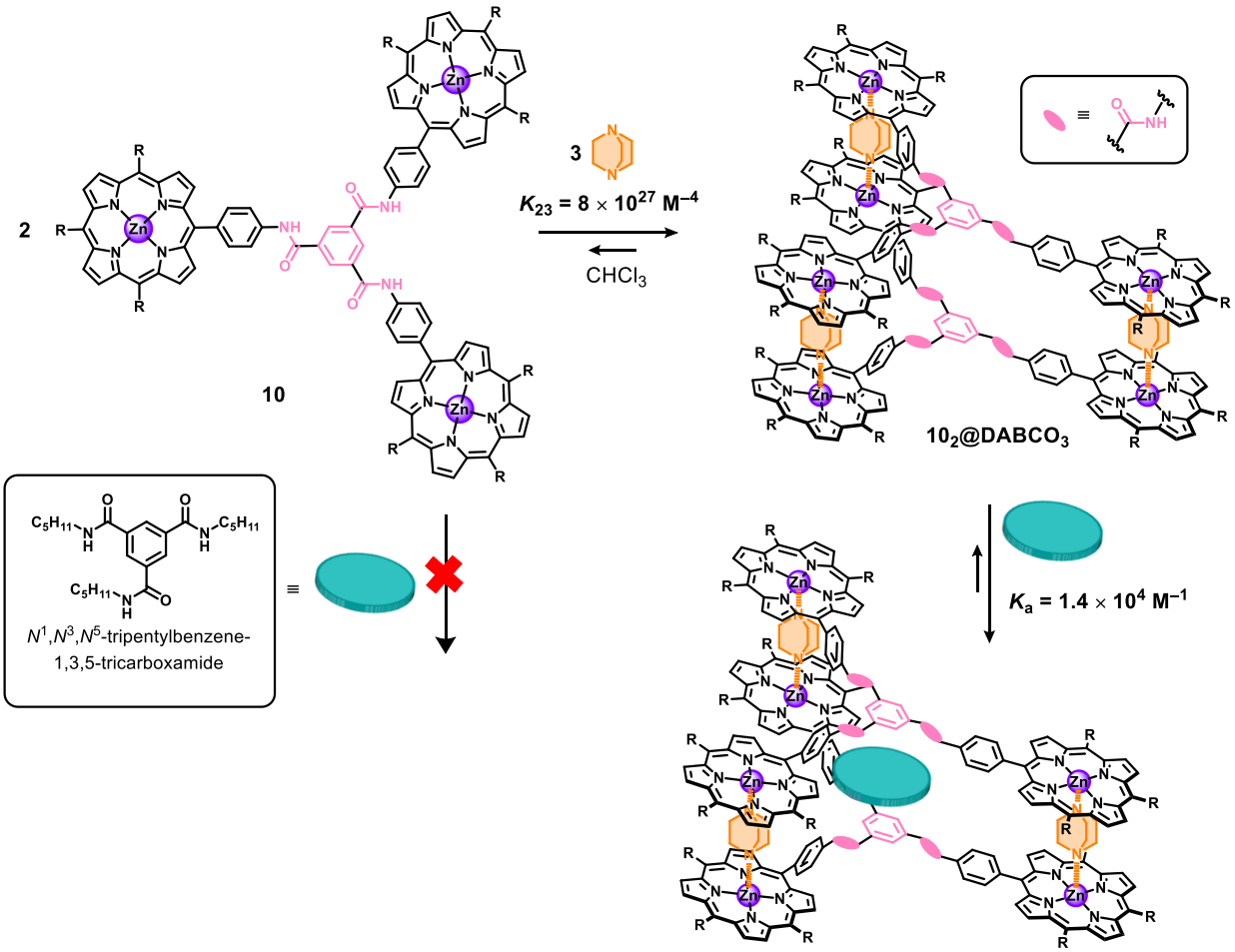

Figure 17. *Structure of the trisporphyrin **10** and the cage it forms upon coordination of DABCO, allowing encapsulation of a guest.* [70]

2.2.2. Multi-pathway allosteric regulation

Commonly in nature, allosteric proteins display multiple allosteric pathways, for example in the case of haemoglobin where it displays both heterotropic and homotropic allosteric control.

In order to design an artificial receptor with multiple levels of allosteric control, as seen with haemoglobin, multiple factors must be taken into account, making their design and synthesis even more non-trivial than simpler allosteric systems. For example, the Jang group were able to design and synthesise a porphyrin tweezer (**11**),[71] which showed positive heterotropic binding of DABCO when chloride is bound or cooperative binding of chloride when DABCO is bound in THF (Figure 18). Utilising the free rotation about the biindole single bond, complexation of the effector fixed the positions of the two faces of the tweezer in a cofacial arrangement. Thus, binding of Cl^- at the biindole bridge increased the binding constant for binding of DABCO by a factor of 12 (to $K_a = 2.48 \times 10^7\ M^{-1}$), and similarly binding of DABCO by the Zn(II)-porphyrin units increased binding of Cl^- by a factor of 9 (to $K_a = 7.1 \times 10^5\ M^{-1}$).

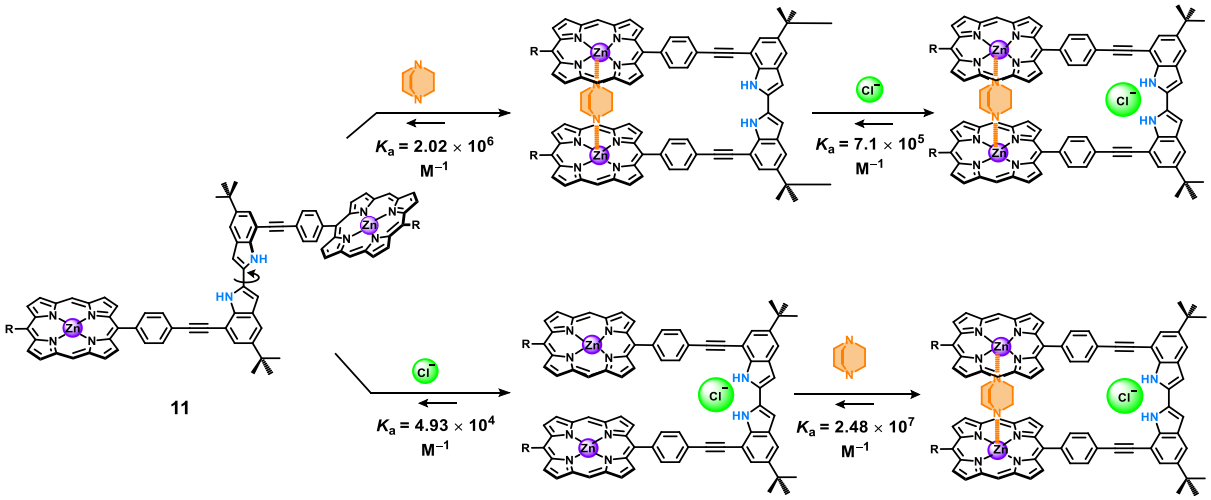

Figure 18. *Allosteric mechanism of the biindole porphyrin tweezer **11** reported by Jang et al.*[71]

However, when extending this work to form a multi-level allosteric host difficulties were found. The group designed and synthesised a porphyrin macrocycle (**12**), featuring two biindole bridges (Figure 19).[72] In the absence of pre-coordination of DABCO, it was seen that there was positive homotropic allosteric control between the two biindole sites, with allosteric cooperativity in the binding of two fluoride ions ($K_2/K_1 = 3.39$), two acetate ions ($K_2/K_1 = 24.5$) or two azide ions ($K_2/K_1 = 35.2$). Similarly to **11**, when DABCO was bound the binding affinity for the first anion significantly increased (by a factor of 74 in the case of fluoride). However, the binding of DABCO was found to switch off the homotropic allosteric effect between the two biindole sites. Thus, the biindole sites became non-cooperative with

respect to one another, with $K_2/K_1 \approx 0.25$ as expected for non-cooperative binding (in the absence of statistical correction). It was hypothesised that due to the intrinsic rigidity of **12**, and further rigidification of the host upon complexation of DABCO, the binding of the first anion did not translate to a further pre-organisation of the host at the second anion binding site when DABCO is complexed.[73]

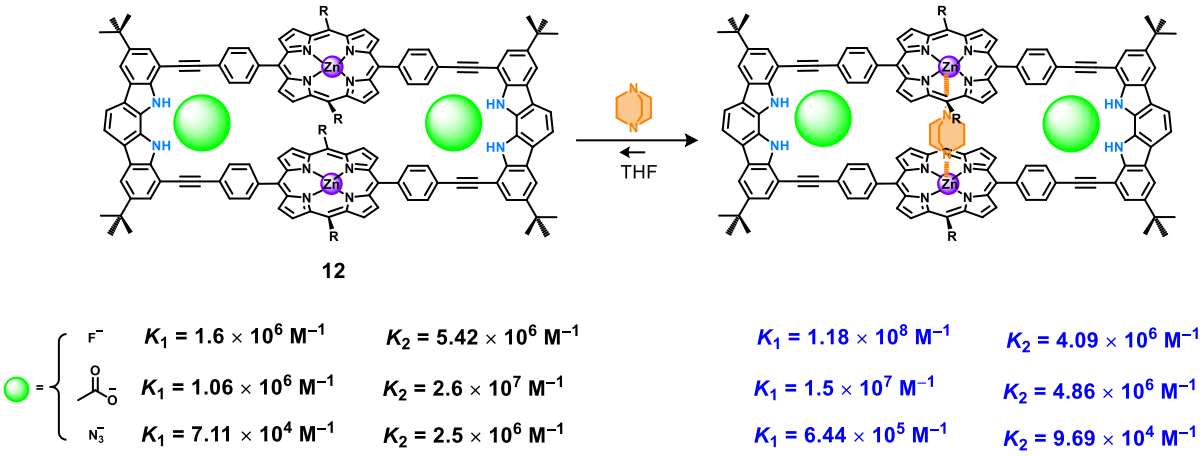

Figure 19. *The allosteric effects displayed by the Jang group's porphyrin macrocycle* ***12****, with the binding constants for binding of the different anions shown before (in black) and after (in blue) complexation of DABCO).*[72]

2.2.3. Multi-dimensional translation of binding events

As seen in the examples cited so far, artificial allosteric systems are often designed to exhibit translation of binding events in one-dimension along one axis. A seemingly less trivial design has led to limited examples of three-dimensional receptors displaying two-dimensional translation of binding events to more than one binding site. This is especially true for systems that display processes analogous to signal amplification due to the need for differing effects upon binding of the first and second guest. Early work from the Shinkai group remain standard examples, where restriction of free rotation in cerium(IV) double decker porphyrin dimers was utilised to afford differing effects upon binding of the second and first guest.

The design of **13** included pyridine groups at the *meso* positions of the porphyrin units, with an approximate interplanar distance of 3.4 Å, allowing for binding of dicarboxylic acids of the

right length (Figure 20).[74] Titration of (1R,2R)-cyclohexane-1,2-dicarboxylic acid (RR-CHDA) in CH_2Cl_2/EtOAc (30:1), was found to produce a sigmoidal curve, indicative of positive cooperative binding of multiple guests. Using the Hill equation, a Hill coefficient of 4 was found, indicating very strong cooperativity between the binding sites, with an estimated total binding constant of K_{tot} = 2.75 × 10^9 M^{-4}. Comparison of the host to a model featuring only one pyridinyl group on each porphyrin, showed that in the absence of multivalency, RR-CHDA could not be bound, underscoring the smaller binding constant for the first guest and the effects of cooperativity.

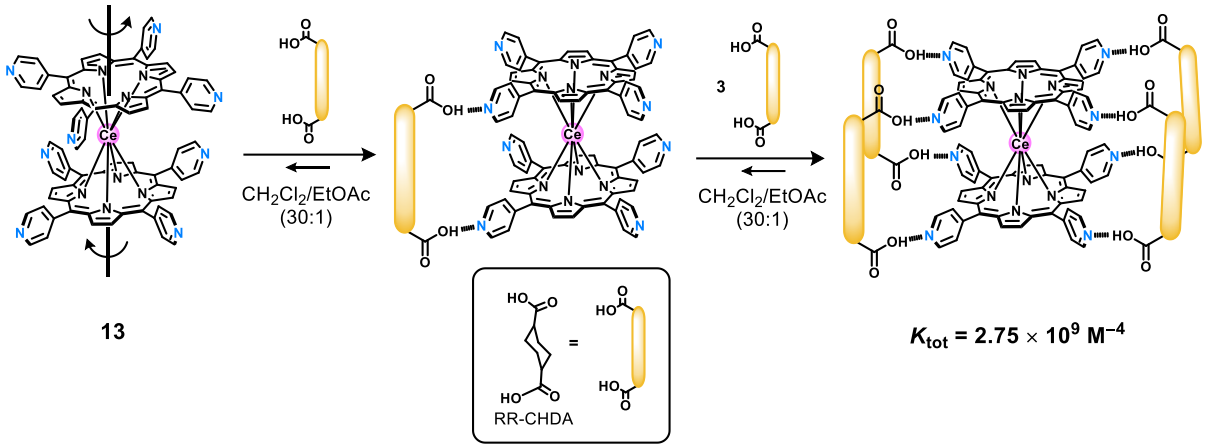

Figure 20. *Skeletal representation of the allosteric mode of action for the Ce(IV)-porphyrin dimer* ***13*** *reported by Shinkai and co-workers.*[74]

This work was further developed to create a prototype molecular spring (**14**), with the group reporting a cerium(IV) double decker featuring ferrocene hinges and 12 pyridine sites (Figure 21).[75] The host was shown to be able to assume an open "extended" conformation, with a large distance between the ferrocene units (3.2 nm) and smaller distance between the cerium centres (1.3 nm), which could be contracted upon cooperative binding of the dicarboxylic acid guests. Titration of RR-CHDA, was shown to lead to a sigmoidal curve with a Hill coefficient of 2.1 and K_{tot} = 10^{14} M^{-6}, suggesting cooperativity albeit to a lesser extent than seen for **13**. Nevertheless, changes in the NMR spectrum and in the CD spectrum showed the bound host assumed the contracted form upon guest complexation, with Fe-Fe distance shortened to 0.5 Å, and the Ce-Ce distance elongated to 3.5 nm according to computational models.

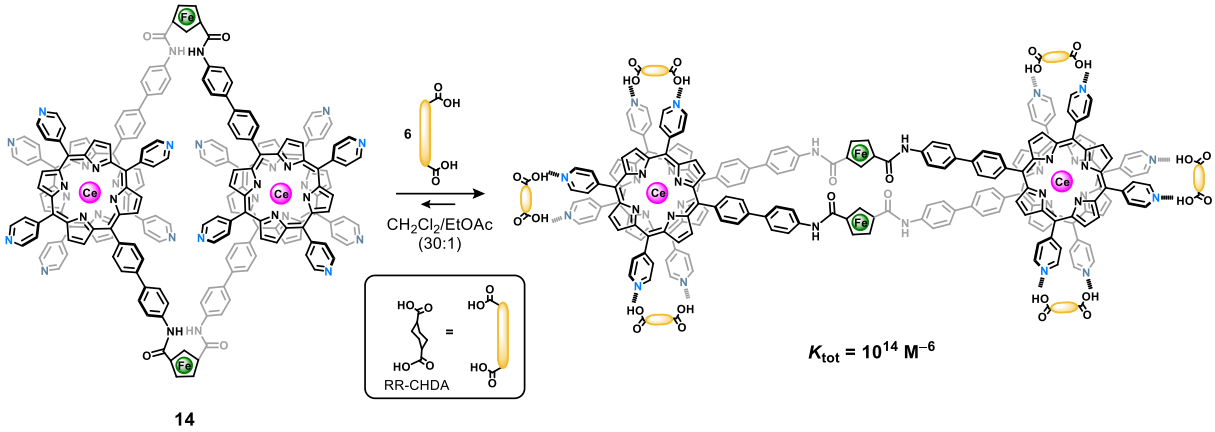

Figure 21. *Illustrative structure of the Shinkai group's molecular spring* ***14*** *in the open and closed form.*[75]

More recently, examples of multi-directional translation of binding events have looked at the use of multiple effectors to simultaneously give rise to conformational changes, similar to the mechanism of the nicotinic acetyl choline receptor.[76] This design has been used by the Heitz group, reporting a porphyrin cage (**15**) featuring triazole ligands embedded into the linkers (Figure 22).[77–79] As π–π interactions were present between the porphyrin units, **15** assumed a collapsed conformation, with an interplanar distance of 3.77 Å measured in the XRD structure. Due to the strength of the interaction, **15** could not encapsulate guests pyrazine or NDI. However, upon addition of Ag^+ ions, the cage was shown to undergo an increase in cavity width to 9.5 Å, with the Ag^+ ions binding to the triazole groups and switching their spatial arrangement from anti-syn-anti-syn, to an all syn configuration. As such, **15@4Ag⁺** was able to bind pyrazine, via ditopic coordination to the two Zn(II) metal centres, at a binding constant of 4.5×10^6 M^{-1} in CH_2Cl_2, amounting to an allosteric on/off control, with a very large amplitude. Similarly, coordination of Ag^+ ions was shown to allow the encapsulation of NDI, via π–π interactions (K_a = 95 M^{-1} in CH_2Cl_2).

The allosterically controlled encapsulation of NDI was also studied within the context of photophysics, where it was observed that a photoinduced electron transfer (from the Zn(II)-porphyrin units to the encapsulated NDI) took place upon irradiation of the porphyrin units, amounting to an allosteric control of the photoinduced electron transfer.[80]

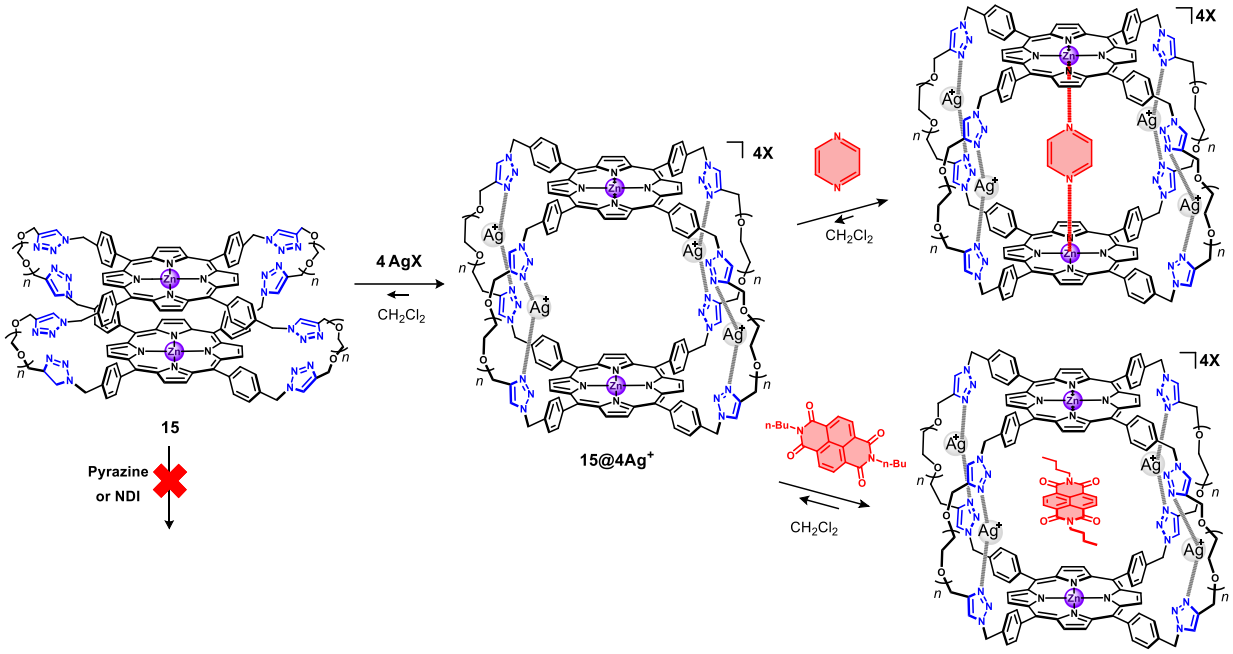

***Figure 22**. Structure and allosteric mechanism of the Heitz group's porphyrin cage **15**, able to encapsulate pyrazine or NDI when in the presence of Ag^+. X = BArF, and n = 1 or 2.*[77]

2.2.4. Allostery within stimuli-responsive units and catalytic systems

The final key features in developing advanced allosteric receptors, more specifically when contemplating the application of such receptors, or more advanced functions, has been the ability to respond to additional stimuli, and/or allosterically control the catalytic activity of an active site.

The Mirkin group reported an early example of an allosterically controlled catalyst (**16**), designing a bis-Zn(II)-porphyrin macrocycle with two Rh(I) metal centres embedded within the linker fragments (Figure 23).[81] By incorporating hemilabile chelating thioether ligands into its structure, it was possible to control the diameter of **16**'s aperture. In the presence of Cl^- and CO ligands, the thioether was displaced, and the aperture of **16** was increased from 3.5 Å to 7 Å. Using this effect, the group were able to display tuneable catalysis of an acyl transfer reaction between pyridyl carbinol and N-acetyl imidazole, previously shown to be accelerated by trimetallic lewis acidic porphyrin assemblies.[82,83] At a catalytic loading of 2% in CH_2Cl_2, **16-open** was shown to have a catalytic turnover rate twice that of **16-closed**, with the

two reactants binding to the Zn(II) centres, placing them in close proximity to one another for the acyl transfer reaction. In contrast, for the reference monomer where such arrangement could not be afforded, the catalytic turnover rate was 1/14th that of **16-open**.

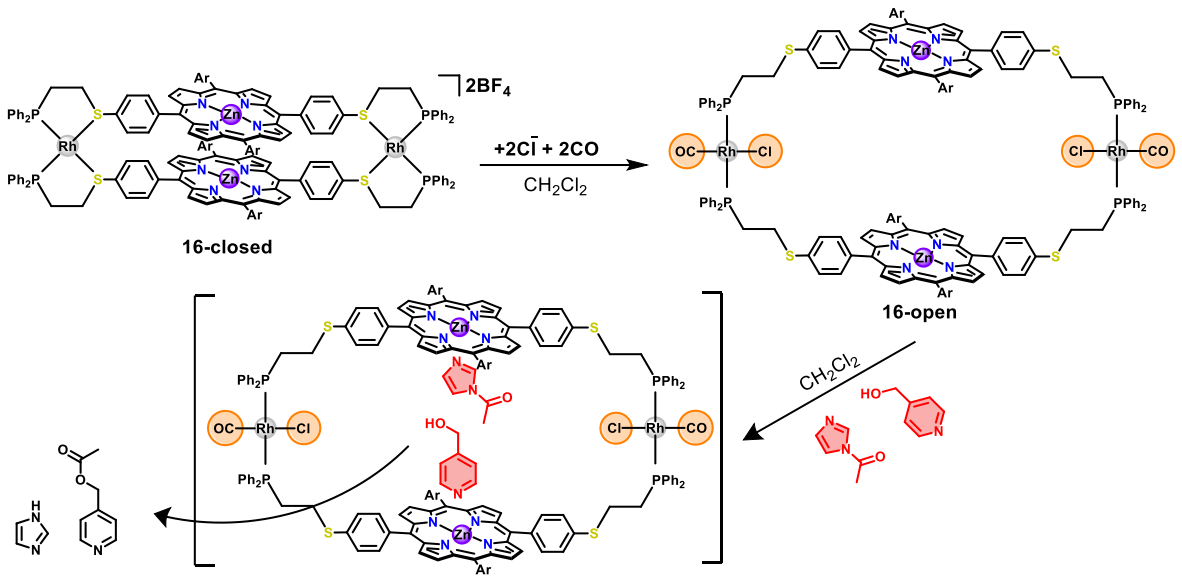

***Figure 23**. Structure of the Mirkin group's porphyrin macrocycle **16** in its open and closed form, and the catalysis of the acyl transfer.*[81]

In terms of additionally stimuli-responsive allosteric systems, examples include the work of the Álvarez group, where the difference in behaviour between a free-base and metalloporphyrin was exploited in a less classical fashion to afford a switching in the behaviour of an octapodal pyrene porphyrin **17-2H** (Figure 24).[84] The receptor was shown to be able to bind fullerenes, forming a 1:2 complex, with binding of fullerene to both faces of the free-base porphyrin. A decrease in the 1:2 binding constants could be seen for the free base receptor (K_1 = 1.4 × 10^4 M^{-1}, K_2 = 3.5 × 10^3 M^{-1} for C_{70} and K_1 = 1.49 × 10^3 M^{-1}, K_2 = 3.71 × 10^2 M^{-1} for C_{60} in toluene) with K_2/K_1 = 0.25, in line with a non-cooperative system. However, it was shown that upon complexation of Zn(II) a very strong negative cooperativity was seen, becoming an off switch for the second binding site, with only formation of the 1:1 complex observed for **17-Zn(II)** (2.69 × 10^4 M^{-1} for C_{70} and 2.3 × 10^3 M^{-1} for C_{60} in toluene). Thus, Zn^{2+} was used as chemical switch to turn on/off cooperativity between the two binding sites, with the effect possibly arising from the changes in planarity of the porphyrin upon coordination of Zn^{2+} indicated via UV-Vis spectroscopy.

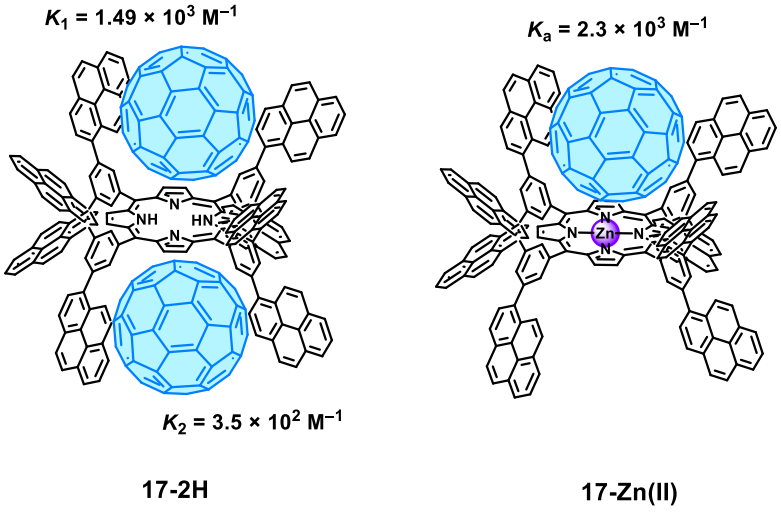

Figure 24. *Structure of the Álvarez group's free-base (**17-2H**) and zinc metalated (**17-Zn(II)**) octapodal pyrene porphyrin hosts, with complexation of fullerene C_{60} and respective binding constants shown.*[84]

The self-locking nano-switch **18** presented by the Schmittel group can be regarded as an example of a stimuli responsive catalytic allosteric system (Figure 25).[85] The receptor, comprised of three freely rotating arms, each incorporating a different recognition unit (a Zn(II)-porphyrin, pyrimidine-pyridine (py-pm) arm and phenanthroline respectively), was shown to be able to assume two states. In its native state, the py-pm arm coordinates to the Zn(II)-porphyrin, blocking the porphyrin site. However, in the presence of Cu(I), the receptor is switched to its second state, with the phenanthroline unit and py-pm both coordinating the Cu(I) guest (K_a = 1.2 × 10^6 M^{-1} in CH_2Cl_2), leaving the Zn(II)-porphyrin free for coordination by guests. Diazastilbene hence coordinates to the Zn(II), at a binding constant 3000 times higher than in the absence of Cu(I) (K_a = 1.6 × 10^3 vs. 0.095 M^{-1} in CH_2Cl_2). Utilising its photosensitising properties, upon irradiation of the porphyrin (419 nm, 30 minutes) **18** (present at a 25 mol% catalyst loading) affords catalysation of the *cis* to *trans* isomerisation of the guest (28:72 ±4).

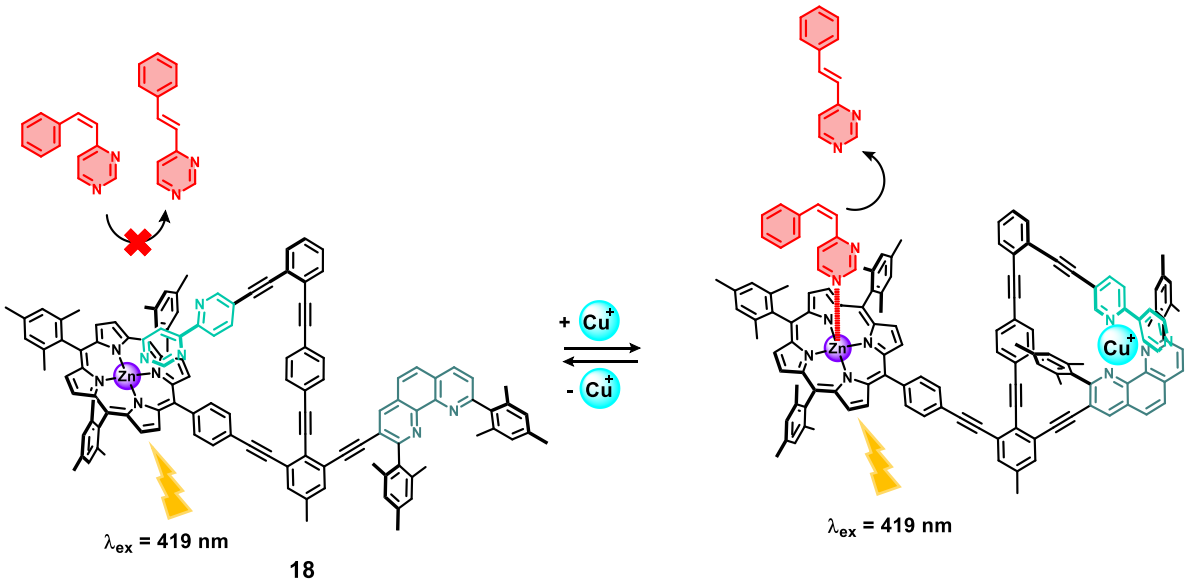

Figure 25. *Structure and mechanism of action of the Schmittel group's self-locking allosteric photocatalyst* ***18****.*[85]

The successful use of porphyrins in all variations of stimuli-responsive systems as structural motifs, recognition sites and molecular switches exemplifies the power of the porphyrin building block in developing complex artificial receptors. Although a number of features key to the development of sophisticated responsive hosts have been achieved, there remain some areas to further develop. For example, in the development of multi-pathway allosteric systems which display simultaneously both homotropic and heterotropic control of guest encapsulation. Development of multi-dimensional allosteric systems featuring more than two enclosed binding pockets is also of interest. Likewise, development of hosts which achieve control using multiple different stimuli, especially further development of multi-state host-guest systems, is worthwhile due to the widened applications that may be afforded.

Therefore, design and synthesis of a multi-responsive allosteric host capable of heterotropic binding of effectors and guests, would be of interest. In order to form a heterotropic allosteric system, the porphyrin unit must be coupled to another recognition group. Additionally, coupling with a stimuli-responsive motif could afford further mechanisms by which control of the host-guest properties is obtained. As such, pairing with a recognition motif able to bind guests and respond to different stimuli could be explored to achieve this system. An example of one such motif is that of the N-substituted acridinium.

3. N-substituted acridinium units in molecular encapsulation

Acridiniums are a class of cationic heterocycle, consisting of an anthracenic structure, with a central pyridyl ring. The extended aromatic structure gives the compounds strong optical properties which have been utilised in DNA labelling and in photoredox catalysis, exploiting the electrochemical properties of the motif.[86–88] Yet of more particular interest, the electro-deficient aromaticity has led to the use of acridiniums as recognition sites, with its stimuli-responsive nature exploited to afford control of guest uptake and release. Similarly to the porphyrin, the acridinium is multi-responsive. Addition of nucleophiles leads to acridane formation, with photo-triggered release of the nucleophile. In addition, N-substituted acridinium can be reduced via electrochemical means to give a radical species which is easily re-oxidised to the acridinium species (Figure 26).[89–91]

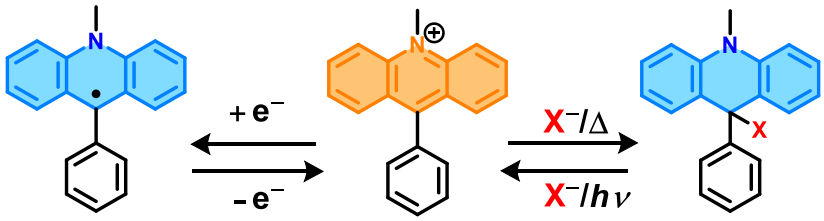

***Figure 26**. Representation of the structures formed upon application of different stimuli to a 9-phenyl N-methyl acridinium.*

3.1. N-substituted acridinium-based receptors

The earliest example of acridinium based receptors is that of Lehn *et al.* of a bisacridinium cavitand **19a** featuring acetylene linkers and its related precursor tweezer **19b** (Figure 27).[92] The water-soluble cavitand was shown to be able to bind anionic and neutral planar guests ($\log K_a$ = 3 - 6), forming 1:1 complexes, with observed hypochromic shifts in the UV-Vis spectra consistent with a π–π stacking structure. The effect was shown to be larger the more stable the host-guest complex, with binding constants seemingly dependent on the aromatic surface area of the guest as opposed to electron density. Interestingly, it was found that the acetylene bridges hindered binding, due to their rigidity, and the distance within the cavity. As such, the acyclic precursors had binding constants 10-100 times larger compared to the cavitands ($\log K_a$

= 4 – 7), highlighting the importance of linkers in determining the efficacy of guest binding. In actuality, the crystal structure of **19a**, showed the cavity to have a height of 7.5 Å (with a width of 4 Å), slightly larger than optimal for π–π interactions (2 × 3.5 Å).

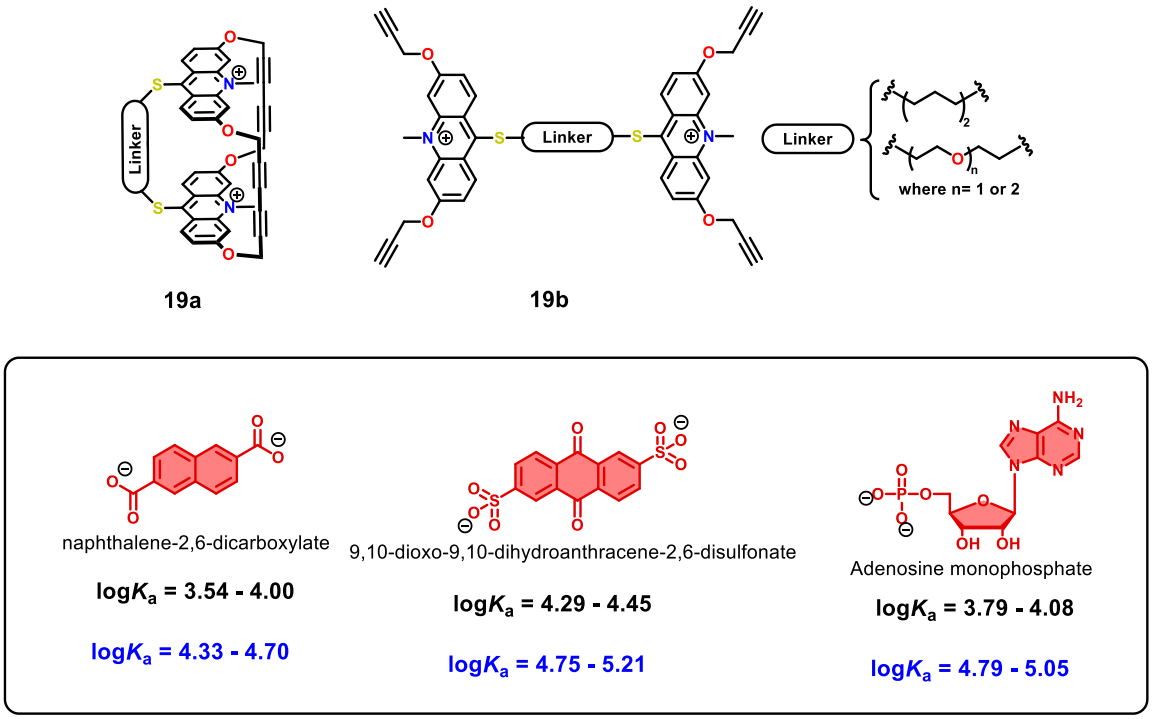

Figure 27. *Structure of the cavitand (**19a**) and tweezer (**19b**) synthesised by Lehn et al., and the range of binding constants of **19a** (in black) and **19b** (in blue) using different linkers with different guests.* [92]

Since then, other acridinium based receptors have been synthesised which utilise the stimuli-responsiveness of the acridinium to afford controlled encapsulation of the guests. In the work of Yoshizawa *et al.*,[93] acridiniums were used to form water-soluble metal-organic capsules, able to encapsulate trifluoroborate-appended cycloalkanes. Yoshizawa then went on to develop a wholly organic water-soluble macrocycle **20** (Figure 28), able to bind long hydrophilic molecules featuring steroid or coumarin motifs, with switchable release upon addition of base.[94] The crystal structure of **20** revealed a cylindrical structure with a 1 nm long cavity. Upon addition of excess aqueous NaOH or $NaHCO_3$, **20** was converted to the acridane derivative **20-OR**, with XRD structure showing a collapsed structure. Upon addition of aqueous HCl, the receptor **20** was recovered, with a fatigue cycle showing no major loss in conversion after 5 cycles. Binding constants and thermodynamic parameters were found via

ITC for the guest CHAPS ($K_a = 7.3 \times 10^3\ M^{-1}$). Via NMR spectroscopy, the binding of the guest was found to proceed via encapsulation of the recognition group of the guest molecule, (with the rest of the guest lying outside the receptor). This suggested possible use of the receptor in binding longer biomolecules and polymers. Similarly, the successive release and reuptake of the guest via addition of base then acid was shown via NMR spectroscopy.

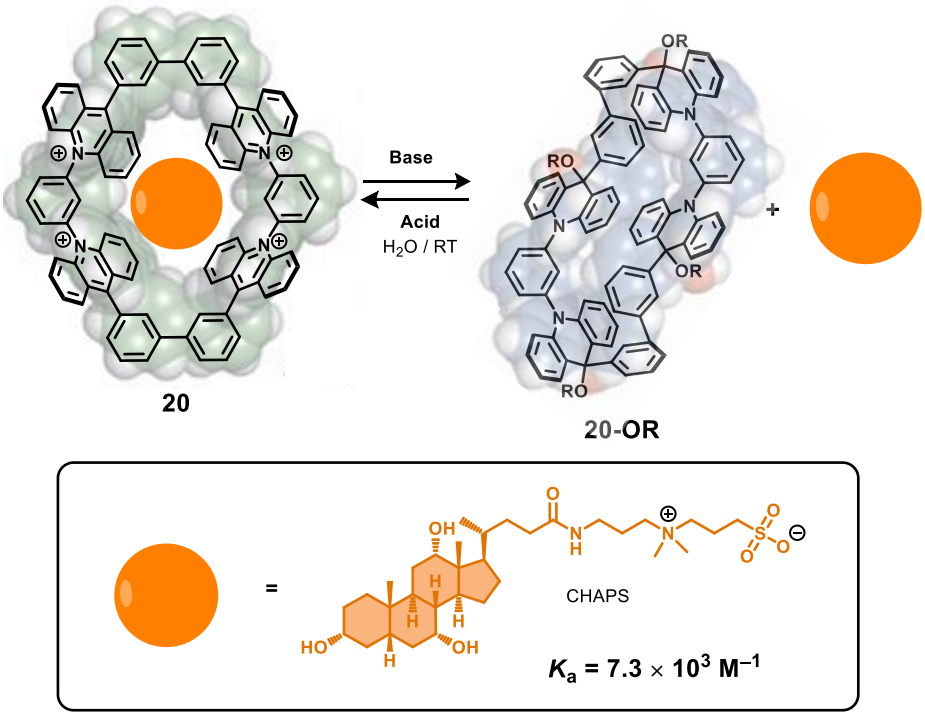

Figure 28. *Structure of the acridinium nano-capsule (**20**) reported by the Yoshizawa group, and the neutral acridane structure (**20-OR**) formed upon exposure to base.* [94]

More recently, our own research group has reported on a series of tweezers and macrocycles, showing binding of various aromatic molecules, and their switchable release upon addition of nucleophiles/base, or reduction of the acridinium. Building on previous work reporting the design and study of bis-acridinium tweezers,[95] a bis-acridinium macrocycle **21** featuring a semi-rigid bipyridylphenyl spacer was reported (Figure 29).[96] The macrocycle was shown to be able to bind polyaromatic molecules, with the highest binding constant being found for perylene ($K_a = 1.2 \times 10^3\ M^{-1}$ in CH_2Cl_2 or $C_2H_4Cl_2$). Significantly, the multi-responsive behaviour of the acridinium units was utilised to tune the binding affinity of the macrocycle, with release of the guest upon addition of OH^- evidenced via UV-Vis spectroscopy. As with Yoshizawa's system, re-aromatisation via addition of TFA led to re-encapsulation of the guest, recovering

the host-guest spectral features. Electrochemical reduction of the acridinium was shown to lead to a dramatic decrease in binding affinity for perylene, (by two orders of magnitude, to K_a = 55 M^{-1}) Thus, a multi-responsive control in the guest uptake and release was shown, utilising electrochemical and chemical stimuli.

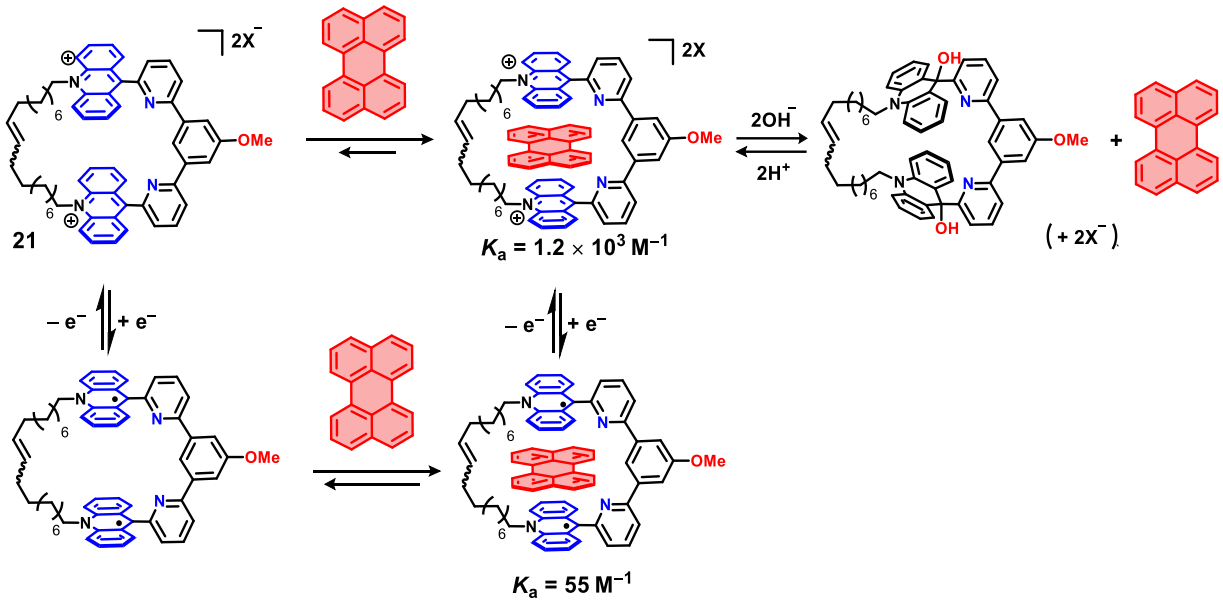

Figure 29. *Structure of the bisacridinium macrocycle* ***21*** *and the complexes it forms in response to different stimuli.* [96]

3.2. Protonated acridines as guests for porphyrinic hosts

Although the pairing of the two motifs opens many perspectives, the coupling of porphyrin and acridinium has not been well explored, with no published examples of metalloporphyrins and acridiniums within a host-guest system, and limited examples of acridinium and free base porphyrin as units within the same system. Most papers involving the two units have focused on the use of the protonated acridine as guests for bis-porphyrin receptors, more specifically bisporphyrin clips.[97,98] The photodynamics of such host-guest complexes were first explored by the group of Fukuzumi, reporting a bis free-base porphyrin clip **22** featuring a diphenyl oxide spacer (Figure 30). **22** was shown via UV-Vis and Fluorescence spectroscopy to be able to bind a simple acridinium (the protonated acridine, AcrH) in a cofacial manner with a binding constant of 9.7 × 10^4 M^{-1} in benzonitrile. Upon irradiation of the complex, electron transfer

from the porphyrin to AcrH was observed to occur, verified via laser photolysis and fluorescence decay experiments, with the charge separated state being long-lived at low temperatures. Similarly, Rath and Chaudhray later explored the encapsulation of AcrH by a bis porphyrin clip **23** featuring a rigid pyrrole linker (Figure 30), able to complex AcrH in dichloromethane with a binding constant of 1.4×10^4 M^{-1}.[99] Here, similarly to the host-guest complexes of Fukuzumi, photoinduced electron transfer was observed, leading to an efficient fluorescence quenching, with 95% quenching of the porphyrin emission, when exciting the Q-band of the porphyrin.

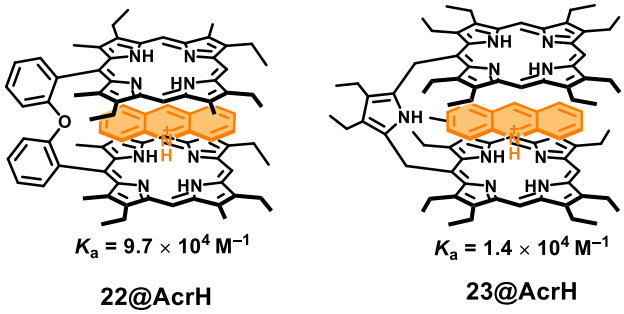

Figure 30. *Host-guest complexes studied by the Fukuzumi group (**22@AcrH**),*[97,98] *and Rath & Chaudray (**23@AcrH**).*[99]

3.3. N-substituted acridiniums covalently linked to porphyrins

Examples of covalently linked porphyrin-acridinium systems are limited to work by Fukuzumi *et al.* in the synthesis of the porphyrin-acridinium triad **24** (Figure 31).[100] Similar to **22@AcrH** and **23@AcrH**, the triad was shown to have quenched fluorescence for both the acridinium and porphyrin due to photoinduced electron transfer. This property was exploited to develop a fluorescence sensor for one-electron reductants such as superoxide, utilising the ability to reduce the acridinium (forming the radical species), and thereby restore the fluorescence of the porphyrin.

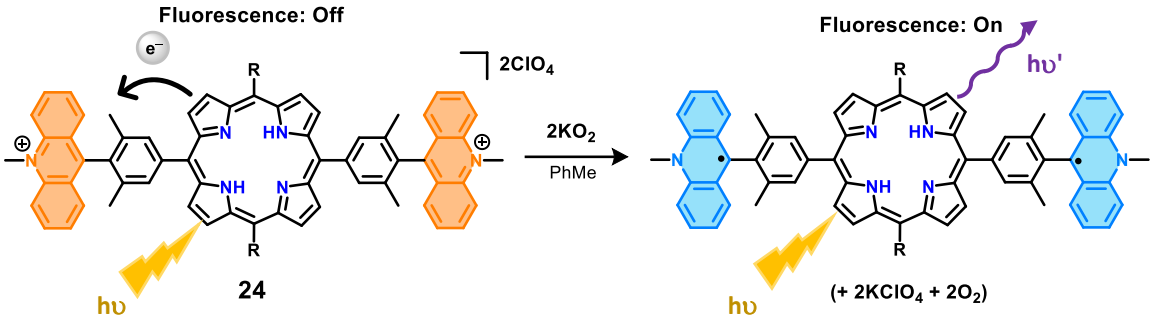

***Figure 31**. The Fukuzumi group's porphyrin-acridinium fluorescence sensor **24** before and after addition of KO_2.*[100]

4. Aims and Objectives

This thesis has aimed to synthesise a family of receptors incorporating the N-alkylated acridinium and the porphyrin as recognitions sites, for the controlled encapsulation of guests. Moreover, in order to take advantage of the different non-covalent interactions that a metalloporphyrin can use to stabilise guest molecules (both metal-ligand coordination and π–π interactions), the design of the receptors incorporated Zn(II)-metallated porphyrins.

Different receptor architectures were designed via exploitation of the multiple functionalisation points of the porphyrin, with formation of the receptors via linking of the two halves of the receptor using flexible linkers (Figure 32). Specifically, a tweezer could be afforded via linking of two porphyrin acridinium conjugates (featuring one N-alkylated acridinium substituent per porphyrin) with one linker group. Similarly, a cage could be obtained by forming four linkers between two porphyrin acridinium conjugates (with four N-alkylated acridinium substituents per porphyrin).

It was hypothesised that such systems would show positive heterotropic allosteric control (Figure 32). In the case of the tweezer, binding of an effector by the porphyrin units, would pre-organise and rigidify the receptor, translating to increased binding affinity at the acridinium site. Given that the acridinium is known to bind planar aromatic guests, effective pre-organisation for binding at the acridinium site, is thus afforded when using an effector which gives a cavity height of approximately 7 Å upon coordination.

Additionally, in the case of the cage, as there are four acridinium sites surrounding the porphyrin, binding of the effector would pre-organise for binding of up to four aromatic guests.

Control in the uptake and release of guests may additionally be achieved via exploitation of the multi-stimuli responsive natures of the porphyrin and acridinium units. More specifically, by exploiting the effects of chemical stimulus (on the acridinium units), and the effect of redox stimulus (on both units) on the binding abilities of the two recognition motifs.

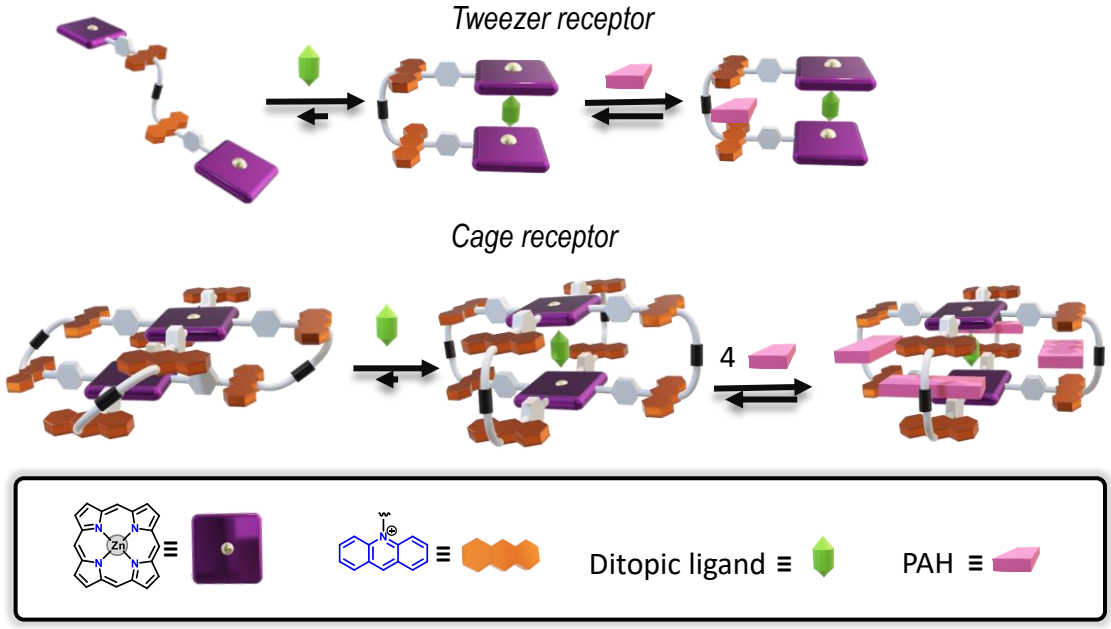

Figure 32. *3D illustration of the tweezer and cage receptor, and the allosteric mechanisms envisioned.*

In order to meet these aims, an efficient means of synthesis had first to be identified. As there were limited examples of porphyrin-acridinium conjugates in the literature, focus was first placed on the covalent attachment of the two motifs, aiming to find an effective route to synthesis of conjugates. The syntheses of the porphyrin-conjugates and the subsequent studies into their properties are detailed in chapter two.

Chapter three details the synthesis of the first receptor: a tweezer, with emphasis on finding efficient means of covalently linking the two faces of the receptors. The results from

investigations into the host-guest properties and effects of different stimuli on the tweezer are thereafter discussed.

Lastly, chapter four covers the synthesis of the cage receptor, and similarly discusses the studies into the host-guest properties of the cage and the effect of chemical stimulus.

5. References

(1) Creeth, J. M.; Gulland, J. M.; Jordan, D. O. 214. Deoxypentose Nucleic Acids. Part III. Viscosity and Streaming Birefringence of Solutions of the Sodium Salt of the Deoxypentose Nucleic Acid of Calf Thymus. *J. Chem. Soc.* **1947**, *5* (1), 1141–1145.

(2) Watson, J. D.; Crick, F. H. Molecular Structure of Nucleic Acids; a Structure for Deoxyribose Nucleic Acid. *Nature* **1953**, *171* (4356), 737–738.

(3) Pedersen, C. J. Cyclic Polyethers and Their Complexes with Metal Salts. *J. Am. Chem. Soc.* **1967**, *89* (26), 7017–7036.

(4) Pedersen, C. J. The Discovery of Crown Ethers (Noble Lecture). *Angew. Chem. Int. Ed.* **1988**, *27* (8), 1021–1027.

(5) Dietrich, B.; Lehn, J. M.; Sauvage, J. P. Diaza Polyoxa-Macrocycles et Macrobicycles. *Tetrahedron Lett.* **1969**, *10* (34), 2885–2888.

(6) Dietrich, B.; Lehn, J. M.; Sauvage, J. P. Les Cryptates. *Tetrahedron Lett.* **1969**, *10* (34), 2889–2892.

(7) Lehn, J.-M. Supramolecular Chemistry—Scope and Perspectives Molecules, Supermolecules, and Molecular Devices(Nobel Lecture). *Angew. Chem. Int. Ed.* **1988**, *27* (1), 89–112.

(8) Cram, D. J. The Design of Molecular Hosts, Guests, and Their Complexes (Nobel Lecture). *Angew. Chem. Int. Ed.* **1988**, *27* (8), 1009–1020.

(9) Cram, D. J.; Kaneda, T.; Helgeson, R. C.; Lein, G. M. Spherands - Ligands Whose Binding of Cations Relieves Enforced Electron-Electron Repulsions. *J. Am. Chem. Soc.* **1979**, *101* (22), 6752–6754.

(10) Fujita, M. Metal-Directed Self-Assembly of Two- and Three-Dimensional Synthetic Receptors. *Chem. Soc. Rev.* **1998**, *27* (6), 417–425.

(11) Ajami, D.; Liu, L.; Rebek, J. Soft Templates in Encapsulation Complexes. *Chem. Soc. Rev* **2015**, *44* (2), 490–499.

(12) Stoddart, J. F. Mechanically Interlocked Molecules (MIMs)—Molecular Shuttles, Switches, and Machines (Nobel Lecture). *Angew. Chem. Int. Ed.* **2017**, *56* (37), 11094–11125.

(13) Sauvage, J. P. From Chemical Topology to Molecular Machines (Nobel Lecture). *Angew. Chem. Int. Ed.* **2017**, *56* (37), 11080–11093.

(14) Butera, E.; Zammataro, A.; Pappalardo, A.; Trusso Sfrazzetto, G. Supramolecular Sensing of Chemical Warfare Agents. *ChemPlusChem* **2021**, *86* (4), 681–695.

(15) Pan, Y.; Hu, X.; Guo, D. Biomedical Applications of Calixarenes: State of the Art and Perspectives. *Angew. Chem. Int. Ed.* **2021**, *60* (6), 2768–2794.

(16) Raynal, M.; Ballester, P.; Vidal-Ferran, A.; van Leeuwen, P. W. N. M. Supramolecular Catalysis. Part 1: Non-Covalent Interactions as a Tool for Building and Modifying Homogeneous Catalysts. *Chem. Soc. Rev.* **2014**, *43* (5), 1660–1733.

(17) Raynal, M.; Ballester, P.; Vidal-Ferran, A.; van Leeuwen, P. W. N. M. Supramolecular Catalysis. Part 2: Artificial Enzyme Mimics. *Chem. Soc. Rev.* **2014**, *43* (5), 1734–1787.

(18) Dale, E. J., Vermeulen, N. A., Juríček, M., Barnes, J. C., Young, R. M., Wasielewski, M. R., & Stoddart, J. F. (2016). Supramolecular *Ex* plorations: *Ex* hibiting the *Ex* tent of *Ex* tended Cationic Cyclophanes. *Acc. Chem. Res.*, *49*(2), 262–273.

(19) Park, J. S.; Sessler, J. L. Tetrathiafulvalene (TTF)-Annulated Calix[4]Pyrroles: Chemically Switchable Systems with Encodable Allosteric Recognition and Logic Gate Functions. *Acc. Chem. Res.* **2018**, *51* (10), 2400–2410.

(20) Goeb, S.; Sallé, M. Electron-Rich Coordination Receptors Based on Tetrathiafulvalene Derivatives: Controlling the Host–Guest Binding. *Acc. Chem. Res.* **2021**, *54* (4), 1043–1055.

(21) Jana, A.; Bähring, S.; Ishida, M.; Goeb, S.; Canevet, D.; Sallé, M.; Jeppesen, J. O.; Sessler, J. L. Functionalised Tetrathiafulvalene- (TTF-) Macrocycles: Recent Trends in Applied Supramolecular Chemistry. *Chem. Soc. Rev.* **2018**, *47* (15), 5614–5645.

(22) Díaz-Moscoso, A.; Ballester, P. Light-Responsive Molecular Containers. *Chem. Commun.* **2017**, *53* (34), 4635–4652.

(23) Geng, W.-C., Sun, H., & Guo, D.-S. Macrocycles containing azo groups: recognition, assembly and application. *J. Incl. Phenom. Macrocycl. Chem.* **2018**. *92*(1–2), 1–79.

(24) Pu, S.-Z.; Sun, Q.; Fan, C.-B.; Wang, R.-J.; Liu, G. Recent Advances in Diarylethene-Based Multi-Responsive Molecular Switches. *J. Mater. Chem. C* **2016**, *4* (15), 3075–3093.

(25) Tian, H.; Yang, S. Recent Progresses on Diarylethene Based Photochromic Switches. *Chem. Soc. Rev.* **2004**, *33* (2), 85–97.

(26) Yu, J.; Qi, D.; Li, J. Design, Synthesis and Applications of Responsive Macrocycles. *Commun. Chem.* **2020**, *3* (1), 189–202.

(27) Bottari, G.; Trukhina, O.; Torres, T. Towards Artificial Photosynthesis: Supramolecular, Donor-Acceptor, Porphyrin-and Phthalocyanine/Carbon Nanostructure Ensembles. *Coord. Chem. Rev.* **2012**, *256*, 2453–2477.

(28) Zhao, J.; Wu, W.; Sun, J.; Guo, S. Triplet Photosensitizers: From Molecular Design to Applications. *Chem. Soc. Rev.* **2013**, *42* (12), 5323–5351.

(29) O'Connor, A. E.; Gallagher, W. M.; Byrne, A. T. Porphyrin and Nonporphyrin Photosensitizers in Oncology: Preclinical and Clinical Advances in Photodynamic Therapy. *Photochem. Photobiol.* **2009**, *85* (5), 1053–1074.

(30) Abrahamse, H.; Hamblin, M. R. New Photosensitizers for Photodynamic Therapy. *Biochem. J.* **2016**, *473* (4), 347–364.

(31) Krause, G. H.; Weis, E. Chlorophyll Fluorescence and Photosynthesis: The Basics. *Annu. Rev. Plant Physiol. Plant Mol. Biol.* **1991**, *42* (1), 313–349.

(32) Milgrom, L. R. *The Colours of Life: An Introduction to the Chemistry of Porphyrins and Related Compounds*; Oxford University Press: Oxford, UK, 1997.

(33) Zhang, W.; Lai, W.; Cao, R. Energy-Related Small Molecule Activation Reactions: Oxygen Reduction and Hydrogen and Oxygen Evolution Reactions Catalyzed by Porphyrin- and Corrole-Based Systems. *Chem. Rev.* **2017**, *117* (4), 3717–3797.

(34) Valderrey, V.; Aragay, G.; Ballester, P. Porphyrin Tweezer Receptors: Binding Studies, Conformational Properties and Applications. *Coord. Chem. Rev.* **2014**, *258–259*, 137–156.

(35) Durot, S.; Taesch, J.; Heitz, V. Multiporphyrinic Cages: Architectures and Functions. *Chem. Rev.* **2014**, *114* (17), 8542–8578.

(36) Mondal, P.; Rath, S. P. Cyclic Metalloporphyrin Dimers: Conformational Flexibility, Applications and Future Prospects. *Coord. Chem. Rev.* **2020**, *405*, 213117–213144.

(37) Elemans, J. A. A. W.; Nolte, R. J. M. Porphyrin Cage Compounds Based on Glycoluril-from Enzyme Mimics to Functional Molecular Machines. *Chem. Commun.* **2019**, *55*, 9590–9605.

(38) Percástegui, E. G.; Jancik, V. Coordination-Driven Assemblies Based on Meso-Substituted Porphyrins: Metal-Organic Cages and a New Type of Meso-Metallaporphyrin Macrocycles. *Coord. Chem. Rev.* **2020**, *407*, 213165–213195.

(39) Ishihara, S.; Labuta, J.; van Rossom, W.; Ishikawa, D.; Minami, K.; Hill, J. P.; Ariga, K. Porphyrin-Based Sensor Nanoarchitectonics in Diverse Physical Detection Modes. *Phys. Chem. Chem. Phys.* **2014**, *16* (21), 9713–9746.

(40) Wezenberg, S. J. Highlight Review Light-Switchable Metal-Organic Cages. *Chem. Lett.* **2020**, *49*(6), 609–615.

(41) Qu, D.-H.; Wang, Q.-C.; Zhang, Q.-W.; Ma, X.; & Tian, H. Photoresponsive Host–Guest Functional Systems. *Chem. Rev.* **2015**, *115*(15), 7543–7588.

(42) Muraoka, T.; Kinbara, K.; Kobayashi, Y.; Aida, T. Light-Driven Open−Close Motion of Chiral Molecular Scissors. *J. Am. Chem. Soc.* **2003**, *125* (19), 5612–5613.

(43) Muraoka, T.; Kinbara, K.; Aida, T. Mechanical Twisting of a Guest by a Photoresponsive Host. *Nature* **2006**, *440* (7083), 512–515.

(44) Gilissen, P. J.; Vanthuyne, N.; Feringa, B. L.; Elemans, J. A. A. W.; Nolte, R. J. M. Light-gated Binding in Double-motorized Porphyrin Cages. *Nat Sci.* **2022**, *2* (1).

(45) Feringa, B. L. The Art of Building Small: From Molecular Switches to Motors (Nobel Lecture). *Angew. Chem. Int. Ed.* **2017**, *56* (37), 11060–11078.

(46) Fukino, T.; Yamagishi, H.; Aida, T. Redox-Responsive Molecular Systems and Materials. *Adv. Mater*. **2017**, *29*(25), 1603888–1603904.

(47) Kahlfuss, C.; Saint-Aman, E.; Bucher, C. Redox-Controlled Intramolecular Motions Triggered by π-Dimerization and Pimerization Processes. In *Organic Redox Systems*; John Wiley & Sons, Inc: Hoboken, NJ, USA, 2015; pp 39–88.

(48) Cai, K.; Zhang, L.; Astumian, R. D.; Stoddart, J. F. Radical-Pairing-Induced Molecular Assembly and Motion. *Nat. Rev. Chem.* **2021**, *5* (7), 447–465.

(49) Iordache, A.; Retegan, M.; Thomas, F.; Royal, G.; Saint-Aman, E.; Bucher, C. Redox-Responsive Porphyrin-Based Molecular Tweezers. *Chem. Eur. J.* **2012**, *18* (25), 7648–7653.

(50) Jokic, D.; Boudon, C.; Pognon, G.; Bonin, M.; Schenk, K. J.; Gross, M.; Weiss, J. Structural and Binding Features of Cofacial Bis-Porphyrins with Calixarene Spacers: Pac-Man Porphyrins That Can Chew. *Chem. Eur. J.* **2005**, *11* (14), 4199–4209.

(51) Dutton, K. G.; Rothschild, D. A.; Pastore, D. B.; Emge, T. J.; Lipke, M. C. The Influence of Redox-Active Linkers on the Stability and Physical Properties of a Highly Electroactive Porphyrin Nanoprism. *Inorg. Chem.* **2020**, *59* (17), 12616–12624.

(52) Mansoor, I. F.; Dutton, K. G.; Rothschild, D. A.; Remsing, R. C.; Lipke, M. C. Uptake, Trapping, and Release of Organometallic Cations by Redox-Active Cationic Hosts. *J. Am. Chem. Soc.* **2021**, *143* (41), 16993–17003.

(53) Endo, K.; Ube, H.; Shionoya, M. Multi-Stimuli-Responsive Interconversion between Bowl- And Capsule-Shaped Self-Assembled Zinc(II) Complexes. *J. Am. Chem. Soc.* **2020**, *142* (1), 407–416.

(54) Jacob, F.; Monod, J. Genetic Regulatory Mechanisms in the Synthesis of Proteins. *J. Mol. Biol.* **1961**, *3* (3), 318–356.

(55) Monod, J.; Jacob, F. General Conclusions: Teleonomic Mechanisms in Cellular Metabolism, Growth, and Differentiation. *Cold Spring Harb. Symp. Quant. Biol.* **1961**, *26*, 389–401.

(56) Changeux, J.-P. 50th Anniversary of the Word “Allosteric.” *Protein Science.* **2011**, *20* (7), 1119–1124.

(57) Monod, J.; Wyman, J.; Changeux, J. On the Nature of Allosteric Transitions: A Plausible Model. *J. Mol. Biol.* **1965**, *12* (1), 88–118.

(58) Koshland, D. E.; Nemethy, J. G.; Filmer, D. Comparison of Experimental Binding Data and Theoretical Models in Proteins Containing Subunits. *Biochemistry* **1966**, *5* (1), 365–385.

(59) Park, S. Y.; Yokoyama, T.; Shibayama, N.; Shiro, Y.; Tame, J. R. H. 1.25 Å Resolution Crystal Structures of Human Haemoglobin in the Oxy, Deoxy and Carbonmonoxy Forms. *J. Mol. Biol.* **2006**, *360* (3), 690–701.

(60) Perutz, M. F. (1970). Stereochemistry of Cooperative Effects in Haemoglobin: Haem–Haem Interaction and the Problem of Allostery. *Nature* **1970**, *228*(5273), 726–734.

(61) Barford, D.; Johnson, L. N. The Allosteric Transition of Glycogen Phosphorylase. *Nature* **1989**, *340* (6235), 609–616.

(62) Berg, J.; Tymoczko, J.; Stryer, L. Phosphorylase Is Regulated by Allosteric Interactions and Reversible Phosphorylation. In *Biochemistry*; W H Freeman, 2002; pp 583–585.

(63) Johnson, L. N.; Acharya, K. R.; Jordan, M. D.; McLaughlin, P. J. Refined Crystal Structure of the Phosphorylase-Heptulose 2-Phosphate-Oligosaccharide-AMP Complex. *J. Mol. Biol.* **1990**, *211* (3), 645–661.

(64) Rebek, J.; Trend, J. E.; Wattley, R. v.; Chakravorti, S. Allosteric Effects in Organic Chemistry. Site-Specific Binding. *J. Am. Chem. Soc.* **1979**, *101* (15), 4333–4337.

(65) Kremer, C.; Lützen, A. Artificial Allosteric Receptors. *Chem. Eur. J.* **2013**, *19* (20), 6162–6196.

(66) Shinkai, S.; Ikeda, M.; Sugasaki, A.; Takeuchi, M. Positive Allosteric Systems Designed on Dynamic Supramolecular Scaffolds: Toward Switching and Amplification of Guest Affinity and Selectivity. *Acc. Chem. Res.* **2001**, *34* (6), 494–503.

(67) Rizzuto, F. J.; von Krbek, L. K. S.; Nitschke, J. R. Strategies for Binding Multiple Guests in Metal–Organic Cages. *Nat. Rev. Chem.* **2019**, *3* (4), 204–222. (67)

(68) Kubo, Y.; Murai, Y.; Yamanaka, J.; Tokita, S.; Ishimaru, Y. A new biphenyl-20-crown-6-derived zinc(II) porphyrin dimer with a potentially heterotropic allostery. *Tetrahedron Lett.* **1999**, *40* (33), 6019–6023.

(69) Kawaguchi, M.; Ikeda, A.; Shinkai, S. A Novel Porphyrin–Homooxacalix[3]Arene Conjugate Which Creates a C3-Symmetrical Capsular Space. *Tetrahedron Lett.* **2001**, *42* (22), 3725–3728.

(70) Ballester, P.; Oliva, A. I.; Costa, A.; Deyà, P. M.; Frontera, A.; Gomila, R. M.; Hunter, C. A. DABCO-Induced Self-Assembly of a Trisporphyrin Double-Decker Cage: Thermodynamic Characterization and Guest Recognition. *J. Am. Chem. Soc.* **2006**, *128* (16), 5560–5569.

(71) Lee, C.-H.; Yoon, H.; Jang, W.-D. Biindole-Bridged Porphyrin Dimer as Allosteric Molecular Tweezers. *Chem. Eur. J.* **2009**, *15* (39), 9972–9976.

(72) Lee, C. H.; Yoon, H.; Kim, P.; Cho, S.; Kim, D.; Jang, W. D. An Indolocarbazole-Bridged Macrocyclic Porphyrin Dimer Having Homotropic Allosterism with Inhibitory Control. *Chem. Commun.* **2011**, *47* (14), 4246–4248.

(73) Park, J. M.; Hong, K.-I.; Lee, H.; Jang, W.-D. Bioinspired Applications of Porphyrin Derivatives. *Acc. Chem. Res.* **2021**, *54* (9), 2249–2260.

(74) Takeuchi, M.; Imada, T.; Shinkai, S. A Strong Positive Allosteric Effect in the Molecular Recognition of Dicarboxylic Acids by a Cerium(IV) Bis[Tetrakis(4-Pyridyl)Porphyrinate] Double Decker. *Angew. Chem. Int. Ed.* **1998**, *37* (15), 2096–2099.

(75) Ikeda, T.; Shinkai, S.; Sada, K.; Takeuchi, M. A Preliminary Step toward Molecular Spring Driven by Cooperative Guest Binding. *Tetrahedron Lett.* **2009**, *50* (17), 2006–2009.

(76) Changeux, J.-P. The Nicotinic Acetylcholine Receptor: A Typical 'Allosteric Machine.' *Phil. Trans. R. Soc. B.* **2018**, *373* (1749), 20170174–20170185.

(77) Djemili, R.; Kocher, L.; Durot, S.; Peuronen, A.; Rissanen, K.; Heitz, V. Positive Allosteric Control of Guests Encapsulation by Metal Binding to Covalent Porphyrin Cages. *Chem. Eur. J.* **2019**, *25* (6), 1481–1487.

(78) Schoepff, L.; Kocher, L.; Durot, S.; Heitz, V. Chemically Induced Breathing of Flexible Porphyrinic Covalent Cages. *J. Org. Chem.* **2017**, *82* (11), 5845–5851.

(79) Kocher, L.; Durot, S.; Heitz, V. Control of the Cavity Size of Flexible Covalent Cages by Silver Coordination to the Peripheral Binding Sites. *Chem. Commun.* **2015**, *51* (67), 13181–13184.

(80) Zanetti-Polzi, L.; Djemili, R.; Durot, S.; Heitz, V.; Daidone, I.; Ventura, B. Allosteric Control of Naphthalene Diimide Encapsulation and Electron Transfer in Porphyrin Containers: Photophysical Studies and Molecular Dynamics Simulation. *Chem. Eur. J.* **2020**, *26* (72), 17514–17524.

(81) Oliveri, C. G.; Gianneschi, N. C.; Nguyen, S. T.; Mirkin, C. A.; Stern, C. L.; Wawrzak, Z.; Pink, M. Supramolecular Allosteric Cofacial Porphyrin Complexes. *J. Am. Chem. Soc.* **2006**, *128* (50), 16286–16296.

(82) Mackay, L. G.; Stephen Wylie, R.; M Sanders, J. K. Catalytic Acyl Transfer by a Cyclic Porphyrin Trimer: Efficient Turnover without Product Inhibition. *J. Am. Chem. Soc* **1994**, *116* (7), 3141–3142.

(83) Wylie, R. S.; Sanders, J. K. M. Modelling the Influence of Porphyrin Supermacrocycles on the Kinetics of Bimolecular Reactions. *Tetrahedron* **1995**, *51* (2), 513–526.

(84) Ferrero, S.; Barbero, H.; Miguel, D.; García-Rodríguez, R.; Álvarez, C. M. Dual-Tweezer Behavior of an Octapodal Pyrene Porphyrin-Based System as a Host for Fullerenes. *J. Org. Chem.* **2019**, *84* (10), 6183–6190.

(85) Schmittel, M.; Pramanik, S.; De, S. A Reversible Nanoswitch as an ON–OFF Photocatalyst. *Chem. Commun.* **2012**, *48* (96), 11730–11732.

(86) Li, Y. Across the Board: Yang Li on Visible-Light Photoredox Catalysis. *ChemSusChem* **2020**, *13* (15), 3937–3939.

(87) Joshi-Pangu, A.; Lévesque, F.; Roth, H. G.; Oliver, S. F.; Campeau, L.-C.; Nicewicz, D.; DiRocco, D. A. Acridinium-Based Photocatalysts: A Sustainable Option in Photoredox Catalysis. *J. Org. Chem.* **2016**, *81* (16), 7244–7249.

(88) Arnold, L. J.; Hammond, P. W.; Wiese, W. A.; Nelson, N. C. Assay Formats Involving Acridinium-Ester-Labeled DNA Probes. *Clin. Chem.* **1989**, *35* (8), 1588–1594.

(89) Zhou, D.; Khatmullin, R.; Walpita, J.; Miller, N. A.; Luk, H. L.; Vyas, S.; Hadad, C. M.; Glusac, K. D. Mechanistic Study of the Photochemical Hydroxide Ion Release from 9-Hydroxy-10-Methyl-9-Phenyl-9,10-Dihydroacridine. *J. Am. Chem. Soc.* **2012**, *134* (28), 11301–11303.

(90) Koper, N. W.; Jonker, S. A.; Verhoeven, J. W.; van Dijk, C. Electrochemistry of the 9-Phenyl-10-Methyl-Acridan/Acridinium Redox System; a High-Potential NADH/NAD $^{+}$ Analogue. *Recl. Trav. Chim. Pays-Bas* **1985**, *104* (11), 296–302.

(91) Jacquot de Rouville, H.-P.; Hu, J.; Heitz, V. N-Substituted Acridinium as a Multi-Responsive Recognition Unit in Supramolecular Chemistry. *ChemPlusChem* **2021**, *86* (1), 110–129.

(92) Claude, S.; Lehn, J.-M.; Schmidt, F.; Vigneron, J.-P. Binding of Nucleosides, Nucleotides and Anionic Planar Substrates by Bis-Intercaland Receptor Molecules. *J. Chem. Soc., Chem. Commun.* **1991**, *17*, 1182–1185.

(93) Yazaki, K.; Sei, Y.; Akita, M.; Yoshizawa, M. Polycationic-Shelled Capsular and Tubular Nanostructures and Their Anionic-Guest Binding Properties. *Chem. Eur. J.* **2016**, *22* (49), 17557–17561.

(94) Kurihara, K.; Yazaki, K.; Akita, M.; Yoshizawa, M. A Switchable Open/Closed Polyaromatic Macrocycle That Shows Reversible Binding of Long Hydrophilic Molecules. *Angew. Chem. Int. Ed.* **2017**, *56* (38), 11360–11364.

(95) Gosset, A.; Xu, Z.; Maurel, F.; Chamoreau, L.-M.; Nowak, S.; Vives, G.; Perruchot, C.; Heitz, V.; Jacquot de Rouville, H.-P. A Chemically-Responsive Bis-Acridinium Receptor. *New J. Chem.* **2018**, *42* (6), 4728–4734.

(96) Hu, J.; Ward, J. S.; Chaumont, A.; Rissanen, K.; Vincent, J.; Heitz, V.; Jacquot de Rouville, H.-P. A Bis-Acridinium Macrocycle as Multi-Responsive Receptor and Selective Phase-Transfer Agent of Perylene. *Angew. Chem. Int. Ed.* **2020**, *59* (51), 23206–23212.

(97) Wada, K.; Mizutani, T.; Matsuoka, H.; Kitagawa, S. A New Strategy for the Design of Water-Soluble Synthetic Receptors: Specific Recognition of DNA Intercalators and Diamines. *Chem. Eur. J.* **2003**, *9* (10), 2368–2380.

(98) Mizutani, T.; Wada, K.; Kitagawa, S. Molecular Recognition of DNA Intercalators at Nanomolar Concentration in Water. *J. Am. Chem. Soc.* **2001**, *123* (26), 6459–6460.

(99) Chaudhary, A.; Rath, S. P. Encapsulation of TCNQ and the Acridinium Ion within a Bisporphyrin Cavity: Synthesis, Structure, and Photophysical and HOMO-LUMO-Gap-Mediated Electron-Transfer Properties. *Chem. Eur. J.* **2012**, *18* (24), 7404–7417.

(100) Kotani, H.; Ohkubo, K.; Crossley, M. J.; Fukuzumi, S. An Efficient Fluorescence Sensor for Superoxide with an Acridinium Ion-Linked Porphyrin Triad. *J. Am. Chem. Soc.* **2011**, *133* (29), 11092–11095.

2

SYNTHESIS AND STUDY OF PORPHYRIN-ACRIDINIUM CONJUGATES

1. Introduction

We first examined the synthetic routes to obtain novel conjugates, aiming to probe the synthetic feasibility of covalent attachment of porphyrin and acridinium units, and to further explore the binding properties.

1.1. Design

In order to afford an allosteric system, key factors must be considered, specifically as they pertain to the efficiency of the allosteric effect. Of high importance is the spacer between the allosteric and active site. Typically, efficient translation of the effects of binding the effector to the secondary binding sites requires a rigid spacer, as use of a flexible spacer can lead to poor translation or loss of the pre-organisation. A convenient spacer used in some examples shown in Chapter 1, is that of a phenyl ring (Figure 1). As a rigid aromatic spacer, it allows translation of rigidification/pre-organisation to the secondary site. Additionally, as a small spacer (relative to the active units) encumbering steric interactions are unlikely to be seen upon pre-organisation of the receptor. Finally, due to steric repulsion between the phenyl protons and that of the *beta* pyrrolic protons and the 1/8 acridinium protons, use of the phenyl spacer should allow for the two motifs to be within the same plane, maximising the effect of the binding activated pre-organisation.

Due to the large differences in polarity between the two recognition units, use of solubilising groups must also be considered in the design of the conjugates, to allow solubility in organic media. This can be aided in several ways, such as 1) via use of a non-coordinating counter anion such as PF_6 and/or 2) via use of solubilising alkyl groups at key functionalisation points. In the latter case, use of solubilising R groups in the AB_3 conjugate is possible. Specifically, the group di-*tert*-butyl benzene is known to enhance the solubility of porphyrins, and as such was chosen.

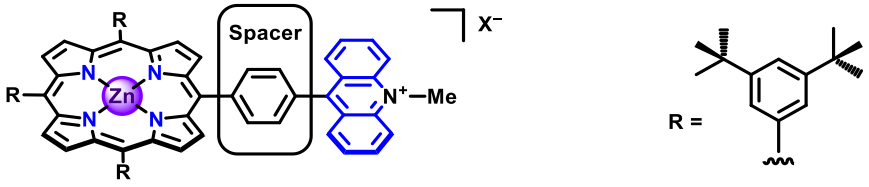

Figure 1. *Illustration of a porphyrin-acridinium conjugate, featuring a phenyl spacer perpendicular to the two active units, and the di-tert-butyl benzyl R group.*

1.2. General routes in porphyrin synthesis and functionalisation

Synthesis of porphyrins has been known since the early 1900s with the first reported syntheses given by Hans Fischer.[1,2] Generally, synthesis is achieved via condensation of pyrroles and aldehydes in the presence of acid and oxidants. Two major methodologies commonly utilised are the Adler-Longo method and the Lindsey method. The Adler-Longo method,[3] building on early work by Rothemund,[4] achieves porphyrin condensation via refluxing of aldehydes and pyrroles in propionic acid, while utilising atmospheric oxygen as the oxidant. The second methodology by Lindsey, *et al.* (Figure 2) consists of a two-step reaction, the 1st step being condensation of aldehydes and pyrroles in the presence of TFA or $BF_3{\cdot}OEt_2$, to reversibly form the porphyrinogen macrocycle at equilibrium, and the following 2nd step, an oxidation using DDQ or chloranil to irreversibly form the porphyrin.[5–8] By carefully monitoring the position of the equilibrium for different aldehydes between the starting materials, side products and the porphyrinogen, Lindsey and co-workers were able to achieve yields as high as 60% in the synthesis of A_4 porphyrins.[8,9] Additionally, although the Adler-Longo method is simpler, the Lindsey method can be advantageous for aldehydes which show poor solubility in propionic acid and/or have acid sensitive substituents.

By using functionalised aldehydes, or β-functionalised pyrroles, *meso* or *beta* substituted porphyrins respectively are readily obtained. Further functionalisation at the peripheries of a porphyrin can also be achieved via different organometallic methodologies.[10] Most commonly, halogenated (or halogenated aryl) porphyrins are used as synthons in metal-halogen exchange reactions or palladium cross coupling reaction, allowing pairing of porphyrins with wide ranging motifs.

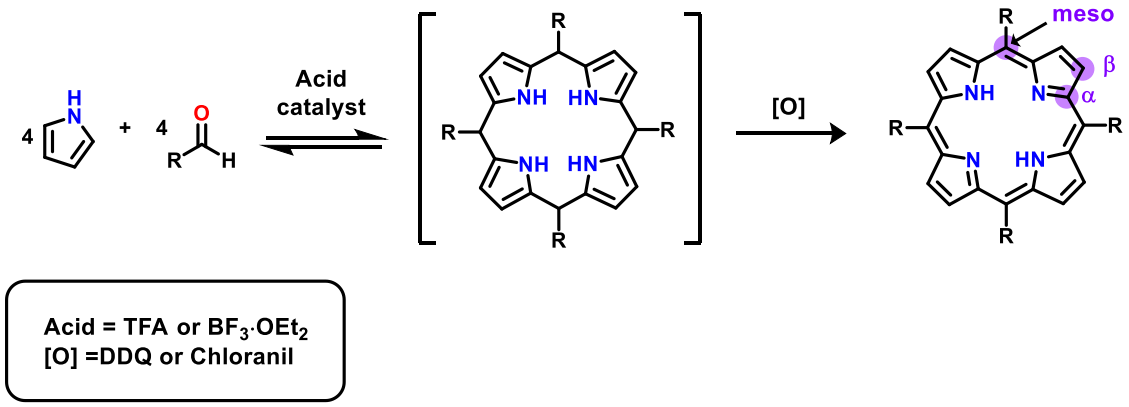

***Figure 2**. General synthesis of a porphyrin via the Lindsey methodology condensation of pyrrole and aldehyde in the presence of acid and oxidant.* [7,8]

1.3. General routes in acridinium synthesis and functionalisation

Acridiniums can be readily accessed using the synthon acridone. The molecule has two key functionalisation points: the carbonyl, and the amine. Stepwise functionalisation at these points allows for the synthesis of acridinium species, with different substituents (Figure 3). In the case of the amine site, alkylation and Ullman amination have been previously reported.[11,12] The substituted acridone can then be reacted at the carbonyl position with organometallic nucleophiles, furnishing an intermediate acridanol species which is readily aromatised to the acridinium upon acid hydrolysis.

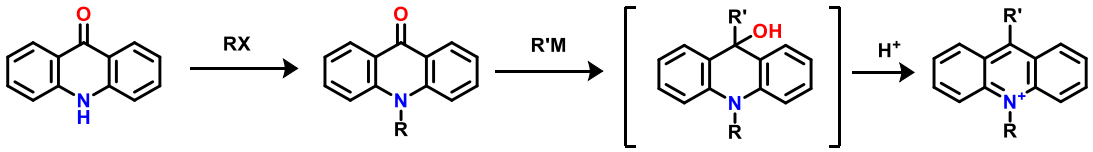

***Figure 3.** General synthesis of an N-substituted acridinium via stepwise functionalisation of 1H-acrid-9-one.*

1.4. Examples of porphyrin-acridinium conjugate syntheses in the literature

As mentioned in Chapter 1 (section 3.3), examples of covalently attached porphyrin-acridinium conjugates are limited to the work of the Fukuzumi group, who reported the porphyrin-acridinium triad **24** (Figure 4).[13] The synthesis of the species was achieved using a

formyl functionalised acridinium (**25**), in turn synthesised via bromination of the photoredox catalyst mesityl methylacridinium followed by a Sommelet reaction to give the cationic aldehyde. Condensation of this species with a 2,2'-dipyrromethane then allowed for the synthesis of the porphyrin-acridinium triad. Although this synthetic route was successful, the yield was very low for the final porphyrin condensation step at 3%.

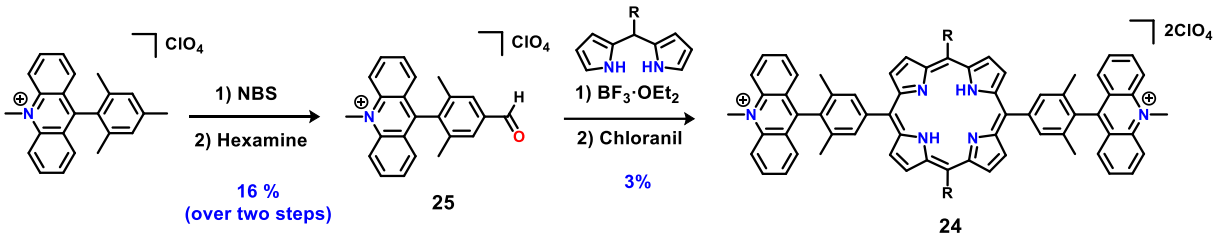

Figure 4. *Synthesis of the Fukuzumi groups' porphyrin-acridinium triad* ***24*** *via porphyrin condensation using a 9-(3,5-dimethylbenzaldehyde-4-yl)-10-methylacridinium* ***25****, (synthesised from the 9-mesityl-10-methylacridnium species).*

2. Attempted synthesis of an AB_3 monoacridinium porphyrin conjugate via Br-Li exchange

Given the typical porphyrin and acridinium synthetic routes and methods of functionalisation, it was proposed that porphyrin-acridinium conjugates may be synthesised via Br-Li exchange of a bromo-aryl functionalised porphyrin. Bromo-aryl porphyrins had been previously shown by the group of Hirel to be useful in the synthesis of carbonyl functionalised porphyrins via such reactions.[14] In the published work specific conditions were used differing from standard procedure for bromo-lithium exchange using n-BuLi; Et_2O at −50 °C was used as the solvent, with THF found to lead to the synthesis of unidentifiable side products and not the desired molecule. In addition, due to the presence of the two internal NH of the porphyrin a two equivalent excess had to be employed, to account for the deprotonation and Li coordination of the internal nitrogen atoms. Taking into account the conditions of the published reaction, a synthetic route was devised to couple a bromo-phenyl functionalised porphyrin and an N-methylated acridone to form a porphyrin-acridinium conjugate (Figure 5).

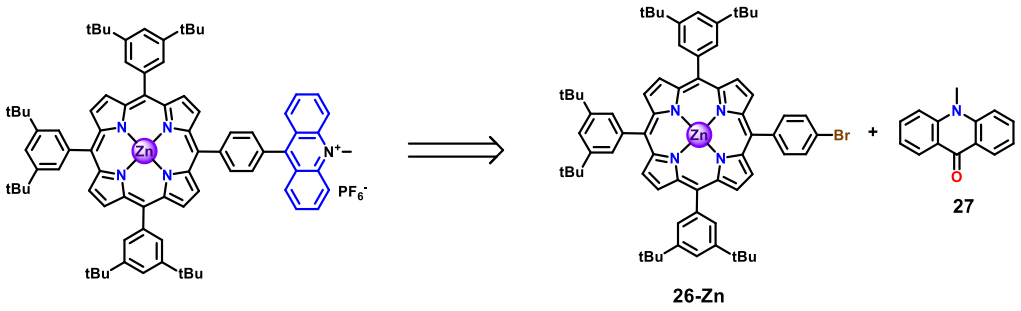

Figure 5. *Retrosynthesis for an AB_3 monoacridinium porphyrin conjugate via metal-halogen exchange.*

Using the Adler and Longo procedure a mono-bromo phenyl "AB_3" porphyrin (**26-2H**) was synthesised at a yield of 7%,[15] utilising di-*tert*-butyl benzyl as the B substituent for its solubilising effects (Figure 6). The obtained porphyrin was then reacted with three equivalents of n-BuLi under dilute conditions in Et_2O at –50°C, to form the lithiated species, before addition of two equivalents of N-methyl acridone. It was believed that in this reaction an intermediate porphyrin-acridanol would be formed (Figure 6), which could then be hydrolysed to the acridinium under acidic conditions similarly to the work of Hirel *et al*. However, it was found that the reaction did not proceed, with return of the starting material: ^{1}H NMR spectroscopy showed no change in the spectrum, suggesting the lithiated species was not formed.

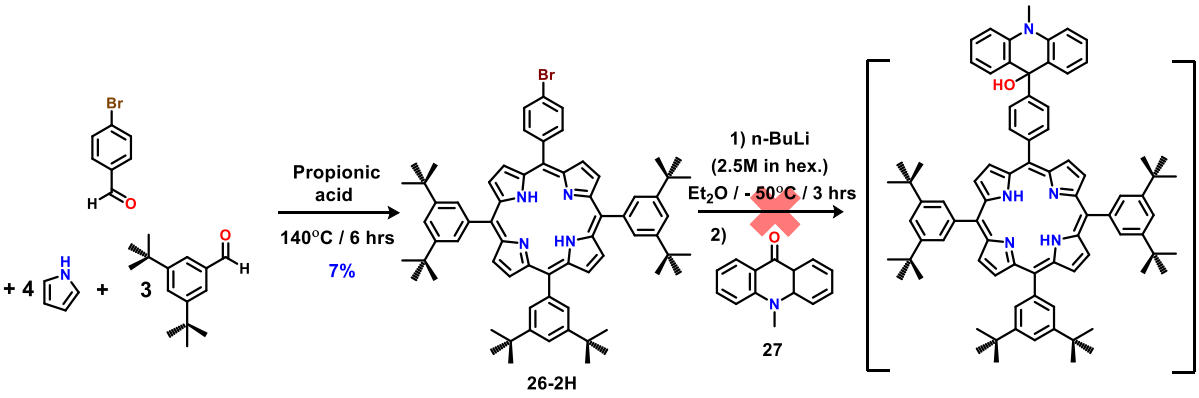

Figure 6. *The proposed reaction scheme for synthesis of an AB_3 mono(N-methyl)acridinium porphyrin conjugate via Br-Li exchange using the bromo-aryl functionalised porphyrin **26-2H** (synthesised according to published work)*[15]***.**

To prevent coordination to the internal nitrogen atoms and outlaw its possible effects, the porphyrin was metalated using $Zn(OAc)_2$, forming the Zn(II)-porphyrin (**26-Zn**), and the

reaction was repeated using the same conditions as stated above. However, similarly to **26-2H**, the reaction was not observed to proceed, with the ^{1}H NMR spectrum of the obtained product appearing similar to the starting material. Therefore, it was concluded that the porphyrin could not be coupled to the acridinium via this method using the published conditions. Later literature analysis revealed that previous works had used higher temperatures of −10 - 0 °C and a larger excess of n-BuLi (6.7 equivalents of n-BuLi) to achieve functionalisation of AB_3 bromo aryl porphyrins,[16,17] suggesting that more forcing conditions may have been necessary to achieve synthesis of the conjugate. However, these works were found after development of other synthetic routes; thus, the alternative conditions were not explored.

3. Synthesis of an AB_3 monoacridinium Zn(II)-porphyrin conjugate via palladium cross coupling

Having been unsuccessful in synthesis of conjugates via Br-Li exchange, we next turned to another common synthetic route: palladium catalysed cross coupling, probing its efficacy using **26-Zn**. It was proposed that via reaction of **26-Zn** with an acridane boronic ester followed by a subsequent oxidation, a diphenyl-spaced porphyrin acridinium conjugate could be afforded (Figure 7). In turn, the acridane boronic ester could be synthesised via palladium cross coupling of a bromo-aryl acridane species.

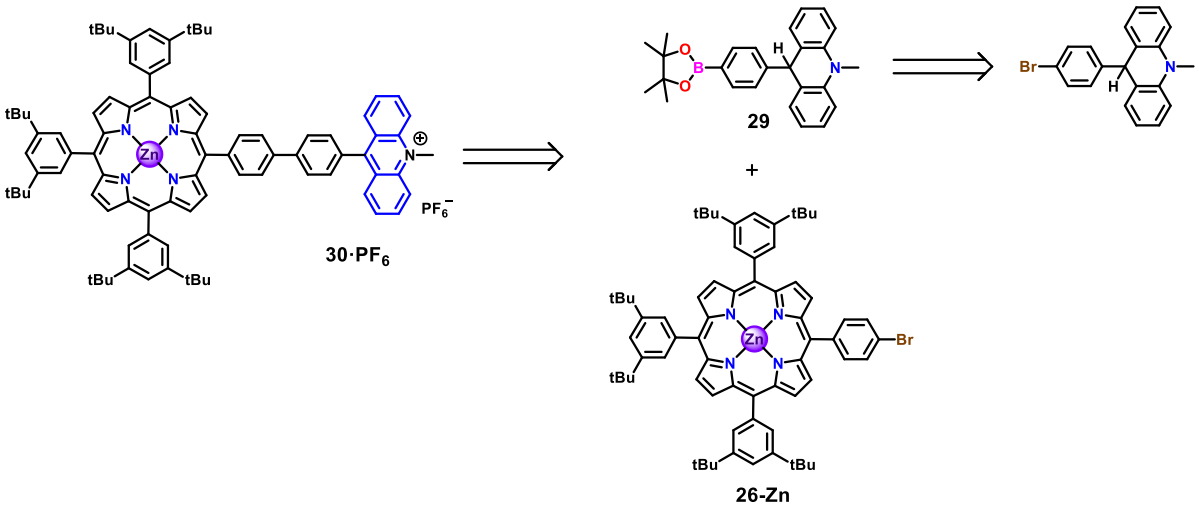

Figure 7. *Retrosynthesis for the synthesis of a monoacridinium porphyrin conjugate (**30·PF$_6$**) via palladium catalysed cross coupling.*

Although functionalisation of acridiniums with boronic esters is theoretically feasible the charged nature of an acridinium boronic ester would make its isolation from the bromophenyl acridinium difficult. As such the acridane form was preferred, with a similar species synthesised and successfully isolated by our research group in previous work.[18]

A bromo phenyl acridinium (**28·PF$_6$**) was first synthesised from 1,4-dibromo benzene, and methyl acridone (**27**) via bromo-lithium exchange (Figure 8). Once in hand, **28·PF$_6$** was then reacted with five equivalents of $LiAlH_4$ (reducing the species to the air-sensitive acridane) and a palladium catalysed cross coupling reaction performed to obtain the boronic ester **29**. This was then reacted in a second Pd-catalysed cross coupling with **26-Zn** to form an acridane-porphyrin. Due to the sensitivity of the acridane, oxidation was immediately carried out using 1.5 equivalents of DDQ to successfully synthesise the biphenyl model **30·PF$_6$** at a yield of 67% for the final two steps. To confirm the coupling of the porphyrin and phenyl acridinium units, the compound was characterised via NMR (^{1}H and ^{13}C), UV-Vis spectroscopy and mass spectrometry.

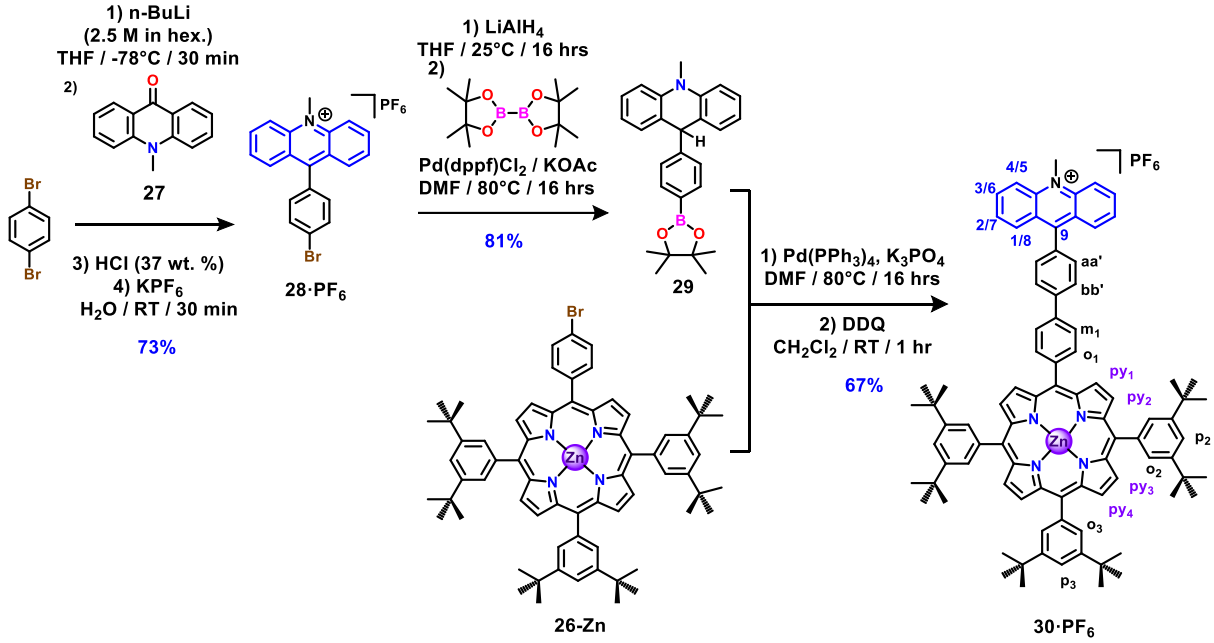

Figure 8. *Synthesis of* ***30·PF$_6$*** *via* palladium cross coupling of an acridane boronic ester (**29**) and a bromo aryl porphyrin (**26-Zn**).

In the ^{1}H NMR characteristic peaks were seen alluding to the presence of an acridinium and a porphyrin. Two doublets at 9.08 and 9.06 ppm (with ^3J = 4.6 Hz) were observed as well as a singlet at 9.02 ppm, consistent with the pyrrolic protons for an AB_3 porphyrin (Figure 9a).

Additionally, in the aromatic region two doublet of doublet of doublets and two doublet of doublets are seen, consistent with the splitting pattern of the acridinium. The absence of a peak between –2 - –3 ppm also confirmed that the porphyrin remained metalated. In the ^{13}C NMR spectrum (Figure 9b), a tell-tale peak was observed at 163 ppm, assigned to the C_9 carbon of the acridinium, with resonance of the positive charge to this position causing the highly deshielded peak.

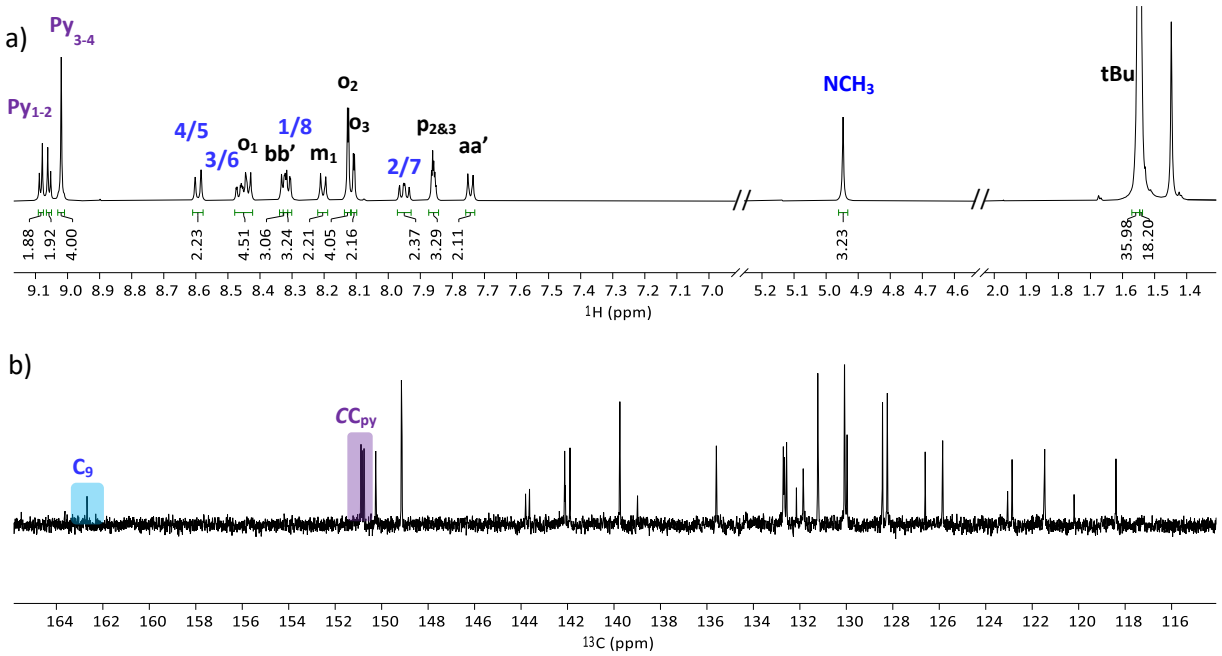

Figure 9. *a) ^{1}H NMR (500 MHz, CD_2Cl_2, 298 K) spectrum and b) ^{13}C NMR (125 MHz, CD_2Cl_2, 298 K) spectrum of* ***30·PF$_6$****. Acridinium chemical shifts are given in blue and the porphyrin chemical shifts in purple.*

In the UV-Vis spectrum of the conjugate (Figure 10) a clear and distinct Soret band at 426 nm (ε = 541 000 L mol^{-1}cm^{-1}) was seen, with the Q-band appearing at 554 (21 600) and 596 nm (8 260). A right-hand shoulder was also observed at the Soret band (450-500 nm), likely due to overlap of an acridinium-centred (π–π* transition) absorbance band. Furthermore, absorption bands observed at 348 (20 900) and 362 nm (30 200) were in-line with an acridinium-centred π-π* transition band.

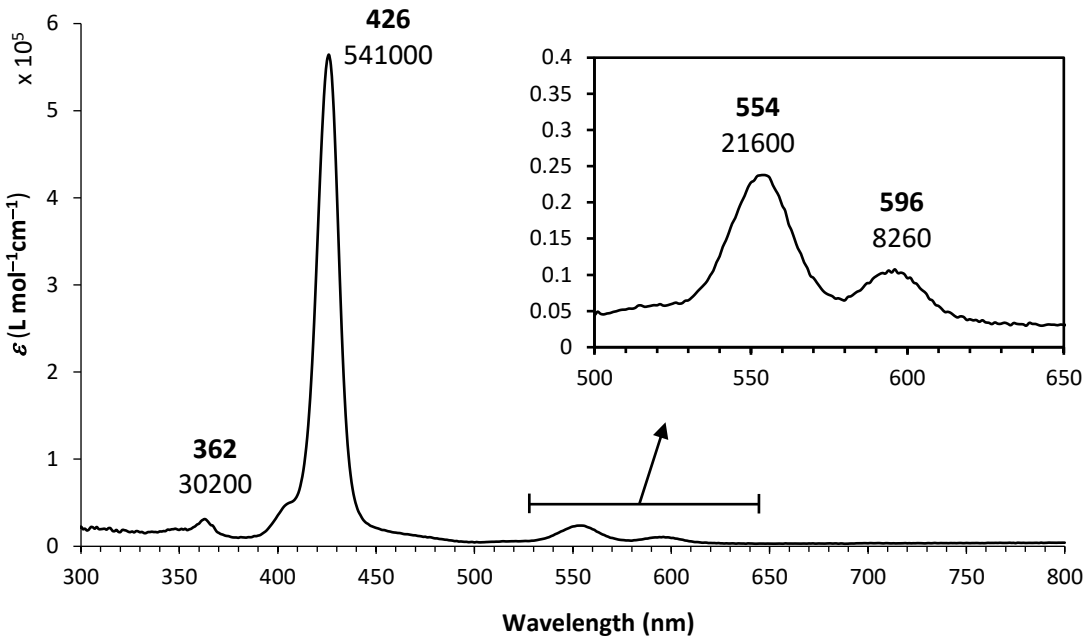

Figure 10. *UV-Vis (CH_2Cl_2, l = 0.5 cm, 298 K,) spectrum of* ***30·PF$_6$*** *(c = 4.75 μM). The values for the peak wavelengths (in bold) and the corresponding extinction coefficients are given.*

Finally, ESI-TOF mass spectrometry gave a mass spectrum with a major mass ion peak equivalent to the calculated monoisotopic mass for the conjugate minus the counterion ($[M]^+$ at m/z = 1280.6458 corresponding to a chemical formula of $C_{88}H_{90}N_5Zn$). The simulated isotopic pattern for the chemical formula was also seen to be in good agreement with that obtained experimentally.

Thus, porphyrin and acridinium units could be coupled via palladium cross coupling, with moderate to high yields for each of the 6 steps. However, this route presented some drawbacks. **30·PF$_6$** featured a diphenyl spacer, in contrast to the initial design. Such a spacer was not ideal due to the potential impact and limit in the efficacy of translation of binding events across the conjugate. Additionally, although the use of the acridane **29** is advantageous for purification, it has a low stability compared to the acridinium, being highly prone to oxidation and therefore sensitive to oxygen. This is due to the gain in aromaticity upon formation of the acridinium. Thus, synthesis of **29** at large scales (and consequently synthesis of the conjugates) might be hindered.

As such, in order to afford the single phenyl spaced conjugate in an efficient manner, attention was turned to a third synthetic pathway taking inspiration from the previous work of the Fukuzumi group: porphyrin condensation using a formyl phenyl acridinium.

4. Synthesis of acridinium porphyrin conjugates via porphyrin condensation

Although the yield achieved by the Fukuzumi group had been low (Figure 4), the route presented some key advantages over palladium catalysed cross coupling which encouraged its pursuit: 1) as the key reactant would be a formyl functionalised acridinium, it would likely be stable in air compared to **29**, in turn allowing the ability to synthesise the reactant in large-scale without fear of degradation. 2) As porphyrin condensation served as the last step, the intermediate could be used to synthesise an entire family of conjugates using one key building block, in contrast to the two previous routes which would require differing porphyrin precursors for each conjugate.

As such, keeping within our design for the conjugates, a synthetic scheme was devised aiming to synthesise conjugates **33·PF$_6$** and **35·2PF$_6$** from a common novel formyl phenyl acridinium building block, which could in turn be synthesised using cheap and commercially available synthons (Figure 11).

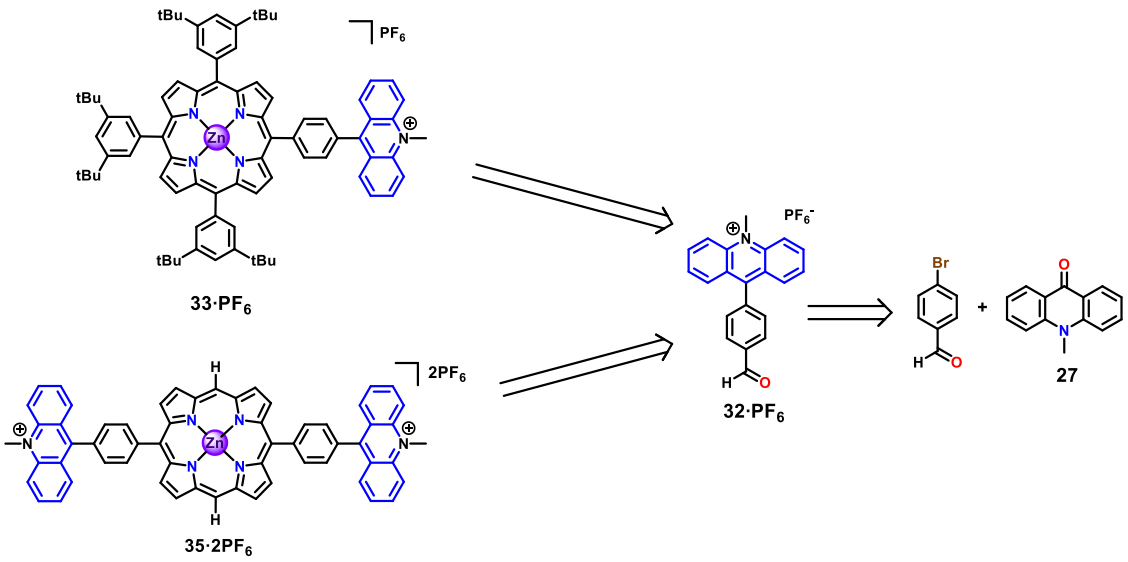

Figure 11. *Retrosynthesis of compounds **33·PF$_6$** and **35·2PF$_6$** via porphyrin condensation using a common formyl phenyl acridinium reactant **32·PF$_6$**.*

4.1. Synthesis of the formyl phenyl acridinium **32·PF$_6$**

Starting from 4-bromo-benzaldehyde dissolved in toluene, a protection step was carried out, reacting the aldehyde with pinacol in the presence of a catalytic amount of *para*-tosylic acid (pTsOH) under refluxing conditions to form the dioxolane analogue (**31**).[19] This protection served to prevent reaction of the aldehyde during the lithiation reaction. With the protected species in hand, the metal halogen exchange was then performed by reacting with n-BuLi, at −78 °C. The lithitated intermediate was then reacted with one equivalent of N-methyl acridone, forming a phenyl-acridanol intermediary species, followed by an acid workup to dehydrate (and thus aromatise) the heterocycle as well as deprotecting the aldehyde in one step. The formed N-methyl formyl-phenyl acridinium chloride salt (**32·Cl**) was then exchanged to the PF_6 salt in an anion metathesis, giving **32·PF$_6$** at a yield of 78% after purification via precipitation from Et_2O (Figure 12). The formation of the aldehyde was confirmed via characteristic peaks for the formyl group in the ^{1}H (10.25 ppm) and ^{13}C (193.3 ppm) NMR spectra, with further structural confirmation given by ESI-TOF mass spectrometry.

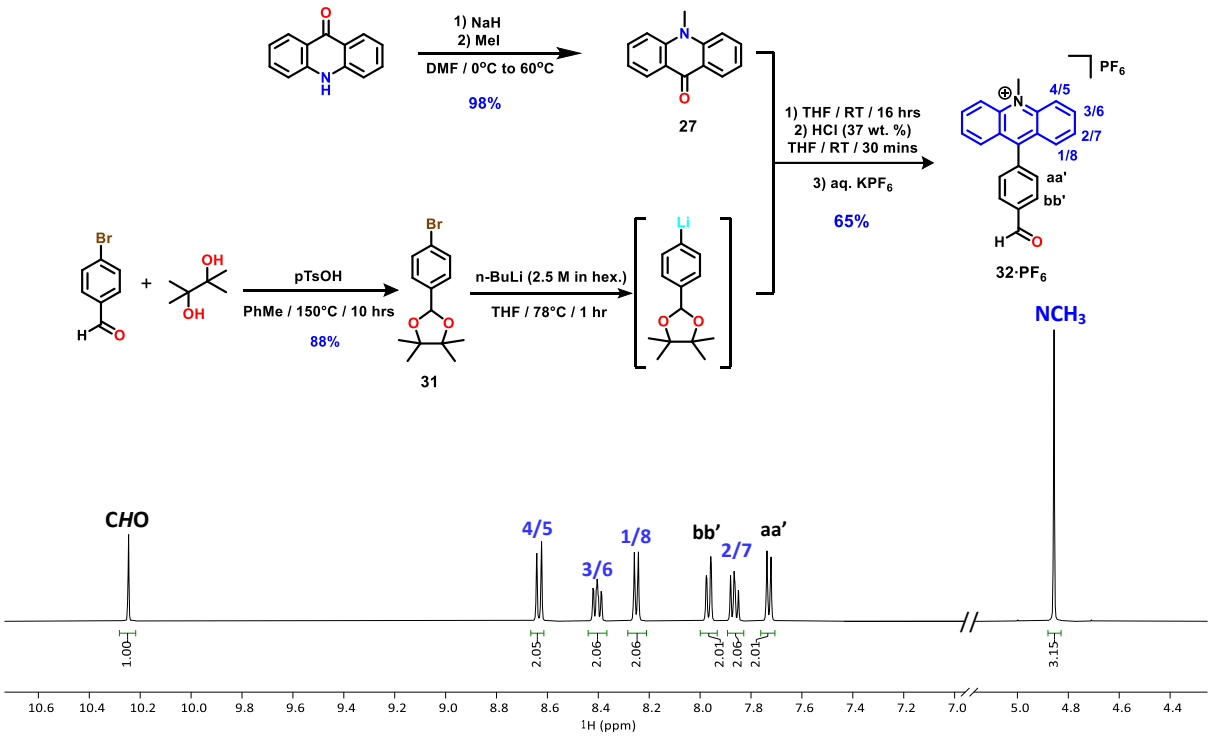

Figure 12. *Synthesis of **32·PF$_6$** from the synthon 4-bromo benzaldehyde and the corresponding ^{1}H NMR (500 MHz, CD_3CN, 298 K) spectrum.*

4.2. Synthesis of the AB_3 monoacridinium Zn(II)-porphyrin conjugate **33·PF$_6$**

Having successfully synthesised the novel reactant, the synthesis of a monoacridinium porphyrin was attempted via porphyrin condensation (Figure 13). Following the Lindsey procedure, **32·PF$_6$** was reacted with 3,5-di-*tert*-butyl benzaldehyde and pyrrole in the presence of TFA, to statistically form the monoacridinium porphyrinogen. This was then oxidised via DDQ, and metalated with Zn(II) to obtain the monoacridinium porphyrin **33·PF$_6$** after purification via column chromatography, at a yield of 12%.

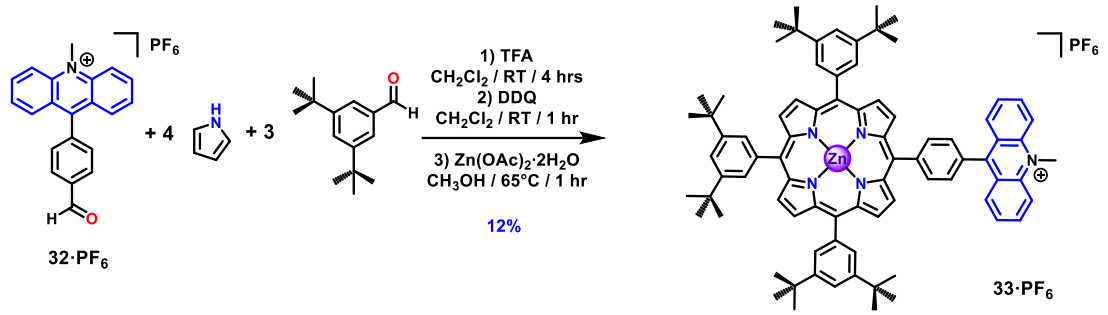

Figure 13. *Synthesis of the conjugate* ***33·PF$_6$*** *from* ***32·PF$_6$*** *via Lindsey-type porphyrin condensation.*

Similarly to **30·PF$_6$**, peaks associated to the porphyrin and acridinium could be observed in the ^{1}H NMR spectrum of **33·PF$_6$** (Figure 14a-ii). However, when comparing the spectra of the two conjugates, differences could be seen, namely a more pronounced distinction between the pyrrolic protons, and downfield shifts of all the peaks for **33·PF$_6$** relative to **30·PF$_6$**. The most significant downfield shifts were seen for the protons of the acridinium, with the size of the shift decreasing with increasing distance from the anisotropic magnetic field induced by the porphyrin ($\Delta\delta H_{1/8}$ = 0.3 ppm, $\Delta\delta H_{2/7}$ = 0.15 ppm, $\Delta\delta H_{4/5\ \&\ 3/6}$ = 0.08 ppm, $\Delta\delta H_{NCH3}$ = 0.07 ppm). The monophenyl spacer of **33·PF$_6$** shortens the distance between the acridinium, and porphyrin compared to the diphenyl-spaced **30·PF$_6$**. As such, the acridinium of **33·PF$_6$** is closer to the deshielded region at the periphery of the porphyrin, giving rise to downfield shifting of the peaks. A similar effect can also be assigned to the downfield shifts of the pyrrolic protons, coupled with increased proximity to the electron-withdrawing acridinium increasing the deshielding effects on the porphyrin. Additionally, the ^{13}C NMR spectrum showed the retained carbon 9 peak of the acridinium (162.78 ppm) and characteristic peaks at approximately 150 ppm for the α-carbons of a porphyrin ring (Figure 14b-ii).

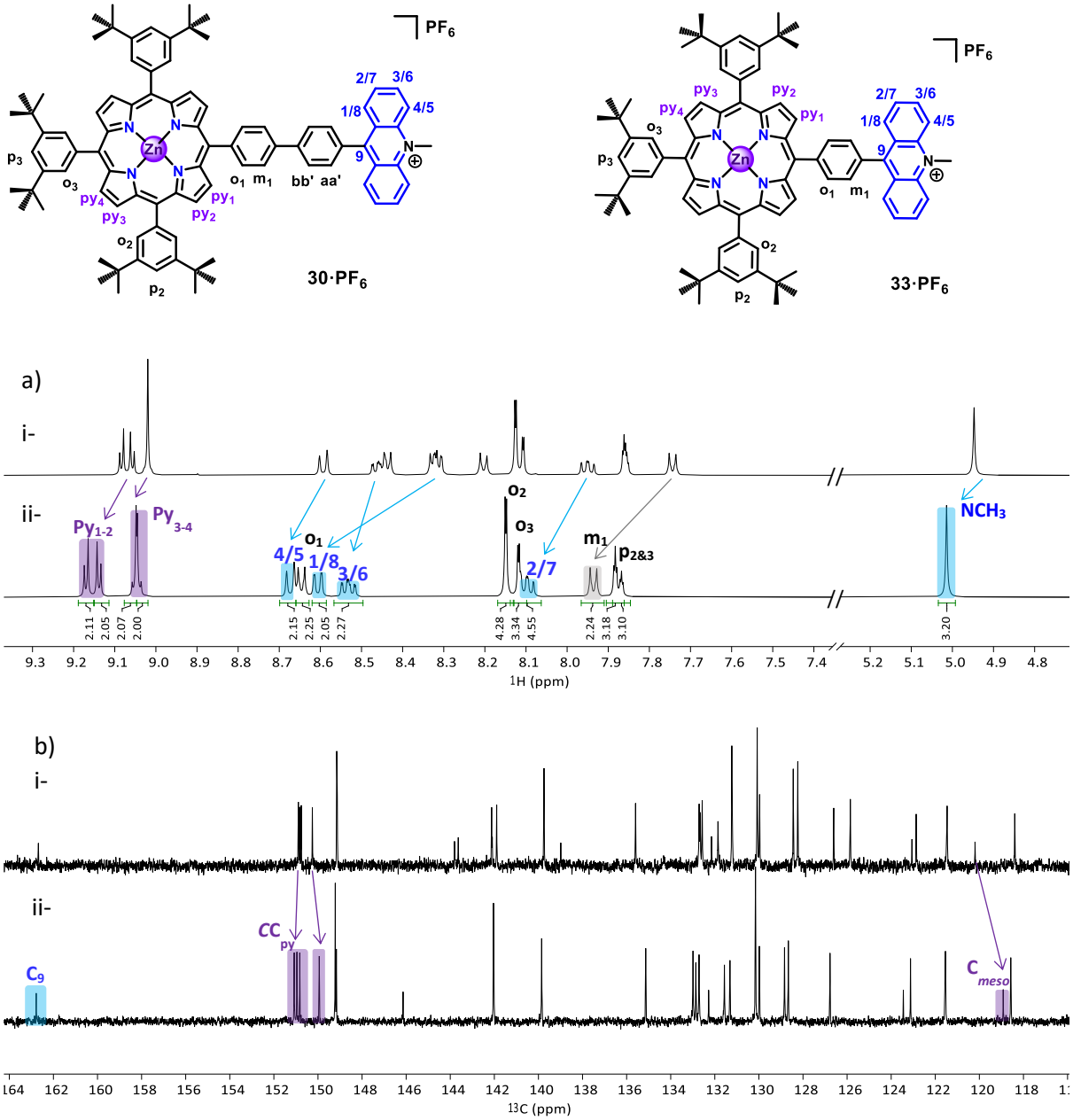

Figure 14. *a) Stacked ^{1}H NMR (500 MHz, CD_2Cl_2, 298 K) spectra of a) i-* ***30·PF₆*** *and b) ii-* ***33·PF₆****. b) Stacked ^{13}C NMR (125 MHz, CD_2Cl_2, 298 K) spectra of i-****30·PF₆*** *and ii-****33·PF₆****. The downfield and upfield shifts are highlighted in blue for the acridinium, in purple for the pyrrolic peaks and in grey for the phenyl protons.*

Additionally, the UV-Vis spectrum for **33·PF₆** (Figure 15) was shown to be similar to that of **33·PF₆** (Figure 8), with features corresponding to the Zn(II)-porphyrin and to the acridinium at similar absorbance maxima and extinction coefficients. Additionally, the mass spectrum showed a major mass ion peak in agreement with that calculated for the conjugate minus the

counterion ([M]$^+$ at m/z = 1204.1680 corresponding to a molecular formula of $C_{82}H_{86}N_5Zn^+$) with a similar isotopic pattern to that simulated.

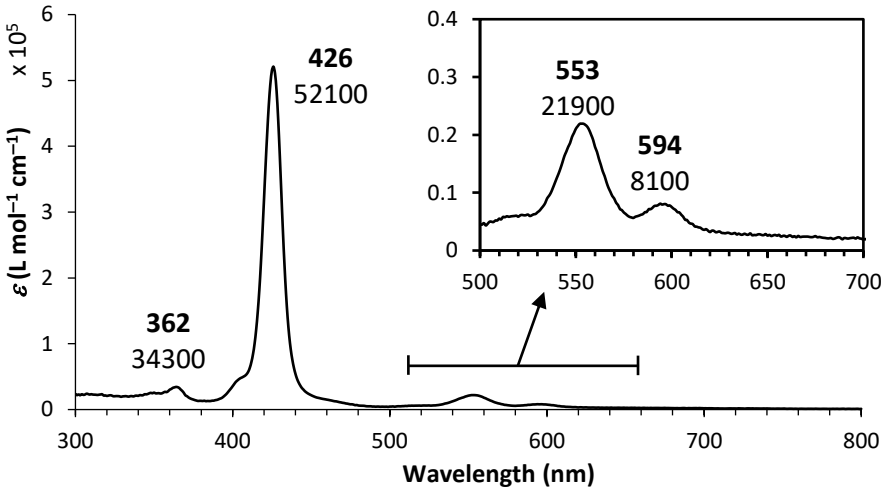

Figure 15. *UV-Visible (CH_2Cl_2, l = 0.5 cm, 298 K) spectrum of* ***33·PF$_6$*** *(c = 4.95 μM).*

4.3. Synthesis of the A_2B_2 bisacridinium Zn(II)-porphyrin conjugate 35·2PF$_6$

As the use of **32·PF$_6$** allowed for direct synthesis of different conjugates, the ability to synthesise an A_2B_2 acridinium porphyrin conjugate via porphyrin condensation was next attempted. Using the same general procedure as **33·PF$_6$**, a synthesised 2,2'-dipyrromethane (**34**) was reacted with **32·PF$_6$** in the presence of TFA, and the formed porphyrinogen subsequently oxidised by DDQ, and metalated with Zn(II) to give **35·2PF$_6$**, with a yield of 29% achieved after purification via column chromatography (Figure 16).

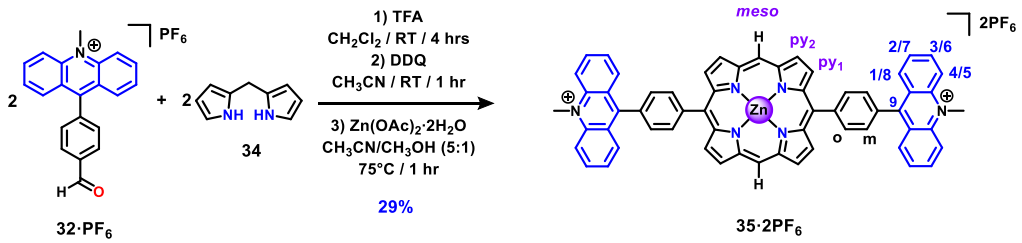

Figure 16. *Synthesis of the A_2B_2 bisacridinium-porphyrin conjugate* ***35·2PF$_6$*** *via porphyrin condensation from the formyl phenyl acridinium* ***32·PF$_6$*** *and 2,2'-dipyrromethane* ***34****.*

In the absence of the solubilising tBu groups, and due to increased π–π stacking interaction, **35·2PF$_6$** was observed to have much reduced solubility in non-polar solvents compared to

30·PF$_6$ and **33·PF$_6$**. However, good solubility was seen for more polar solvents, leading to characterisation via NMR and UV-Vis spectroscopy in acetonitrile. In line with the increased symmetry of the molecule (D_{2h}, compared to C_{2v} for **30·PF$_6$** & **33·PF$_6$**), only two pyrrolic peaks could be seen in the ^{1}H NMR spectrum (doublets at 9.65 and 9.4 ppm, ^3J = 4.4 Hz), with a peak at 10.49 ppm characteristic of the porphyrin *meso*-protons (Figure 17a). The acridinium peaks in contrast remained unchanged and preserved. The ^{13}C NMR spectrum also supported formation of the bisacridinium conjugate (Figure 17b), with a peak at 107.2 ppm, consistent with the unsubstituted *meso*-carbons.

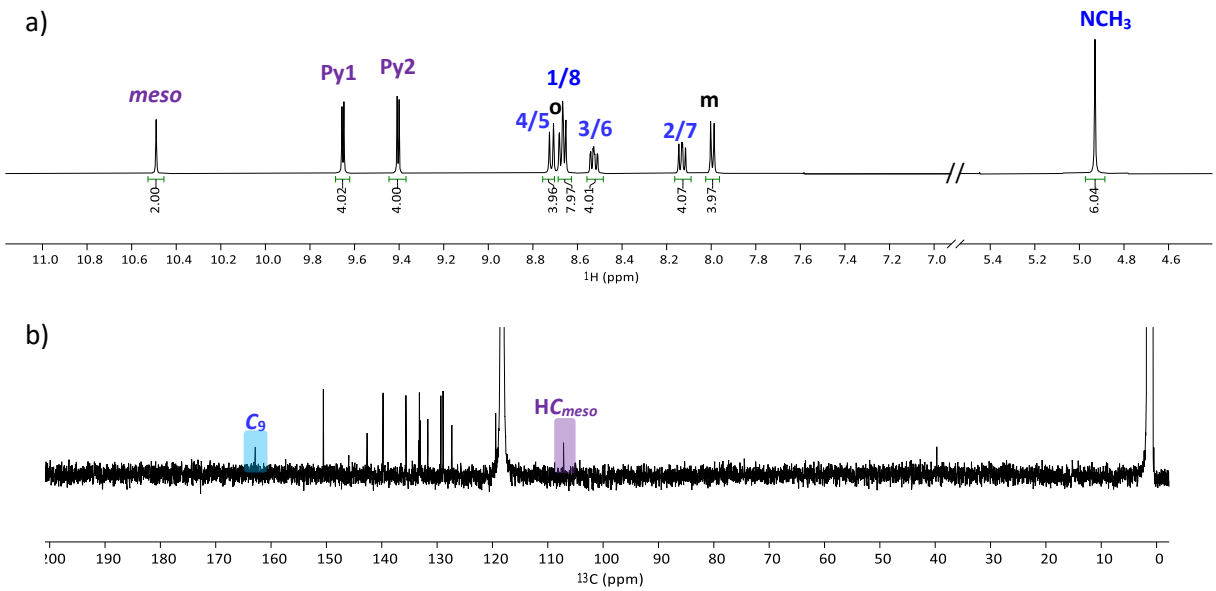

Figure 17. *a) ^{1}H NMR (500 MHz, CD_3CN, 298 K) and b) ^{13}C NMR (125 MHz, CD_3CN, 298 K) spectra of* ***35·2PF$_6$****.*

Furthermore, the mass spectrum obtained showed a major mass ion peak equal to that calculated for **35^{2+}** with an isotopic pattern complementary to the simulated spectrum ($[M]^{2+}$ at m/z = 454.1268 corresponding to a molecular formula of $C_{60}H_{40}N_6Zn^{2+}$). Similarly, the UV-Vis spectrum of the conjugate contained transition bands consistent with the acridinium (at 348 and 362 nm) and Zn(II)-metalated porphyrin (Soret band at 411 nm and Q-bands at 545 & 586 nm) units (Figure 18).

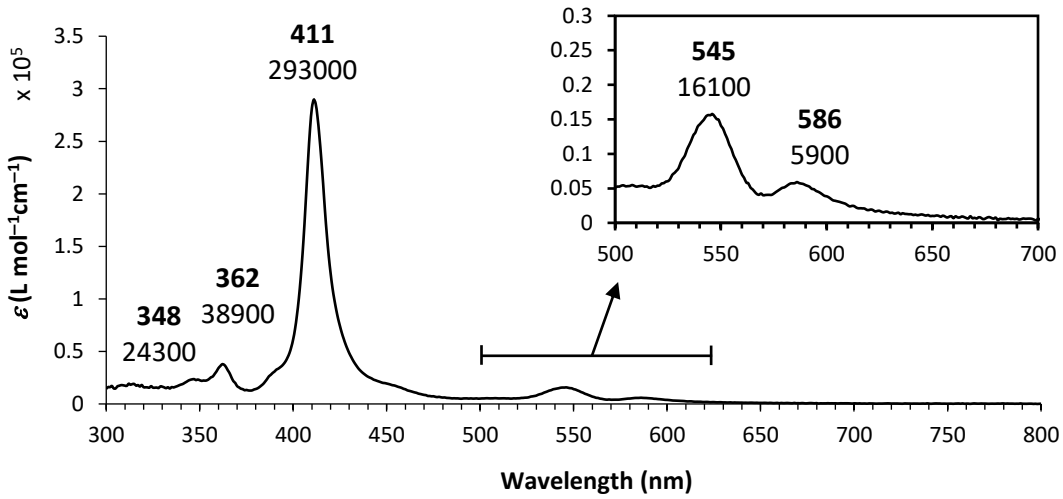

Figure 18. *UV-Vis (CH_3CN, l = 0.1 cm, 298 K) spectrum of* ***35·2PF$_6$*** *(c = 34.0 μM).*

Thus, it was concluded that porphyrin acridinium conjugates were most easily afforded via porphyrin condensation, with the ability to access a family of conjugates directly from the powerful building block **32·PF$_6$**.

5. Study of the A_2B_2 bisacridinium Zn(II)-porphyrin conjugate 35·2PF$_6$

To further investigate the properties of the conjugates, more specifically **35·2PF$_6$**, computational (caried out by Dr. Christophe Gourlaouen at the Institut de Chimie de Strasbourg, Université de Strasbourg), photophysical (carried out by Dr. Barbara Ventura and Daniel Sanchez-Resa at ISOF-Bologna) and electrochemical studies were conducted. The synthesis and results of the studies have recently been published.[20]

5.1. Computational studies

In order to probe the nature and localization of the frontier orbitals of **35·2PF$_6$**, DFT calculations were performed. Via symmetry-less optimization of **35·2PF$_6$**, a structure was obtained featuring the porphyrin and acridinium units lying within the same horizontal plane, and the phenyl rings orthogonal to the motifs at a dihedral angle of 88°. Analysis of the structure revealed degeneracy in both the HOMOs and LUMOs (Figure 19). The HOMOs were

found to be localised on the porphyrin as a near degenerate set of orbitals at energy levels of –5.74 and –5.65 eV.

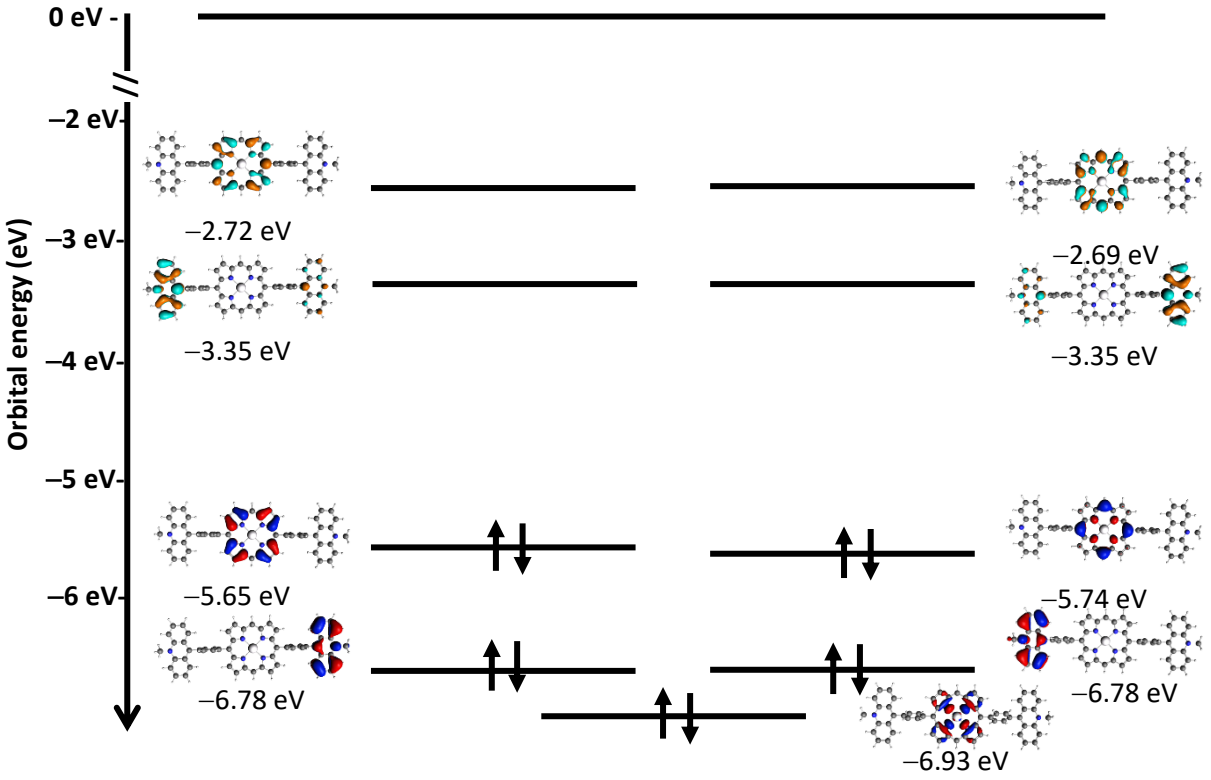

Figure 19. *Calculated molecular orbitals diagram for the conjugate* ***35·2PF$_6$****.*

Further calculations allowed the simulation of a theoretical absorption spectrum (Figure 20), which showed similar spectral features to that obtained experimentally. Namely, an intense band at 406 nm (similar to the experimental value of 411 nm), and three smaller bands at 332, 512 and 610 nm respectively (consistent with the experimental values of 362, 545 and 586 nm). The band at 406 nm was found to be composed of overlapping transition bands, with absorbance maxima at 397 and 406 nm for the two porphyrin-centred π–π* transitions, and at 408 nm for the comparatively lower intensity acridinium-centred π–π* transitions. The band at 332 nm, was composed of two acridinium π–π* transitions, and the band at 512 nm, composed of two porphyrin-based π–π* transitions. Interestingly, the lowest energy transition at 610 nm was shown to be due to a charge transfer from the porphyrin to one of the acridinium units.

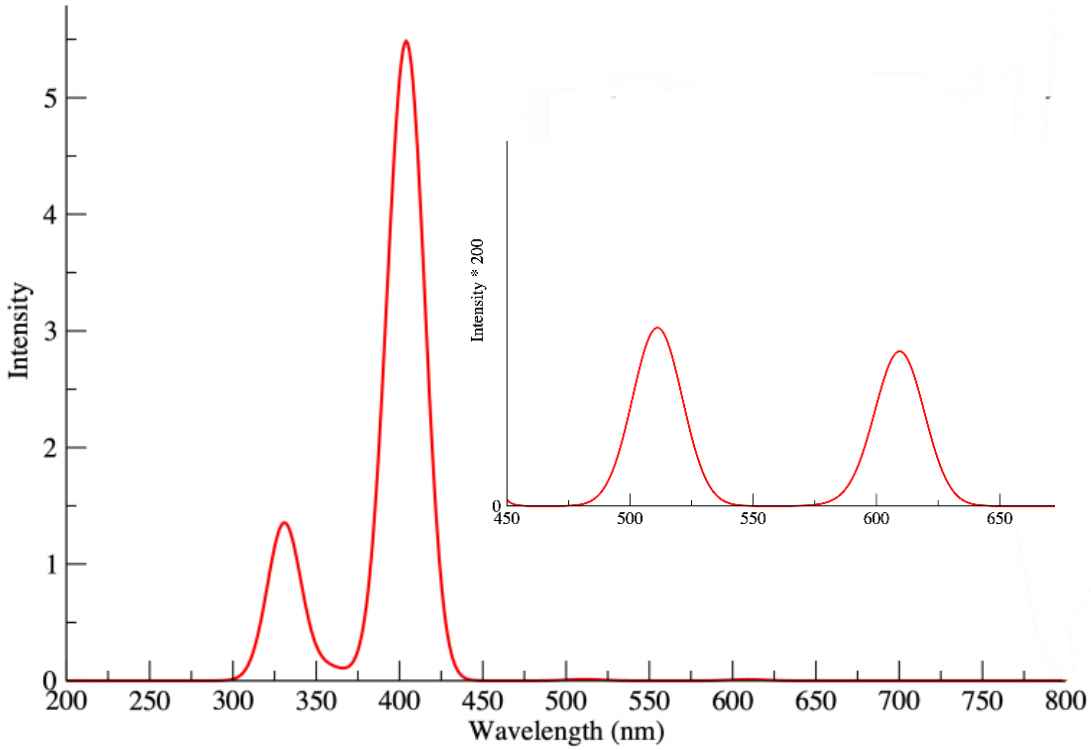

λ_{abs}	f_{osc}	%	Depleted orbital	Populated Orbital
610	$1.01\ 10^{-2}$	100%	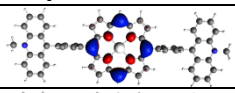	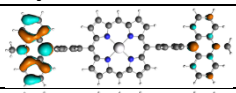
512	$6.87\ 10^{-3}$	51%	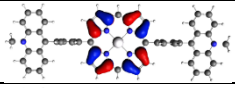	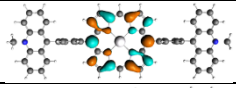
		48%	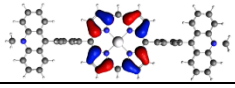	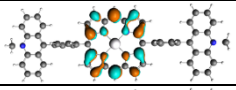
510	$5.65\ 10^{-3}$	52%	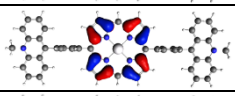	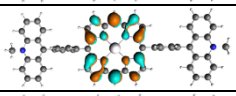
		46%	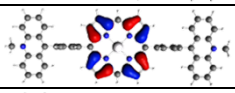	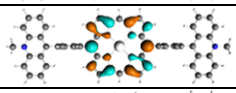
408	2.44	49%	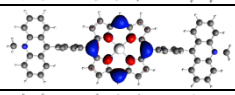	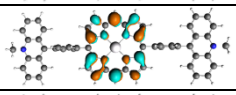
		47%	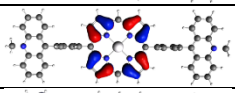	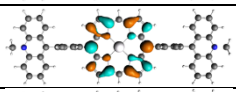
406	1.61	36%	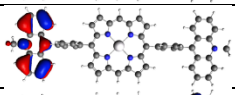	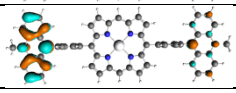
		20%	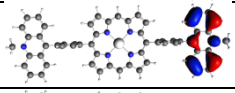	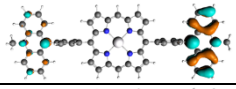
		15%	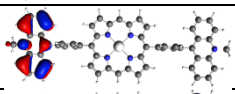	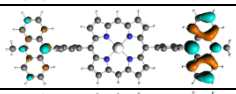
		10%	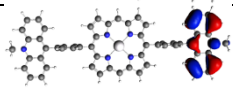	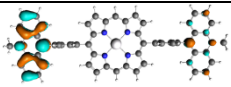

397	2.07	42%	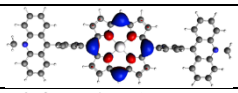	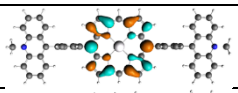
		38%	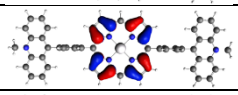	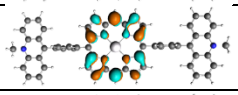
331	0.84	48%	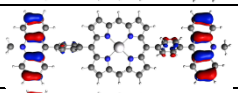	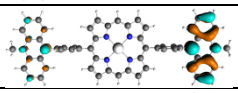
		23%	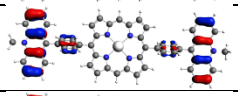	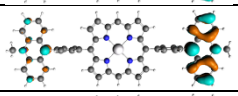
		13%	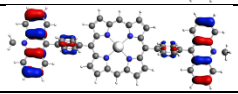	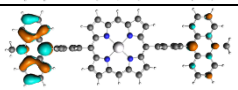

Figure 20. *Theoretical absorption spectrum of* ***35·2PF$_6$*** *in CH_3CN and the character of the singlet states generating the absorption bands in the absorption spectra of* ***35·2PF$_6$.***

The charge transfer transition was further probed, investigating the properties of the charge-separated state via calculations in the presence and absence of an imposed C_2 symmetry. In the symmetry optimised structure, it was found that the structure became significantly distorted upon relaxation of the excited state, with decrease in the dihedral Phenyl-Acridinium angle to 77.2°, and an even larger decrease for the Phenyl-Porphyrin dihedral angle to 59.9°. The optimised structure was calculated to emit at 693 nm. When C_2 symmetry was not imposed, the structure was observed to undergo more significant distortion, with curving of the structure (Figure 21). Due to the lack of symmetry, delocalisation was not preserved, leading to localisation of the electron on one of the two acridinium units, thus generating two minima. The barrier between the two minima was calculated to be very low, at 302 cm^{-1}, allowing free oscillation of the exciton, and giving rise to an averaged symmetrical conformer.

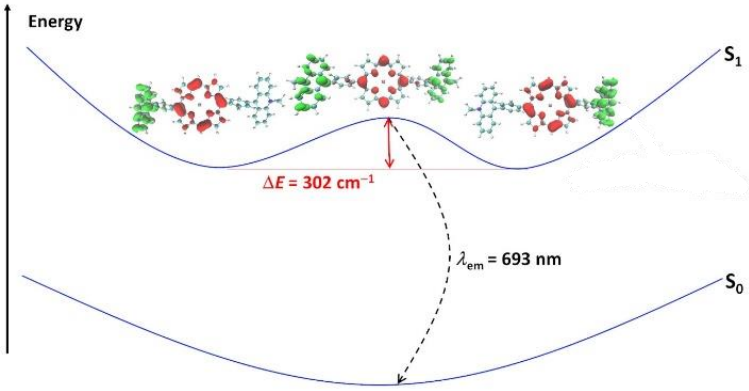

Figure 21. *Schematic representation of the energy diagram for the relaxation of* ***35·2PF$_6$*** *from the charge separated state to the ground state.*

5.2. Electrochemical Study

The electrochemical properties of the molecule were next investigated via cyclic voltammetry (Figure 22). Although the compound showed good solubility in acetonitrile, it was found that in the presence of $TBAPF_6$, the solubility was drastically reduced. As such, cyclic voltammograms were recorded in another polar solvent with a similar dielectric constant: DMF (ε_r = 35.94 vs. 36.71 for CH_3CN).

Typically, within a 1.5 to −1.6 voltage window a Zn(II)-porphyrin exhibits two reversible ring-centred single electron oxidations and a reversible ring-centred reduction. [21,22] In contrast, the phenyl acridinium typically exhibits two reductions, one reversible wave and an irreversible wave at a more negative potential.[23] However, deviations from typical behaviour could be seen for **35·2PF$_6$**. Scanning within the 1 to −1 voltage window (Figure 22) revealed a reversible wave in the cathodic regime (E_{red} = −0.475 V vs SCE and $E_{1/2}$ = −0.442 V vs SCE) and an irreversible wave in the anodic regime (E_{ox} = +0.949 V vs SCE), with similar peak current (I = 7.3 μA), suggesting an equal number of electrons in the two processes. The equal peak heights of the two peaks was further confirmed via rotating disk electrode (RDE) measurements in benzonitrile. The reversible wave was assigned to the one electron reductions of the two acridinium fragments ($2Acr^+ + 2e^- \rightleftarrows 2Acr^{\cdot}$), with the two acridinium units not expected to be in electronic communication with one another, and hence to be reduced at the same potential. This was further supported by the degeneracy of the LUMOs calculated computationally. Given the peak height, the irreversible wave could then be assigned to a bi-electronic oxidation of the porphyrin to give a dicationic porphyrin ($Por \rightarrow Por^{2+} + 2e^-$), with irreversibility likely due to chemical reaction of the formed dication porphyrin unit with either solvent molecules or with the non-oxidised porphyrin to form oligomers.[24–27] Based on these values, an estimate for the HOMO-LUMO gap was obtained equalling 1.39 eV, smaller than that calculated computationally (2.3 eV, Figure 19).

When expanding the voltage window to 1.5 to −1.6, two additional peaks were observed in the cathodic regime (E_{red} = −1.34 V vs SCE and E_{red} = −1.43 V vs SCE), at smaller current heights than see for the two premier waves. Based on the electrochemistry of porphyrins and acridiniums, [22,23] it was determined that the two peaks belonged to reduction of the "acridinium" radical to form a carbanion ($Acr^{\cdot} + e^- \rightarrow Acr^-$) and a reduction of the porphyrin to

form a radical anion (Por + $e^- \rightarrow Por^{\cdot -}$). Formation of the carbanion was further supported by the reduced intensity of the acridinium re-oxidation peak (E_{ox} = –0.409 V vs SCE). The carbanion is known to be highly reactive, reacting with solvent molecules, leading to a reduced amount of the species in the solution.[23] However, due to the close E_{red} values it could not be said with certainty which peak belonged to which of the two processes (i.e., whether E_{red} = –1.34 V belonged to the porphyrin reduction and E_{red} = –1.43 V to the acridinium radical reduction, or vice versa).

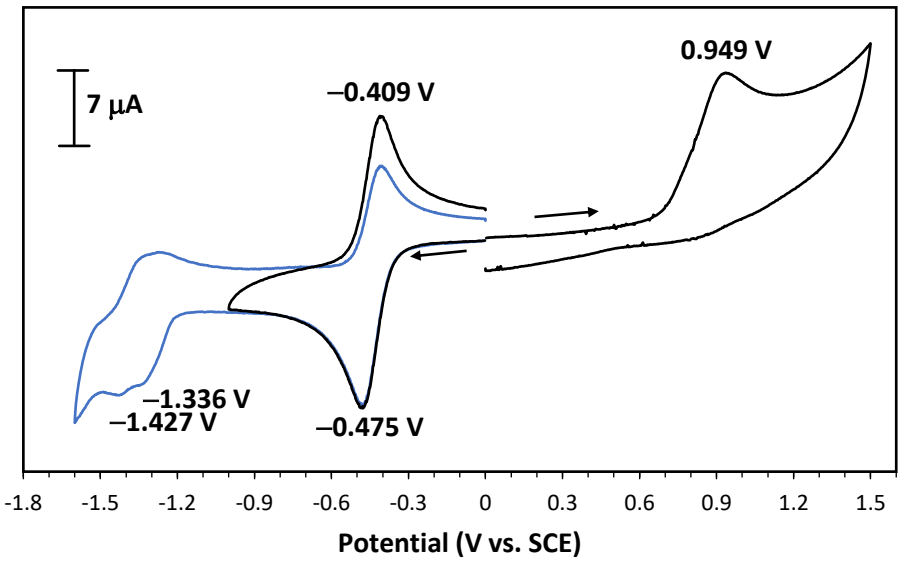

Figure 22. *Cyclic voltammograms (DMF, WE: Pt, CE: Pt, RE: Hg/Hg_2Cl_2/KCl sat., 100 mV s^{-1}) of a solution of* ***35·2PF$_6$*** *(c = 1.00 mM) in the presence of $TBAPF_6$ as supporting electrolyte (c = 0.1 mol L^{-1}).*

5.3. Photophysical Study (conducted by Dr. Barbara Ventura, Bologna)

Although both the acridinium and the porphyrin are known to fluoresce, none of the three synthesised conjugates were observed to be fluorescent. Via comparison to model compounds (namely **32·PF$_6$** and Zn(II)-bisphenyl porphyrin **Zn-bP**) the efficiency of the observed fluorescence quenching in **35·2PF$_6$** was quantified (Table 1). When exciting at 543 nm (selectively exciting the porphyrin), at both room temperature and at 77 K strong quenching of the emission of both the porphyrin and acridinium units of **35·2PF$_6$** (Figure 23) was observed, with emission quantum yield smaller than could be measured via steady state experiments (<0.0001). When compared to the emission quantum yield found for **Zn-bP** (0.035) and for **32·PF$_6$** (0.045), this accounted for a near quantitative quenching of emission.

Table 1 *[a] Emission maxima were obtained from corrected spectra. [b] Fluorescence quantum yields were measured with reference to meso-tetraphenylporphyrin (TPP) in aerated toluene as a standard for the porphyrin units and with reference to Coumarin 153 in ethanol for the acridinium units. [c] Fluorescence lifetimes are given in nanoseconds, with excitation at 465 nm for* ***Zn-bP*** *and at 368 nm for* ***32·PF$_6$****. [d] Selective excitation of the Zn(II)-porphyrin unit at 543 nm gives a yield below the minimum value measurable with steady-state experiments (i.e. 1 × 10^{-4}).*

		RT			**77K**		
		λ_{max} (nm)[a]	ϕ_{em}[b]	τ (ns)[c]	λ_{max} (nm)[a]	τ (ns)[c]	***E*** (eV)
32·PF$_6$		515	0.045	1.73	471, 500	2.70 (20%); 16.6 (80%)	2.63
Zn-bP	Zn-bP^1	588, 638	0.035	2.30	605, 648	2.31	2.05
	Zn-bP^3				794		1.56
35·2PF$_6$		590, 642[d]	<1 × 10^{-4} [d]				

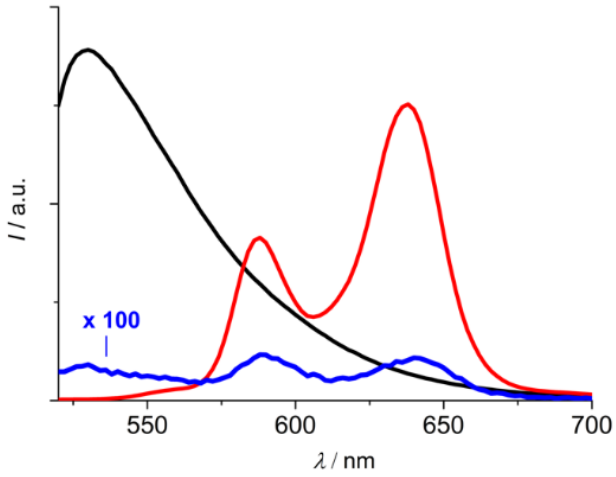

Figure 23. *Uncorrected emission spectra of the CH$_3$CN solutions of* ***35·2PF$_6$*** *(blue) and models* ***32·PF$_6$*** *(black) and* ***Zn-bP*** *(red), isoabsorbing at 262 nm (A$_{262}$ = 0.1), with λ$_{exc}$=262 nm. The blue spectrum has been multiplied by a factor of 100.*

To ascertain the mechanism of the fluorescence quenching, pump probe transient absorption spectroscopy was performed on **35·2PF$_6$**. The measurements were conducted at two excitation wavelengths, allowing for predominant excitation of the acridinium units (at 360 nm) and selective excitation of the porphyrin (at 543 nm). The obtained transient absorption spectra for **35·2PF$_6$** supported the formation of a charge separated state with features

corresponding to the formation of the π-radical cation Zn-porphyrin and the radical acridinium species.[28] In contrast, the two models **ZnbP** and **32·PF$_6$** were found to both form triplet excited states. The kinetics of the process was confirmed to be ultra-fast, with formation of the charge-separated (CS) state in 0.3 ps when exciting at 560 nm, and even faster at less than 0.3 ps, when exciting at 360 nm, with a lifetime of approximately 0.7 ps.

The energy of the charge-separated state (1.39 eV) was approximated as $E_{ox} - E_{red}$, using the oxidation potential of the porphyrin unit (E_{ox} = 0.949 V vs. SCE) and the reduction potential of the acridinium unit (E_{red} = −0.475 V vs. SCE). Based on the collected data, an energy level diagram was obtainable which confirmed that the photoinduced electron transfer was thermodynamically favourable, with the CS state being a lower lying excited state than the triplet excited states of the acridinium and porphyrin (Figure 24).

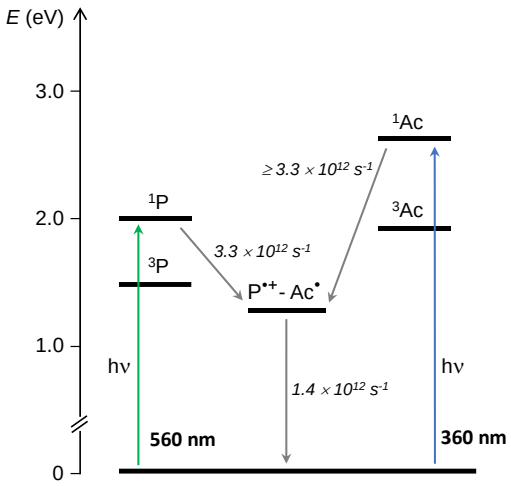

Figure 24. *Energy level diagram and kinetics of the photoinduced processes occurring in the conjugate* ***35·2PF$_6$*** *in CH_3CN, with "P" denoting the porphyrin unit, and "Ac" denoting the acridinium unit.*

5.4. Binding studies of 35·2PF$_6$

To support the hypothesis that porphyrin-acridinium conjugates can display positive allosteric control, **35·2PF$_6$** was used to probe the binding abilities of porphyrin-acridinium systems.

5.4.1. Choice of effector and guest

The use of porphyrins allows flexibility in the choice of effector, as both metal-ligand coordination, and π–π interactions can be formed. As metal-ligand coordination is a stronger interaction, preference is given to ditopic ligands as an effector, to ensure effective pre-organisation of the receptor. To a similar end, the size and length of the effector will inform the shape and size of the guest binding cavity, as such effectors of suitable length must be chosen. We chose to bind polyaromatic molecules at the acridinium sites, and thus an approximate interplanar distance of 7 Å was required, accounting for the π–π interaction above and below the guest, (typically 3.5 Å). The most suitable effector for this was determined to be DABCO, being approximately 2.7 Å long giving an approximate interplanar Zn-Zn distance of 7 Å when internally complexed as seen in crystal XRD structures of host-guest porphyrin receptor@DABCO complexes.[29] Furthermore, DABCO was effective in pre-organising for the binding of aromatic guests in the porphyrin cage **10_2@(DABCO)$_3$** (Chapter 1, section 2.2.1).[30] Additionally, as a ditopic ligand bound via metal-ligand coordination, use of DABCO ensures no competition between the effector and the guest, a risk that may be present if an aromatic effector were used.

5.4.2. Binding of DABCO

Thus, the binding ability of **35·2PF$_6$** with regards to DABCO was investigated via ^{1}H NMR spectroscopy. 0.5 equivalents of DABCO were added to one equivalent of **35·2PF$_6$** in acetonitrile at a five millimolar concentration (Figure 25). The ^{1}H NMR spectrum of the solution showed clear upfield shifts of the porphyrin protons ($\Delta\delta H_{meso}$ = 0.4 ppm, $\Delta\delta H_{py1\text{-}2}$ = 0.3 ppm), suggesting increased electronic shielding, synonymous with an induced magnetic field effect from increased proximity between the conjugates. In addition, a broad peak associated to DABCO was seen at −3.8 ppm, significantly shifted upfield from the chemical shift of free DABCO (2.7 ppm), in accordance with the formation of the sandwiched complex. In contrast, the acridinium protons were not observed to be as upfield shifted as the porphyrin protons ($\Delta\delta H_{1/8}$ = 0.1 ppm), likely due to both the smaller induced anisotropic magnetic field of the acridinium, and the ability of DABCO to act as a rotor making the acridinium units not as eclipsed as the porphyrin units.

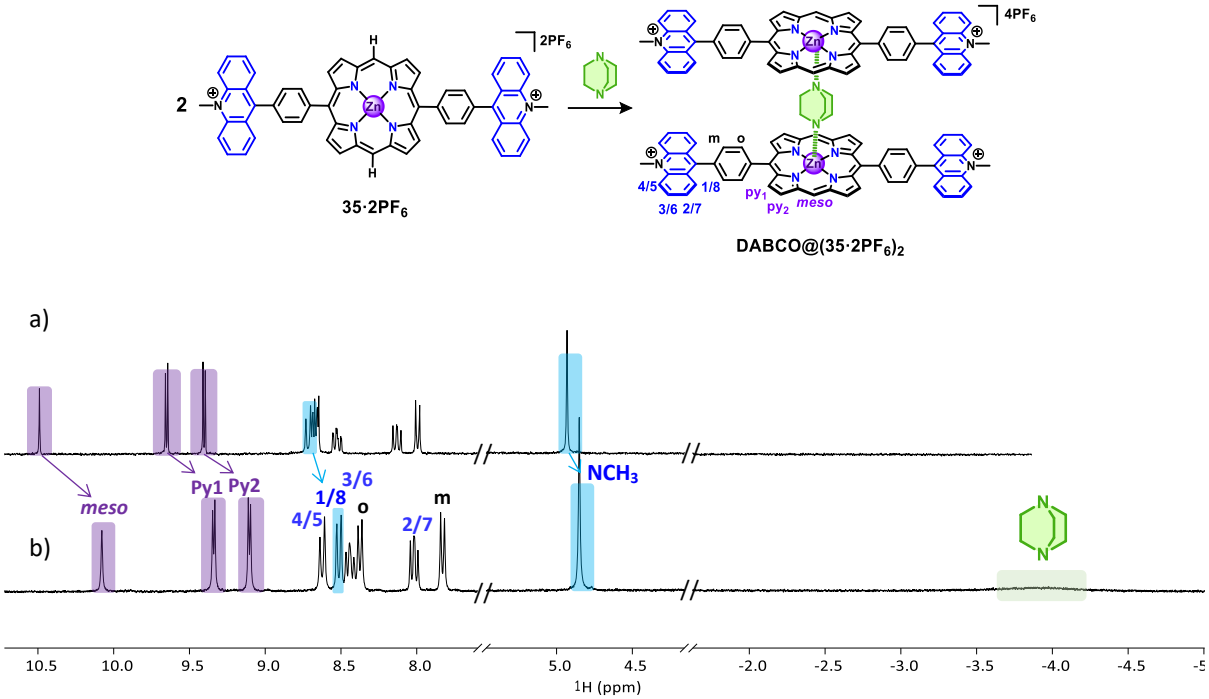

Figure 25. *^{1}H NMR (500 MHz, CD_3CN, 5.00 mM, 298 K) Spectra stack of a) **35·2PF$_6$** upon addition of b) 0.5 equivalents of DABCO. Upfield shifts are highlighted in purple for the pyrrolic protons and in blue for the acridinium protons.*

5.4.3. Binding of Pyrene

The ability of the sandwiched complex to bind pyrene was then explored, with an equivalent of pyrene added to the solution. The ^{1}H NMR spectrum of the solution showed little change to the peaks associated with the porphyrin (Figure 26). However, noticeable upfield shifts were seen for the acridinium peaks ($\Delta\delta H_{4/5}$ = 0.1 ppm, $\Delta\delta H_{3/6}$ = 0.06 ppm and $\Delta\delta H_{(1/8\ \&\ 2/7)}$ = 0.05 ppm), again suggesting an increase in electronic shielding associated to binding of pyrene via π–π interactions. The peak associated with DABCO was also seen to be shifted upfield to –4.4 ppm, suggesting an overall stabilisation of the complex upon addition of pyrene, further supporting binding of pyrene. In addition, the pyrene peaks were seen to be shifted upfield in comparison to the ^{1}H NMR spectrum of free pyrene, assigned to an induced magnetic field effect experienced upon binding by the acridinium units.

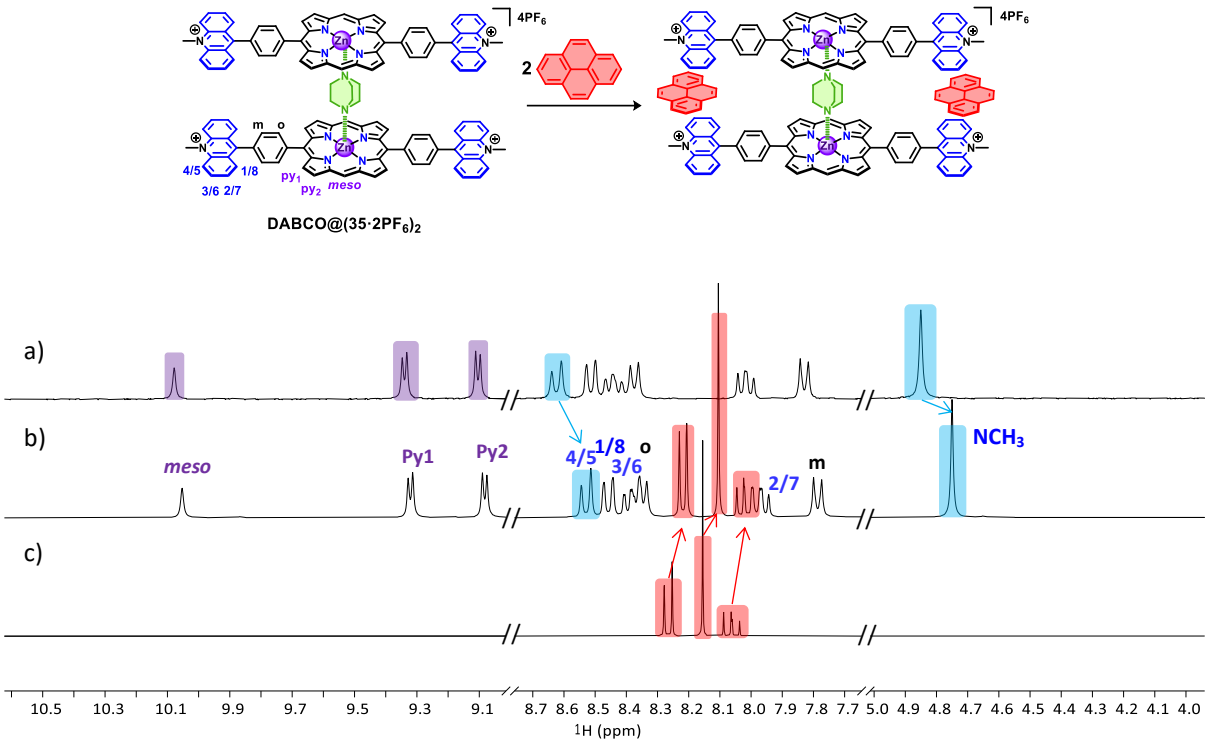

Figure 26. *Stacked ^{1}H NMR (500 MHz, CD_3CN, 2.50 mM, 298 K) spectra of a)* ***DABCO@35·2PF$_6$*** *upon addition of b) one equivalent of pyrene. An NMR spectrum of c) pyrene is included for comparison.*

Furthermore, evidence of an allosteric process was given by the control ^{1}H NMR experiment of **35·2PF$_6$** and pyrene without DABCO in the same conditions, which showed little to no change in chemical shifts, suggesting that in the absence of pre-organisation via DABCO complexation, the acridinium units could not bind pyrene (Figure 27).

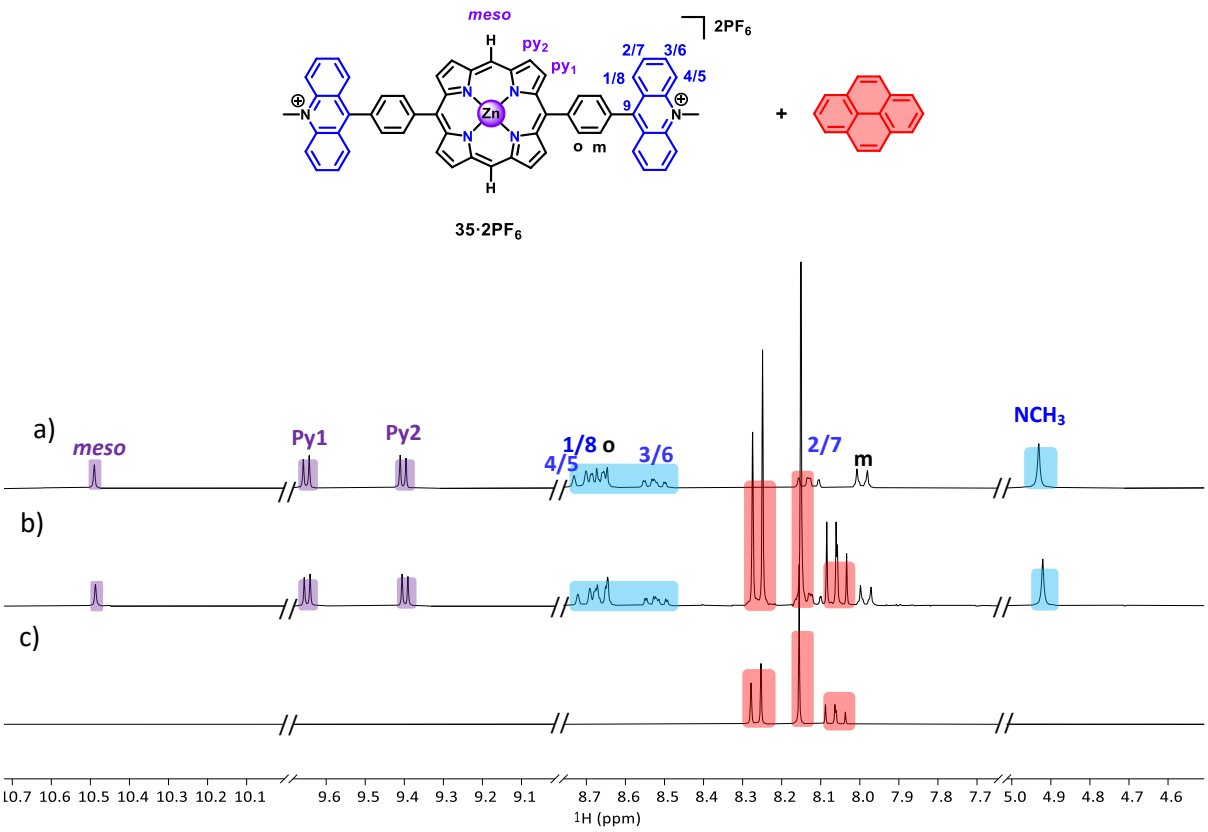

Figure 27. *^{1}H NMR (400 MHz, CD_3CN, 5.00 mM, 298 K) Spectra stack of a) **35·2PF$_6$** upon addition of b) one equivalent of pyrene. A ^{1}H NMR spectrum of c) pyrene is included for comparison.*

Therefore, it was concluded that the bisacridinium porphyrin was capable of forming a supramolecular receptor, with addition of DABCO resulting in the formation of a sandwiched Zn(II)porphyrin-DABCO-Zn(II)porphyrin complex, able to bind pyrene at the acridinium sites.

6. Conclusion

In conclusion, two effective synthetic pathways were found for connecting a porphyrin unit to acridinium unit(s). In particular, synthesis via porphyrin condensation using a novel and powerful reactant was found to be most efficient, allowing gram-scale synthesis of the stable key intermediate, and synthesis of different acridinium-porphyrin conjugates. Via this route, two conjugates were successfully synthesised and characterised, an AB_3 and A_2B_2 conjugate. The properties of the A_2B_2 conjugate with regards to its photophysics and electrochemistry have been studied, with key peculiar properties found. Via cyclic voltammetry, the porphyrin

was shown to undergo an uncommon bi-electronic oxidation. In addition, the conjugates were all observed to have highly quenched fluorescence, with photoinduced electron transfer evidenced for the bisacridinium Zn(II)-porphyrin conjugate via transient absorption spectroscopy. Finally, the ability of the A_2B_2 conjugate to bind DABCO and form a sandwiched complex was exhibited via ^1H NMR spectroscopy, with the complexes ability to bind pyrene further probed. Revealing upfield shifts in the spectrum supported binding of pyrene by the sandwiched complex at the acridinium site, consistent with the hypothesis that positive allosteric control can be exhibited in porphyrin-acridinium systems.

7. References

(1) Fischer, H.; Zeile, K. Synthese Des Hämatoporphyrins, Protoporphyrins Und Hämins. *Justus Liebigs Ann. Chem.* **1929**, *468* (1), 98–116.

(2) Fischer, H. On Haemin and the Relationships between Haemin and Chlorophyll. *Nobel Lecture Dec* **1930**, *11*.

(3) Adler, A. D.; Longo, F. R.; Finarelli, J. D.; Goldmacher, J.; Assour, J.; Korsakoff, L. A Simplified Synthesis for Meso-Tetraphenylporphine. *J.Org. Chem.* **1967**, *32* (2), 476–476.

(4) Rothemund, P. Formation of Porphyrins from Pyrrole and Aldehydes. *J. Am. Chem. Soc.* **1935**, *57* (10), 2010–2011.

(5) Lindsey, J. S. The Synthesis of Meso-Substituted Porphyrins, In *Metalloporphyrins Catalyzed Oxidations. Catalysis by Metal Complexes*; Montanari. F., Casella, L. H., Eds.; Springer: Dordrecht, Netherlands, 1994; pp 49–86.

(6) Lindsey, J. S. Synthetic Routes to Meso -Patterned Porphyrins. *Acc. Chem. Res.* **2010**, *43* (2), 300–311.

(7) Lindsey, J. S.; Hsu, H. C.; Schreiman, I. C. Synthesis of Tetraphenylporphyrins under Very Mild Conditions. *Tetrahedron Lett.* **1986**, *27* (41), 4969–4970.

(8) Lindsey, J. S.; Schreiman, I. C.; Hsu, H. C.; Kearney, P. C.; Marguerettaz, A. M. Rothemund and Adler-Longo Reactions Revisited: Synthesis of Tetraphenylporphyrins under Equilibrium Conditions. *J. Org. Chem.* **1987**, *52* (5), 827–836.

(9) Geier, G. R.; Lindsey, J. S. Effects of Aldehyde or Dipyrromethane Substituents on the Reaction Course Leading to Meso-Substituted Porphyrins. *Tetrahedron* **2004**, *60* (50), 11435–11444.

(10) Hiroto, S.; Miyake, Y.; Shinokubo, H. Synthesis and Functionalization of Porphyrins through Organometallic Methodologies. *Chem. Rev.* **2017**, *117* (4), 2910–3043.

(11) Kurihara, K.; Yazaki, K.; Akita, M.; Yoshizawa, M. A Switchable Open/Closed Polyaromatic Macrocycle That Shows Reversible Binding of Long Hydrophilic Molecules. *Angew. Chem. Int. Ed.* **2017**, *56* (38), 11360–11364.

(12) Hu, J.; Ward, J. S.; Chaumont, A.; Rissanen, K.; Vincent, J.; Heitz, V.; Jacquot de Rouville, H. A Bis-Acridinium Macrocycle as Multi-Responsive Receptor and Selective Phase-Transfer Agent of Perylene. *Angew. Chem. Int. Ed.* **2020**, *59* (51), 23206–23212.

(13) Kotani, H.; Ohkubo, K.; Crossley, M. J.; Fukuzumi, S. An Efficient Fluorescence Sensor for Superoxide with an Acridinium Ion-Linked Porphyrin Triad. *J. Am. Chem. Soc.* **2011**, *133* (29), 11092–11095.

(14) Önal, E.; Ahsen, V.; Pécaut, J.; Luneau, D.; Hirel, C. Bromine–Lithium Exchange as a Straightforward Method to Obtain Meso-Tetrakis(4-Formylphenyl)Porphyrin: A Versatile Intermediate. *Tetrahedron Lett.* **2015**, *56* (37), 5157–5160.

(15) Nöll, G.; Daub, J.; Lutz, M.; Rurack, K. Synthesis, Spectroscopic Properties, and Electropolymerization of Azulene Dyads. *J. Org. Chem.* **2011**, *76* (12), 4859–4873.

(16) Hammel, D.; Kautz, C.; Müllen, K. Funktionalisierte *Meso* -Arylporphyrine Als Edukte Für Die Synthese von Oligoporphyrinylen. *Chem. Ber.* **1990**, *123* (6), 1353–1356.

(17) Wennerström, O.; Ericsson, H.; Raston, I.; Svensson, susanne; Pimlott, W. Meso-Tetra(Meso-Tetraphenylporphyrinyl)Porphyrin, a Macrocycle with Five Covalently Linked Porphyrin Units. *Tetrahedron Lett.* **1989**, *30* (9), 1129–1132.

(18) Jacquot de Rouville, H.-P.; Zorn, N.; Leize-Wagner, E.; Heitz, V. Entwined Dimers Formation from Self-Complementary Bis-Acridiniums. *Chem. Commun.* **2018**, *4*, 10966–10969.

(19) McKiernan, G. J.; Hartley, R. C. Boronate Titanium Alkylidene Reagents for Diversity-Based Synthesis of Benzofurans. *Org. Lett.* **2003**, *5* (23), 4389–4392.

(20) Edo-Osagie, A.; Sánchez-Resa, D.; Serillon, D.; Bandini, E.; Gourlaouen, C.; Jacquot de Rouville, H.-P.; Ventura, B.; Heitz, V. Synthesis, Electronic and Photophysical Properties of a Bisacridinium-Zn(II) Porphyrin Conjugate. *C. R. Chim.* **2021**, *24* (S3), 47–55.

(21) Diers, J. R.; Kirmaier, C.; Taniguchi, M.; Lindsey, J. S.; Bocian, D. F.; Holten, D. A Perspective on the Redox Properties of Tetrapyrrole Macrocycles. *Phys. Chem. Chem. Phys.* **2021**, *23* (35), 19130–19140.

(22) Kadish, K. M.; van Caemelbecke, E. Electrochemistry of Porphyrins and Related Macrocycles. *J. Solid State Electrochem.* **2003**, *7*, 254–258.

(23) Koper, N. W.; Jonker, S. A.; Verhoeven, J. W.; van Dijk, C. Electrochemistry of the 9-Phenyl-10-Methyl-Acridan/Acridinium Redox System; a High-Potential NADH/NAD $^{+}$ Analogue. *Recl. Trav. Chim. Pays-Bas* **1985**, *104* (11), 296–302.

(24) Ogawa, T.; Ogawa, T.; Nishimoto, Y.; Ono, N.; Yoshida, N.; Osukua, A. One-Pot Electrochemical Formation of Meso,Meso-Linked Porphyrin Arrays. *Chem. Commun.* **1998**, *3*, 337–338.

(25) Devillers, C. H.; Lucas, D.; Dime, A. K. D.; Rousselin, Y.; Mugnier, Y. Exploring the Redox Reactivity of Magnesium Porphine. Insight into the Origins of Electropolymerisation. *Dalton Trans.* **2010**, *39* (9), 2404–2411.

(26) Dime, A. K. D.; Devillers, C. H.; Cattey, H.; Habermeyer, B.; Lucas, D. Control over the Oxidative Reactivity of Metalloporphyrins. Efficient Electrosynthesis of Meso,Meso-Linked Zinc Porphyrin Dimer. *Dalton Trans.* **2012**, *41* (3), 929–936.

(27) Osuka, A.; Shimidzu, H. Meso, Meso-Linked Porphyrin Arrays. *Angew. Chem. Int. Ed. Engl.* **1997**, *36* (12), 135–137.

(28) Fajer, J.; Borg, D. C.; Forman, A.; Dolphin, D.; Felton, R. H. ..Pi.-Cation Radicals and Dications of Metalloporphyrins. *J. Am. Chem. Soc.* **1970**, *92* (11), 3451–3459.

(29) Schoepff, L.; Kocher, L.; Durot, S.; Heitz, V. Chemically Induced Breathing of Flexible Porphyrinic Covalent Cages. *J. Org. Chem.* **2017**, *82* (11), 5845–5851.

(30) Ballester, P.; Oliva, A. I.; Costa, A.; Deyà, P. M.; Frontera, A.; Gomila, R. M.; Hunter, C. A. DABCO-Induced Self-Assembly of a Trisporphyrin Double-Decker Cage: Thermodynamic Characterization and Guest Recognition. *J. Am. Chem. Soc.* **2006**, *128* (16), 5560–5569.

3

SYNTHESIS AND STUDY OF A PORPHYRIN-ACRIDINIUM TWEEZER

1. Introduction

Having identified an efficient synthetic pathway for the coupling of porphyrins and acridiniums and established the exhibition of positive allosteric control in the binding of guests, we then looked to the synthesis of covalently attached porphyrin-acridinium conjugates. As the porphyrin-acridinium conjugates had been afforded with the acridinium at the *meso* substituents, the presence of up to four acridinium units per porphyrin was allowed, making the synthesis of different receptors possible including tweezers, macrocycles, cryptands and cages. However, due to their relative simplicity in comparison to the other architectures, the synthesis of molecular tweezers was first attempted.

1.1. Design and rationalisation of a porphyrin-acridinium tweezer

Molecular tweezers can be defined as a class of receptors featuring two recognition units, joined by a single linker. The first reported tweezer was given by Whitlock,[1] with countless tweezers reported since.[2–5] Tweezers can be grouped into three general classes based on the rigidity of the linker, whether it is:

1) Rigid: Where minimal flexibility is present, typically in the form of a few rotatable bonds, such as in the Jang groups' biindole bridged tweezer **11** (Chapter 1, section 2.2.2).[6]
2) Semi-flexible: Where partial flexibility is seen, such as in the Weiss group's pac-man tweezer **5** (Chapter 1, section 1.2).[7]
3) Flexible: Where full flexibility is seen, allowing for a larger range of accessible conformations.

The rigidity of the linker greatly informs the binding properties of the tweezer and its selectivity towards different guests. Use of rigid linkers can allow for higher binding constants in complexation. However, within the context of allosteric control a flexible linker can be preferrable to afford a larger allosteric effect. Thus, a flexible linker was proposed in the design of the porphyrin-acridinium tweezer (Figure 1).

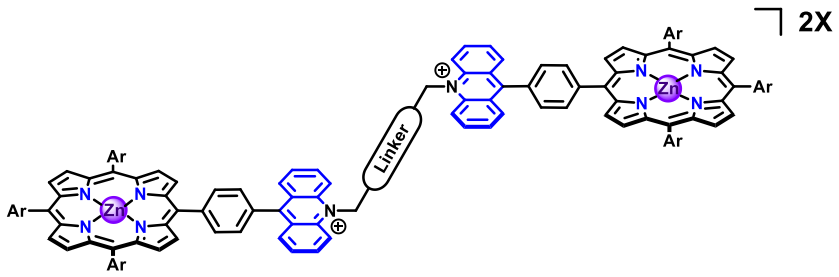

***Figure 1**. Illustration of the proposed design for the porphyrin-acridinium tweezer.*

In synthesising covalent molecular tweezers, there are two general approaches. The first is a termolecular reaction where two tweezer fragments are reacted with a doubly functionalised linker fragment to afford the tweezer. The second approach is direct attachment of two fragments which are functionalised with a group that can be reacted together to form the tweezer in a bimolecular reaction. The latter is preferrable as the reaction allows for the formation of only one product in contrast to the former. Given the two-step functionalisation required to synthesise an acridinium from an acridone (Chapter 2, section 1.3), attachment of a "linker" group to the acridinium was possible and so synthesis via the second route was pursued.

Attachment of the linker as part of the functionalisation of the acridinium was advantageous in minimising the number of synthetic steps. However, it presented some considerations. Namely, the linker group used would need to be robust to the conditions of both the synthesis of the acridinium (where strong nucleophiles are used) and of the porphyrin (where acid catalysts are used). Additionally, as the linking of the two halves of the receptors would be the last synthetic step, care also had to be taken in the choice of linking reaction. As previously discussed (Chapter 1, section 3), the acridinium is sensitive to nucleophilic addition. Additionally, the Zn(II)-porphyrin is readily demetallated when exposed to strong acids. Although the acridinium can be easily reformed via addition of acid, and the free base porphyrin is facile to remetallate, to avoid any issues high yielding linking reactions with mild conditions (without use of acids or bases/nucleophiles) were preferred. With these requirements in mind, and due to the ease of N-alkylation of the acridone synthon, alkenyl chains were chosen as the flexible linker, with formation of the receptor via olefin metathesis.

1.2. Alkene metathesis and retrosynthesis of a porphyrin-acridinium tweezer

The catalysis of olefin metathesis has been known since 1955, and is commonly used in ring closing, ring opening and cross metathesis.[8] The three most utilised catalysts are the 1st and 2nd generation Grubbs' catalysts,[9] and Schrock's catalyst (Figure 2).[10] In the presence of the catalyst, olefin metathesis is reversible, putting the reaction under thermodynamic control and allowing accumulating formation of the most stable product. The Grubbs' catalysts specifically are known to have high functional group tolerance as well as being less air and moisture sensitive than the Schrock catalyst. Thus, they can be used with a wide array of substituents, making use of the Grubbs' catalysts preferrable for synthesis of receptors. Accordingly, the Grubbs' catalysts (both generations) have been used to synthesise a number of molecular receptors and mechanically interlocked molecules.[11–21]

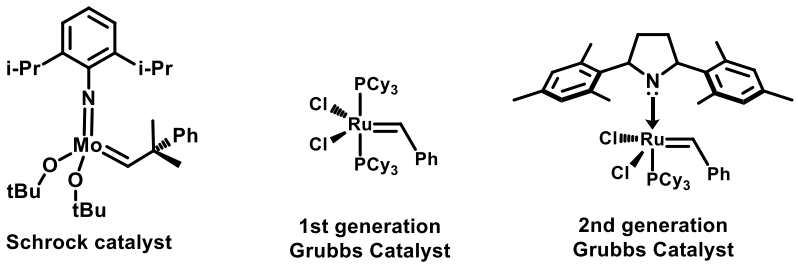

Figure 2. *Structures of the olefin metathesis catalysts.*

The main consideration in Grubbs catalysed olefin metathesis is the solvent used. As dissociation of the tris cyclohexyl phosphine ligand is a key factor in the mechanism for both catalysts (forming the active species),[22,23] coordinating solvents will block the active site of the catalyst. Most commonly, dichloromethane is used as the solvent in Grubbs catalysed alkene metathesis, due to its suitably low polarity. As the monoacridinium porphyrin conjugate **33·PF$_6$** showed solubility in CH_2Cl_2, it was expected that attachment of an alkenyl chain to the structure would also provide a suitably soluble tweezer precursor, which could be derivatized to the tweezer (Figure 3).

The final consideration for the design and synthesis of the tweezer was in the length of the alkenyl chain. Previous work within our research group had revealed the importance of chain length in determining the efficiency of the alkene metathesis. Specifically, in the synthesis of the bis acridinium macrocycle **21** (Chapter 1, section 3.1) via alkene metathesis; using a hexenyl or octenyl functionalised acyclic precursor was found to lead to a mixture of products,

with the decenyl functionalised analogue proceeding efficiently to the macrocycle.[14] Thus, to ensure efficient synthesis of the porphyrin-acridinium receptors a decenyl functionalisation was chosen for the tweezer precursor.

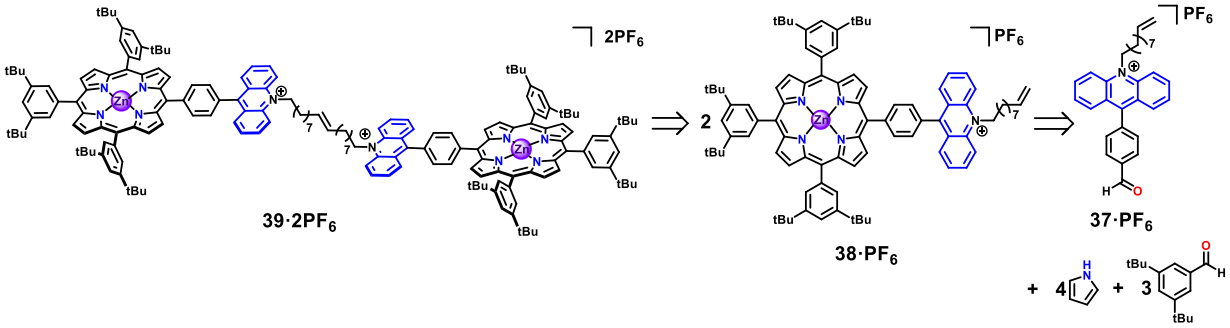

***Figure 3**. Retrosynthesis of a porphyrin-acridinium tweezer.*

2. Synthesis of a mono(N-decenyl)acridinium porphyrin tweezer precursor

In order to afford the decenyl functionalised formyl phenyl acridinium, alkylation of the starting synthon, 9-(10H)acridone was first performed via deprotonation using NaH, and the nucleophilic species then reacted with 10-bromo-decene, giving the N-decenyl acridone (**36**) at a yield of 70% after purification (Figure 4). The N-decenyl formyl phenyl acridinium was then synthesised via the same synthetic route as followed for **32·PF$_6$** (Chapter 2, section 4.1), obtaining the product at a moderate yield of 65%. Formation of **37·PF$_6$** was confirmed via NMR spectroscopy (Figure 5) and mass spectrometry.

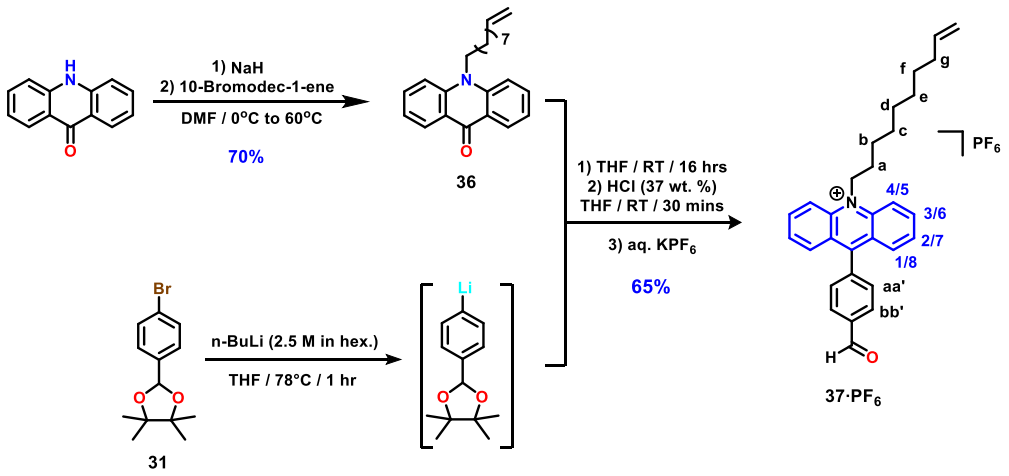

***Figure 4.** Synthesis of the formylphenyl N-(decenyl)acridinium **37·PF$_6$** from the N-decenylacridone **36**.*

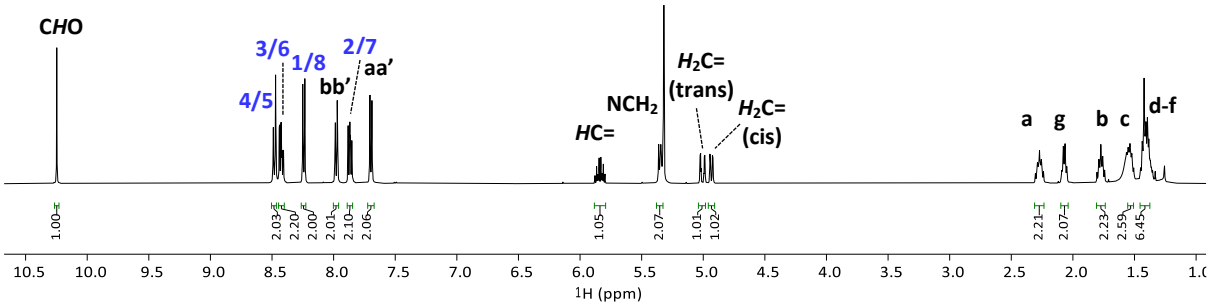

Figure 5. *^{1}H NMR (500 MHz, CD_2Cl_2, 298 K) spectrum of* ***37·PF$_6$****.*

The formed **37·PF$_6$** was then used in the same general procedure as followed for the mono(N-methyl)acridinium porphyrin conjugate **33·PF$_6$** (Chapter 2, section 4.2), to afford the monoacridinium porphyrin **38·PF$_6$** (Figure 6). In contrast to the previous conjugates, it was found that **38·PF$_6$** could not be easily isolated from the side products via column chromatography alone. However, when coupled with crystallisation, a pure product could be obtained, with a yield of 12%.

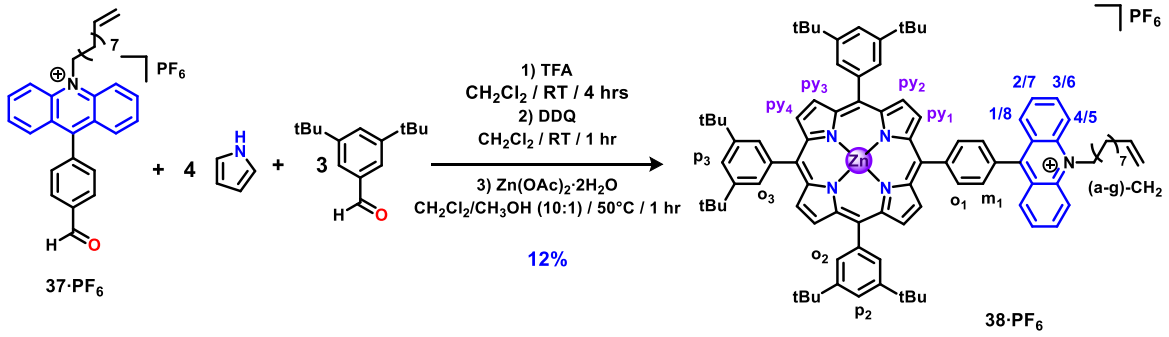

Figure 6. *Illustrative schematic showing the synthesis of the mono(N-decenyl)acridinium porphyrin conjugate* ***38·PF$_6$*** *from* ***37·PF$_6$****.*

The NMR spectra of the N-decenyl conjugate **38·PF$_6$** were observed to look much the same as the N-methyl conjugate **33·PF$_6$**, except for the presence of additional peaks in the alkyl region and peaks associated to the alkene group (Figure 7). Additionally, in accordance with a change from a methyl to a methylene group, the multiplicity of the nitrogen adjacent alkyl changed from a singlet to a multiplet in the ^{1}H NMR spectrum.

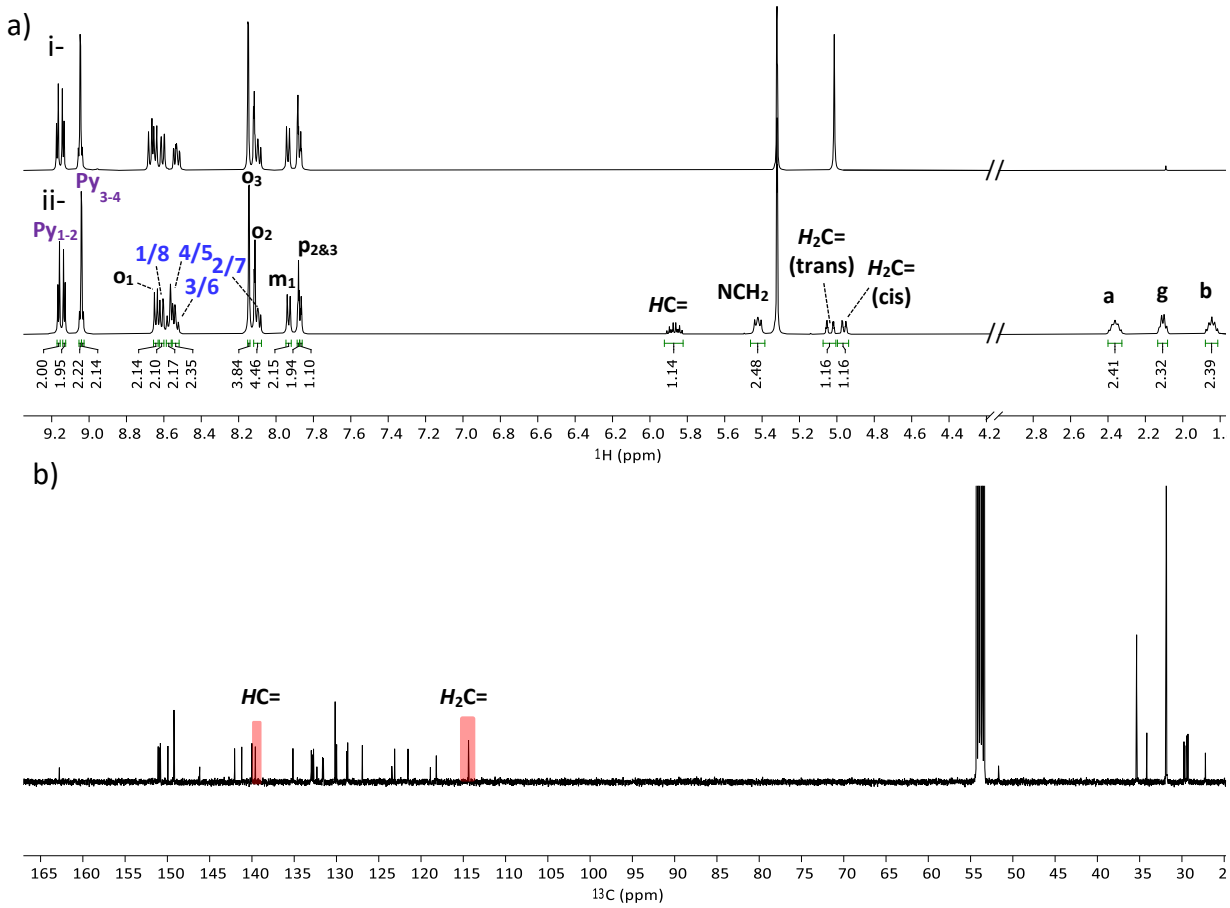

***Figure 7**. a) ^{1}H NMR (500 MHz, CD_2Cl_2, 298 K) spectrum of i- the mono(N-methyl)acridinium porphyrin conjugate **33·PF$_6$** and ii- the mono(N-decenyl)acridinium porphyrin conjugate **38·PF$_6$**. b) ^{13}C NMR (125 MHz, CD_2Cl_2, 298 K) spectrum of the conjugate **38·PF$_6$**.*

Mass spectrometry was seen to give a major mass ion peak in agreement with the chemical formula of the conjugate without the counter ions ($[M]^+$ at m/z = 1328.7402 corresponding to a molecular formula of $C_{91}H_{102}N_5Zn^+$, Figure 8). An additional peak at m/z = 664.3711 (30% intensity of the major mass ion peak) was seen assigned to a 2+ charged species of the same chemical formula as the major mass ion peak, indicating oxidation of the species during ionisation to form a radical-dicationic species.

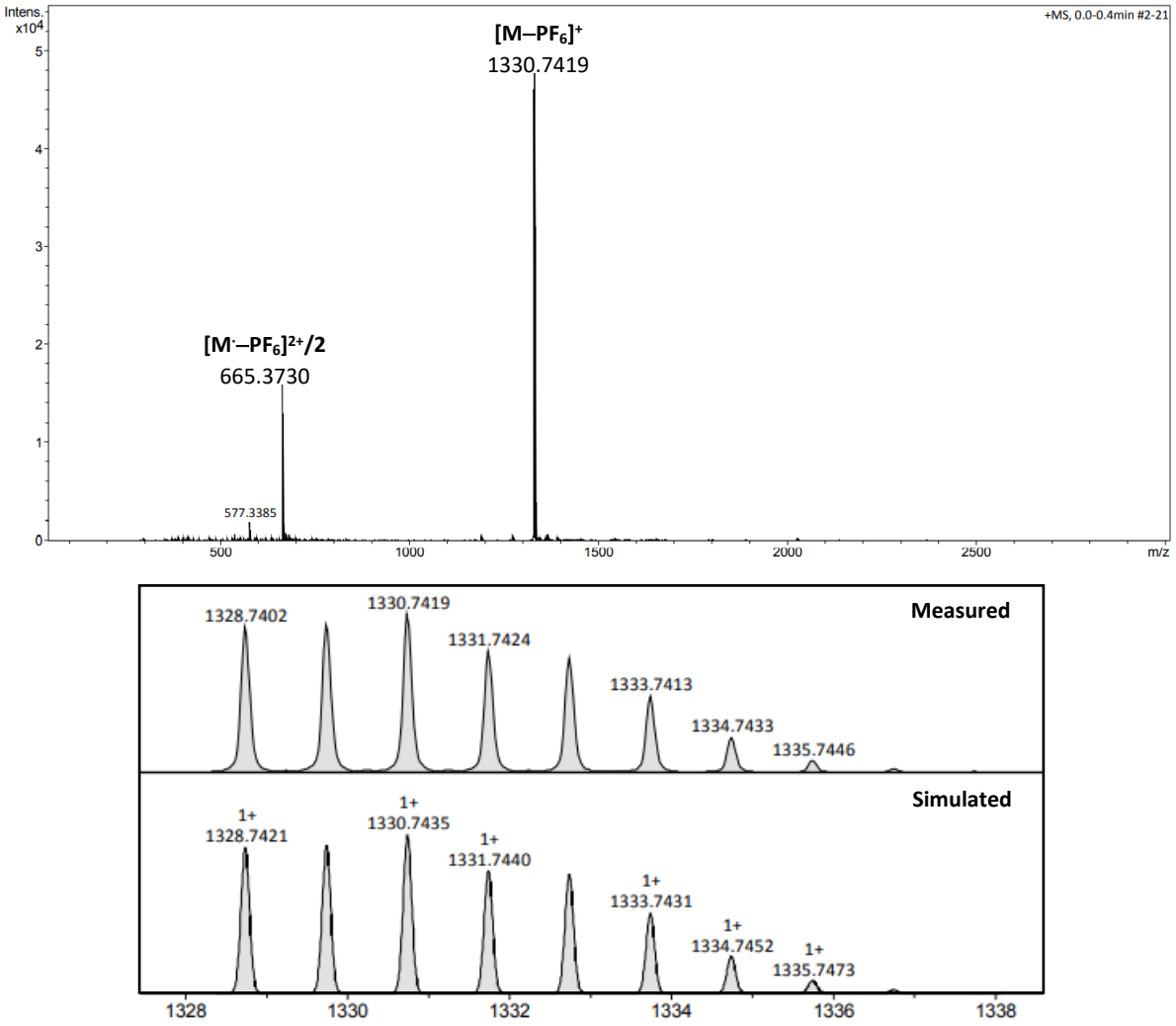

Figure 8. *High resolution mass (ESI-TOF) spectrum of* ***38·PF$_6$****, with a zoom-insert of the major mass ion peak* ***38$^+$****, showing the measured and simulated isotopic pattern.*

Similarly, when comparing the UV-Vis spectra of **38·PF$_6$** and **33·PF$_6$**, no hypsochromic/bathochromic shifts for any of the bands were observed (Figure 9). However, a slight decrease in intensity for the Soret band was seen (378 000 L mol^{-1} cm^{-1} at λ_{max} = 426 nm for **38·PF$_6$**, compared to 521 000 L mol^{-1} cm^{-1} for **33·PF$_6$**).

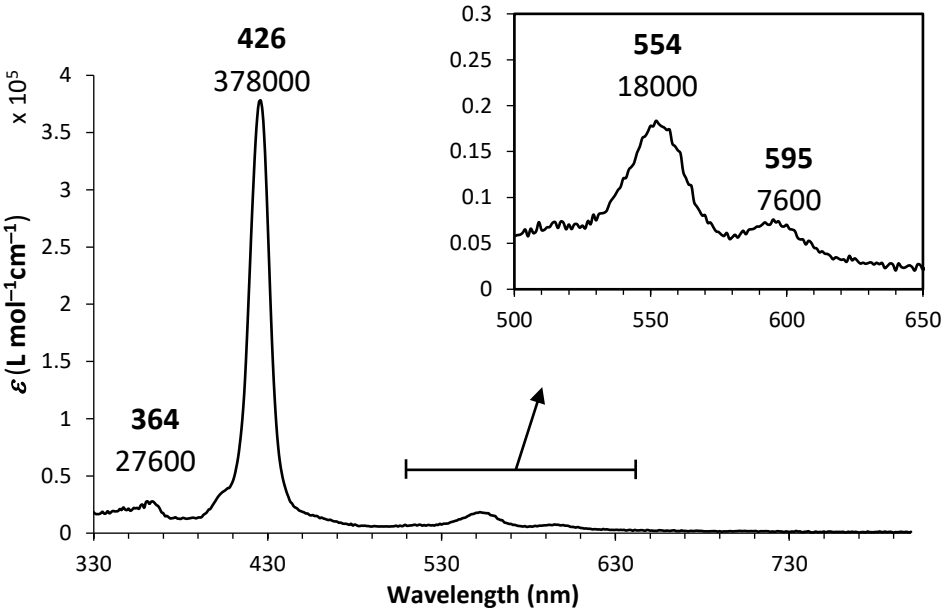

Figure 9. *UV-Vis (CH_2Cl_2, l = 0.2 cm, 298 K) spectrum of* ***38·PF$_6$*** *(c = 7.45 μM).*

3. Synthesis and characterisation of the porphyrin-acridinium tweezer 39·2PF$_6$

With the tweezer precursor **38·PF$_6$** in hand, synthesis of a tweezer via olefin metathesis was then attempted. Employing the Grubbs (I) catalyst at a 10 mol% loading, olefin metathesis was carried out on **38·PF$_6$** (Figure 10), obtaining the tweezer **39·2PF$_6$** at a yield of 77% after purification via column chromatography.

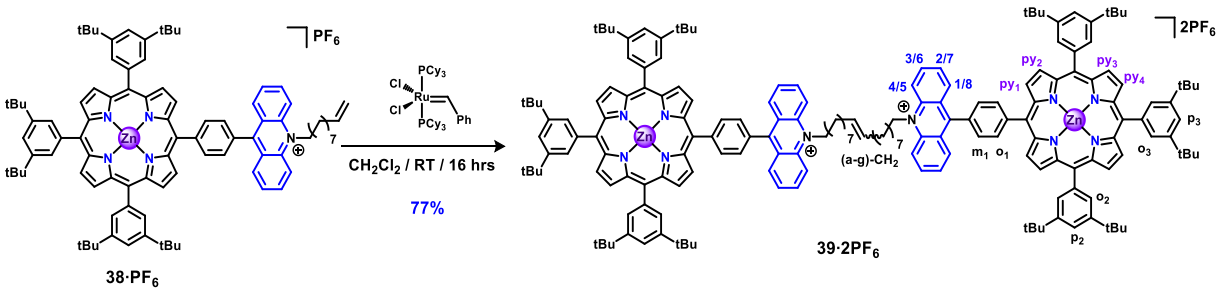

Figure 10. *Synthesis of* ***39·2PF$_6$*** *from* ***38·PF$_6$****, via olefin metathesis using the Grubbs (I) catalyst.*

The tweezer **39·2PF$_6$** was characterised via NMR spectroscopy, with disappearance of the three vinylic protons seen in the ^{1}H NMR spectrum (Figure 11a), replaced with a multiplet at 5.5 ppm, in agreement with formation of a symmetrised di-substituted alkene bond via alkene metathesis. A small shoulder peak was also seen at 5.45 ppm, overlapping the NCH_2 protons,

indicating formation of both the *trans* and *cis* alkene isomers. This was further supported by the observable shoulder peak seen for the allylic methylene protons at 2.15 ppm, with the relative integrals giving a 3:1 ratio of *trans*:*cis*. Additionally, no other significant changes to the aromatic or aliphatic peaks were seen, suggesting that there was no interaction between the two linked faces of **39·2PF$_6$**, in accordance with the use of a highly flexible linker, and the presence of bulky *meso* aryl groups on the porphyrin units. Similarly, in the ^{13}C NMR spectrum (Figure 11b) only one peak could be seen for the alkene carbons (losing the two distinct alkenyl carbon peaks seen for **38·PF$_6$**) with the remaining peaks remaining mostly unchanged. Thus, successful metathesis was concluded.

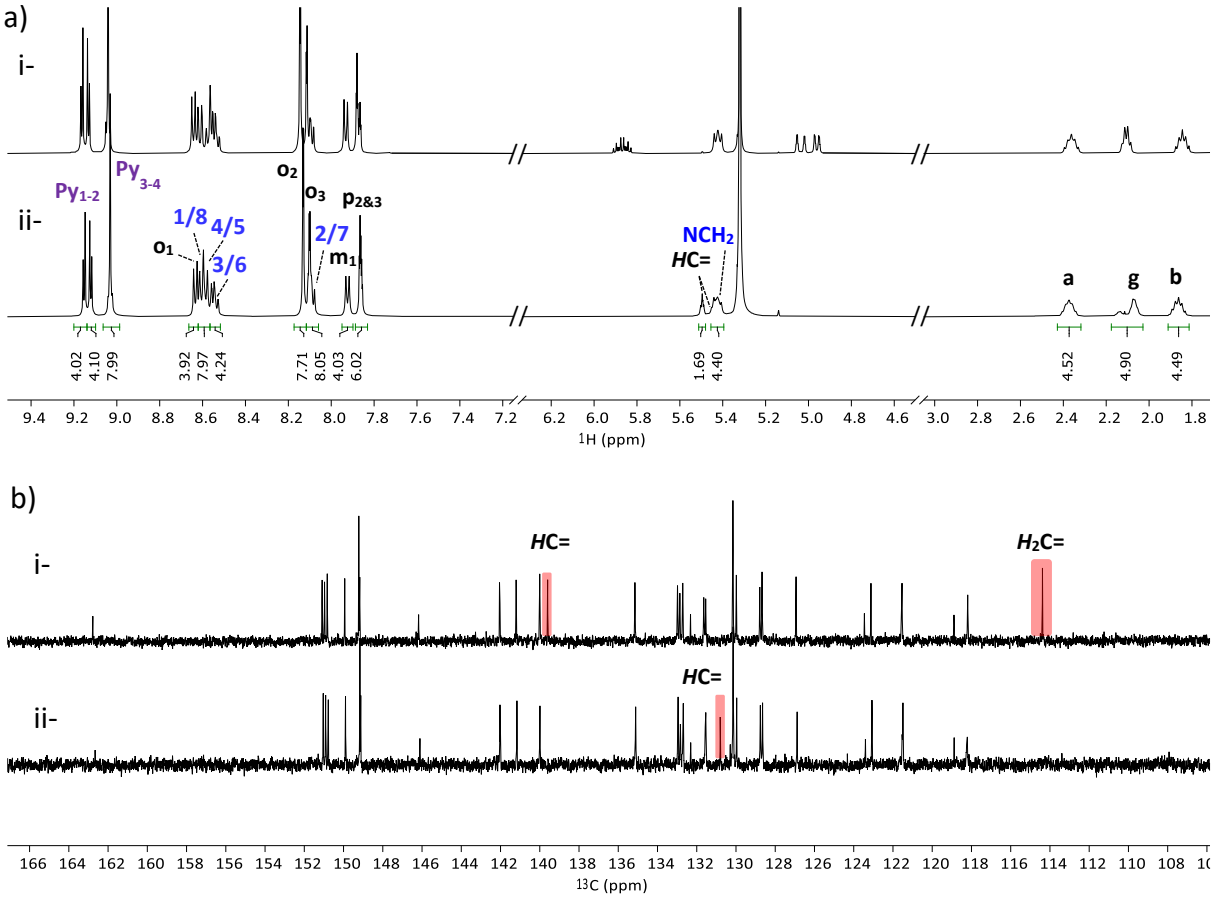

Figure 11. *Stacked a) ^{1}H NMR (500 MHz, CD_2Cl_2, 298 K) and b) ^{13}C NMR (125 MHz, CD_2Cl_2, 298 K) spectra of i-* ***38·PF$_6$*** *and ii-* ***39·2PF$_6$****.*

Formation of **39·2PF$_6$** was further supported by mass spectrometry (Figure 12), showing both a major mass ion peak and isotopic pattern in good agreement with that calculated for **39^{2+}**/2 ([M]$^{+}$ at m/z = 1314.7243 corresponding to a molecular formula of $C_{180}H_{200}N_{10}Zn_2^{2+}$).

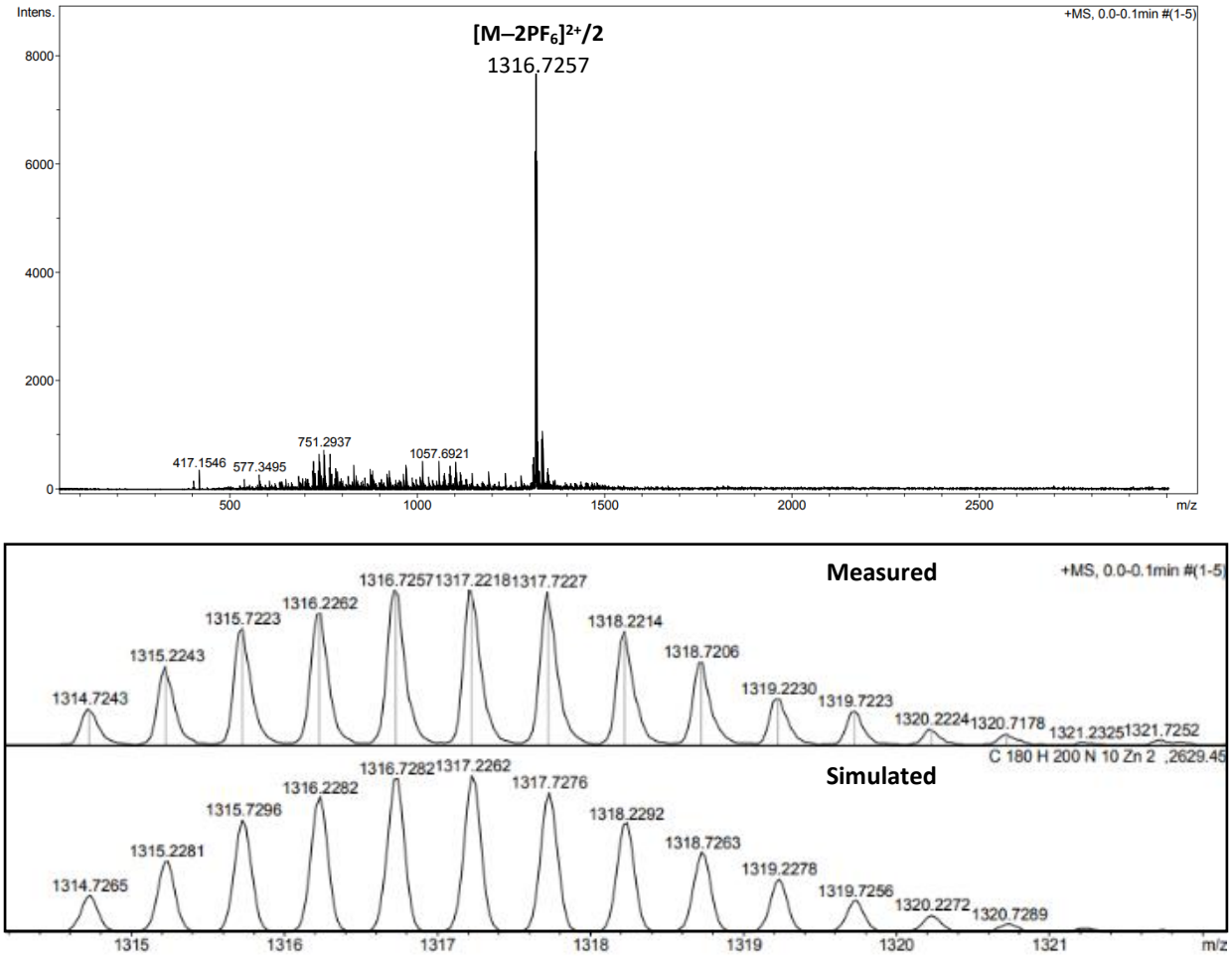

***Figure 12**. Mass (ESI-TOF) spectrum of the tweezer **39·2PF$_6$**, with a zoom insert of the major mass ion peak **39^{2+}**/2, showing the isotopic pattern measured and simulated.*

Finally, UV-Vis spectroscopy showed that covalently linking the monomers led to higher extinction coefficients for all bands by a factor of approximately 2.4, supporting the presence of two porphyrin and two acridinium units (Figure 13). In accordance with the NMR spectra, no hypsochromic or bathochromic shifts could be seen for any of the absorbance bands, when comparing to the precursor **38·PF$_6$**.

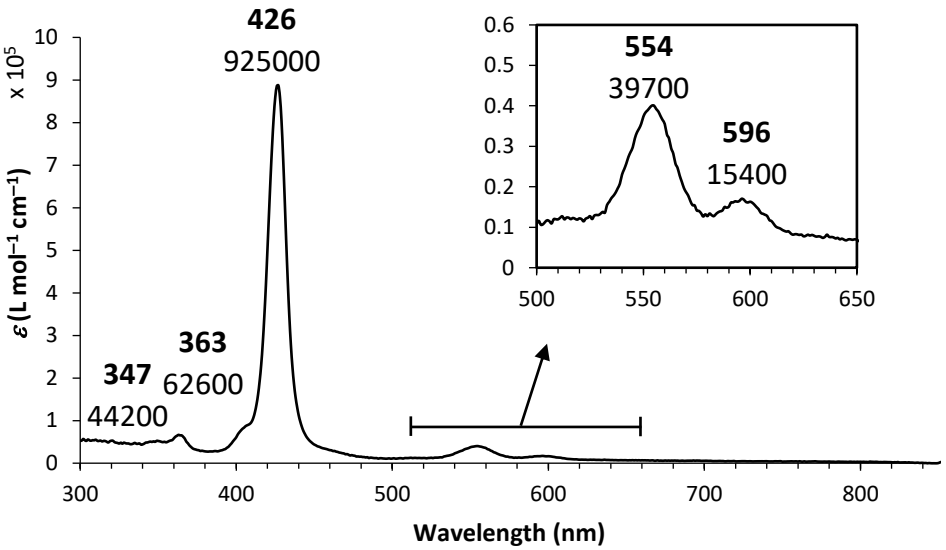

Figure 13. *UV-Vis (CH_2Cl_2, l = 1 cm, 298 K) spectrum of the tweezer* ***39·2PF$_6$*** *(c = 1.00 μM).*

4. Binding studies of the porphyrin-acridinium tweezer 39·2PF$_6$

4.1. Study of the complexation of DABCO by 39·2PF$_6$ and its effects on the binding of polyaromatic hydrocarbons

The ability of the tweezer **39·2PF$_6$** to bind DABCO was probed via ^{1}H NMR (Figure 14), with addition of 1 equivalent of DABCO to a millimolar solution of **39·2PF$_6$** in CD_2Cl_2 giving rise to a characteristic upfield shifted peak for DABCO at –4.6 ppm (*cf*. free DABCO at 2.7 ppm) in the ^{1}H NMR spectrum. This was comparable to that seen for the bisacridinium porphyrin conjugate **35·2PF$_6$** (Chapter 2, section 5.4.2) with a much narrower peak observed for **39·2PF$_6$**, indicating an induced magnetic field effect on the DABCO ligand from ditopic complexation by the Zn(II)-porphyrin units. Additionally, as similarly seen for **35·2PF$_6$** the peaks associated with **39·2PF$_6$** were also upfield shifted, with the most significant being for the pyrrolic protons of the porphyrin at –0.4 ppm, further supporting formation of the macrocyclic complex (**DABCO@39·2PF$_6$**).

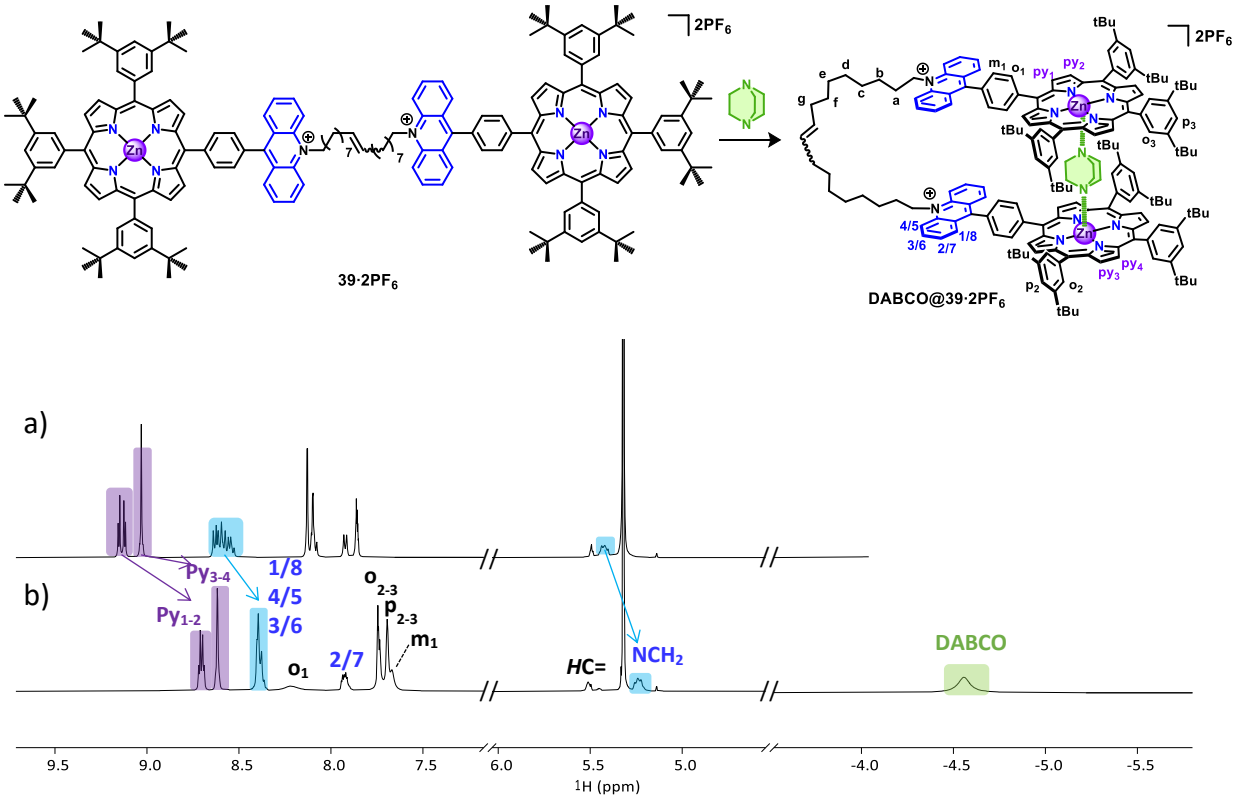

Figure 14. *Stacked ^{1}H NMR (500 MHz, CD_2Cl_2, 1.00 mM, 298 K) spectra of tweezer a)* ***39·2PF$_6$*** *and b)* ***DABCO@39·2PF$_6$****.*

To corroborate these results, DOSY experiments were conducted, with clear differences in the diffusion of **39·2PF$_6$** seen in the presence and in the absence of DABCO. In the absence of DABCO, **39·2PF$_6$** was shown to diffuse as a single species with a diffusion coefficient of 3.8 × 10^{-6} cm^2 s^{-1}. Upon addition of DABCO, a single diffusing species was similarly seen, with the DABCO peak diffusing with the same coefficient as those of **39·2PF$_6$**, in agreement with formation of **DABCO@39·2PF$_6$**. The complex had a larger diffusion coefficient of 4.5 × 10^{-6} cm^2 s^{-1}, giving a hydrodynamic radius of 1.11 nm when assuming a spherical model (Table 1). The energy minimised (MMFF, Spartan'20, Wavefunction, Inc., Irvine, CA) structure of **DABCO@39·2PF$_6$**, was shown to extend outside of a sphere with a 1.11 nm radius, most specifically for the alkenyl chain. This is likely due to the flexibility of the alkenyl linker, and the deviation from a spherical shape.

Table 1. *Data from the DOSY NMR experiments recorded for* ***39·2PF$_6$*** *and* ***DABCO@39·2PF$_6$****.* ***R_h*** *of* ***39·2PF$_6$*** *is not provided as* ***39·2PF$_6$*** *is a highly flexible species meaning the conformation in solution cannot be easily determined.*

Species	Solvent	D ($\times 10^{-6}$ cm^2 s^{-1})	R_h (Å)
DABCO@39·2PF$_6$	CD_2Cl_2	4.50 (± 0.16)	11.1
39·2PF$_6$	CD_2Cl_2	3.80 (± 0.1)	–

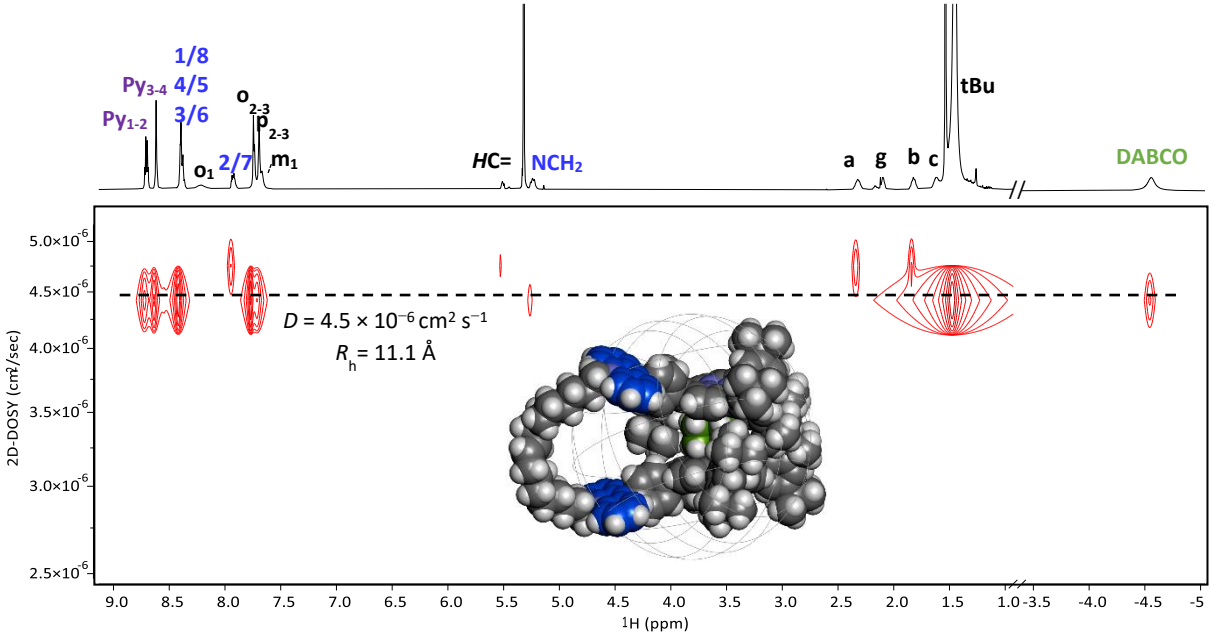

Figure 15*. ^{1}H DOSY NMR (600 MHz, CD_2Cl_2, 1.00 mM, 298 K) spectrum of* ***DABCO@39·2PF$_6$*** *and the energy minimised (Spartan'20) model of the complex, within a superimposed sphere (radius = 1.11 nm).*

In addition, UV-Vis titrations were used to determine the binding constant (Figure 16). Addition of up to 4 equivalents of DABCO to a micromolar solution of **39·2PF$_6$** in CH_2Cl_2, gave rise to a bathochromic shift of the Soret band by 2 nm (from 426 nm to 428 nm), with an isosbestic point at 427 nm. Additionally, a narrowing of the Soret band width was observed, in agreement with formation of the less flexible 1:1 macrocyclic complex **DABCO@39·2PF$_6$** from the comparatively more flexible **39·2PF$_6$**.

Further addition of up to 320 equivalents (Figure 16), gave rise to a second process with further bathochromic shifts (and a broadening) of the Soret band, and a second local isosbestic point (at 431 nm). These results indicated binding of a second DABCO ligand at

larger equivalents, breaking the macrocyclic receptor to form an acyclic host:(guest)$_2$ species. Fitting to a 1:2 binding model gave averaged binding constants of K_{11} = 2.0 (±0.3) × 10^6 and K_{12} = 6.0 (±0.6) × 10^3 M^{-1} for the 1:1 and 1:2 complexes. The 1:1 value was similar to values found for another reported porphyrin tweezer with a flexible/semi-flexible linker in the same solvent.[24]

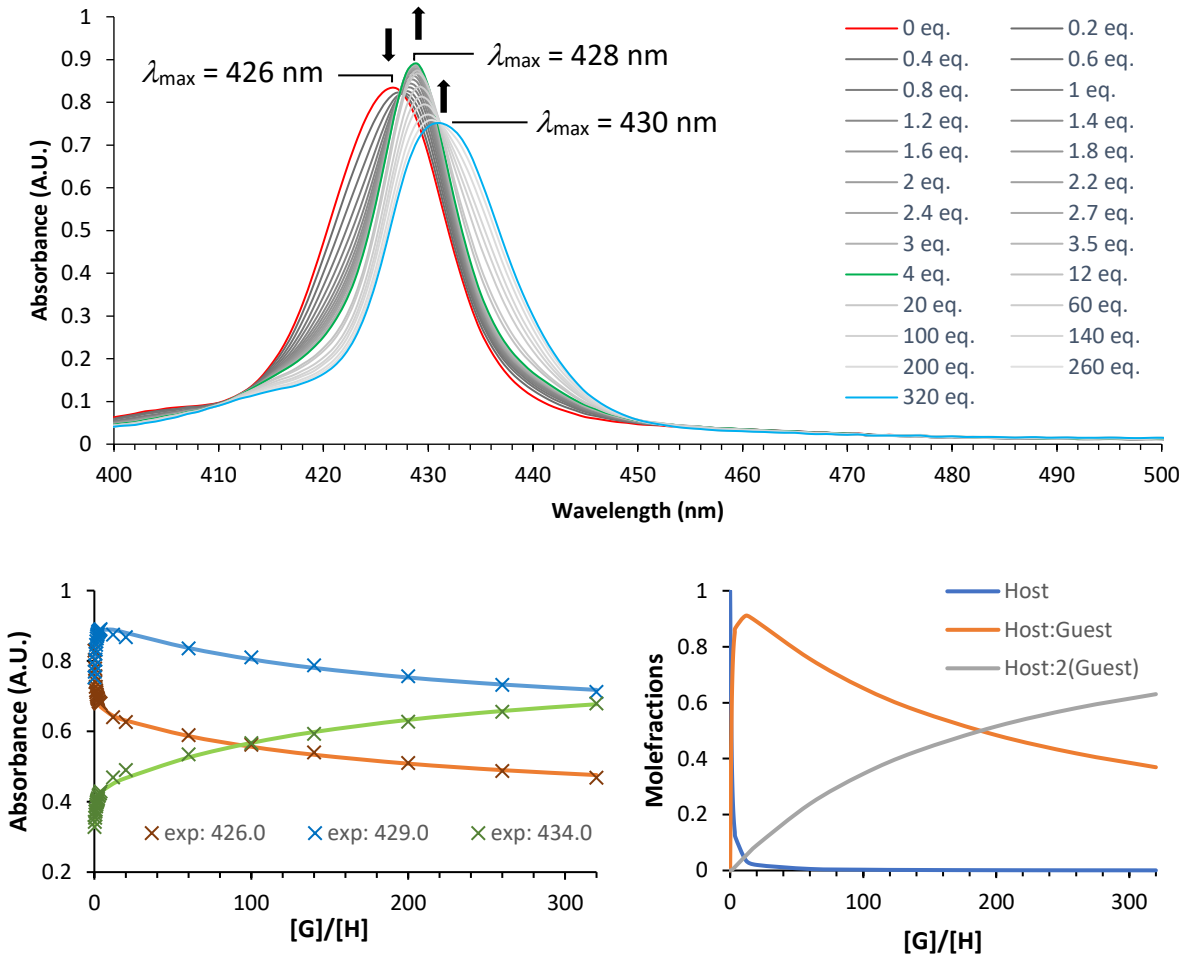

Figure 16. *UV-Vis (CH_2Cl_2, l = 1 cm, 298 K) titration of* ***39·2PF$_6$*** *(c = 1.00 μM) with up to 320 equivalents of DABCO. The non-linear regression fit of the data and the calculated speciation diagram are provided.*

To allow comparison, titrations were also conducted on the equivalent model AB_3 monoacridinium porphyrin **33·PF$_6$** (Figure 17), at a two micromolar concentration in CH_2Cl_2. It was found that addition of up to 50 equivalents, led to a larger bathochromic shift for the Soret band ($\Delta\lambda_{max}$ = + 7 nm) than seen for the 1:1 process of **39·2PF$_6$** with formation of one species suggested by the presence of one isosbestic point at 431 nm. Fitting to a 1:1 binding

model gave a binding constant of 1.06 (±0.03) × 10^5 M^{-1}, 20 times smaller than seen for **39·2PF$_6$** (Table 2), further supporting a ditopic binding of biPy by **39·2PF$_6$**.

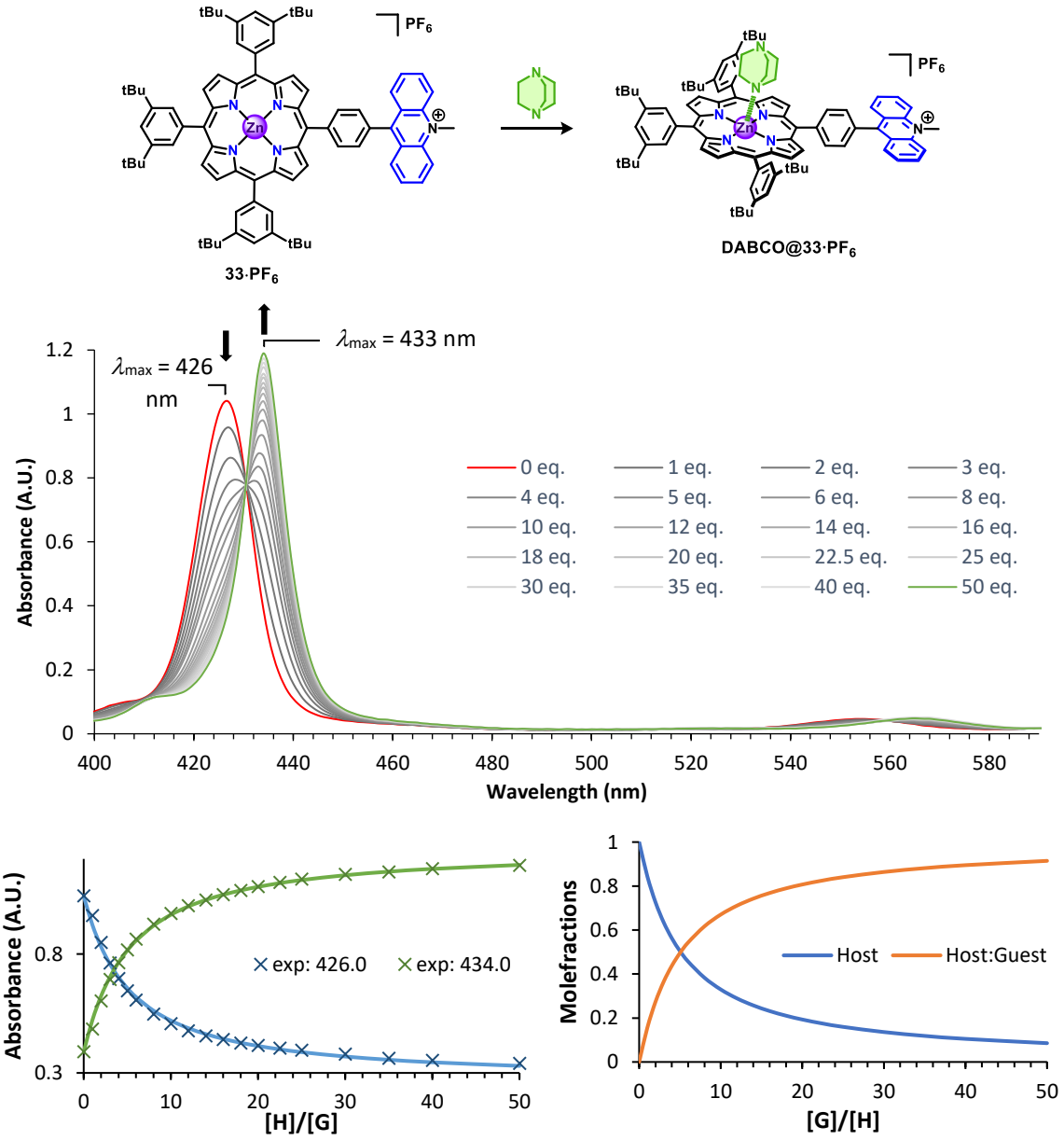

Figure 17. *UV-Vis (CH_2Cl_2, l = 1 cm, 298 K) titration of* ***33·PF$_6$*** *(c = 2.00 μM) with up to 50 equivalents of DABCO, and the non-linear regression fit, along with the accompanying calculated speciation diagram.*

Table 2. *Binding constants obtained via UV-Vis titrations of the two species* ***33·PF$_6$*** *and* ***39·2PF$_6$,*** *with the guest* ***DABCO****.*

Species	Guest	Solvent	K_a (L mol^{-1})
33·PF$_6$	**DABCO**	CH_2Cl_2	1×10^5
39·2PF$_6$	**DABCO**	CH_2Cl_2	$K_{11} = 2 \times 10^6$ $K_{12} = 6 \times 10^3$

We then looked to explore the ability of the **DABCO@39·2PF$_6$** complex to bind polyaromatic molecules, assessing the efficacy of DABCO as an effector for allosterically enhanced binding of polyaromatic molecules. A binding experiment was first carried out for the macrocyclic complex with perylene (Figure 18), with addition of 1 equivalent of perylene to a 1 millimolar solution of **DABCO@39·2PF$_6$** in CD_2Cl_2 leading to no major change to the ^{1}H NMR spectrum.

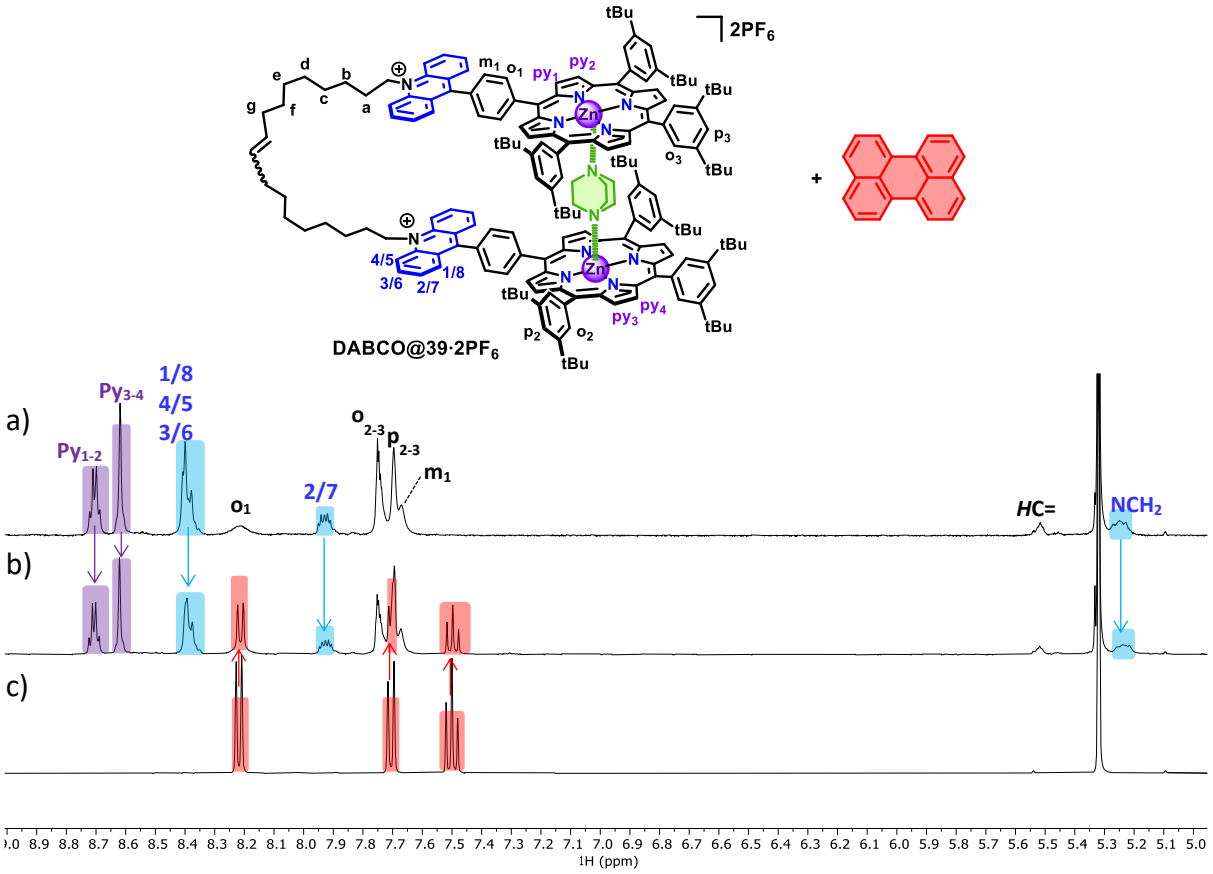

Figure 18. *Stacked ^{1}H NMR (400 MHz, CD_2Cl_2, 1.00 mM, 298 K) spectra of a) the macrocyclic complex and b) upon addition of 1 eq. of perylene. A ^{1}H NMR spectrum of c) perylene is provided for comparison.*

Switching to the polyaromatic molecule pyrene (Figure 19), addition of one equivalent to the **DABCO@39·2PF$_6$** solution at the same concentration, gave rise to a slight broadening of all peaks associated with **39·2PF$_6$.** However, no significant upfield shifts were seen. Addition of a further equivalent of pyrene was not seen to lead to further change, and an increase in concentration to five millimolar did not have significant impact. As a result, it was concluded that there was not a strong interaction between pyrene and **DABCO@39·2PF$_6$**.

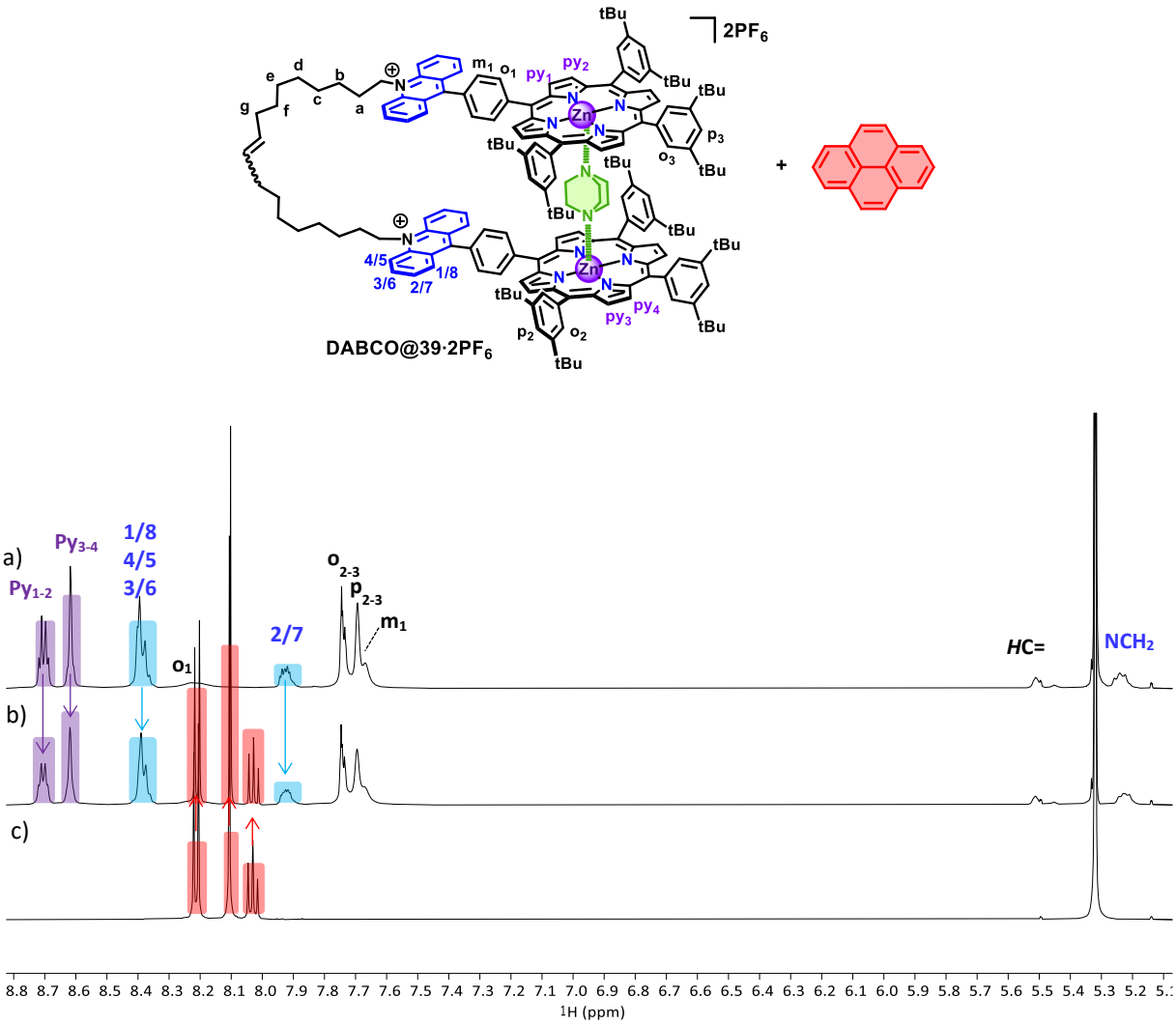

Figure 19. *Stacked ^{1}H NMR (500 MHz, CD_2Cl_2, 1.00 mM, 298 K) spectra of a)* ***DABCO@39·2PF$_6$*** *upon addition of b) two equivalents of pyrene. A spectrum of c) pyrene is included for comparison.*

Based on the results of the NMR experiments, we hypothesised that steric interactions may occur between the di-*tert*-butyl groups of the two porphyrin units upon complexation of DABCO, inhibiting binding of the polyaromatic guest. Steric interactions between the groups

would disfavour the eclipsed conformation required to have efficient π–π interaction with a polyaromatic guest at the acridinium binding site (Figure 20). This hypothesis was supported by computational studies (carried out by Dr. Dylan Serillon, University of Barcelona), modelling the interaction of **39·2PF$_6$** with DABCO, showing unfavourable interactions between the aryl substituents upon complexation of DABCO when in an eclipsed conformation.

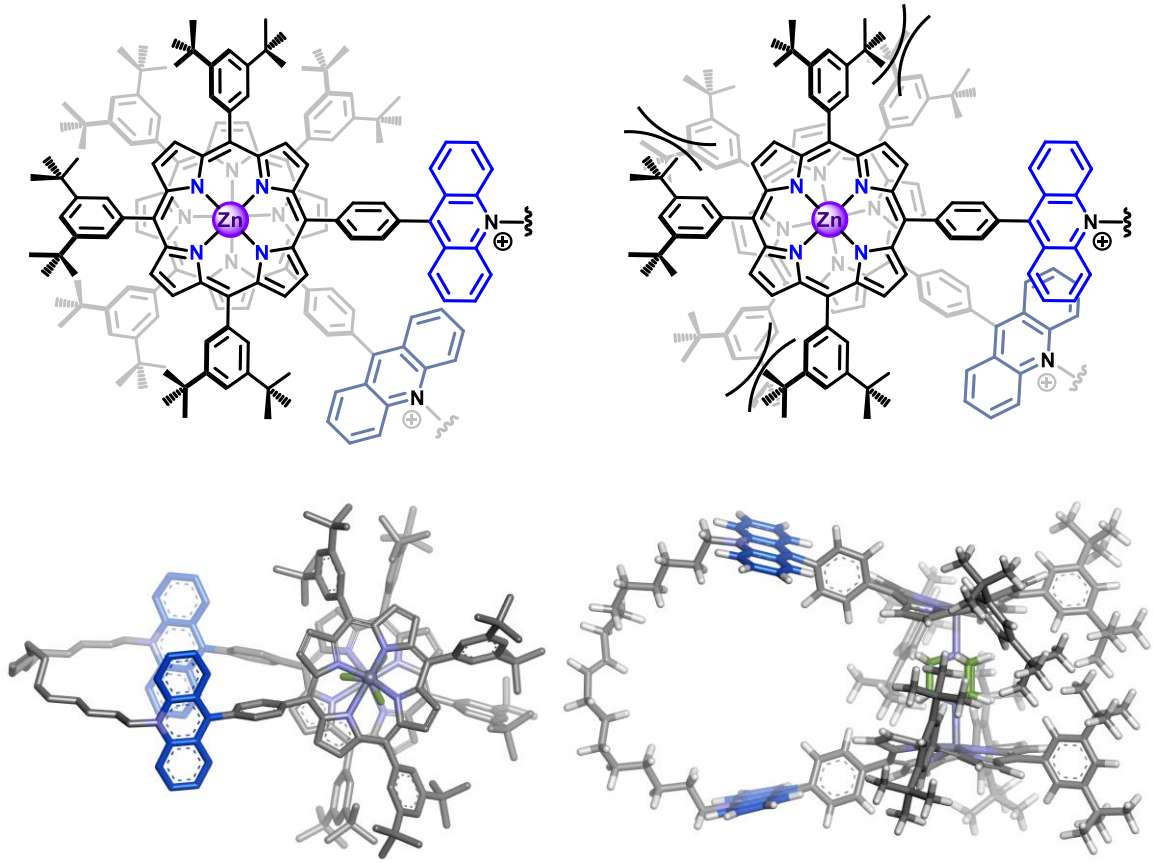

***Figure 20**. Illustration of the off-set conformation, the steric interactions encountered when the di-tert-butyl groups are close to one another, and the computed energy-minimised (Spartan'20) three-dimensional model of the off-set conformation*

To assess whether any change in behaviour was observed in the absence of DABCO, a ^{1}H NMR spectrum was recorded for a millimolar solution of **39·2PF$_6$** with an equivalent of pyrene in CD_2Cl_2 (Figure 21). However, as seen with **DABCO@39·2PF$_6$** little change was seen in the spectra, with no broadening or shifts of the peaks. As such it was concluded that **39·2PF$_6$** could not bind poly aromatic guests in the absence of an effector.

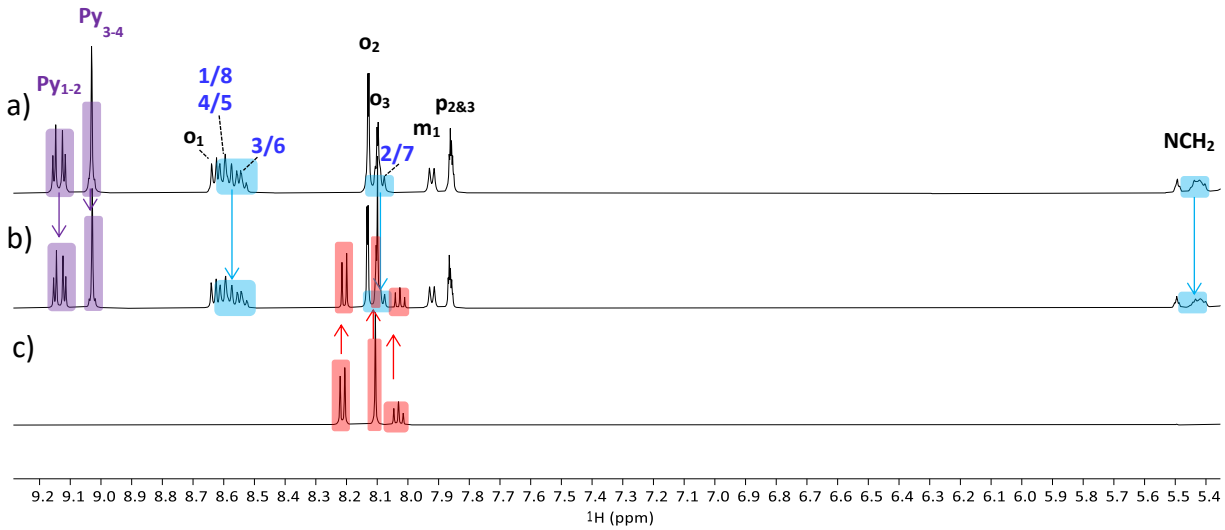

Figure 21. *Stacked ^{1}H NMR (500 MHz, CD_2Cl_2, 2.00 mM, 298 K) spectra, showing a)* ***39·2PF$_6$*** *before and b) after addition of one equivalent of pyrene. A spectrum of c) pyrene is provided for comparison.*

To avoid steric interactions between the faces of **39·2PF$_6$**, the larger effector 4,4'-bipyridine (biPy) was explored, with the ligand having a length more than twice that of DABCO (7.1 Å vs. 2.7Å, Figure 22), ensuring no steric interactions between the two faces of the receptor upon complexation of the ligand.

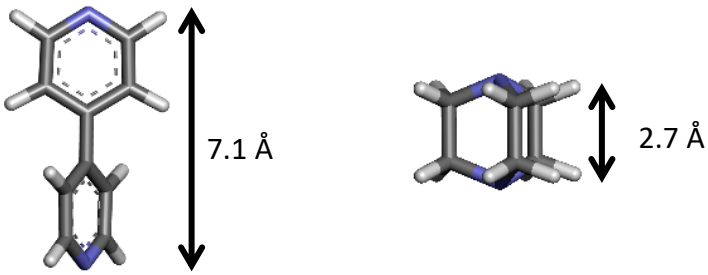

Figure 22. *Energy-minimised (Spartan'20) structures of the two ditopic ligands biPy and DABCO, with their respective N-N lengths.*

4.2. Study of the complexation of biPy by **39·2PF$_6$** and its effects on pyrene complexation

In order to confirm the ability of **39·2PF$_6$** to complex biPy and form a macrocyclic receptor, one equivalent of biPy was added to a solution of **39·2PF$_6$** in CD_2Cl_2, and a ^{1}H NMR spectrum recorded (Figure 23). Notable changes in the spectrum were seen upon addition of biPy, with upfield shifts of the pyrrolic protons ($\Delta\delta H_{Py1\text{-}4}$ ppm = – 0.25 ppm), and upfield shifts of smaller magnitude for the acridinium peaks ($\Delta\delta H_{1/8}$ = – 0.1 ppm). In addition, broad peaks for biPy were observed at significantly upfield shifted chemical shifts (H_β = 4.94 and H_α = 2.32 ppm, in comparison to free 4,4'-bipyridine: H_α = 8.72 and H_β = 7.57 ppm), indicating an induced magnetic field effect, suggesting formation of the macrocyclic receptor **biPy@39·2PF$_6$**.

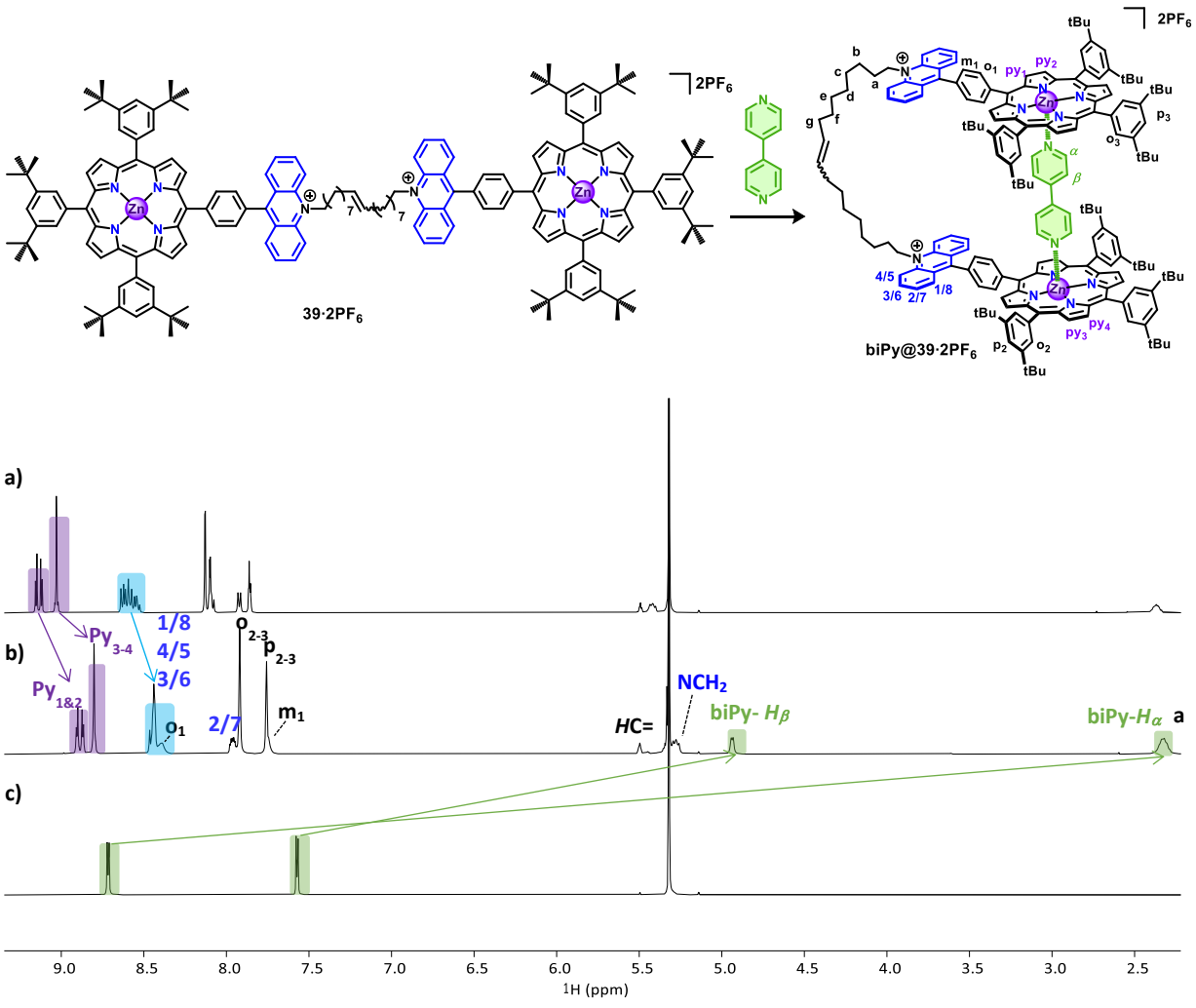

Figure 23. *Stacked ^{1}H NMR (500 MHz, CD_2Cl_2, 1.90 mM, 298 K) spectra of a)* **39·2PF$_6$**, *b)* ***biPy*@39·2PF$_6$** *and c) biPy.*

Evidence of complexation of biPy was further given via ^{1}H DOSY NMR (Figure 24), which showed a single diffusing species with the same diffusion coefficient (D = 3.8 × 10^6 cm^2 s^{-1}) for both the biPy protons and the protons of **39·2PF$_6$** (similar to that found for **39·2PF$_6$** alone, Table 3), giving a hydrodynamic radius of 13.2 Å when using a spherical model. The energy-minimised model of **biPy@39·2PF$_6$** was shown to be in agreement with the DOSY experiments, being close in size to a superimposed sphere (with 1.32 nm radius). Similarly to **DABCO@39·2PF$_6$**, the alkenyl chain was shown to partially extend outside the sphere (Figure 24).

Table 3. *Data from the DOSY NMR experiments recorded for **39·2PF$_6$** and **biPy@39·2PF$_6$***

Species	Solvent	D (× 10^6 cm^2 s^{-1})	R_h (Å)
biPy@39·2PF$_6$	CD_2Cl_2	3.80 (± 0.15)	13.2
39·2PF$_6$	CD_2Cl_2	3.80 (± 0.1)	–

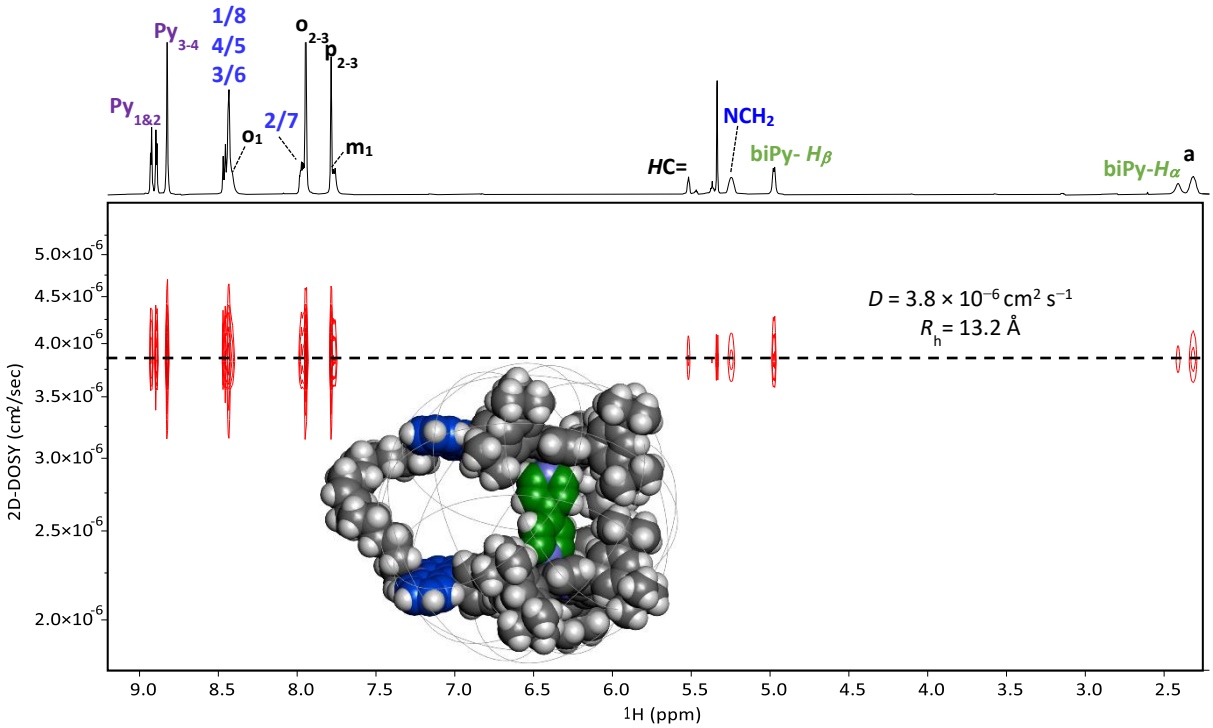

Figure 24. *^{1}H DOSY NMR (600 MHz, CD_2Cl_2, 1.90 mM, 298 K) spectrum and the energy-minimised structure of **biPy@39·2PF$_6$**, within a superimposed sphere (radius = 1.32 nm).*

The complexation of biPy was further probed via UV-Vis titrations, with up to 188 equivalents of 4,4'-bipyridine added to a micromolar solution of **39·2PF$_6$** in CH_2Cl_2. Overlayed spectra showed the presence of one isosbestic point (at 427 nm) up to 13 equivalents before slight

bathochromic shifting, with a second local isosbestic point at 433 nm (Figure 25). Fitting to a 1:2 model gave averaged binding constants of K_{11} of = 1.8 (± 0.1) ×10^5 L mol^{-1}, and K_{12} = 799 (± 130) L mol^{-1}. The 1:1 value was again found to be similar to binding constants found for other porphyrin tweezers with flexible/semi-flexible linkers.[24,25]

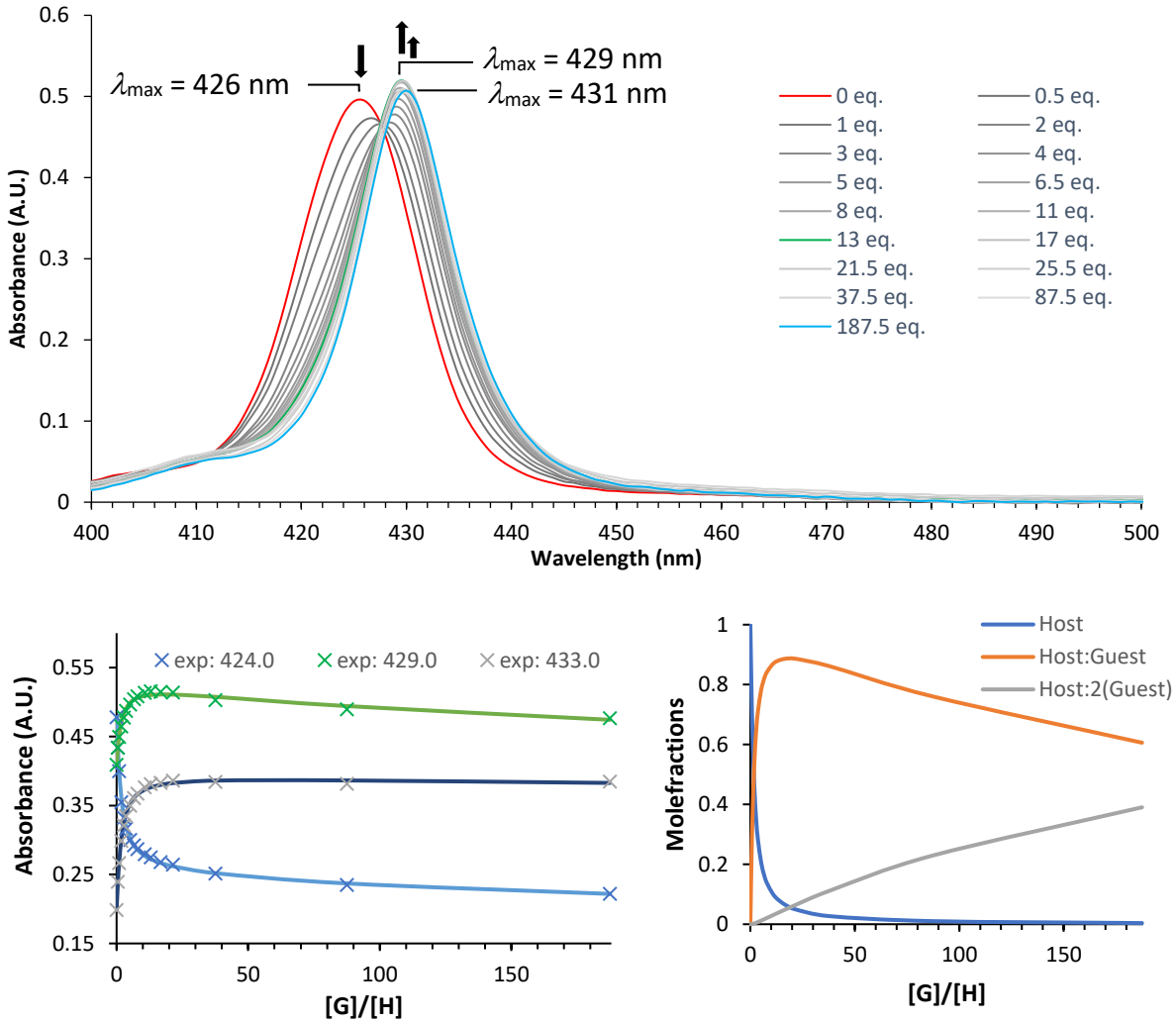

Figure 25. *UV-Vis (CH_2Cl_2, l = 0.1 cm, 298 K) titration of* ***39·2PF$_6$*** *(c = 5.28 μM) with up to 188 equivalents of biPy with the non-linear regression fit and calculated speciation diagram.*

For comparison, UV-Vis titration with **33·PF$_6$** at five micromolar in CH_2Cl_2 were conducted (Figure 26). As seen with DABCO, addition of increasing equivalents of biPy (up to 2000 equivalents) led to larger bathochromic shifts (6 nm) than seen in the 1:1 process of **39·2PF$_6$**, with a single isosbestic point at 430 nm supporting formation of one species as expected. Fitting to a 1:1 binding model gave an averaged binding constant of 3.85 (± 0.15) × 10^3 M^{-1}, 47 times smaller than that seen for **biPy@39·2PF$_6$** (Table 4).

Table 4. *Binding constants obtained for the monoacridinium porphyrin conjugate* ***33·PF$_6$*** *and the tweezer* ***39·2PF$_6$*** *when titrated with biPy in CH_2Cl_2.*

Species	Guest	Solvent	K_a (L mol^{-1})
33·PF$_6$	**biPy**	CH_2Cl_2	3.8×10^3
39·2PF$_6$	**biPy**	CH_2Cl_2	$K_{11} = 1.8 \times 10^5$ K_{12} =799

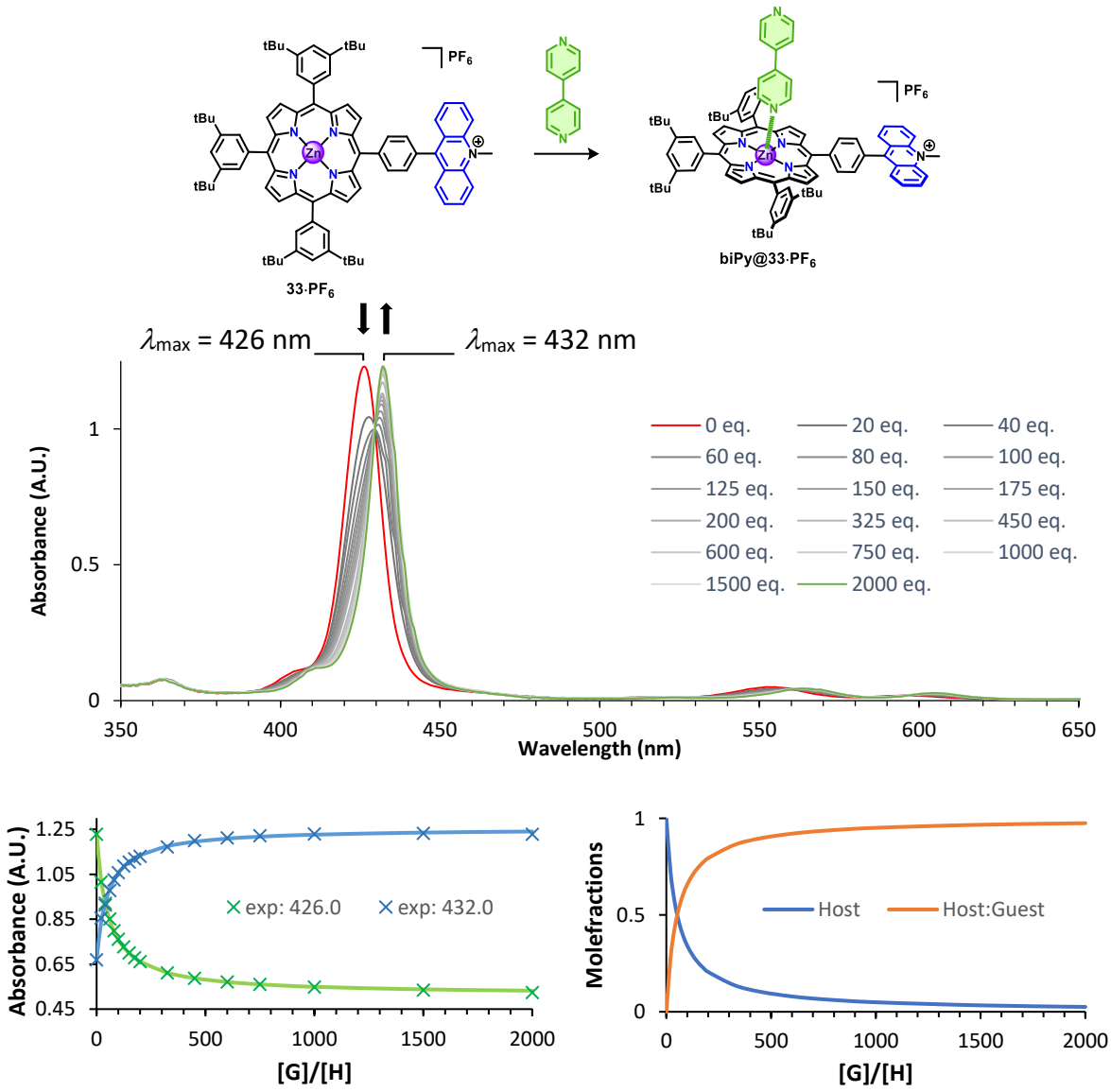

Figure 26. *UV-Vis (CH_2Cl_2, l = 0.5 cm, 298 K) titration of* ***33·PF$_6$*** *(c = 4.95 μM) with up to 2000 equivalents of biPy, and the non-linear regression fit with the accompanying calculated speciation diagram.*

The efficacy of the pre-organisation with biPy for the complexation of polyaromatic guests was probed. Due to the larger size of biPy relative to DABCO (Figure 22) it was expected that the complex should be able to bind aromatic guests such as ferrocene, which was previously utilised as a template to form the tetracationic molecular square Cyclobis(paraquat-4,4'-biphenylene) by the Stoddart group,[26,27] and similarly explored by the group as an allosteric guest.[28] Additionally, **biPy@39·2PF$_6$** may be able to bind polyaromatic molecules such as pyrene or perylene or alternatively two polyaromatic hydrocarbons in a double-decker π-stacked formation.

When studying the ability of **biPy@39·2PF$_6$** to bind taller aromatic guests, ferrocene was found to be a poor guest for the receptor likely due to its small aromatic surface area, with seemingly no significant association between **biPy@39·2PF$_6$** and guest, as assessed via ^{1}H NMR spectroscopy.

However, addition of pyrene to a two millimolar solution of **biPy@39·2PF$_6$** (with 1 eq. of biPy giving 88% complex) in CD_2Cl_2 was seen to lead to changes in the ^{1}H NMR spectrum (Figure 27). Addition of 12 equivalents of pyrene led to small upfield shifts of the acridinium peaks, with the most clearly defined being for the NCH_2 protons ($\Delta\delta NCH_2$= –0.070 ppm). This suggested possible increased electronic shielding of the acridinium protons upon addition of pyrene, in line with an acridinium-pyrene π–π interaction, as opposed to the expected downfield shift in the case of a CH-π interaction. The peaks of the pyrene protons were also observed to be upfield shifted by 0.02 ppm. Furthermore, upfield shifts of the biPy peaks ($\Delta\delta H_\beta$ ppm= –0.052 ppm) were also seen as well as sharpening of the aromatic peaks associated to **39·2PF$_6$**, suggesting a possible stabilising effect on the complex. Upon further addition of pyrene (up to 50 equivalents), downfield shifts of the porphyrin protons were observed. This could suggest a reduction in the tilting motion of the porphyrin units, reducing the contribution of the induced magnetic field effect on the chemical shifts of the pyrrolic protons. Alternatively, the downfield shift may be due to an anisotropic magnetic field effect from the bound pyrene molecules on the pyrrolic protons.

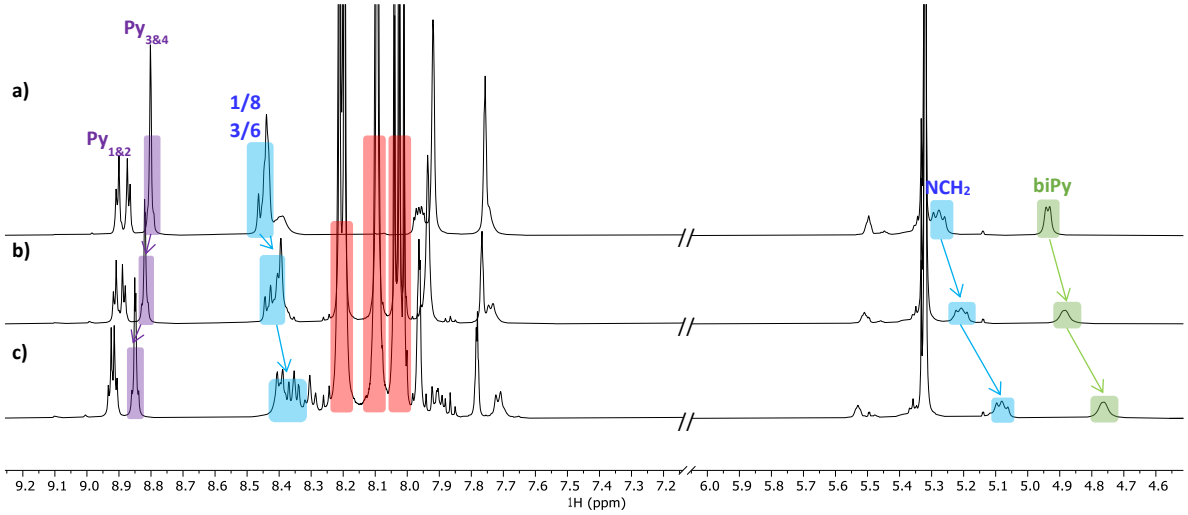

***Figure 27**. Stacked ^{1}H NMR (500 MHz, CD_2Cl_2, 1.90 mM, 298 K) spectra of a) **biPy@39·2PF$_6$**, b) **biPy@39·2PF$_6$** after addition of 12 eq. of pyrene and c) **biPy@39·2PF$_6$** after addition of 40 eq. of pyrene.*

To further probe the binding of pyrene, a ^{1}H NMR titration was performed with up to 360 equivalents of pyrene added to the solution. Fitting to a 1:1 binding model gave a low binding constant of <2 M^{-1}, while fitting of the curve to an instantaneous 1:2 binding model gave a binding constant of 25 M^{-2} (Figure 28).

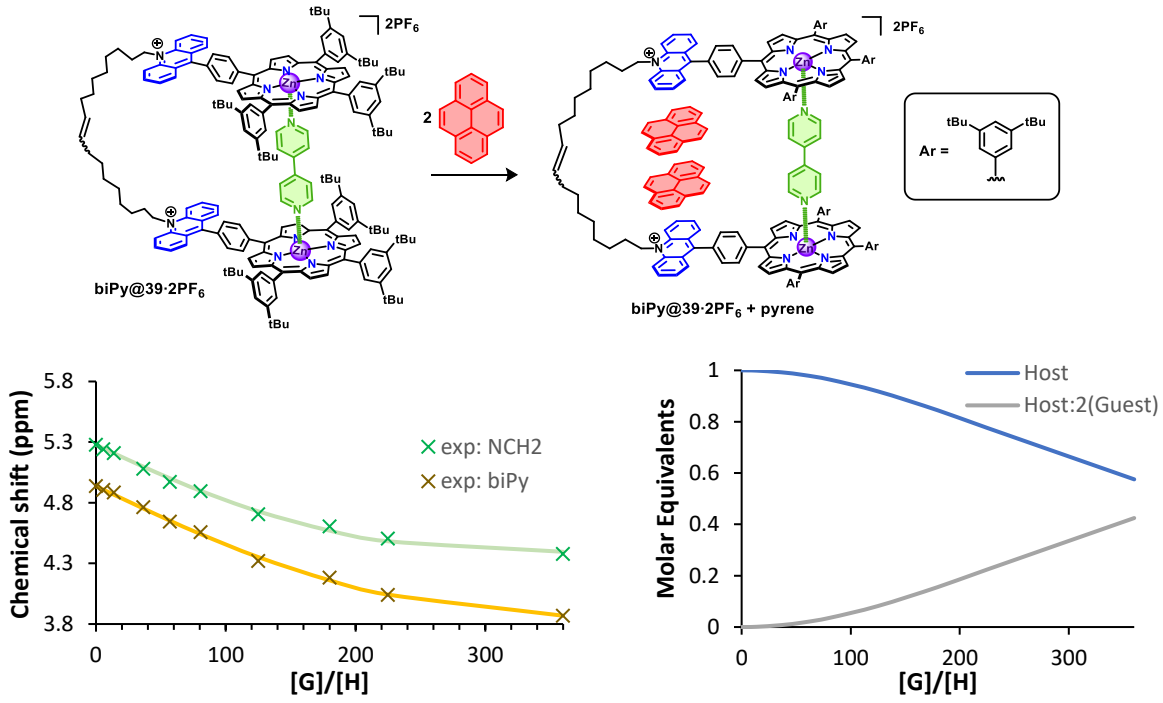

***Figure 28.** The obtained curve of the NMR titration and the non-linear regression fit for an instantaneous 1:2 model, with the calculated speciation diagram.*

5. Studies on the switchable nature of the porphyrin-acridinium tweezer 39·2PF$_6$

In addition to the binding properties of **39·2PF$_6$**, studies into its switchable properties were also conducted. As discussed in Chapter 1, both the acridinium and the porphyrin are multi-responsive unts. Thus, investigations into the effect of chemical and redox stimuli on the properties of **39·2PF$_6$** were conducted.

5.1. Study of the effects of chemical stimulus in the form of nucleophiles

As shown with the Yoshizawa group's macrocycle **20**,[29] and our research group's macrocycle **21**,[14] the acridinium is chemically responsive via nucleophilic addition to the C_9 position. Therefore, the ability of the tweezer to respond to chemical stimuli in the form of hydroxide ions was first probed.

5.1.1. NMR and Mass spectrometry studies of the chemo-switching process

Addition of 2.2 equivalents of TBAOH (40 wt.% in methanol) to a millimolar solution of **39·2PF$_6$** in CD_2Cl_2, was seen to lead to dramatic changes in the ^{1}H and ^{13}C NMR spectra. Large upfield shifts were observed for all acridinium/acridanol protons in the aromatic region of the ^{1}H NMR spectrum, in-line with loss of aromaticity upon sp3 hybridisation of the C_9 position (Figure 29a). In addition, the NCH_2 protons were similarly upfield shifted ($\Delta\delta$ = –1.2 ppm), due to the loss of the electron withdrawing nature of the acridinium, and no longer being in the direct periphery of an aromatic system (and as such experiencing a weaker anisotropic magnetic field effect). In contrast, the pyrrolic protons were not observed to be as upfield shifted, with the pyrrolic protons closest to the acridinium/acridanol unit seen to be most affected ($\Delta\delta H_{py1}$ = –0.3 ppm), emphasising that the reaction with the nucleophile was localised to the acridinium.

Similarly, in the ^{13}C NMR spectrum (Figure 29b) large upfield shifts were seen for the 9-carbon due to the change in hybridisation from sp^2 to sp^3 ($\Delta\delta C_9$= –85 ppm), consistent with a dearomatisation of the acridinium to form the acridanol (Figure 29).

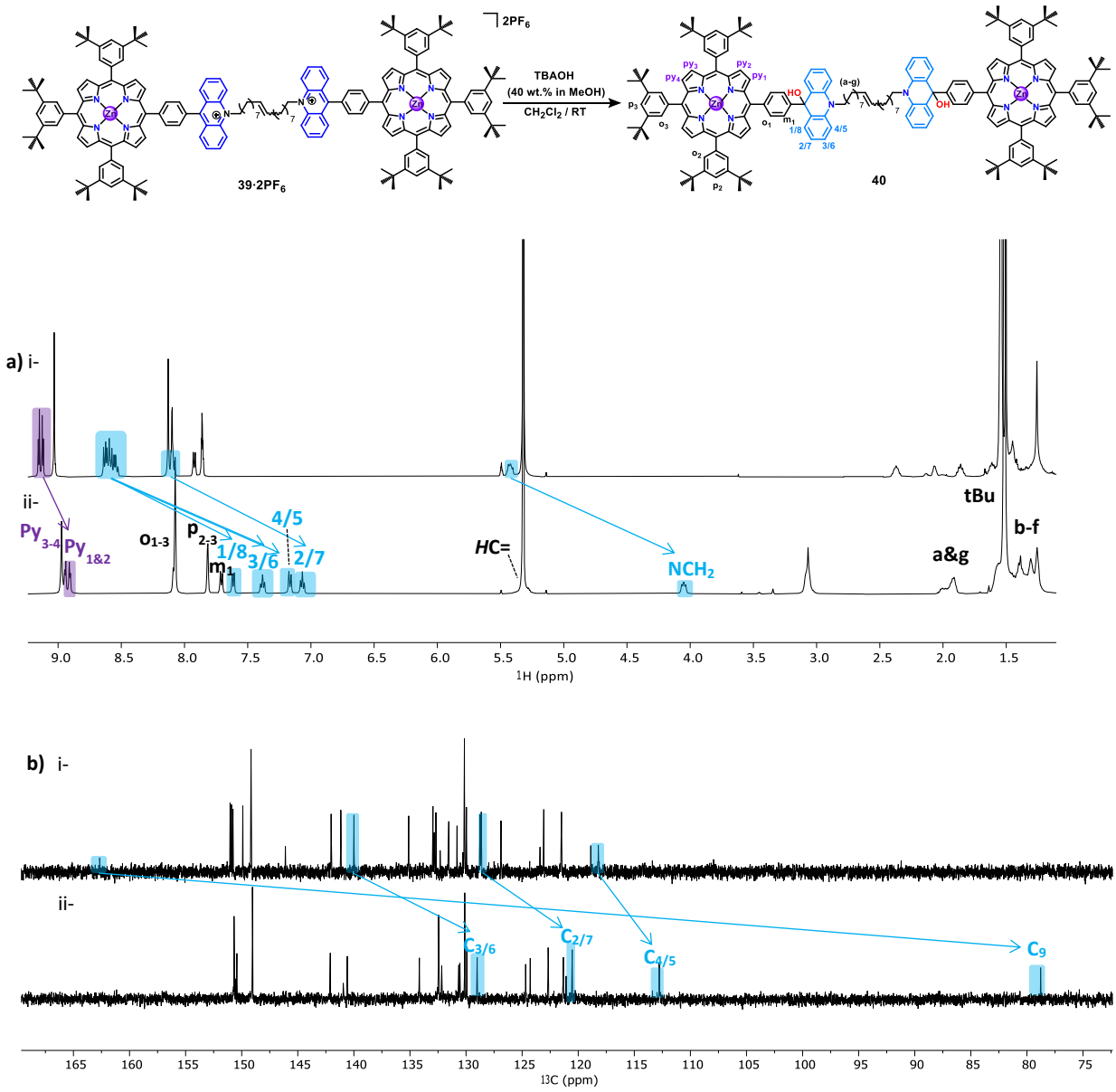

Figure 29. *Stacked a) ^{1}H NMR (500 MHz, CD_2Cl_2, 1.00 mM, 298 K) and b) ^{13}C NMR (125 MHz, CD_2Cl_2, 1.00 mM, 298 K) spectra of i-* ***39·2PF$_6$*** *and ii-* ***40*** *formed after addition of TBAOH.*

Further characterisation of the molecule was attempted via electrospray ionisation mass spectrometry. However due to the ionisation method and the sensitivity of the C-OH bond, it was found that the major ion obtained was that of the acridinium-porphyrin tweezer ($[M-2OH]^{2+}$, m/z = 1314.73, Figure 30). Nevertheless, mass ion peaks related to various other derivative structures of the tweezer formed upon ionisation were seen, including $[M-OH]^{+}$ (m/z = 2646.46), $[M-2OH+H]^{+}$ (m/z = 2630.46) and $[M-2OH+MeO]^{+}$ (m/z = 2660.47), at intensities of < 5% relative to the major mass ion peak. In the case of the latter two species, the hydro and methoxy group are likely due to ionisation of the solvent mixture (CH_3OH/H_2O).

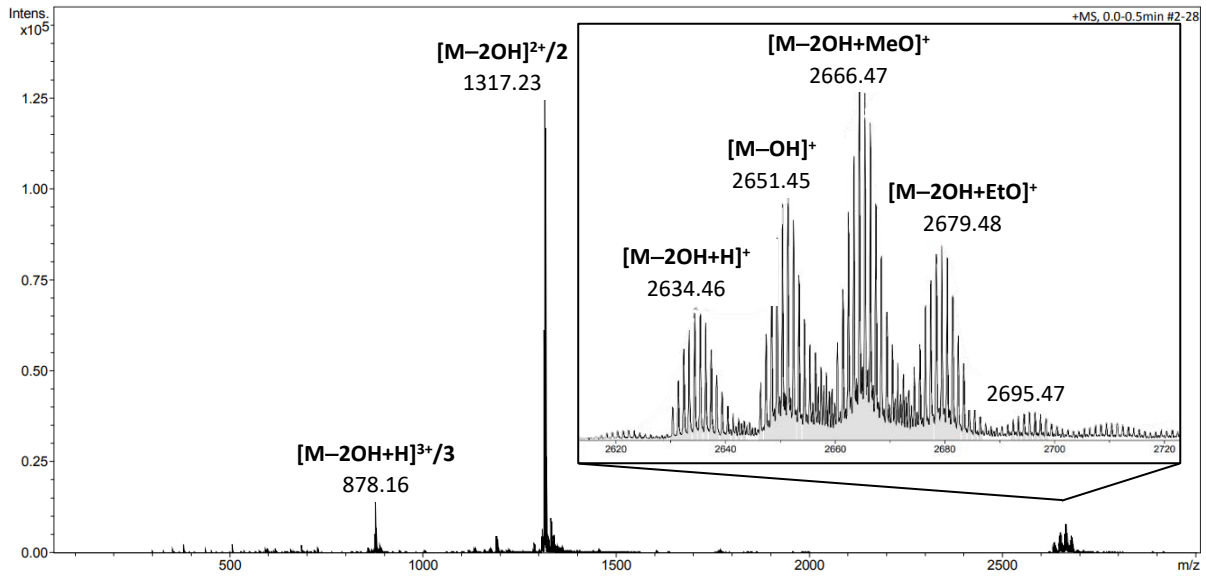

Figure 30. *Mass spectrum (ESI-TOF) obtained for* ***40****, with zoom-insert of the region m/z = 2600 - 2700, showing the singly charged derivative species.*

5.1.2. UV-Vis study of the chemo-switching process

Due to the large change in aromaticity upon nucleophilic addition, UV-Vis spectroscopy could be used to follow and confirm the formation of the acridanol species, with the phenyl acridanol known to have a π–π* transition absorbance band at a wavelength significantly bathochromically shifted compared to the phenyl acridinium.[30] Accordingly , it was observed that addition of 2.2 equivalents of TBAOH to **39·2PF$_6$** led to a flattening of the acridinium π-π* bands, (λ_{max} = 363 & 348 nm) and the rise of a new bathochromically shifted band at around 300 nm, in-line with formation of the acridanol species (Figure 31). However, upon subsequent addition of 2.2 equivalents of TFA, flattening of the acridanol band and recovery of the acridinium π-π* bands and was seen, with a similar absorbance intensity to the band prior to addition of the nucleophile. This indicated near quantitative conversion back to the acridinium. Additionally, no demetallation of the Zn(II)-porphyrin units could be observed for the Q-bands, in accordance with the higher reactivity and acid-sensitivity of the acridanol relative to the Zn(II)-porphyrin. Via a fatigue cycle, it was found that no significant drop in conversion was seen after five cycles, indicating a robust species. (Figure 31).

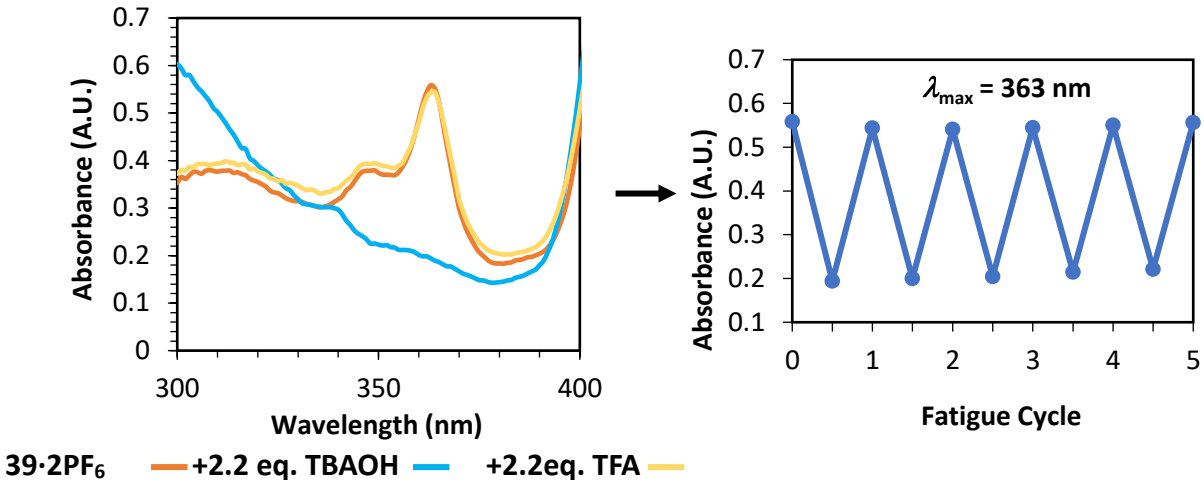

Figure 31. *Overlayed UV-Vis spectra (CH_2Cl_2, 0.1 mM, l = 0.1 cm, 298 K) of* **39·2PF$_6$** *showing the effect of addition of 2.2 equivalents of TBAOH, followed by 2.2 equivalents of TFA on the acridinium's π–π* band.*

5.1.3. Fluorescence study of the chemo-switching process

In addition, the effects of chemical stimulus were probed via fluorescence spectroscopy with no fluorescence seen for **39·2PF$_6$** upon excitation of the Zn(II)-porphyrin Q-band (at 562 nm).

Transient absorption spectroscopy experiments conducted by collaborators Dr. Barbara Ventura and Daniel Sanchez-Resá, showed that the spectra of **39·2PF$_6$** contained features corresponding to both the radical cation Zn(II)-porphyrin and the acridinium radical species. This was in accordance with photoinduced electron transfer from the Zn(II)-porphyrin to the acridinium, forming the charge-separated state (Figure 32). This species was again observed to be short-lived, relaxing to the ground state within 1 ps.

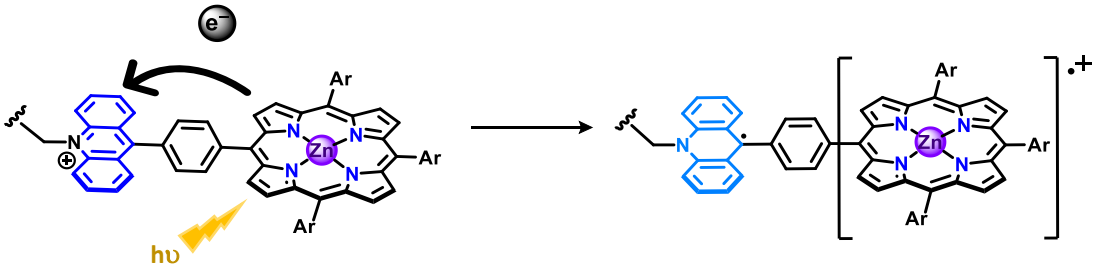

Figure 32. *Illustrative schematic of the photo-induced electron transfer process that takes place upon excitation of the porphyrin units of* ***39·2PF$_6$****.*

In contrast, for **40** fluorescence of the porphyrin units was observed upon excitation of the Zn(II)-porphyrin units' Q-band at 553 nm (Figure 33). When exciting the acridanol units (at 292 nm) the fluorescence of the acridanol species was seen to be quenched, and that of the Zn(II)-porphyrin units sensitised, indicating energy transfer from the acridanol units to the porphyrin units upon excitation. Thus, chemical stimulus could be used as a fluorescence switch, with addition of nucleophiles also giving rise to a change from electron to energy transfer.

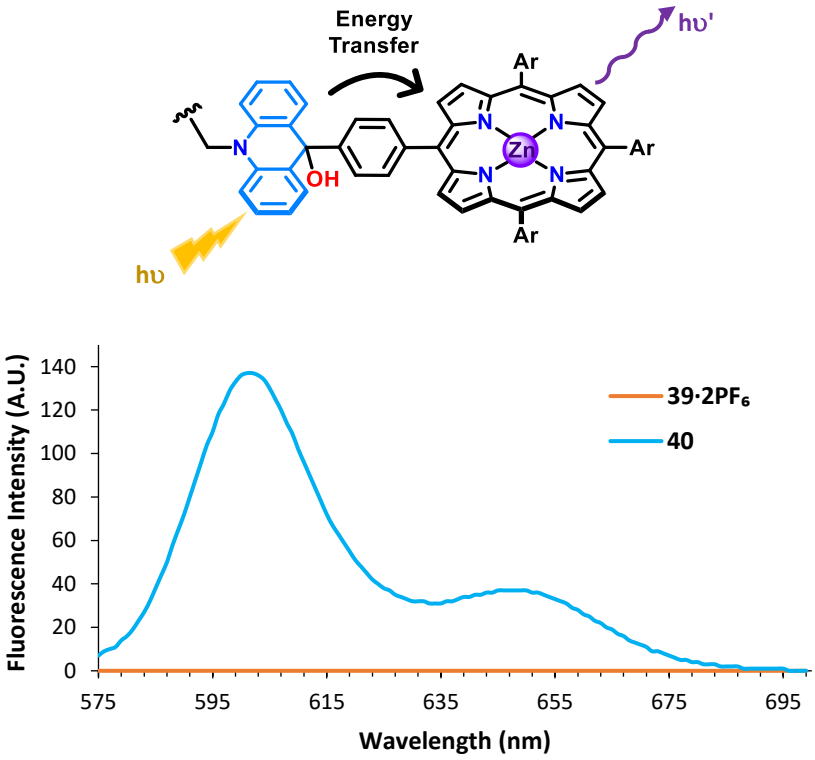

Figure 33. *Overlayed fluorescence spectra (CH_2Cl_2, 298 K) showing the intensity of fluorescence of* ***39·2PF₆*** *and* ***40*** *(c = 5.00 μM) upon excitation of the Zn(II)-porphyrin Q band (λ_{ex} = 553 nm).*

5.2. Effects of chemo-switching on the binding of biPy

The ability of **40** to bind biPy was assessed via NMR and UV-Vis spectroscopy. Addition of an equivalent of biPy to a millimolar solution of **40** in CD_2Cl_2 gave rise to similar changes in the ^{1}H NMR spectrum as seen previously with **39·2PF₆** (Figure 34). The biPy protons were significantly shifted with respect to free biPy ($\Delta\delta H_{biPy\text{-}\alpha}$ = –6.4 ppm, $\Delta\delta H_{biPy\text{-}\beta}$ = –2.7 ppm), in accordance with its binding to the two Zn(II)-porphyrin units. Additionally, upfield shifts could

be seen for the porphyrin protons, most significantly for the pyrrolic protons ($\Delta\delta H_{py}$ = –0.25 ppm). Interestingly, in contrast to the acridinium protons of **39·2PF$_6$**, the acridanol peaks were not observed to be upfield shifted, likely due to the loss of planarity and increased flexibility upon dearomatisation.

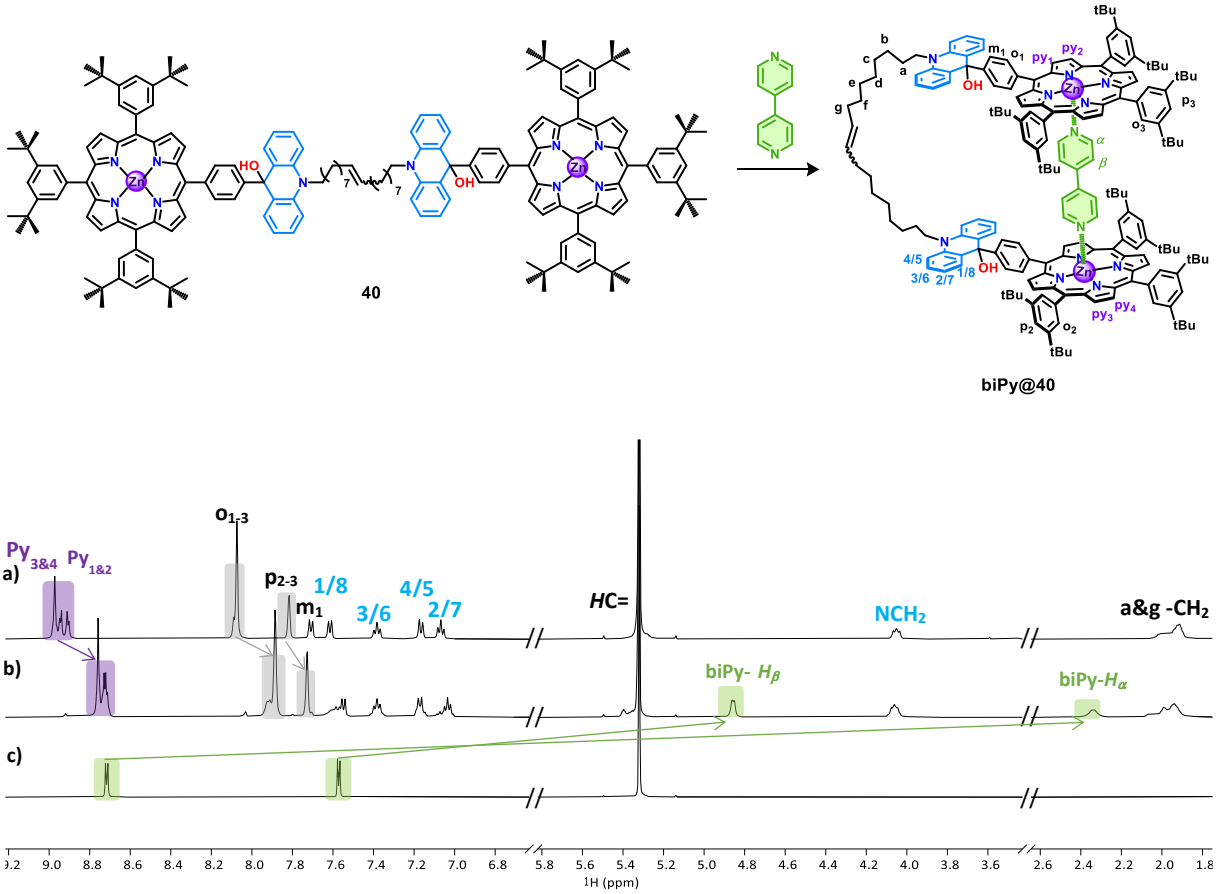

Figure 34. *Stacked ^{1}H NMR (500 MHz, CD_2Cl_2, 2.03 mM, 298 K) spectra of a)* ***40*** *upon addition of b) one equivalent of biPy forming* ***biPy@40****. A ^{1}H NMR spectrum of c) 4,4'-bipyridine is included for comparison.*

DOSY NMR further confirmed the complexation of biPy (Figure 35), which diffused with the same diffusion coefficient as **40** (4.05×10^{-6} cm^{2}s^{-1}). The diffusion coefficient for the complex was slightly larger than found for **40** alone (3.75×10^{-6} cm^{2}s^{-1}, Table 5) in contrast to **39·2PF$_6$**, with a hydrodynamic radius of 1.24 nm calculated for **biPy@40**. As with **biPy@39·2PF$_6$**, the energy minimised (Spartan'20) structure **biPy@40** was shown to agree with the DOSY experiments, being close in-size to a superimposed sphere of the same radius (1.24 nm), with the flexible alkenyl chain partially extending past the radius of the sphere (Figure 35).

Table 5. *Data from the DOSY NMR experiments recorded for* ***39·2PF$_6$*** *and* ***biPy@39·2PF$_6$****.*

Species	Solvent	D (× 10^6 cm^2 s^{-1})	R_h (Å)
biPy@40	CD_2Cl_2	4.05 (± 0.11)	12.4
40	CD_2Cl_2	3.75 (± 0.09)	–

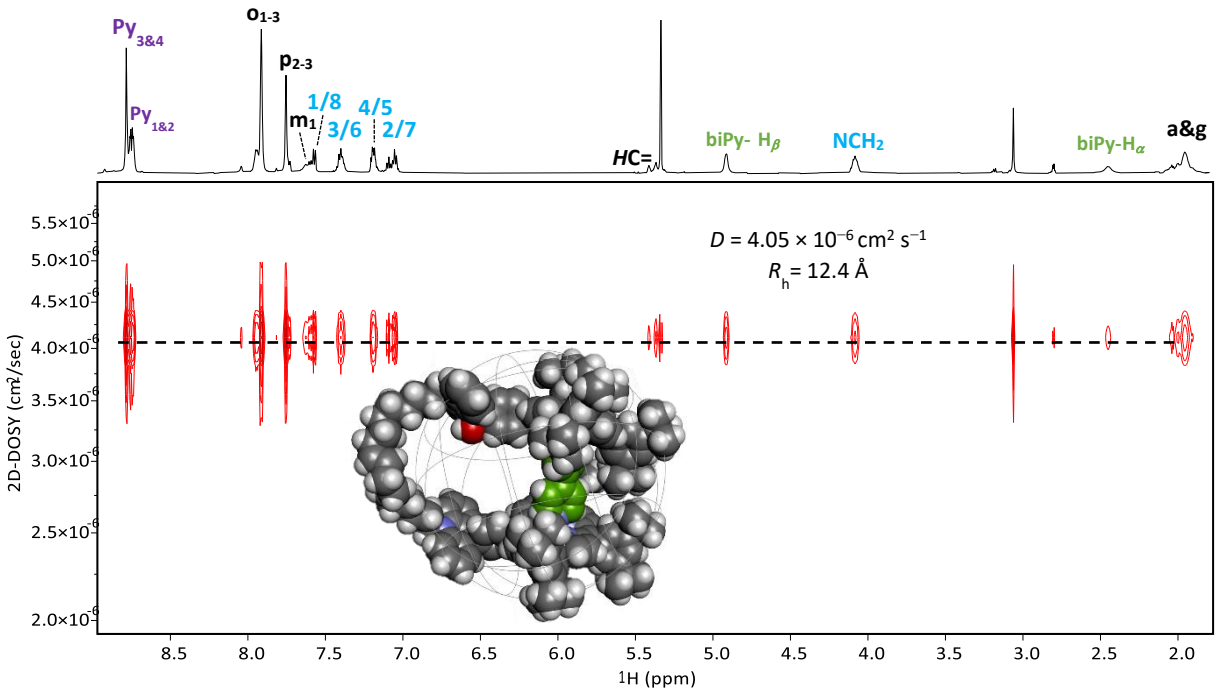

Figure 35. *^{1}H DOSY NMR (600 MHz, CD_2Cl_2, 2.03 mM, 298 K) spectrum of* ***biPy@40*** *(diffusion coefficient and hydrodynamic radius are displayed), and the energy minimised (Spartan'20) structure of the complex within a sphere of radius = R_h.*

UV-Vis titrations in CH_2Cl_2 at micromolar concentrations (Figure 36) revealed little difference between **biPy@39·2PF$_6$** and **biPy@40**. Addition of up to 488 equivalents of biPy was seen to lead to similar changes in the Soret band, with an initial bathochromic shift by 3 nm upon addition of up to 11 equivalents (local isosbestic point at 427 nm), and further bathochromic shifts upon addition of further excess (second local isosbestic point at 432 nm). Accordingly, association constants similar to those found for **39·2PF$_6$** (Table 6), were found for both the 1:1 **biPy@40** species (K_{11} = 1.4 (±0.3) × 10^5 M^{-1}) and the 1:2 **(biPy)$_2$@40** species (K_{12} = 870 (± 200) M^{-1}).

Table 6. *Binding constants obtained via UV-Vis titrations of the two tweezers* ***40*** *and* ***39·2PF$_6$****, with biPy.*

Species	Guest	Solvent	K_a (L mol^{-1})
40	**biPy**	CH_2Cl_2	$K_{11} = 1.4 \times 10^5$ $K_{12} = 870$
39·2PF$_6$	**biPy**	CH_2Cl_2	$K_{11} = 1.8 \times 10^5$ $K_{12} = 799$

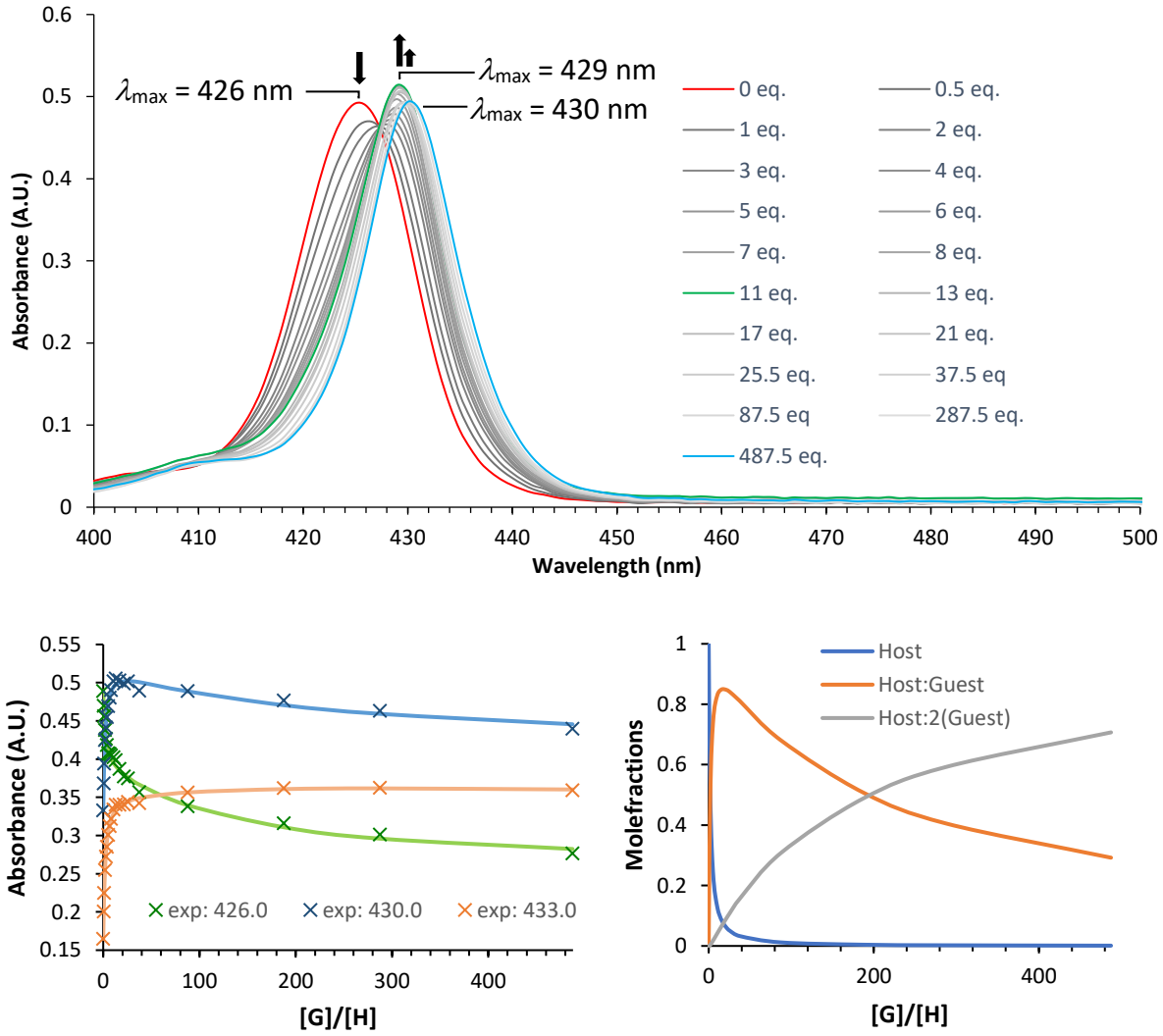

Figure 36. *UV-Vis (CH_2Cl_2, l = 0.1 cm, 298 K) titration of* ***40*** *(c = 5.74 μM) with up to 488 equivalents of biPy, with the non-linear regression fit of the obtained curves, and the calculated speciation diagram.*

5.3. Study of the effects of redox stimulus

Initial cyclic voltammograms of **39·2PF$_6$** showed, a reversible oxidation wave for the two porphyrin units at $E_{1/2}$ = 0.750 V vs. SCE, and a reversible wave for the reduction of the two acridinium units at $E_{1/2}$ = −0.535 V vs. SCE (Figure 37a). Upon addition of an equivalent of biPy (Fig. 37b), a notable cathodic shift was seen for the oxidation wave ($\Delta E_{1/2}$ = −57 mV). This was assigned to the donation of electron density from biPy upon coordination to the Zn(II)-porphyrin, which would decrease the required potential to oxidise the porphyrin.

The redox properties of **40** were also investigated, to quantify the effects of the acridinium relative to the acridanol, and further probe the effect of ligand coordination in mediating the ease with which the porphyrin species is oxidised. Initial recorded cyclic voltammograms showed, similarly to **39·2PF$_6$**, the presence of a reversible wave for the porphyrin (Figure 37c). Regarding the porphyrin, it was found that switching to the acridanol species significantly increased the ease of oxidation of the porphyrin by approximately 48 mV. Addition of biPy was shown to have a similar effect as seen for **39·2PF$_6$** (Figure 37d), with coordination of biPy increasing the electron density of the porphyrin components. However, the shift was to a lower degree ($\Delta E_{1/2}$ = −19 mV) than seen for **39·2PF$_6$**, thought to be due to the absence of the electron withdrawing acridinium moiety.

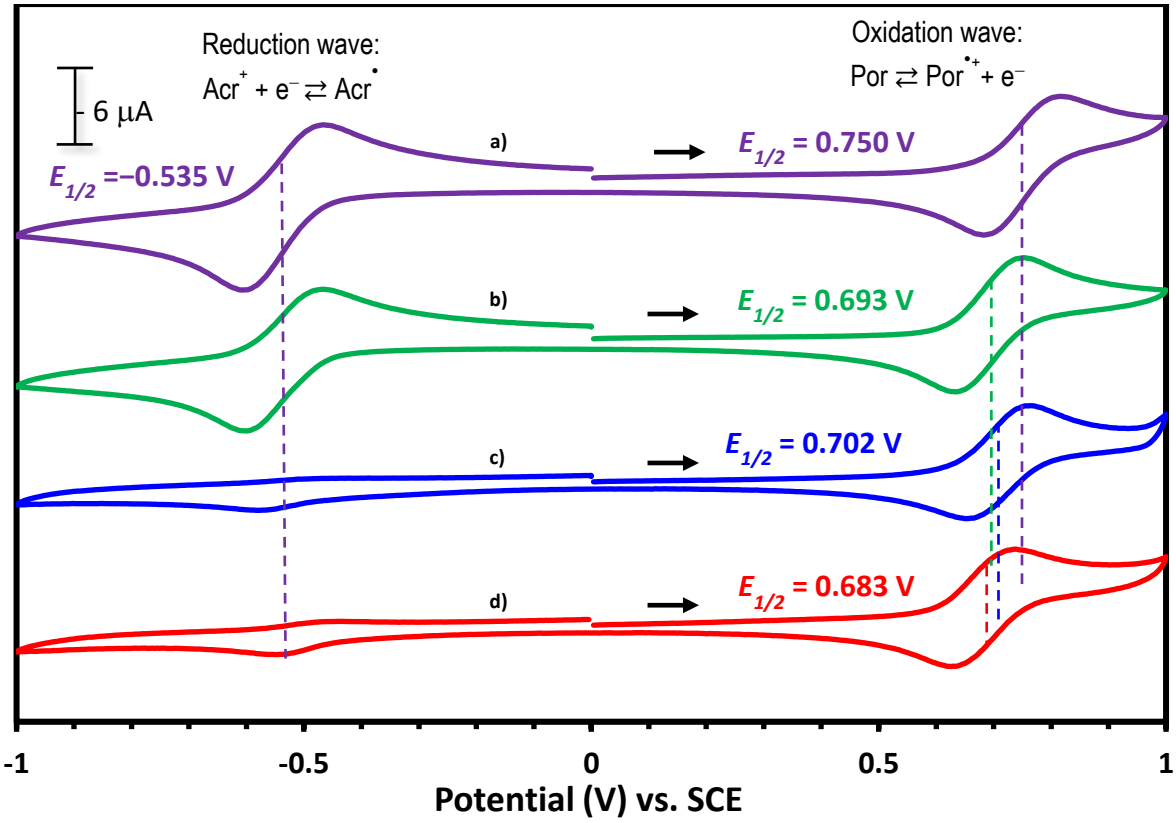

Figure 37. *Stacked cyclic voltammograms ($C_2H_4Cl_2$, 1.00 mM, 0.1 M $TBAPF_6$, 100 mV/s, WE: Pt, CE: Pt, Ref: $Hg/Hg_2Cl_2/KCl$ sat., 298 K) comparing the E_{ox} and E_{red} of a)* ***39·2PF6****, b)* ***biPy@39·2PF6****, c)* ***40****, and d)* ***biPy@40****.*

A thermodynamic cycle was used to quantify the oxidation effect on the biPy binding constants (Figure 38), with decreased binding constants found for both tweezers (Table 7). However, the extent of this decrease was not equivalent for the two tweezers. For the oxidised form of the porphyrin-acridinium tweezer (**39**$^{4+}$) the binding constant was estimated as 2.1 × 10^3 M^{-1} (approximately 86 times larger than that found for **39·2PF6** (K_a = 1.8 × 10^5 M^{-1}). In contrast, for the oxidised form of the porphyrin-acridanol tweezer (**40**$^{2+}$) the binding constant was estimated to be 3.1 × 10^4 M^{-1}, 4.5 times smaller than that found for **40** (K_a = 1.4 × 10^5 M^{-1}).

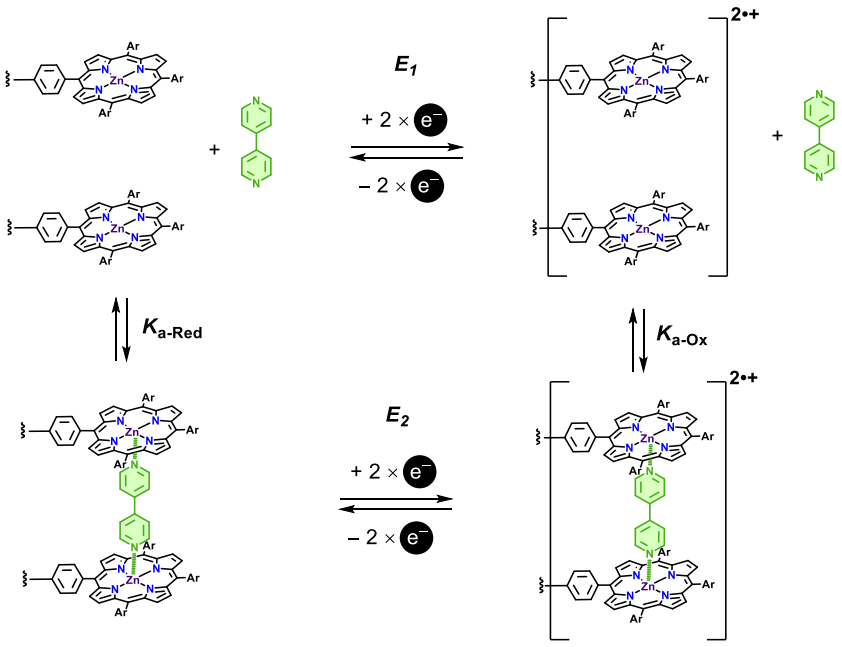

Figure 38. *Square scheme for the oxidation of the porphyrin tweezer, showing the thermodynamic cycle which allows calculation of the binding constant for the oxidised tweezers.*

This feature amounted to a remote control of biPy binding via chemical and redox stimuli at the acridinium/acridanol site, illustrating the differing properties of the eight distinct states accessible from **39·2PF$_6$** (Figure 39). As such, the binding and switching studies showed that **39·2PF$_6$** is a flexible and complex multi-responsive receptor, able to bind DABCO or biPy, respond to chemical and/or redox stimulus, and further use stimuli to control and tune binding affinity.

Table 7. *showing the associated binding constants for the tweezers, and the effect of oxidation on these value*

	39^{2+} + biPy ⇄ biPy@39^{2+}	**39^{4+}+ biPy ⇄ biPy@39^{4+}**	**40+ biPy ⇄ biPy@40**	**40^{2+}+ biPy ⇄ biPy@40^{2+}**
K_a (L mol^{-1})	1.8×10^5	2.1×10^3	1.4×10^5	3.1×10^4

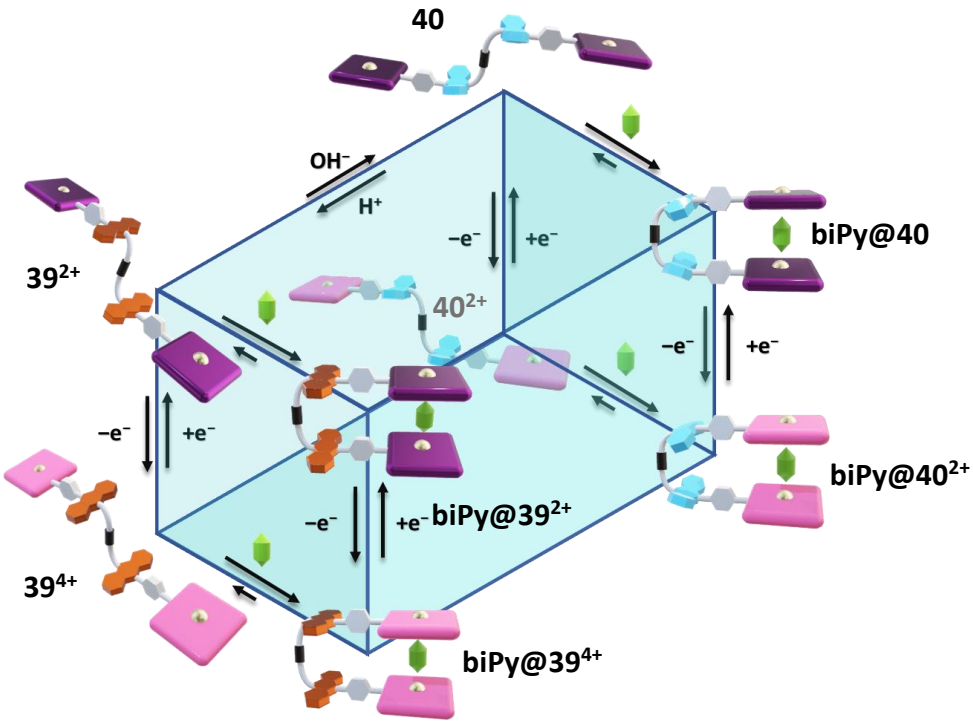

Figure 39. *Cubic graphical diagram illustrating the eight distinct states which can be accessed from* ***39·2PF$_6$****.*

6. Conclusions

In conclusion, a porphyrin-acridinium tweezer has been successfully synthesised via olefin metathesis. Due to the flexible linker, the tweezer is able to bind both DABCO and 4,4'-bipyridine to form macrocyclic complexes at binding constants 20 and 40 times higher than the related mono acridinium porphyrin conjugate. The ability of the macrocyclic complexes to encapsulate pyrene were probed for both, with DABCO found to be a poor effector for the tweezer due to the presence of steric clashes.

In addition, the multi-stimuli responsive nature of both moieties has been exploited, with the ability to form a neutral tweezer via addition of nucleophiles. This was not initially seen to affect the binding properties with regards to complexation of 4,4'-bipyridine. However, when combining chemical and redox stimulus, the ability to remotely control the binding of 4,4'-bipyridine was revealed with dearomatisation of the acridinium shown to tune and lessen the effect of oxidation, leading to characterisation of a multi-state system.

7. References

(1) Chen, C. W.; Whitlock, H. W. Molecular Tweezers: A Simple Model of Bifunctional Intercalation. *J. Am. Chem. Soc.* **1978**, *100* (15), 4921–4922.

(2) Gakh, A. A. *Molecular Devices*; John Wiley & Sons, Inc.: Hoboken, NJ, USA, 2018.

(3) Hardouin–Lerouge, M.; Hudhomme, P.; Sallé, M. Molecular Clips and Tweezers Hosting Neutral Guests. *Chem. Soc. Rev.* **2011**, *40* (1), 30–43.

(4) Han, Y.; Tian, Y.; Li, Z.; Wang, F. Donor-Acceptor-Type Supramolecular Polymers on the Basis of Preorganized Molecular Tweezers/ Guest Complexation. *Chem. Soc. Rev* **2018**, *47*, 5165–5176.

(5) Valderrey, V.; Aragay, G.; Ballester, P. Porphyrin Tweezer Receptors: Binding Studies, Conformational Properties and Applications. *Coord. Chem. Rev.* **2014**, *258–259*, 137–156.

(6) Lee, C.-H.; Yoon, H.; Jang, W.-D. Biindole-Bridged Porphyrin Dimer as Allosteric Molecular Tweezers. *Chem. Eur. J.* **2009**, *15* (39), 9972–9976.

(7) Jokic, D.; Boudon, C.; Pognon, G.; Bonin, M.; Schenk, K. J.; Gross, M.; Weiss, J. Structural and Binding Features of Cofacial Bis-Porphyrins with Calixarene Spacers: Pac-Man Porphyrins That Can Chew. *Chem. Eur. J.* **2005**, *11* (14), 4199–4209.

(8) Grubbs, R. H. Introduction. In *Handbook of Metathesis*; Grubbs, R. H., Ed.; Wiley-VCH Verlag GmbH: Weinheim, Germany, 2003; pp 1–3.

(9) Grubbs, R. H. Olefin-Metathesis Catalysts for the Preparation of Molecules and Materials (Nobel Lecture). *Angew. Chem. Int. Ed.* **2006**, *45* (23), 3760–3765.

(10) Schrock, R. R. Multiple Metal–Carbon Bonds for Catalytic Metathesis Reactions (Nobel Lecture). *Angew. Chem. Int. Ed.* **2006**, *45* (23), 3748–3759.

(11) Quaglio, D.; Zappia, G.; de Paolis, E.; Balducci, S.; Botta, B.; Ghirga, F. Olefin Metathesis Reaction as a Locking Tool for Macrocycle and Mechanomolecule Construction. *Org. Chem. Front.* **2018**, *5* (20), 3022–3055.

(12) Zhu, B.; Chen, H.; Lin, W.; Ye, Y.; Wu, J.; Li, S. Template-Directed Synthesis of Flexible Porphyrin Nanocage and Nanorings via One-Step Olefin Metathesis. *J. Am. Chem. Soc.* **2014**, *136* (43), 15126–15129.

(13) Taesch, J.; Heitz, V.; Topić, F.; Rissanen, K. Templated Synthesis of a Large and Flexible Covalent Porphyrinic Cage Bearing Orthogonal Recognition Sites. *Chem. Commun.* **2012**, *48* (42), 5118–5120.

(14) Hu, J.; Ward, J. S.; Chaumont, A.; Rissanen, K.; Vincent, J.; Heitz, V.; Jacquot de Rouville, H.-P. A Bis-Acridinium Macrocycle as Multi-Responsive Receptor and Selective Phase-Transfer Agent of Perylene. *Angew. Chem. Int. Ed.* **2020**, *59* (51), 23206–23212.

(15) Mongin, C.; Ardoy, A.; Mereau, R.; Bassani, D.; Bibal, B. Singlet Oxygen Stimulus for Switchable Functional Organic Cages. *Chem. Sci.* **2020**, *11* (6), 1478–1484.

(16) Bakker, J. M.; Langford, S. J.; Latter, M. J.; Lee, K. A.; Woodward, C. P. Template-Directed Assembly of a Macrocyclic Porphyrin Tetramer Using Olefin Metathesis. *Aus. J. Chem.* **2005**, *58* (11), 757–761.

(17) van Gerven, P. C. M.; Elemans, J. A. A. W.; Gerritsen, J. W.; Speller, S.; Nolte, R. J. M.; Rowan, A. E. Dynamic Combinatorial Olefin Metathesis: Templated Synthesis of Porphyrin Boxes. *Chem. Commun.* **2005**, *28*, 3535–3537.

(18) Ishida, T.; Morisaki, Y.; Chujo, Y. Synthesis of Covalently Bonded Nanostructure from Two Porphyrin Molecular Wires Leading to a Molecular Tube. *Tetrahedron Lett.* **2006**, *47* (30), 5265–5268.

(19) Youm, K.-T.; Nguyen, S. T.; Hupp, J. T. Hollow Porphyrin Prisms: Modular Formation of Permanent, Torsionally Rigid Nanostructures via Templated Olefin Metathesis. *Chem. Commun.* **2008**, *29*, 3375–3377.

(20) Kang, B.; Kurutz, J. W.; Youm, K.-T.; Totten, R. K.; Hupp, J. T.; Nguyen, S. T. Catalytically Active Supramolecular Porphyrin Boxes: Acceleration of the Methanolysis of Phosphate Triesters via a Combination of Increased Local Nucleophilicity and Reactant Encapsulation. *Chem. Sci.* **2012**, *3* (6), 1938–1944.

(21) Totten, R. K.; Ryan, P.; Kang, B.; Lee, S. J.; Broadbelt, L. J.; Snurr, R. Q.; Hupp, J. T.; Nguyen, S. T. Enhanced Catalytic Decomposition of a Phosphate Triester by Modularly Accessible Bimetallic Porphyrin Dyads and Dimers. *Chem. Commun.* **2012**, *48* (35), 4178–4180.

(22) Sanford, M. S.; Love, J. A.; Grubbs, R. H. Mechanism and Activity of Ruthenium Olefin Metathesis Catalysts. *J. Am. Chem. Soc.* **2001**, *123* (27), 6543–6554.

(23) Dias, E. L.; Nguyen, S. T.; Grubbs, R. H. Well-Defined Ruthenium Olefin Metathesis Catalysts: Mechanism and Activity. *J. Am. Chem. Soc.* **1997**, *119* (17), 3887–3897.

(24) Solladié, N.; Aziat, F.; Bouatra, S.; Rein, R. Bis-Porphyrin Tweezers: Rigid or Flexible Linkers for Better Adjustment of the Cavity to Bidentate Bases of Various Size. *J. Porphyr. Phthalocyanines* **2008**, *12* (12), 1250–1260.

(25) Lee, Y. J.; Kang, B.; Seo, J. Metalloporphyrin Dimers Bridged by a Peptoid Helix: Host-Guest Interaction and Chiral Recognition. *Molecules* **2018**, *23* (11), 2741–2754.

(26) Ashton, P. R.; Menzer, S.; Raymo, F. M.; Shimizu, G. K. H.; Stoddart, J. F.; Williams, D. J. The Template-Directed Synthesis of Cyclobis(Paraquat-4,4′-Biphenylene). *Chem. Commun.* **1996**, *4*, 487–490.

(27) Asakawa, M.; Ashton, P. R.; Menzer, S.; Raymo, F. M.; Stoddart, J. F.; White, A. J. P.; Williams, D. J. Cyclobis(Paraquat-4,4′-Biphenylene)–an Organic Molecular Square. *Chem. Eur. J.* **1996**, *2* (7), 877–893.

(28) Henkelis, J. J.; Blackburn, A. K.; Dale, E. J.; Vermeulen, N. A.; Nassar, M. S.; Stoddart, J. F. Allosteric Modulation of Substrate Binding within a Tetracationic Molecular Receptor. *J. Am. Chem. Soc.* **2015**, *137* (41), 13252–13255.

(29) Kurihara, K.; Yazaki, K.; Akita, M.; Yoshizawa, M. A Switchable Open/Closed Polyaromatic Macrocycle That Shows Reversible Binding of Long Hydrophilic Molecules. *Angew. Chem. Int. Ed.* **2017**, *56* (38), 11360–11364.

(30) Zhou, D.; Khatmullin, R.; Walpita, J.; Miller, N. A.; Luk, H. L.; Vyas, S.; Hadad, C. M.; Glusac, K. D. Mechanistic Study of the Photochemical Hydroxide Ion Release from 9-Hydroxy-10-Methyl-9-Phenyl-9,10-Dihydroacridine. *J. Am. Chem. Soc.* **2012**, *134* (28), 11301–11303.

4

SYNTHESIS AND STUDY OF THE CAGE RECEPTOR

1. Introduction

Having synthesised the tweezer successfully via alkene metathesis and evidenced the role of the acridinium units in modulating the properties of the host, attention was turned to synthesis of the cage. As stated and shown with the syntheses of **33·PF$_6$** and **35·2PF$_6$** (Chapter 2, section 4), synthesis via porphyrin condensation allows for the direct attainment of differently *meso* substituted conjugates. Thus, focus was placed on the synthesis of a *tetrakis* alkene-functionalised acridinium porphyrin conjugate which would enable synthesis of a molecular cage via olefin metathesis (Figure 1).

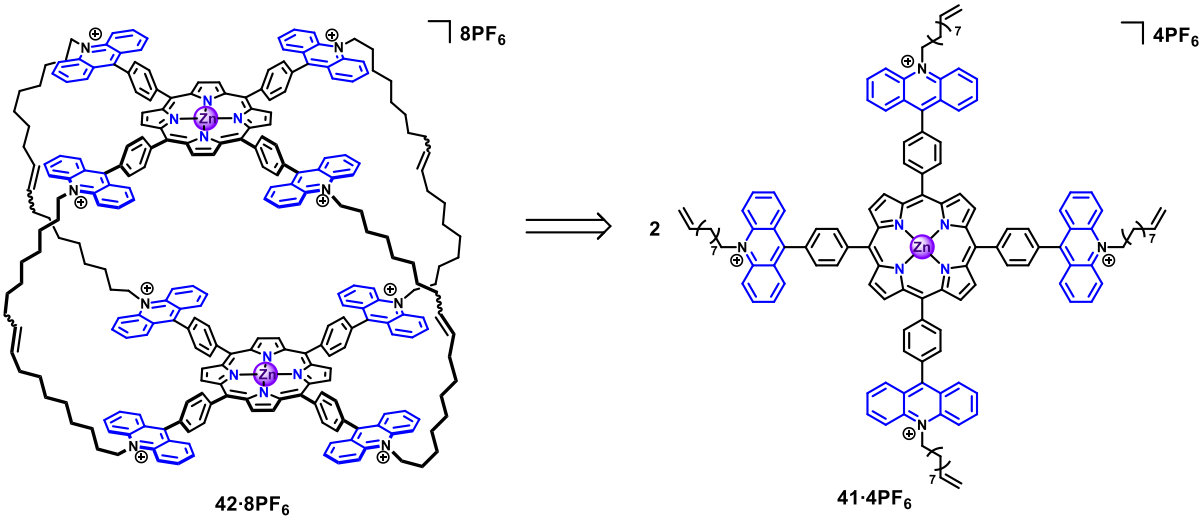

Figure 1. *Retrosynthetic scheme for the synthesis of an octaacridinium porphyrin cage (**42·8PF$_6$**) via olefin metathesis of a tetrakisacridinium porphyrin conjugate (**41·4PF$_6$**).*

In direct contrast to molecular tweezers, molecular cages have three-dimensional enclosed cavities. Despite this, the general allosteric mechanism envisioned for the porphyrin-acridinium tweezer would apply for the porphyrin-acridinium cage. Additionally, as a multitopic host with multiple acridinium binding sites, the cage could potentially bind up to four polyaromatic molecules (when using DABCO as an effector). Finally, as the cage would feature more acridinium units than the tweezer, the response of the host to different stimuli (chemical and redox) would be more pronounced, with the eight acridinium units giving a larger cumulative effect than the two of the tweezer.

2. Synthesis of an A_4 porphyrin-acridinium conjugate via porphyrin condensation

Using the same general porphyrin condensation methodology as used for previous conjugates (Chapter 2, section 4 and Chapter 3, section 2), synthesis of the tetrakisacridinium porphyrin conjugate was pursued via reaction of the formyl functionalised (N-decenyl)acridinium **37·PF$_6$** with pyrrole in the presence of TFA, followed by oxidation using DDQ (Figure 2).

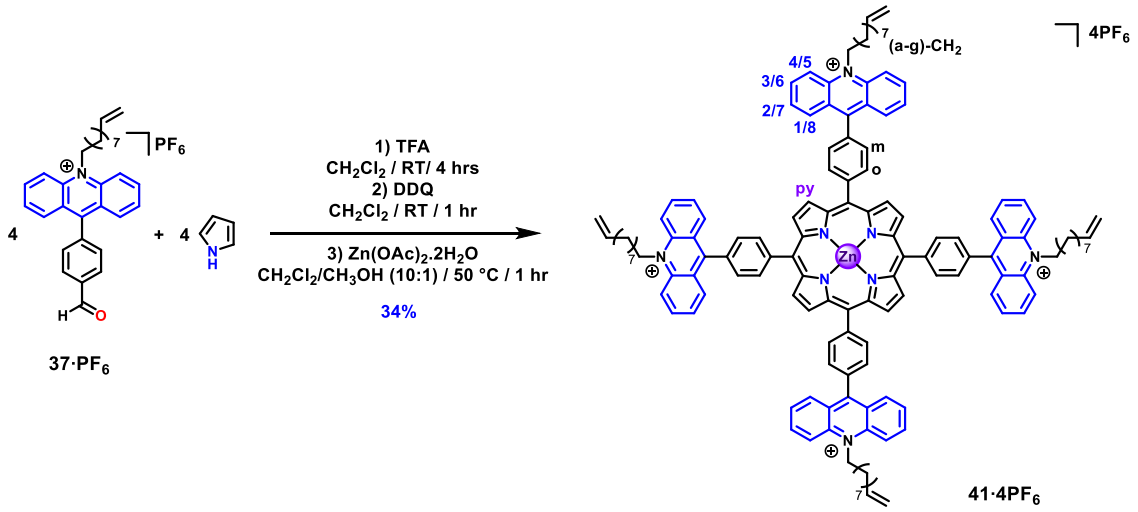

Figure 2. *Illustrative scheme for the synthesis of the tetrakis acridinium porphyrin conjugate* ***41·4PF$_6$.***

As with the tweezer precursor **38·PF$_6$**, it was observed that the conjugate could not be easily isolated from pyrrolic oligomeric side products via column chromatography alone. Fortunately, due to the limited solubility of the conjugate in chloroform, and the contrasting higher solubility of the side products, precipitation of the conjugate from chloroform could be used to further isolate the conjugate. Thus, purification via combined column chromatography and precipitation followed by metalation afforded the product **41·4PF$_6$** at a yield of 34%.

Advantageously for olefin metathesis, and despite the higher number of acridinium units, **41·4PF$_6$** showed good solubility in dichloromethane. The ^{1}H NMR spectrum in CD_2Cl_2 showed the presence of the expected singlet for the eight pyrrolic protons, reflecting the higher symmetry (D4h) of the conjugate compared to **38·PF$_6$** and **39·2PF$_6$** (Figure 3a-i). This was similarly reflected in the ^{13}C NMR spectrum (Figure 3b) by the appearance of a lone peak at 150 ppm for the *alpha* pyrrolic carbons of the porphyrin, in contrast to the four peaks seen for **38·PF$_6$** and **39·2PF$_6$** (Chapter 3, section 3: Figure 11). Interestingly, the ^{1}H NMR spectrum

was observed to dramatically change in CD_3CN (Figure 3a-ii), more specifically with regards to the acridinium protons, which were seen to be narrower and more widely spread in the aromatic region, whereas in CD_2Cl_2 the acridinium peaks were comparatively broadened and overlapped in the case of the 3/6 and 4/5 protons. The 4/5 and NCH_2 protons were observed to be the most changed, being upfield shifted in the CD_2Cl_2 spectrum ($\Delta\delta H_{4/5}$ = 0.21 ppm and $\Delta\delta NCH_2$ = 0.05 ppm).

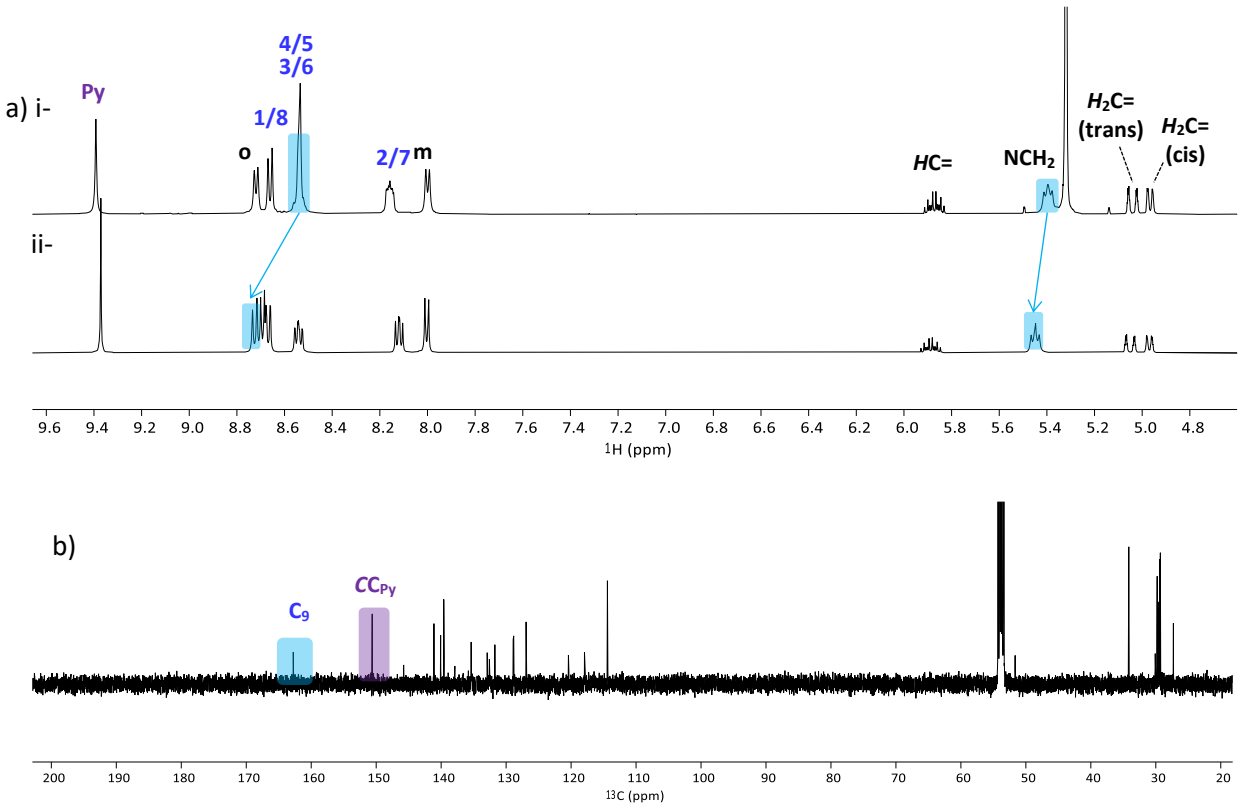

Figure 3. *a) ^1H NMR (500 MHz, 298 K) in i- CD_2Cl_2 and ii- CD_3CN and b) ^{13}C NMR (125 MHz, CD_2Cl_2, 298 K) spectra of the cage precursor* ***41·4PF$_6$.***

MS and UV-Vis further confirmed the synthesis of **41·4PF$_6$**, with a larger molar extinction coefficient for the acridinium π–π* bands (364 nm, ε = 87200 L mol^{-1} cm^{-1}) than found for the monoacridinium porphyrin conjugates (**30·PF$_6$**, **33·PF$_6$** and **38·PF$_6$**), in line with the presence of more than one acridinium unit (Figure 4). The Q-band of **41·4PF$_6$** was observed to be bathochromically shifted relative to **38·PF$_6$** (556 nm: $\Delta\lambda_{max}$ = + 3 nm and 603 nm: $\Delta\lambda_{max}$ = + 7 nm), indicating reduction in the HOMO-LUMO gap of **41·4PF$_6$** compared to **38·PF$_6$**, in-line with the increased number of acridinium units.

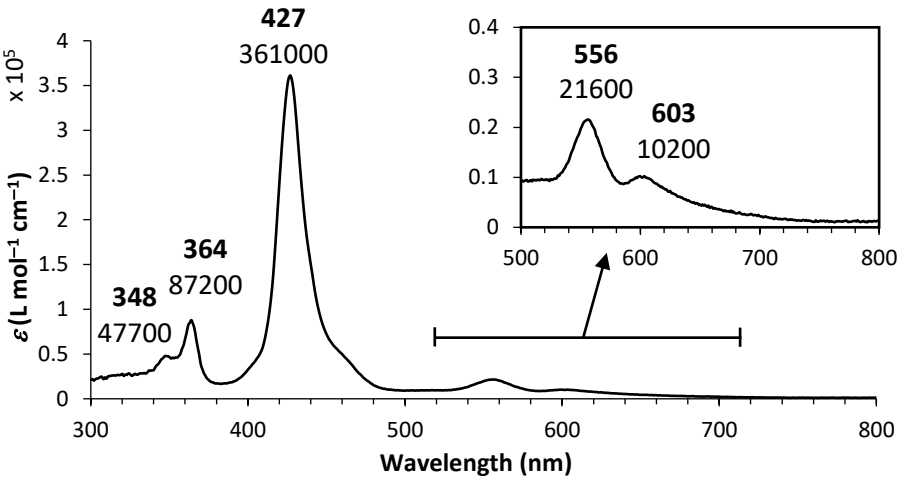

Figure 4. *UV-Vis (CH_2Cl_2, l = 1 cm, 298 K) spectrum of the cage precursor* ***41·4PF$_6$*** *(c = 3.00 μM) Distinct bands associated to the porphyrin (427 – 603 nm) and the acridinium (348 - 364 nm) are seen.*

Additionally, needle-like crystals were prepared via vapour diffusion of Et_2O into a solution of **41·4PF$_6$** in CH_3CN and analysed via X-ray diffraction (Figure 5). Due to the high flexibility of the alkenyl chains, disorder in two of the chains could not be removed, limiting the quality of the structure obtained. Regardless, the structures of the active units were still clearly seen and well-resolved, with the presence of the phenyl acridinium units at the *meso* position of the porphyrin, and a general co-planarity between the acridinium and porphyrin units. In contrast, as calculated for **35·2PF$_6$**, the phenyl spacers were found to be perpendicular to the active units (average dihedral angle = 60°). The cell unit was calculated to have a triclinic space group (P $\bar{1}$ (No. 2)), with the compound packing as sheets, at a 45° angle to the b and a axes of the cell unit.

When observing the packing of the crystal, it was found that there were short contact interactions between the porphyrin unit and the acridinium unit of two separate stacked conjugates at average lengths of 3.5 Å, suggesting π–π interactions between the porphyrin and acridinium in the solid-state structure.

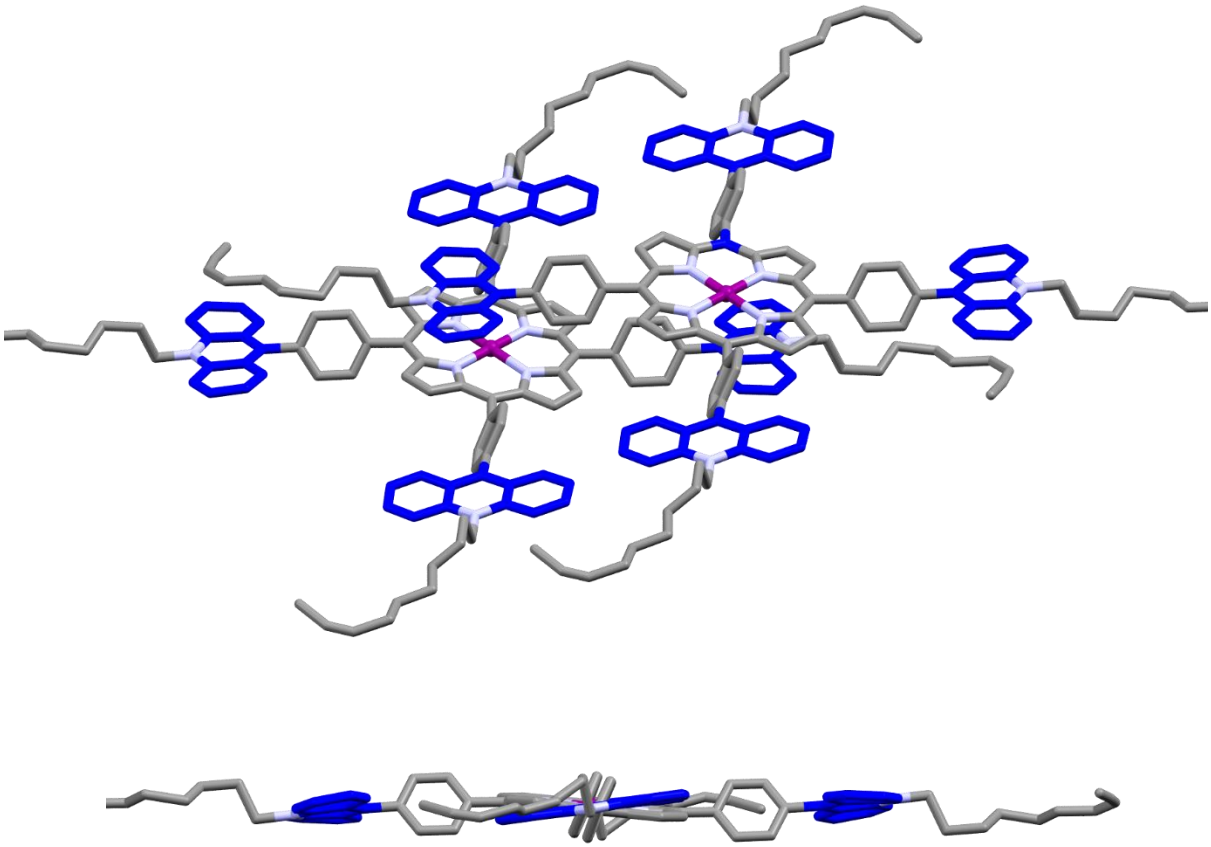

Figure 5. *XRD crystal structure of the cage precursor* ***41·4PF$_6$*** *from two points of view, showing the structure and coplanarity of the active units. For clarity, solvent, counter anions and disorder in the two alkenyl chains has been removed.*

3. Synthesis of a porphyrin-acridinium cage via olefin metathesis

As **41·4PF$_6$** had four alkenyl chains, different products could be formed including oligomers. Thus, we first explored the suitability of different ditopic ligands to act as templates for the cage, via formation of sandwiched complexes, to favour intramolecular ring-closing reactions versus oligomer formation.

Since complexation of ligands to the active form of the Grubbs' catalyst blocks the active site of the catalyst, it was necessary to use a template with a high binding constant for the Zn(II)-porphyrin. As DABCO has a binding constant for monomeric porphyrins typically in the order of 10^5 M^{-1} for a 1:1 complex,[1] and had been successfully used in similar porphyrin cage syntheses, [2,3] the use of DABCO was first explored, via addition of 0.5 equivalents of DABCO

to a millimolar solution of **41·4PF$_6$** in CD_2Cl_2. However, it was found that addition of DABCO led to precipitation of **41·4PF$_6$** forming a complex insoluble in non-polar solvents.

In contrast, when exploring the typically less strongly binding biPy ($K_a \approx 10^3 - 10^4\ M^{-1}$) [4,5] as a template, addition of half an equivalent of biPy to a millimolar solution of the conjugate in CD_2Cl_2 did not lead to any precipitation. Furthermore, the ^{1}H NMR spectrum of the solution showed key changes suggesting formation of the sandwiched complex, including upfield shifts of both the pyrrolic ($\Delta\delta H_{py} = -0.25$ ppm) and acridinium protons ($\Delta\delta H_{1\text{-}8} < -0.1$ ppm), in-line with an induced magnetic field effect (Figure 6). In addition, broad peaks at 5.1 and 2.5 ppm were seen, assigned to the complexed biPy *beta* and *alpha* protons respectively.

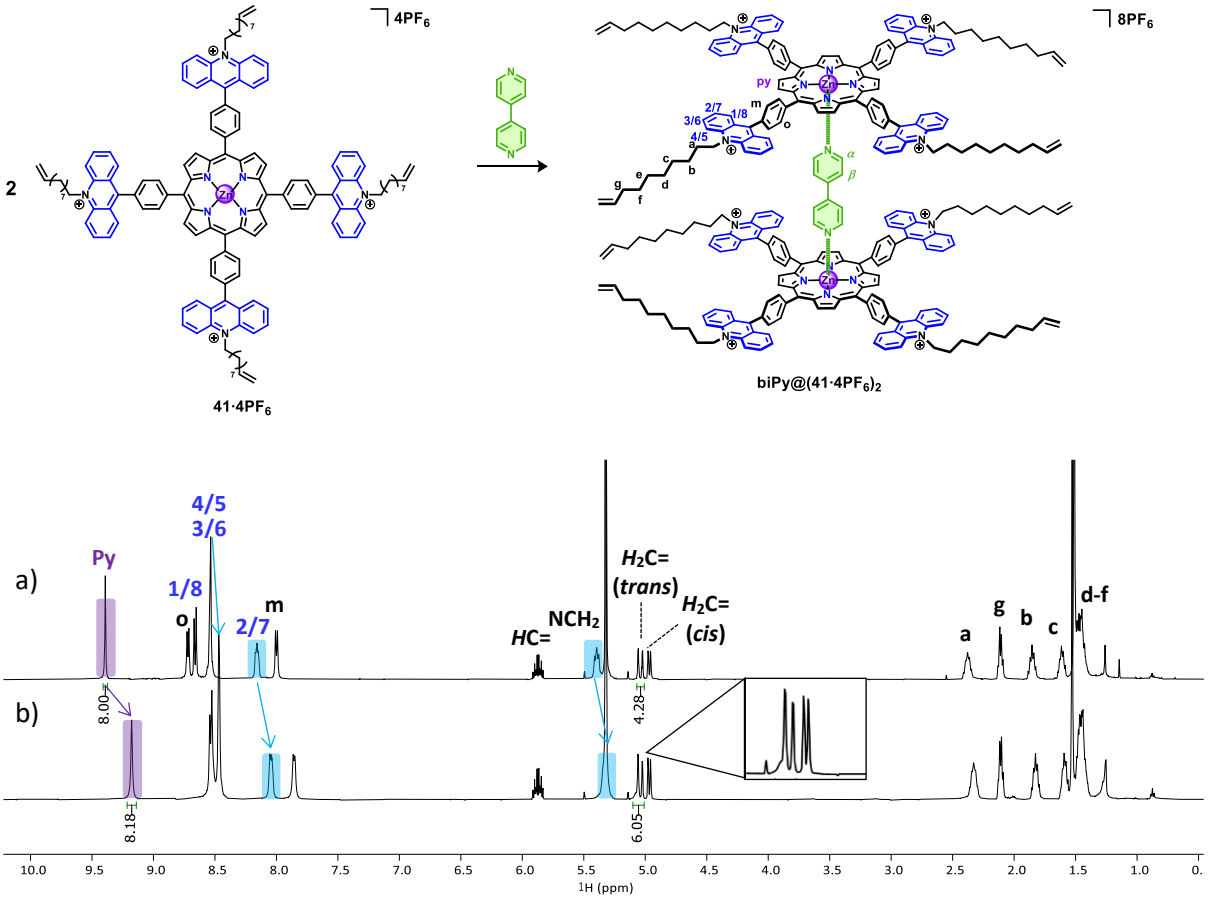

Figure 6. *Stacked ^{1}H (500 MHz, CD_2Cl_2, 298 K) spectra showing the cage precursor **41·4PF$_6$** a) before and b) after addition of 0.5 equivalents of biPy.*

As with the tweezer, the synthesis of the cage was achieved via olefin metathesis using Grubbs' 1st generation catalyst for its high functional group tolerance and relative stability. Initial trials in the synthesis (conducted at room temperature in CH_2Cl_2 at sub millimolar concentrations) revealed that although total consumption of **41·4PF$_6$** could be had with one

catalyst load of 20 mol% (as assessed via TLC), the cage formed was not fully closed, with only three of the four links made (as assessed via mass spectrometry). Thus, in order to form the fully closed cage, a second catalyst loading was required, with reaction for 16 hours after the initial catalyst loading, and a further eight hours after the second catalyst loading completing the four required metathesis reactions.

After testing different eluents for purification via column chromatography, it was found that a solution of 80:5:15 CH_2Cl_2/CH_3OH/CH_3CN (0.02 M KPF_6) gave good results, with KPF_6 decreasing adherence of the cage to the stationary silica phase, while the polarity of the eluent gave a suitable retention factor (R_f) value of < 0.5.

To remove biPy further purification was required. Fortunately, removal of the template was achievable via subsequent column chromatography using a CH_3CN KPF_6 (0.04 M) solution as the eluent. The combination of the two chromatographic methods allowed for the isolation of the cage **42·8PF$_6$** at a yield of 49%.

Curiously, **42·8PF$_6$** showed much reduced solubility compared to the conjugate in CH_2Cl_2 (Figure 7), with ^{1}H NMR spectra in the deuterated solvent returning poorly resolved broad-base peaks in the absence of the template, which were hard to distinguish from one another. However, a peak assignable to the pyrrolic protons was seen (9.39 ppm), and the lack of terminal alkene peaks notable. Additionally, broad peaks for the CH_2 protons were observed in the alkyl region. Although the cage showed high solubility in polar solvents such as CD_3CN, DMSO and DMF, ^{1}H NMR spectra in these solvents returned even broader peaks.

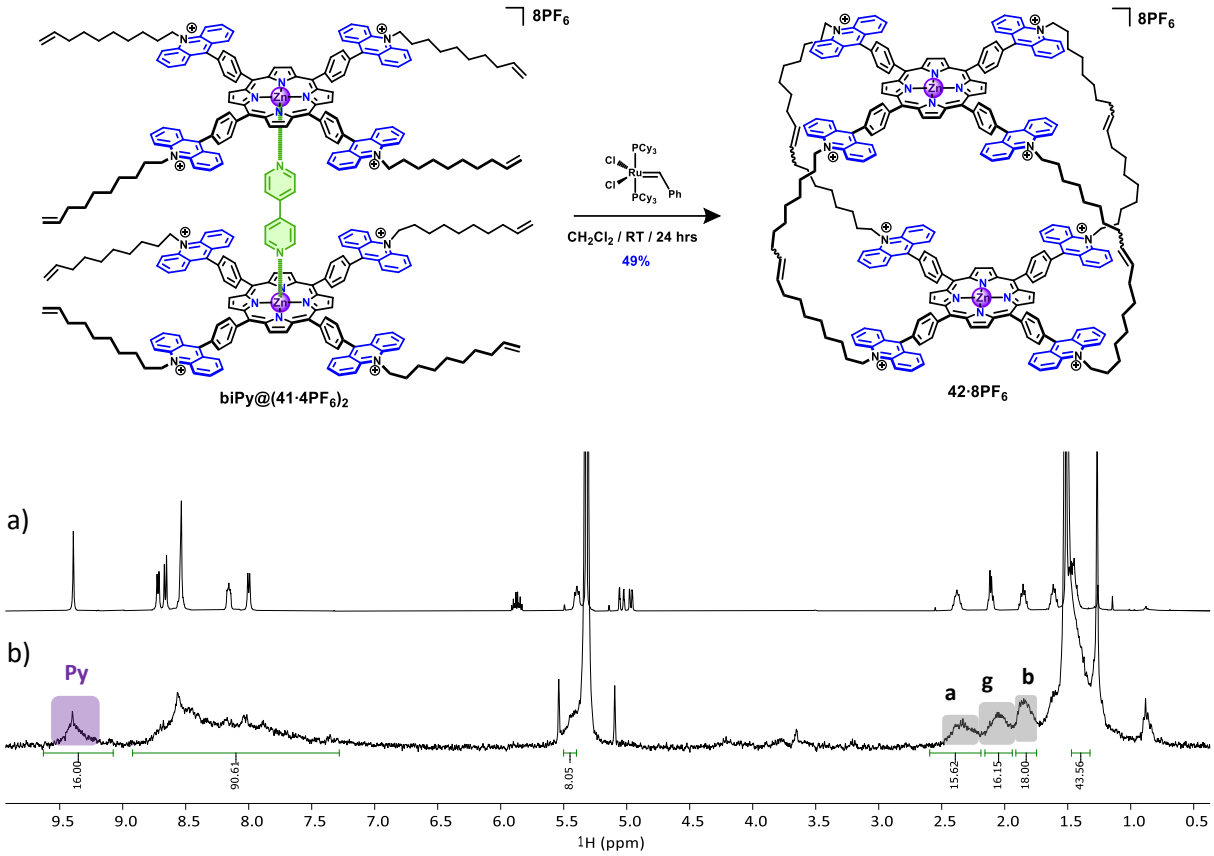

Figure 7. *Stacked ^{1}H NMR (500 MHz, CD_2Cl_2, 298 K) spectra of a)* ***41·4PF$_6$*** *and b) the cage* ***42·8PF$_6$****. The pyrrolic protons and CH_2 protons are highlighted in purple and grey respectively.*

UV-Vis spectra of **42·8PF$_6$** were recorded in both CH_2Cl_2 and in CH_3CN, and compared to the UV-Vis spectra of the cage precursor **41·4PF$_6$** in the corresponding solvent at two times intensity (Figure 8). In both solvents, bathochromic shifting of the Soret band of the porphyrin by $\Delta\lambda_{max}$ = –3 - –4 nm compared to the **41·4PF$_6$** spectra was observed. Additionally, in CH_2Cl_2 bathochromic shifts were also seen in the Q-band, while in CH_3CN a slight hypsochromic shift was seen ($\Delta\lambda_{max}$ = +1 - 2 nm). Hypochromic shifts of the Soret band were seen in both solvents, by 20% in CH_2Cl_2, and 35 % in CH_3CN (with broadening of the Soret band mid-height width). However, in both solvents no significant changes to the acridinium π–π* band (348 - 364 nm) were observed, showing good agreement with the **41·4PF$_6$** spectra in this region. Thus, intramolecular parallel offset π–π interaction between the porphyrin units was indicated, with seemingly no interaction between the porphyrin and acridinium units in solution.

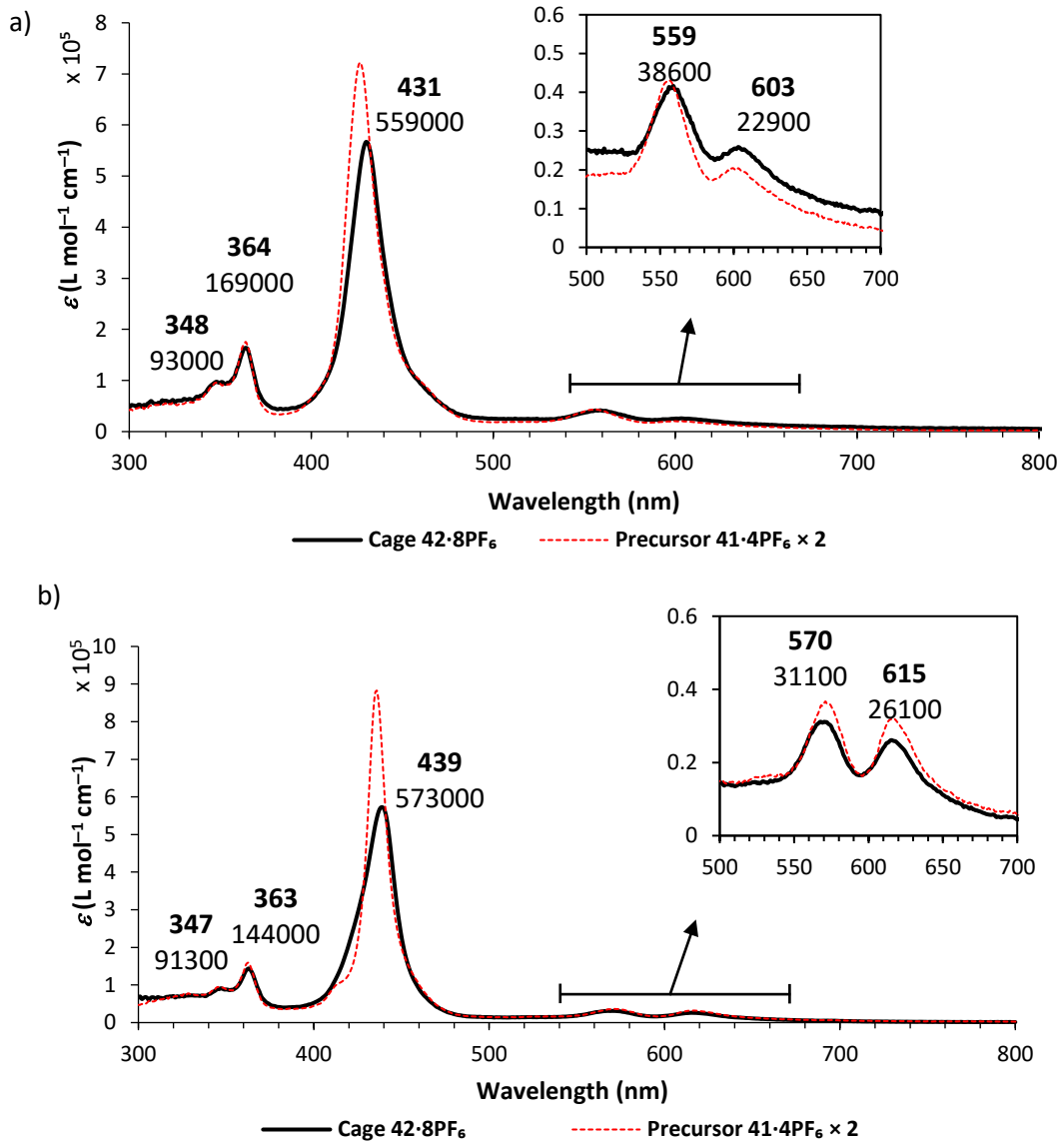

Figure 8. *Overlayed UV-Vis (l = 1 cm, 298 K) spectra of the cage* ***42·8PF₆*** *(displayed in black) and* ***41·4PF₆*** *at two times intensity (displayed in red) in a) CH_2Cl_2 (c = 1.00 μM) and in b) CH_3CN (c = 1.00 μM). The absorbance maxima and corresponding extinction coefficients for* ***42·8PF₆*** *are given above the associated band.*

The cage was unambiguously detected via mass spectroscopy as major mass ion peaks, at different multiple charges (Figure 9). The highest intensity peak was seen to be a 7+ charged species equivalent to the cage molecular formula without the counter anions ($[M–8PF_6]^{7+}$ at m/z = 539.4090), suggesting a single electron reduction during ionisation. Additionally, peaks for the 8+ charged species ($[M–8PF_6]^{8+}$ at m/z = 471.8561) and a 7+ charged species where a PF_6^- counter anion is retained ($[M–7PF_6]^{7+}$ at m/z = 559.9734) were present at 60% and 20% relative to the major mass ion peak.

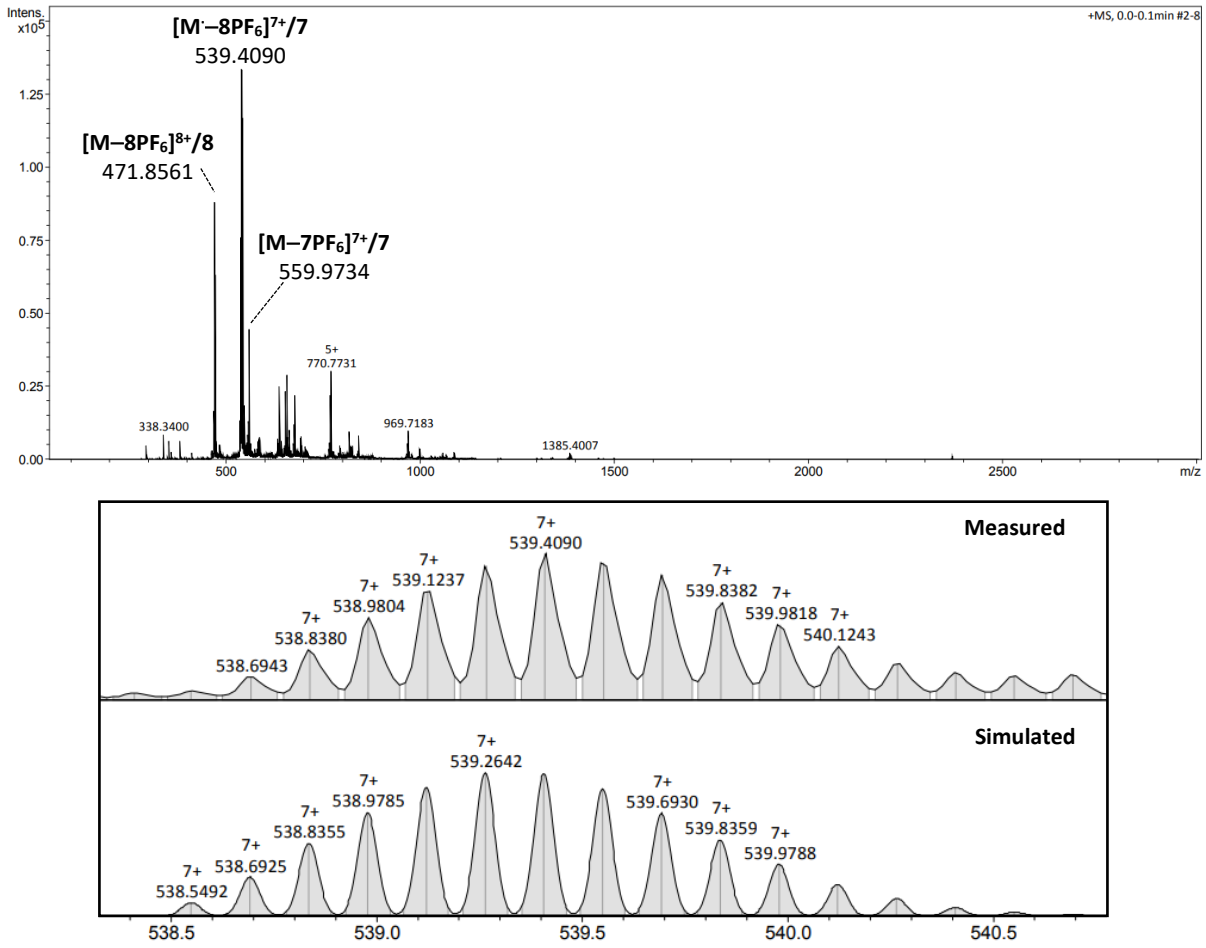

Figure 9. *High resolution mass (ESI-TOF) spectrum of* ***42·8PF$_6$*** *with zoom-insert of the major mass ion peak* ***42^{7+}/7.***

4. Binding studies of the acridinium porphyrin hexafluorophosphate cage

4.1. Study of the complexation of bipy by 42·8PF$_6$

Although the cage gave broad NMR spectra, it was observed that upon addition of an equivalent of biPy to a millimolar solution of **42·8PF$_6$** in CD_2Cl_2/CD_3CN (9:1) peaks became narrow, and a lone distinguishable peak could be seen for the pyrrolic protons, as well as distinct peaks for the inward facing and outward facing *meta* (7.72 and 7.84 ppm) and *ortho* (at 8.32 and 8.56 ppm) phenyl protons (Figure 10). Additionally, two peaks were seen for the alkene protons representing the *trans* and *cis* isomers. Finally, a narrow upfield shifted peak could be seen for the *beta* protons of the biPy ligand, in-line with internalisation and complexation within the cage.

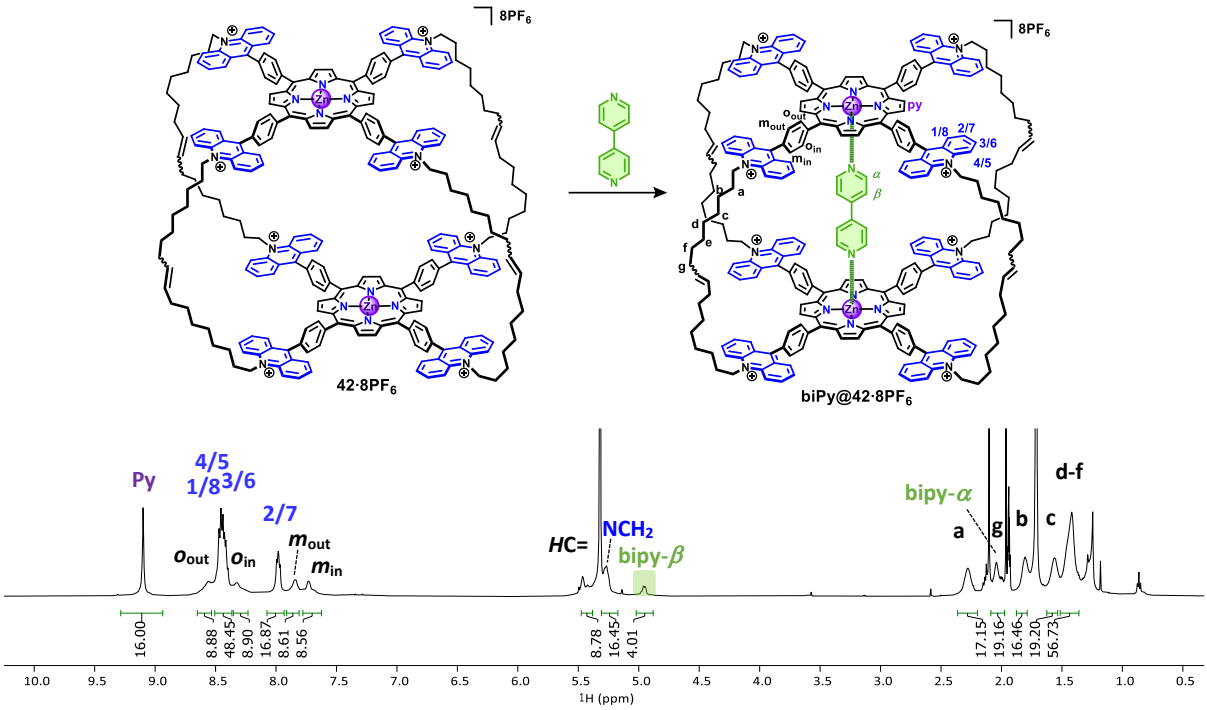

Figure 10. *^{1}H NMR (500 MHz, CD_2Cl_2/CD_3CN (9:1), 1.00 mM, 298 K) spectrum of* ***biPy@42·8PF$_6$.***

To further confirm the complexation of biPy, DOSY NMR spectra were recorded for the solution (Figure 11), where it was found that the cage and bipyridine ran at similar diffusion coefficients (2.80×10^{-6} cm^2 s^{-1}), further supporting complexation of biPy by the cage. Due to the mixed solvent system used (CD_2Cl_2/CD_3CN (9:1 v/v)), the true viscosity of the solution is not known. However, if assuming a viscosity close to or equivalent to the major solvent (CD_2Cl_2 = 4.353×10^{-4} Pa s), a hydrodynamic radius of 17.9 Å is calculated based on a spherical model, equivalent to a volume of 24023 Å^3. This was in-line with what was expected based on the dimensions of the crystal structure cell unit of **41·4PF$_6$** (b axis = 17.9 Å, Figure 5), as well as being an expectedly larger complex compared to the **biPy@39·2PF$_6$** complex (Table 1). Additionally, an energy-minimised structure of **biPy@42·8PF$_6$** was seen to agree with the derived radius, having a similar size to that of a superimposed sphere (with radius = 1.79 nm).

Table 1. *Diffusion coefficients and hydrodynamic radii of* ***biPy@42·8PF$_6$*** *and* ***biPy@39·2PF$_6$.***

Species	Solvent	D ($\times 10^6$ cm^2 s^{-1})	R_h (Å)
biPy@42·8PF$_6$	CD_2Cl_2/CD_3CN (9:1)	2.80 (± 0.13)	17.9
biPy@39·2PF$_6$	CD_2Cl_2	3.80 (± 0.15)	13.2

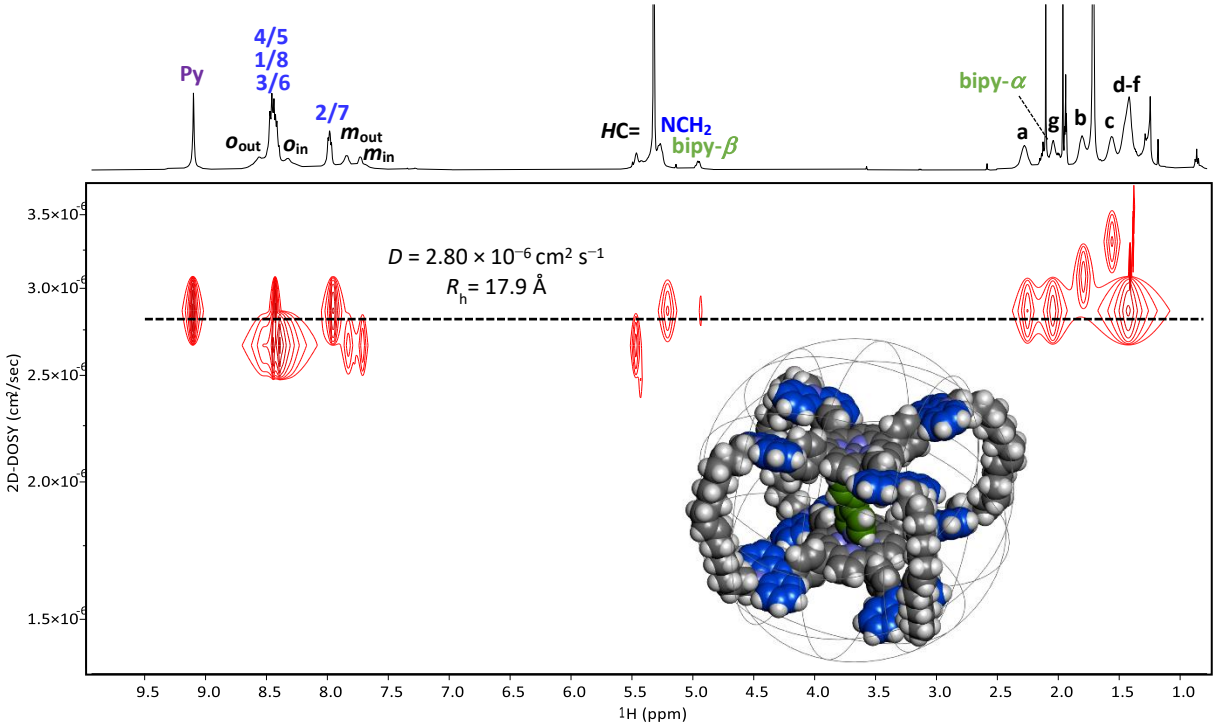

Figure 11. *^{1}H DOSY NMR (600 MHz, CD_2Cl_2/CD_3CN (9:1), 1.00 mM, 298 K) spectrum of the* ***biPy@42·8PF$_6$*** *complex, and the energy-minimised (Spartan'20) structure within a sphere of radius = R_h.*

UV-Vis titrations were conducted to ascertain the binding constant for formation of the complex (Figure 12). Addition of increasing amounts of biPy (up to 10 equivalents) to a solution of the cage in CH_2Cl_2 (0.1% CH_3CN) led to hyperchromic shifting by a factor of 1.3 in-line with removal of the π–π interaction between the porphyrin units. In contrast, no major changes were seen for the acridinium-centred band at 348 – 364 nm, supporting interaction with the porphyrin and not the acridinium units, as expected. Slight decrease in the band width was also observed for the Soret band (in-line with a rigidification of the cage) and an isosbestic point at 423 nm, supporting the formation of a single 1:1 host:guest complex. Fitting to a 1:1 model gave an averaged binding constant of 4.2 (± 0.7) × 10^6 M^{-1}, around 23 times larger than that seen for the tweezer **39·2PF$_6$** (at 1.8 × 10^5 M^{-1}), as expected for a less flexible species (in comparison to the tweezer).

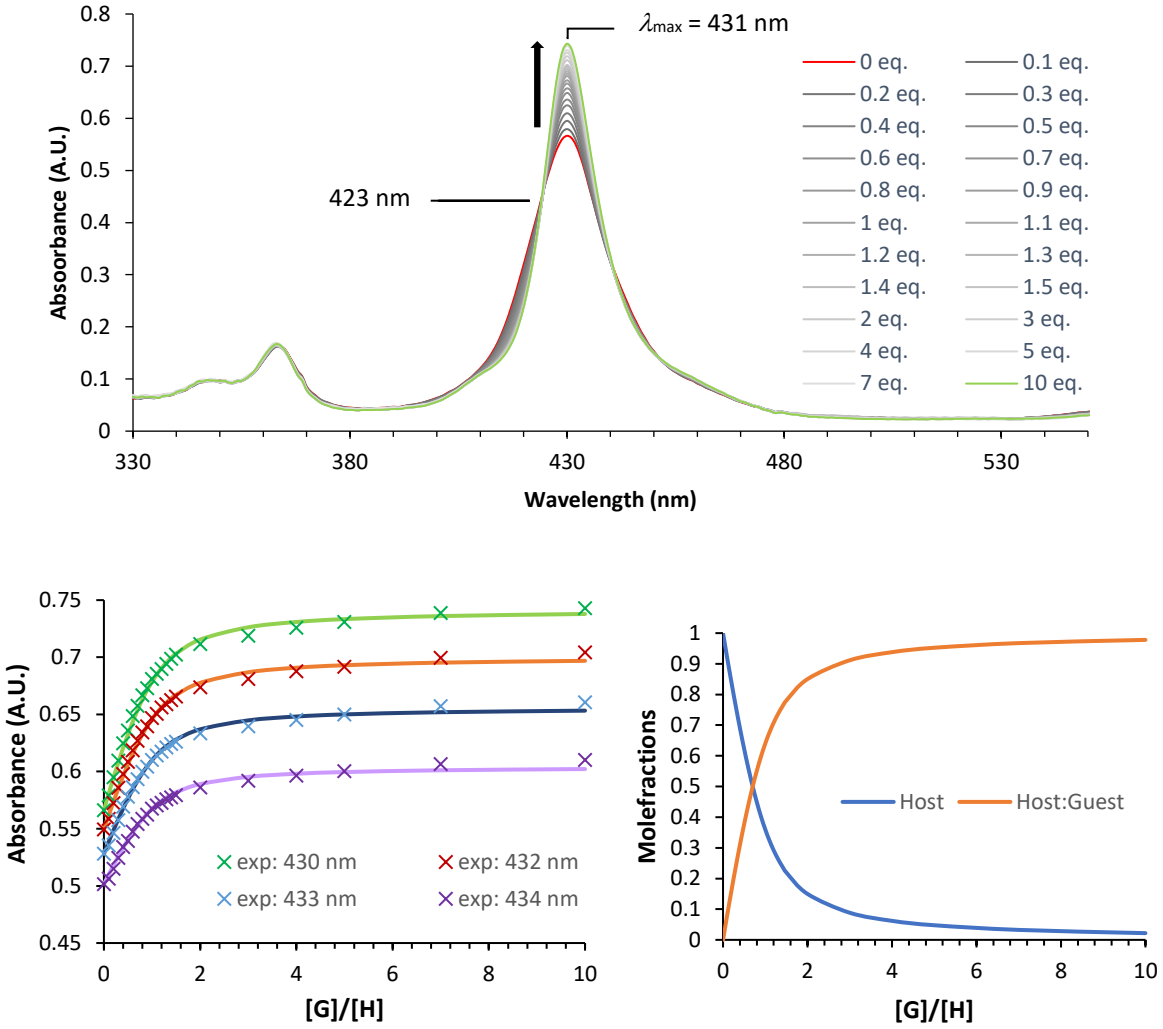

Figure 12. *UV-Vis (CH_2Cl_2 (0.1% CH_3CN), l = 1 cm, 298 K) titration of* ***42·8PF$_6$*** *(c = 1.00 μM) with up to 10 equivalents of biPy, and the non-linear regression fit of the obtained curve with the speciation diagram.*

4.2. Study of the complexation of DABCO by 42·8PF$_6$

The ability of **42·8PF$_6$** to bind DABCO was also explored. As was the case for biPy, addition of one equivalent of DABCO to a solution of the cage in CD_3CN, gave a ^{1}H NMR spectrum with narrow peaks for the cage in contrast to that seen for the free cage (Figure 13). A narrow peak for DABCO could be seen at –4.6 ppm, significantly upfield shifted from free DABCO, indicating internal ditopic binding of DABCO. Interestingly, only a subtle distinction was seen between the inward-facing and outward-facing *meta* and *ortho* protons of the phenyl spacers.

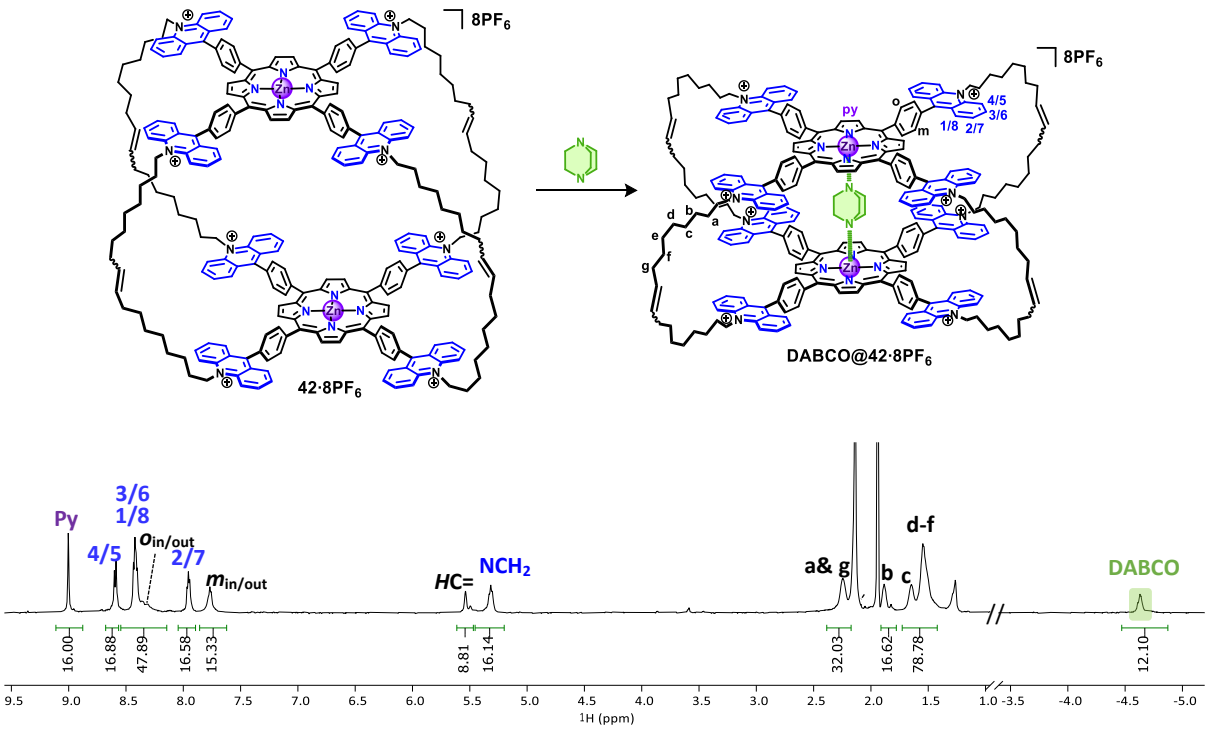

Figure 13. *^{1}H NMR (500 MHz, CD_3CN, 1.00 mM, 298 K) spectrum of* ***DABCO@42·8PF$_6$****.*

Using NOESY NMR (Figure 14a), a through space correlation could be seen between the DABCO protons and the pyrrolic protons of the porphyrin units. DOSY NMR recorded in acetonitrile showed all peaks to move with a similar coefficient ($D = 3.65 \times 10^6$ cm^2 s^{-1}), further supporting complexation of DABCO (Figure 14b). Using the diffusion coefficient and the viscosity of acetonitrile (3.57×10^{-4} Pa s), a hydrodynamic radius of 16.7 Å was calculated, with an approximate volume of 19660 Å^3 when assuming a spherical model. This was in good agreement with that calculated for the **biPy@42·8PF$_6$** complex, and with the **DABCO@39·2PF$_6$** complex (Table 2), being expectedly larger than the latter complex, given the larger aromatic surface area of the tetrakisacridinium porphyrin unit. Additionally, an energy-minimised structure of **DABCO@39·2PF$_6$** was seen to have a similar size to that of superimposed sphere with a radius of 1.67 nm.

Table 2. *Diffusion coefficients and hydrodynamic radii for the DABCO complexes of* ***42·8PF$_6$*** *and* ***39·2PF$_6$****.*

Species	Solvent	D (× 10^6 cm^2 s^{-1})	R_h (Å)
DABCO@42·8PF$_6$	CD_3CN	3.65 (± 0.07)	16.7
DABCO@39·2PF$_6$	CD_2Cl_2	4.50 (± 0.16)	11.1

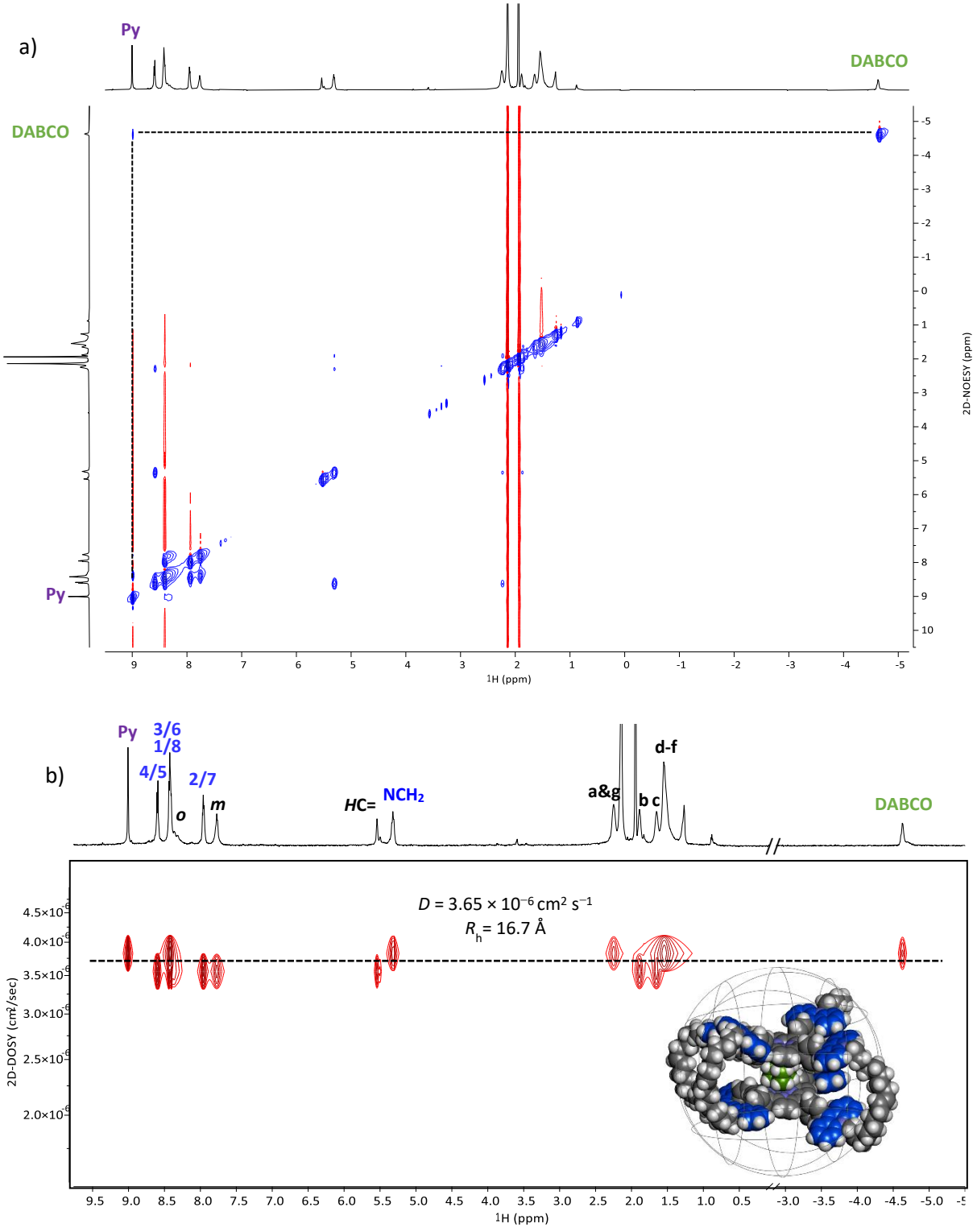

Figure 14. *a) 2D NOESY NMR (500 MHz, CD_3CN, 1.00 mM, 298 K) spectrum of the* ***DABCO@42·8PF$_6$*** *complex. The distinct correlation between the DABCO and pyrrolic protons is highlighted with dashed lines. b) ^{1}H DOSY NMR (600 MHz, CD_3CN, 1.00 mM, 298 K) spectrum of the* ***DABCO@42·8PF$_6$*** *complex, and the energy-minimised (Spartan'20) structure within a superimposed sphere with radius = R_h.*

UV-Vis titrations were caried out at micromolar concentrations in CH_3CN (Figure 15). Addition of increasing equivalents of DABCO to the **42·8PF$_6$** solution was seen to lead to a large hypsochromic shift from 439 nm to 426 nm, in addition to a slight decrease in the band width, consistent with a constriction in flexibility. In addition, an isosbestic point could be seen at 432 nm suggesting formation of one complex. As such, the obtained curve was fit to a 1:1 binding model, with an averaged binding constant of 4.5 (±0.2) × 10^5 M^{-1} obtained.

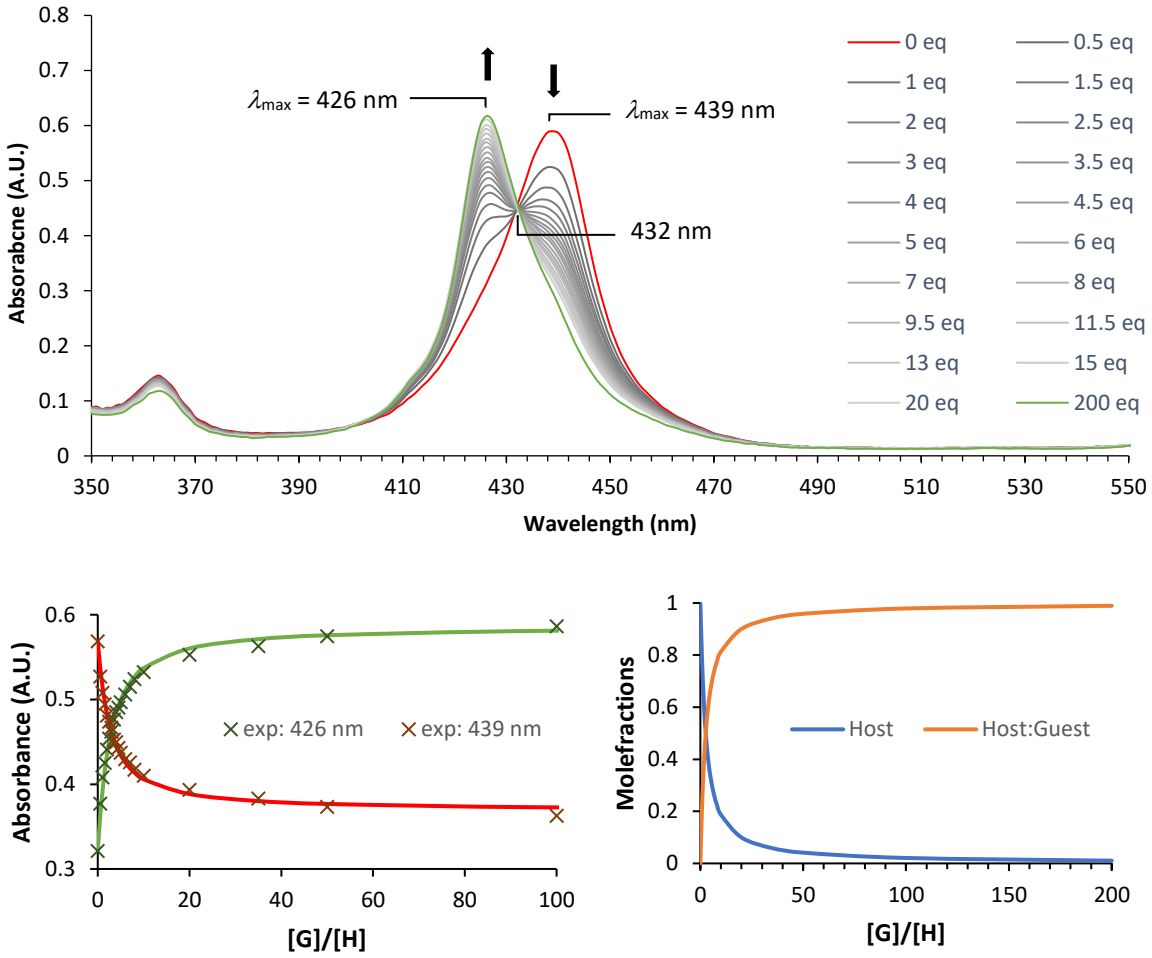

Figure 15. *UV-Vis (CH_3CN, l = 1 cm, 298 K) titration of* ***42·8PF$_6$*** *(c = 1.00 μM) with up to 200 equivalents of DABCO, and the non-linear regression fit of the obtained curve with the accompanying speciation diagram.*

4.3. Preliminary investigation into the allosteric binding of pyrene

Having evidenced the formation of the **DABCO@42·8PF$_6$** complex, attention was turned to the capacity of the complex to bind polyaromatic molecules. Due to the poor solubility of the complex in other solvents CD_3CN was used, despite the somewhat limited solubility of poly aromatic hydrocarbons in this solvent. Adding 5 equivalents of pyrene to a solution of the **DABCO@42·8PF$_6$** complex in CD_3CN, was seen to lead to significant changes to the ^{1}H NMR spectrum (Figure 16), namely upfield shifts of the pyrene molecule by 0.04 ppm, and upfield shifts of the NCH_2 (–0.064 ppm) and 4/5 (– 0.092 ppm) protons of the acridinium, indicating an induced magnetic field effect in-line with binding of the pyrene molecules via π–π stacking interactions. However, due to the limited solubility of poly aromatic hydrocarbons in acetonitrile, studies in this solvent were limited. Thus, in order to allow study in non-polar solvents (such as dichloromethane) anion metathesis was performed.

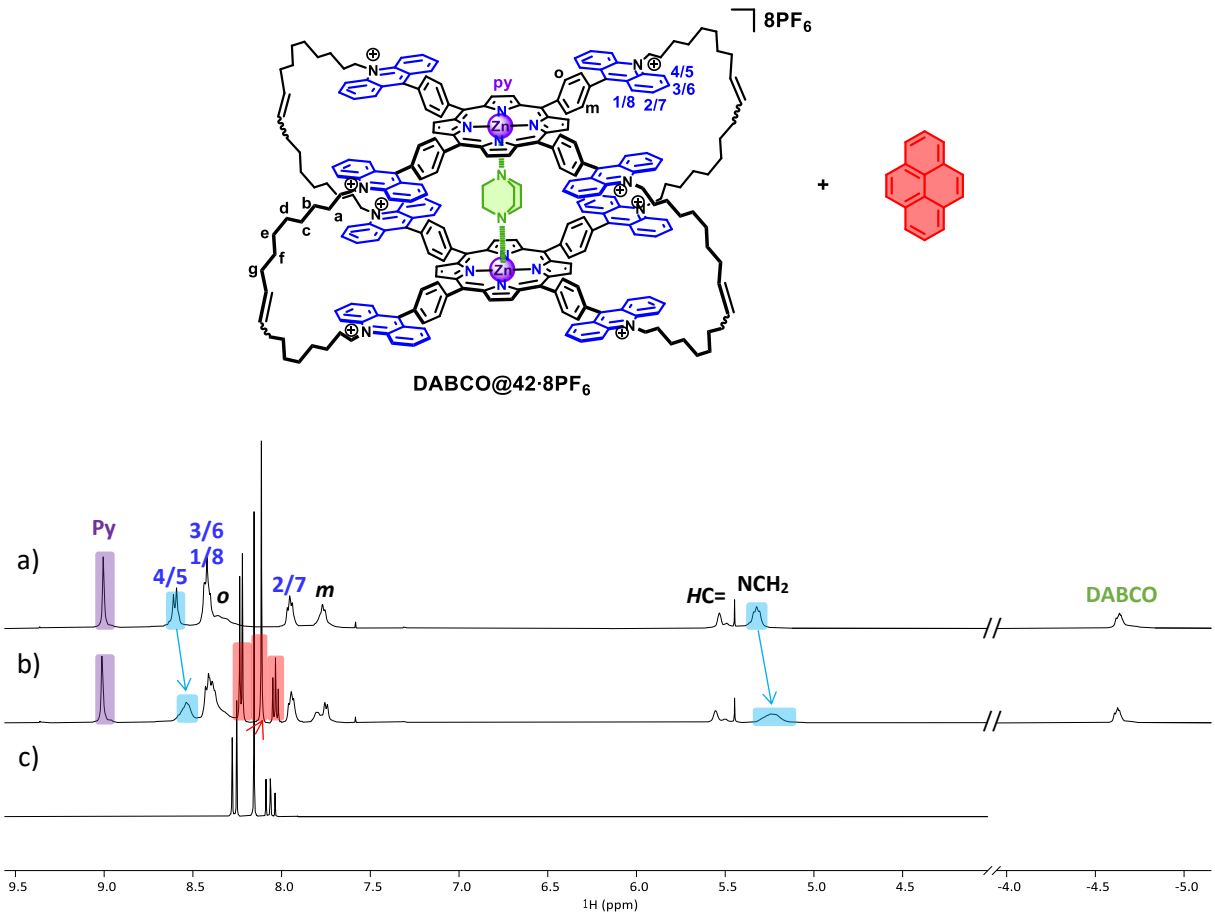

***Figure 16**. Stacked ^{1}H NMR (500 MHz, CD_3CN, 0.5 mM, 298 K) spectra of a) the complex **DABCO@42·8PF$_6$** and b) **DABCO@42·8PF$_6$** plus pyrene (5 equivalents). A spectrum of c) pyrene is provided for comparison.*

5. Synthesis, characterisation, and study of the cage BArF salt (42·8BArF)

Due to the high solubility and non-coordinating properties, **42·8PF$_6$** was exchanged to the BArF analogue, with anion metathesis conducted using NaBArF in CH_2Cl_2 to give **42·8BArF** in quantitative yields (Figure 17). Full exchange to BArF was confirmed via ^{19}F NMR, showing a lone singlet for the BArF molecules.

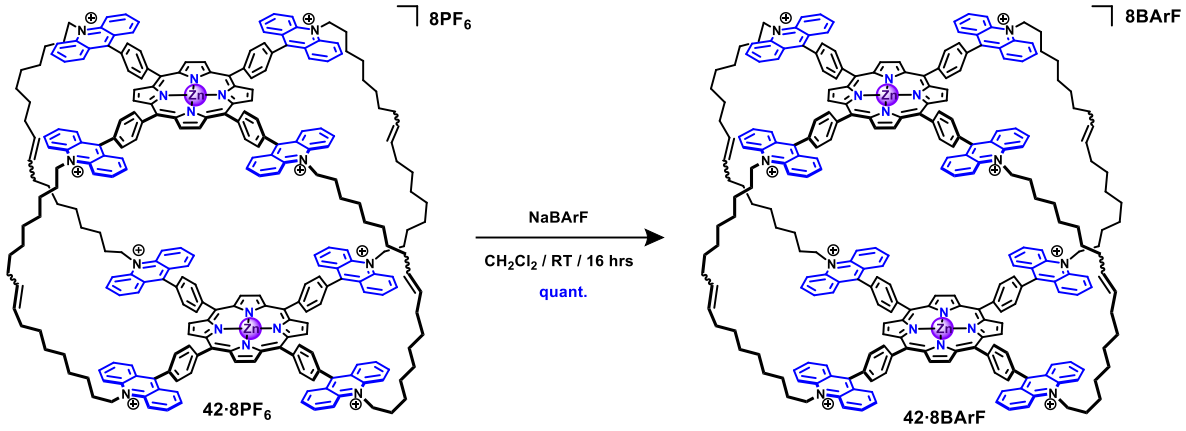

Figure 17. *Synthesis of the cage* ***42·8BArF*** *via anion metathesis of* ***42·8PF$_6$****.*

Upon formation of the BArF salt, immediate distinctions could be seen. The cage showed significantly improved solubility in CH_2Cl_2 compared to the PF_6 salt, with the ability to see narrow peaks in the ^1H NMR spectrum (Figure 18b). Additionally, separate peaks were noticeable for the inward facing and outward facing *meta* and *ortho* phenyl protons. When comparing the cage to the BArF analogue of the cage precursor **41·4BArF** (Figure 18a), it was found that many of the peaks were significantly upfield shifted, including for the BArF counterion, suggesting a possible interaction between the cage and the counterion. Small shoulder peaks were also seen in the aromatic region of the spectrum, most noticeably for the pyrrolic protons. It was hypothesised that this may be due to slow conversion (relative to the NMR timescale) to conformations of the cage with wider apertures (indicated by their downfield shifted chemical shifts relative to the more intense peaks). Investigation of this assertion was limited due to the low boiling point of CH_2Cl_2 (hindering variable temperature NMR experiments), and the return to broadness seen in the NMR spectra when using alternative solvents (including $CHCl_3$ and CD_3CN). However, when exploring the binding of ditopic ligands, the resulting spectra of the complexes was seen to give a single set of peaks in the aromatic region, supporting the presence of one species in solution.

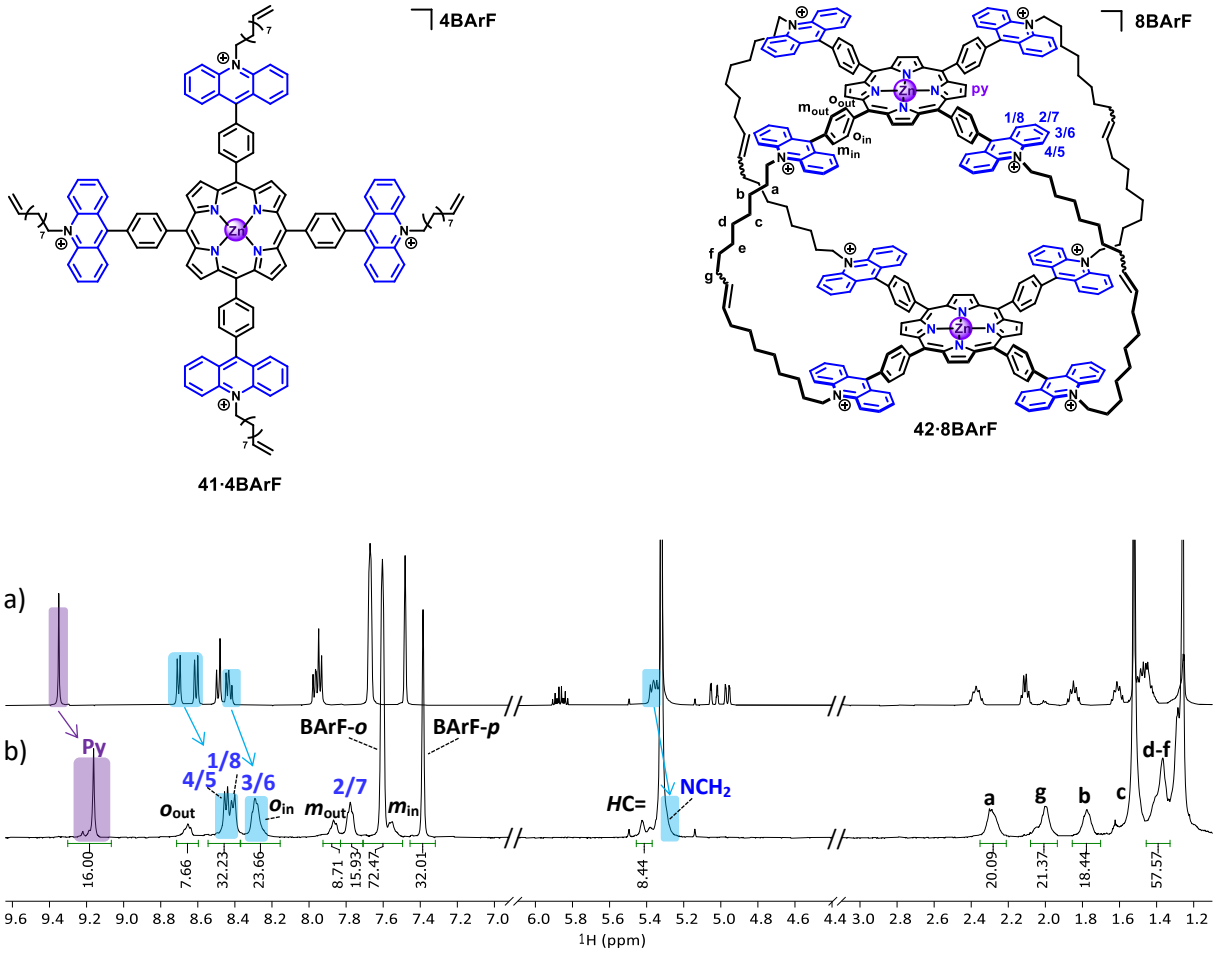

Figure 18. *Stacked ^{1}H NMR (500 MHz, CD_2Cl_2, 298 K) spetra of a) the cage precursor* ***41·4BArF*** *and b) the cage* ***42·8BArF****.*

DOSY NMR spectra were recorded for NaBArF, the cage precursor **41·4BArF** and the cage **42·8BArF**. A diffusion coefficient of 2.92 × 10^{-6} cm^2 s^{-1} was found for the major peaks of the cage **42·8BArF**, corresponding to a hydrodynamic radius of 17.2 Å (Figure 19). The $BArF^-$ ions were not observed to have a diffusion coefficient the same as the cage (3.77 × 10^{-6} cm^2 s^{-1}), however the diffusion coefficient measured was less than half the value for NaBArF (8.38 × 10^{-6} cm^2 s^{-1}, Table 3). Thus, interactions between the cage and the $BArF^-$ counterions were concluded to take place, and the difference in the broadness of the ^{1}H NMR peaks in comparison to **42·8PF$_6$** partly ascribed to this interaction. However, the exact nature of the interaction and its localisation could not be ascertained, although the upfield shift did suggest shielding via an induced magnetic field.

Table 3. *Diffusion coefficients and hydrodynamic radii of the salts* ***42·8BArF****,* ***41·4BArF*** *and NaBArF, obtained via DOSY NMR experiments.*

Species		Solvent	D (× 10^6 cm^2 s^{-1})	R_h (Å)
42·8BArF	$\mathbf{42^{8+}}$	CD_2Cl_2	2.92 (± 0.14)	17.2
	BArF	CD_2Cl_2	3.77 (± 0.01)	-
41·4BArF	$\mathbf{41^{4+}}$	CD_2Cl_2	3.55 (± 0.05)	14.1
	BArF	CD_2Cl_2	4.95 (± 0.01)	-
NaBArF	**BArF**	CD_2Cl_2	8.38 (± 0.05)	5.98

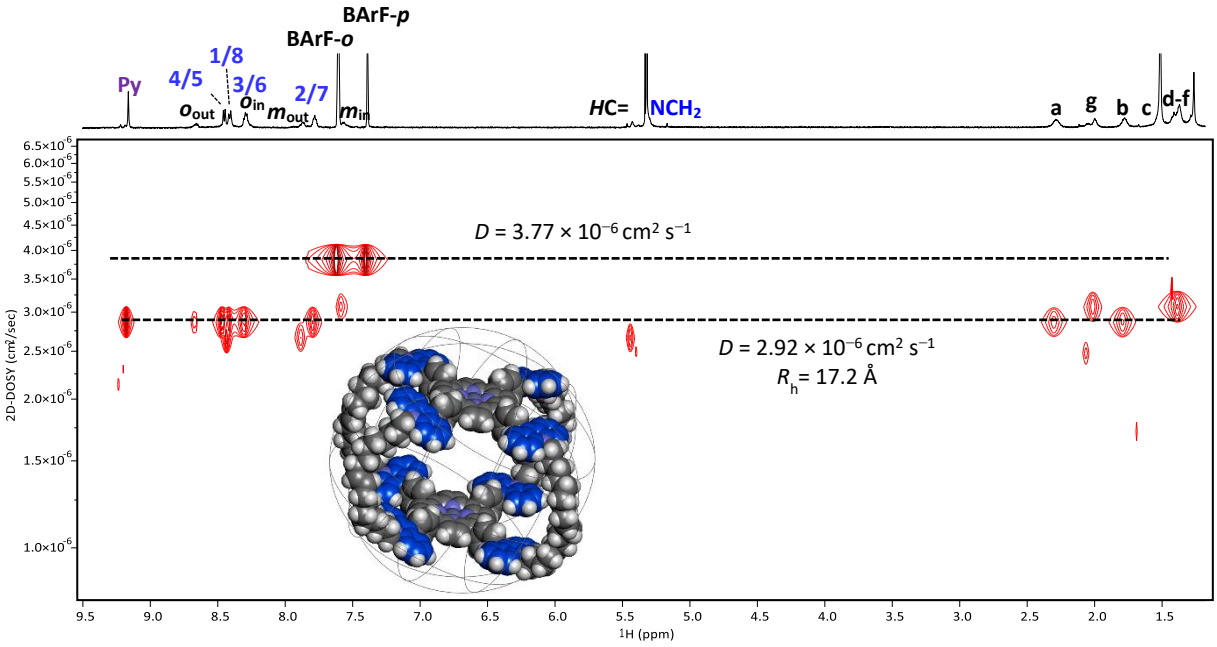

Figure 19. *^{1}H DOSY (600 MHz, CD_2Cl_2, 1.00 mM, 298 K) NMR spectra, of* ***42·8BArF*** *and the energy-minimised (Spartan'20) structure of* $\mathbf{42^{8+}}$ *within a superimposed sphere of radius = R_h.*

Similarly to the ^{1}H NMR spectrum, metathesis to the BArF salt was seen to present marked differences in the UV-Vis spectrum compared to **42·8PF$_6$** (Figure 20). Where hypochromic and bathochromic shifts of the Soret band were observed in the case of **42·8PF$_6$**, for **42·8BArF** a good agreement was seen between its spectrum and that of **42·4BArF** (at two times intensity). A slight broadening was seen for the Soret band, with no changes to the Q-band implying that **42·8BArF** did not form the intramolecular parallel offset π–π interactions indicated with **42·8PF$_6$**.

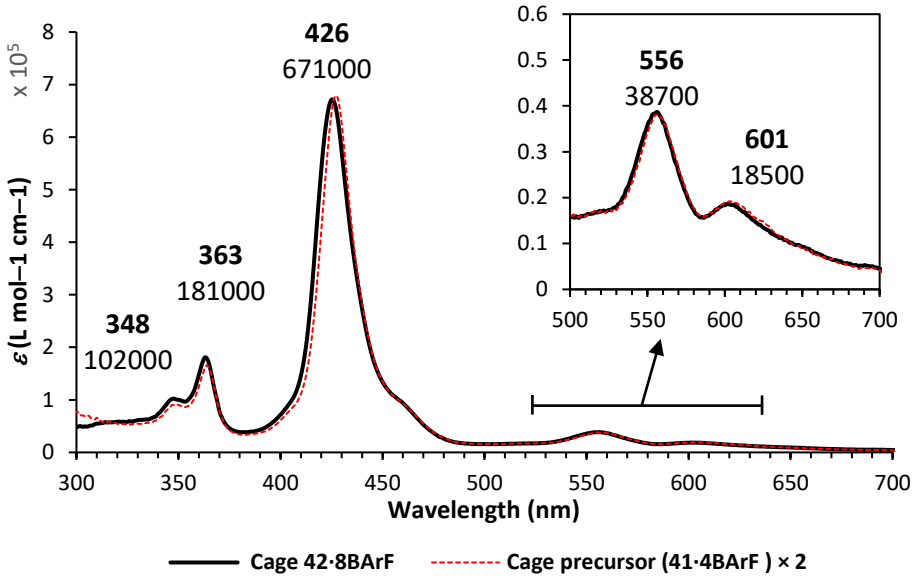

Figure 20. *Overlayed UV-Vis (CH_2Cl_2, l = 1 cm, 298 K) spectra of* ***42·8BArF*** *(in black, c = 2.00 μM) and* ***41·4BArF*** *(in red, at two times intensity).*

6. Binding Studies of the cage with BArF as the counter ion (42·8BArF)

6.1. Study of the complexation of biPy

To further investigate the effects of anion metathesis, the ability of **42·8BArF** bind biPy was probed. Addition of an equivalent of biPy to a millimolar solution of the cage in CD_2Cl_2 was seen to lead to resolution of the pyrrolic protons in to one singlet for the 16 pyrrolic protons, upfield shifted by 0.094 ppm compared to the major pyrrolic proton of **42·8BArF** (Figure 21). The difference in chemical shifts between the outward and inward-facing *meta* and *ortho* phenyl protons was also seen to become smaller. This suggested a decreasing anisotropic magnetic field effect, that might be seen with a widening of the cage aperture upon complexation of biPy. A slight downfield shift of the $BArF^-$ ions' protons was also observed suggesting an interruption or reorganisation of the interaction between the $BArF^-$ ions and the cage. This trend was also seen in the ^{19}F NMR spectrum, which showed a slight downfield shift by 0.06 ppm (from –62.89 to –62.83 ppm). Tell-tale narrow upfield shifted protons could also be seen for biPy at 4.9 and 2.4 ppm for the *beta* and *alpha* biPy protons respectively, indicating internal complexation of biPy by the cage.

As similarly seen with the tweezer **39·2PF$_6$**, upfield shifts of the acridinium protons were also observed, although to a lesser extent ($\Delta\delta H_{4/5}$ = 0.045 ppm, vs 0.1 ppm for **biPy@39·2PF$_6$**).

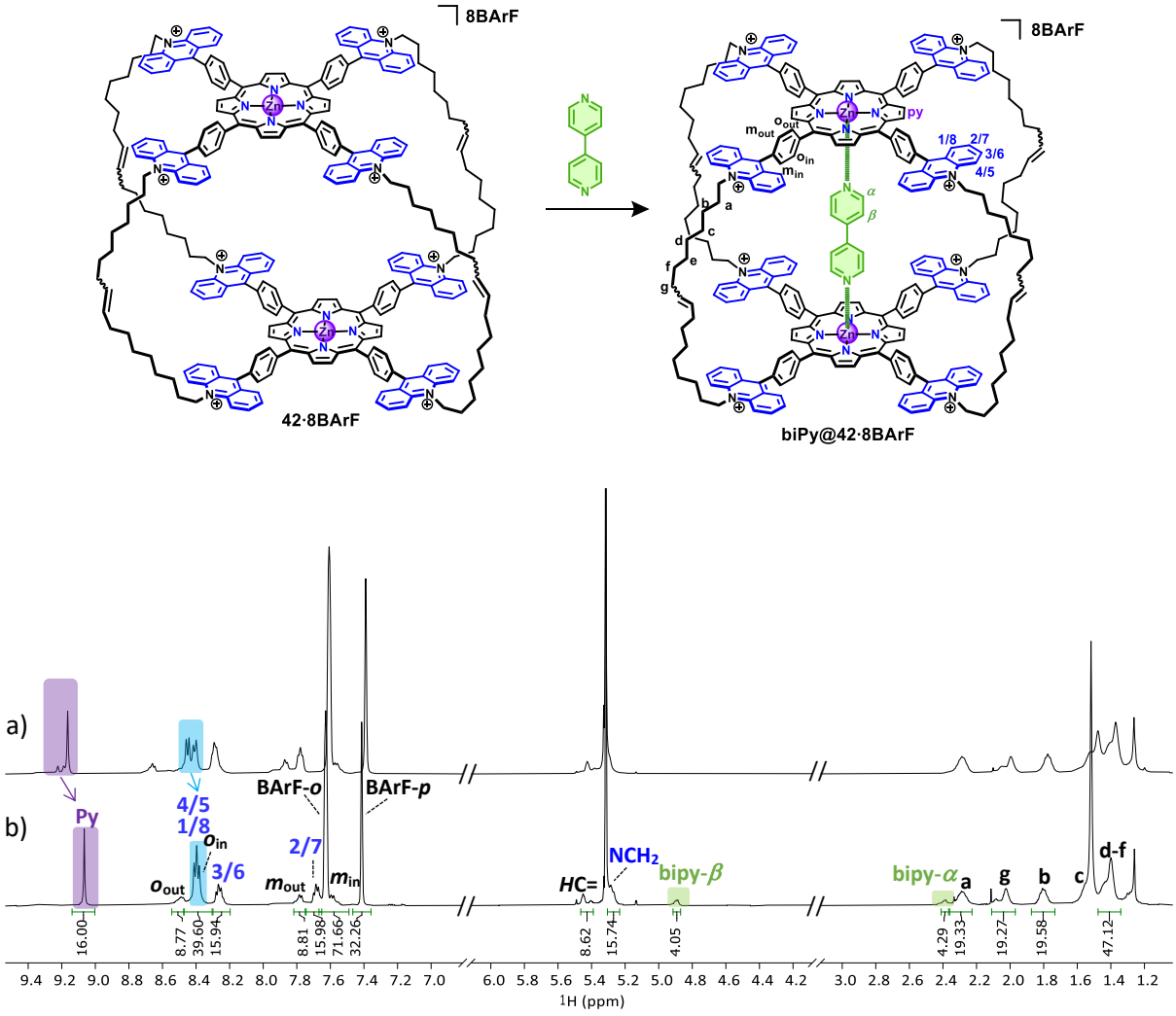

Figure 21. *Stacked ^{1}H (500 MHz, CD_2Cl_2, 1.00 mM, 298 K) NMR spectra of a)* ***42·8BArF*** *and b) the* ***biPy@42·8BArF*** *complex formed upon addition of an equvalent of bipy to the solution.*

The cage and biPy were observed to have the same diffusion coefficient (2.85 × 10^{-6} cm^2 s^{-1}) via DOSY NMR, with an approximate hydrodynamic radius of 17.6 Å (Figure 22). This value was similar to that obtained for the **biPy@42·8PF$_6$** complex, and slightly larger than that obtained for the free cage. The $BArF^-$ ions were still found to diffuse at a similarly slower rate (3.71 × 10^{-6} cm^2 s^{-1}) in comparison to NaBArF, suggesting that the interaction between the cage and counterions remained, with the downfield shift of the BArF protons indicating a possible change in the arrangement of the interaction. Additionally, as was seen with **biPy@42·8PF$_6$**, the energy-minimised structure of the complex was found to be similar in size to a sphere of radius = 1.76 nm (Figure 22).

Table 4. *Diffusion coefficients and hydrodynamic radii of the* ***biPy@42·8PF$_6$*** *and* ***biPy@42·8BArF*** *complexes.*

Species		Solvent	D (× 10^6 cm^2 s^{-1})	R_h (Å)
bipy@42·8BArF	**bipy@42^{8+}**	CD_2Cl_2	2.85 (± 0.13)	17.6
	BArF	CD_2Cl_2	3.71	-
biPy@42·8PF$_6$		CD_2Cl_2/CD_3CN (9:1)	2.80 (± 0.13)	17.9

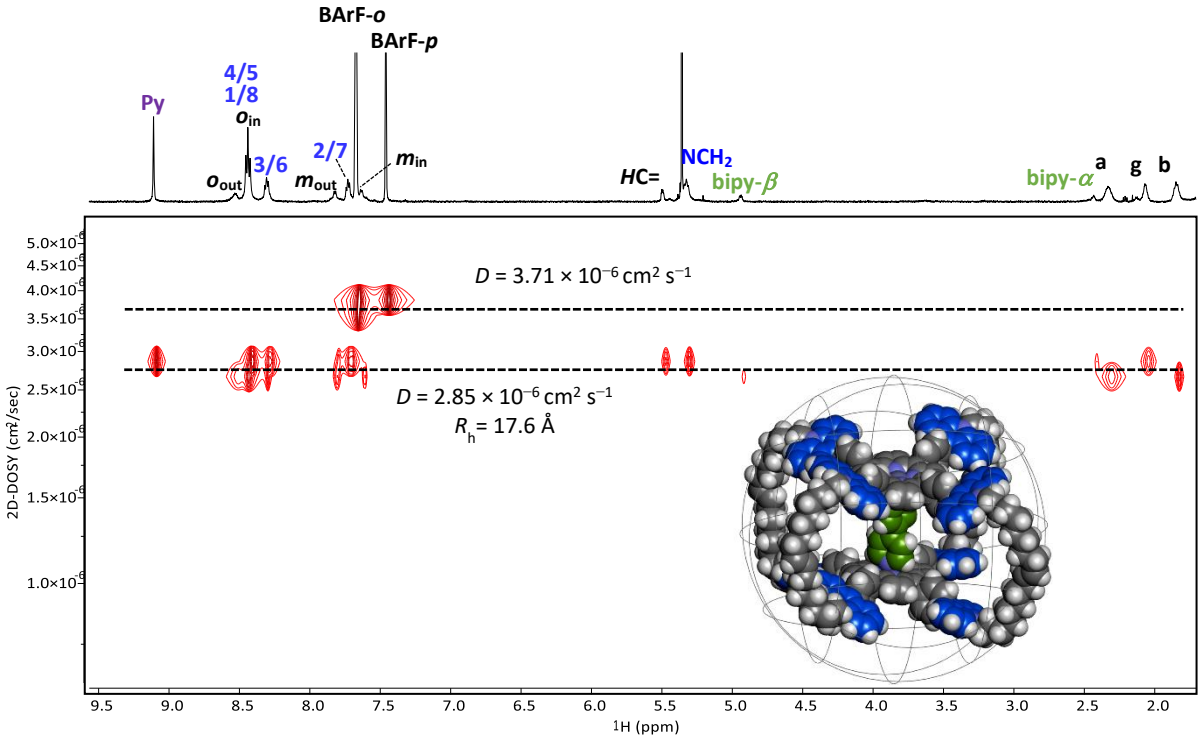

Figure 22. *^{1}H DOSY (600 MHz, CD_2Cl_2, 1.00 mM, 298 K) NMR spectrum of the* ***biPy@42·8BArF*** *complex, and the energy-minimised (Spartan'20) structure of* ***biPy@42^{8+}*** *within a superimposed sphere with radius = R_h.*

In UV-Vis titrations conducted in CH_2Cl_2 at sub-micromolar concentrations (Figure 23), addition of increasing equivalents of biPy (up to 10 equivalents) to **42·8BArF** was seen to lead to a bathochromic shift of the Soret band by 4 nm (to 430 nm). Additionally, a hyperchromic shift of the Soret band by a factor of 1.3 was seen, in line with the hyperchromic shift seen for **42·8PF$_6$**. In addition, a narrowing of the Soret band could also be seen, consistent with a less conformationally flexible complex. Strangely, a single isosbestic point was not seen, instead the overlayed spectra showed two isosbestic points at 426 nm (from 0-1 eq.) and 425

nm (from 1.1 to 10 eq.). However, fitting to a 1:2 binding model was not observed to give a better residual error than the 1:1 model. One possible hypothesis indicated by the closeness of the two isosbestic points is that they may be due to a displacement of $BArF^-$ ions. Via fitting to a 1:1 model an averaged binding constant of 1.3 (±0.2) × 10^7 M^{-1} was found, 72 times larger than that found for **39·2PF$_6$**, and three times larger than that found for **42·8PF$_6$**.

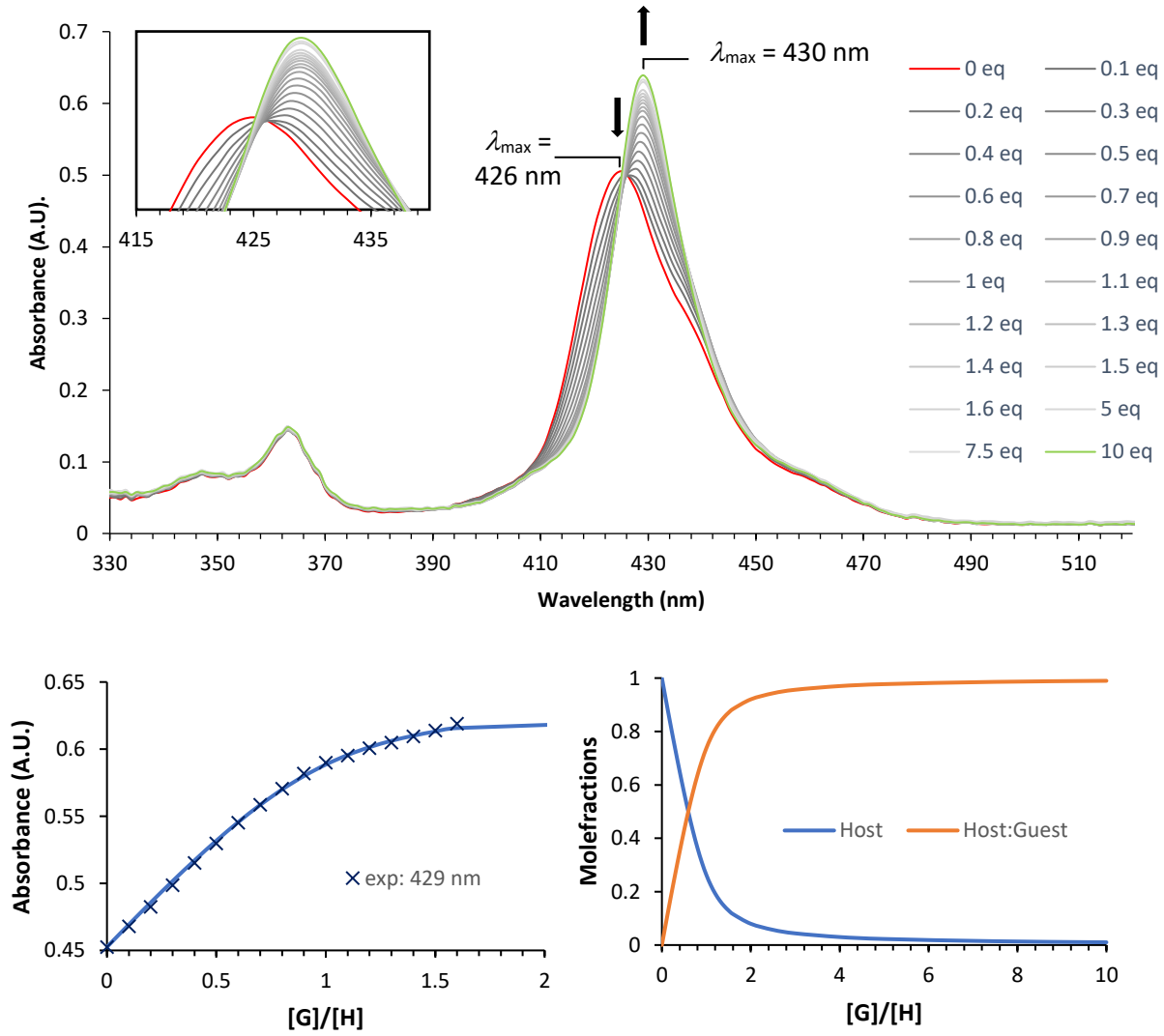

Figure 23. *UV-Vis (CH_2Cl_2, l = 1 cm, 298 K) titration of* ***42·8BArF*** *(c = 0.75 μM) with biPy (up to 10 equivalents), and the non-linear regression fit of the obtained titration curve, with the calculated speciation diagram.*

6.2. Study of the complexation of DABCO

Formation of the 1:1 **DABCO@42·8BArF** complex was also explored via NMR spectroscopies. Addition of one equivalent of DABCO to a millimolar solution of **42·8BArF** in CD_2Cl_2 gave (similarly to biPy) a single set of peaks, with a singlet for the 16 pyrrolic protons. The pyrrolic protons were seen to be upfield shifted by 0.29 ppm relative to the most intense pyrrolic peak of the cage (Figure 24). In addition, an upfield shifted peak was observed for the DABCO protons at −4.1 ppm (compared to free DABCO at 2.7 ppm), indicating internalisation and complexation at the Zn(II)-porphyrin site. Distinction from the **biPy@42·8BArF** spectrum was seen in the phenyl protons, with the difference in chemical shift between the inward and outward-facing *ortho* protons increasing relative to the spectra of **42·8BArF**. However, this was not seen for the *meta* protons where the difference in chemical shift was seen to become smaller. This could be due to the unequal anisotropic effects of the acridinium and porphyrin units. The large difference between the inward and outward-facing protons seen for **DABCO@42·8BArF** was in direct contrast to that seen for the complex **DABCO@42·8PF$_6$**, where little separation was seen between the inward and outward-facing protons (Figure 13).

Interestingly, downfield shifts of the BArF protons could again be seen upon addition of DABCO ($\Delta\delta H_{BArF}$ = +0.093 ppm), with the difference being larger than seen with **biPy@42·8BArF**. The ^{19}F NMR followed the trend, with a downfield shift by 0.14 ppm suggesting a possible rearrangement of the intermolecular BArF-cage interaction.

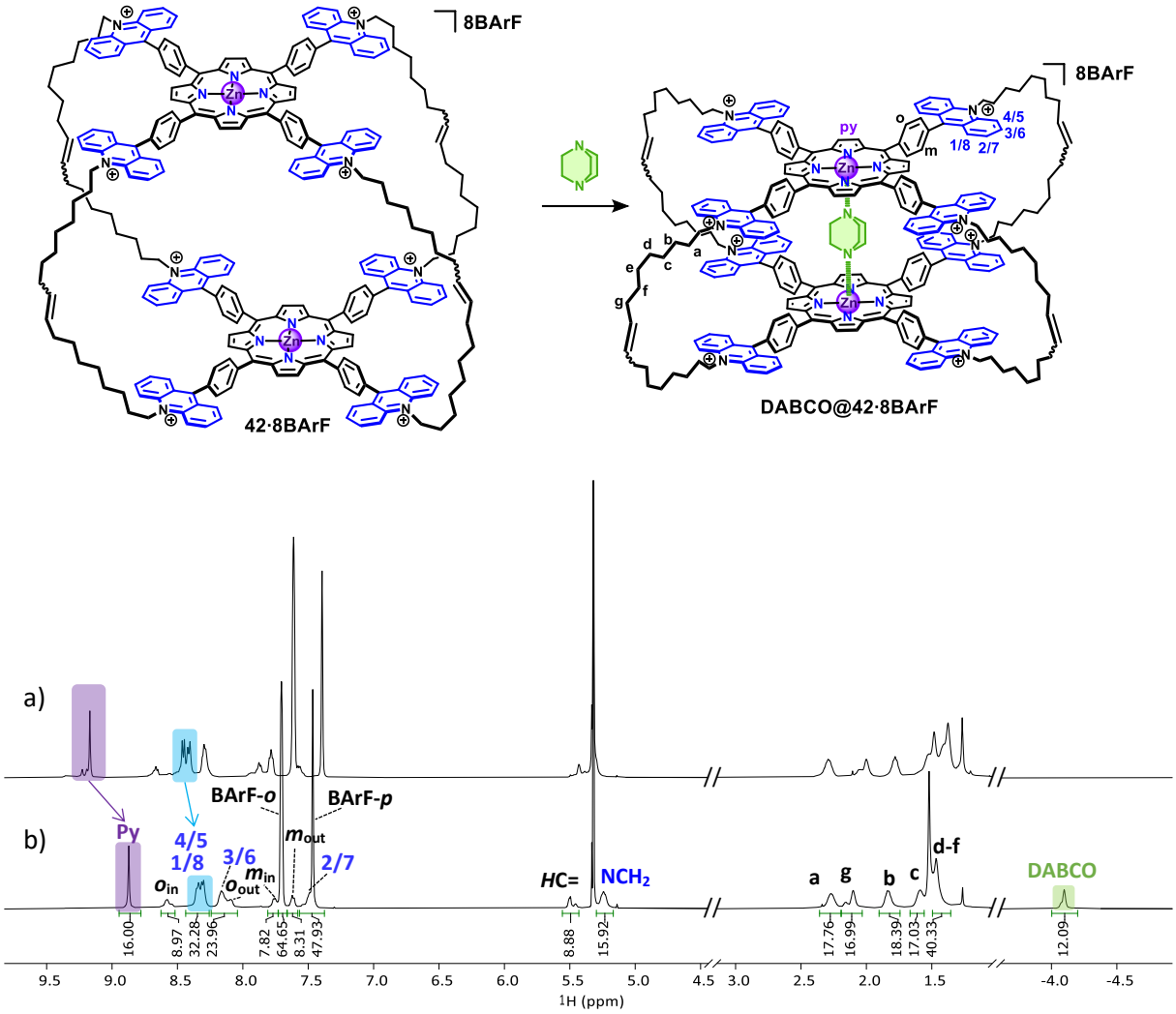

***Figure 24**. Stacked ^1H (500 MHz, CD_2Cl_2, 1.00 mM, 298 K) NMR spectra, showing a) **42·8BArF** and b) **DABCO@42·8BArF**.*

NOESY NMR confirmed binding of DABCO, with correlation between the pyrrolic protons and DABCO, and additionally between the inward-facing *ortho* protons and DABCO (Figure 25).

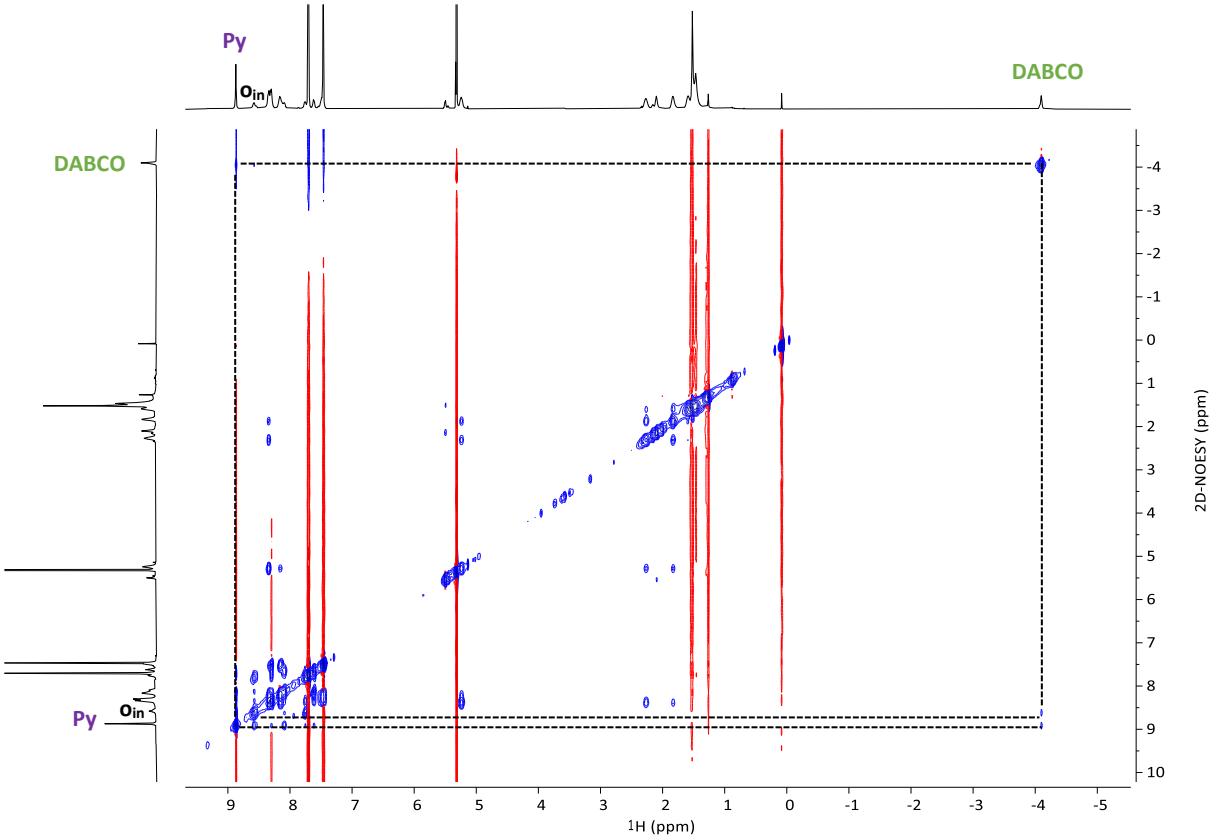

Figure 25. *2D-NOESY NMR (500 MHz, CD_2Cl_2, 1.00 mM, 298 K) spectrum for* ***DABCO@42·8BArF****.*

DOSY NMR experiments showed all peaks (excluding the BArF protons) to diffuse with the same diffusion coefficient (2.86×10^6 cm^2 s^{-1}), giving a calculated hydrodynamic radius of 17.5 Å, and volume of 22543 Å^3 using a spherical model, slightly larger than that obtained for **DABCO@42·8PF$_6$** (Table 5). In addition, as with **biPy@42·8BArF**, interaction between the cage and the BArF$^-$ ion appeared to still be present, with a diffusion coefficient of 3.65×10^{-6} cm^2 s^{-1} found for the BArF$^-$ ions, suggesting that the downfield shifts seen in the 1D spectra were due to rearrangement of the interaction between the cage and the BArF$^-$ ions.

Table 5. *Diffusion coefficients and hydrodynamic radii of the* ***DABCO@42·8BArF*** *and* ***DABCO@42·8PF$_6$*** *complexes.*

Species		Solvent	D ($\times 10^6$ cm^2 s^{-1})	R_h (Å)
DABCO@42·8BArF	**DABCO@42^{8+}**	CD_2Cl_2	2.86 (± 0.05)	17.5
	BArF	CD_2Cl_2	3.65 (± 0.02)	-
DABCO@42·8PF$_6$		CD_3CN	3.65 (± 0.07)	16.7

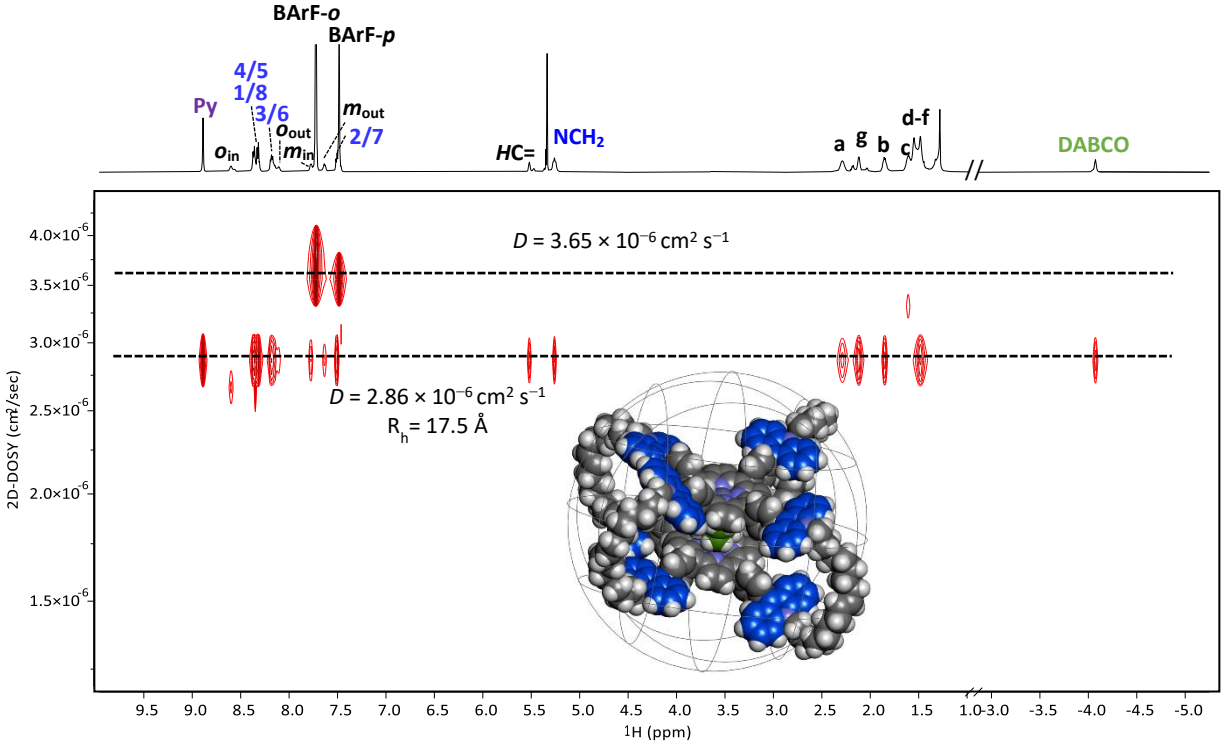

Figure 26. *^{1}H DOSY (600 MHz, CD_2Cl_2, 1.00 mM, 298 K) NMR spectrum for* ***DABCO@42·8BArF****, and the energy-minimised (Spartan'20) structure of* ***DABCO@42^{8+}*** *within a superimposed sphere (of radius = R_h).*

UV-Vis titrations in CH_2Cl_2 revealed hyperchromic shifts of the Soret band by a factor of 1.2, with a smaller shift in the absorbance maxima wavelength (Figure 27). A general thinning of the Soret band was also observed, in-line with a less conformationally flexible complex. In contrast to what was found with biPy, a single isosbestic point was observed at 419 nm, supporting formation of one complex. Fitting to a 1:1 model gave a binding constant of 1.2 (±0.2) × 10^7 M^{-1}, similar to that obtained for biPy.

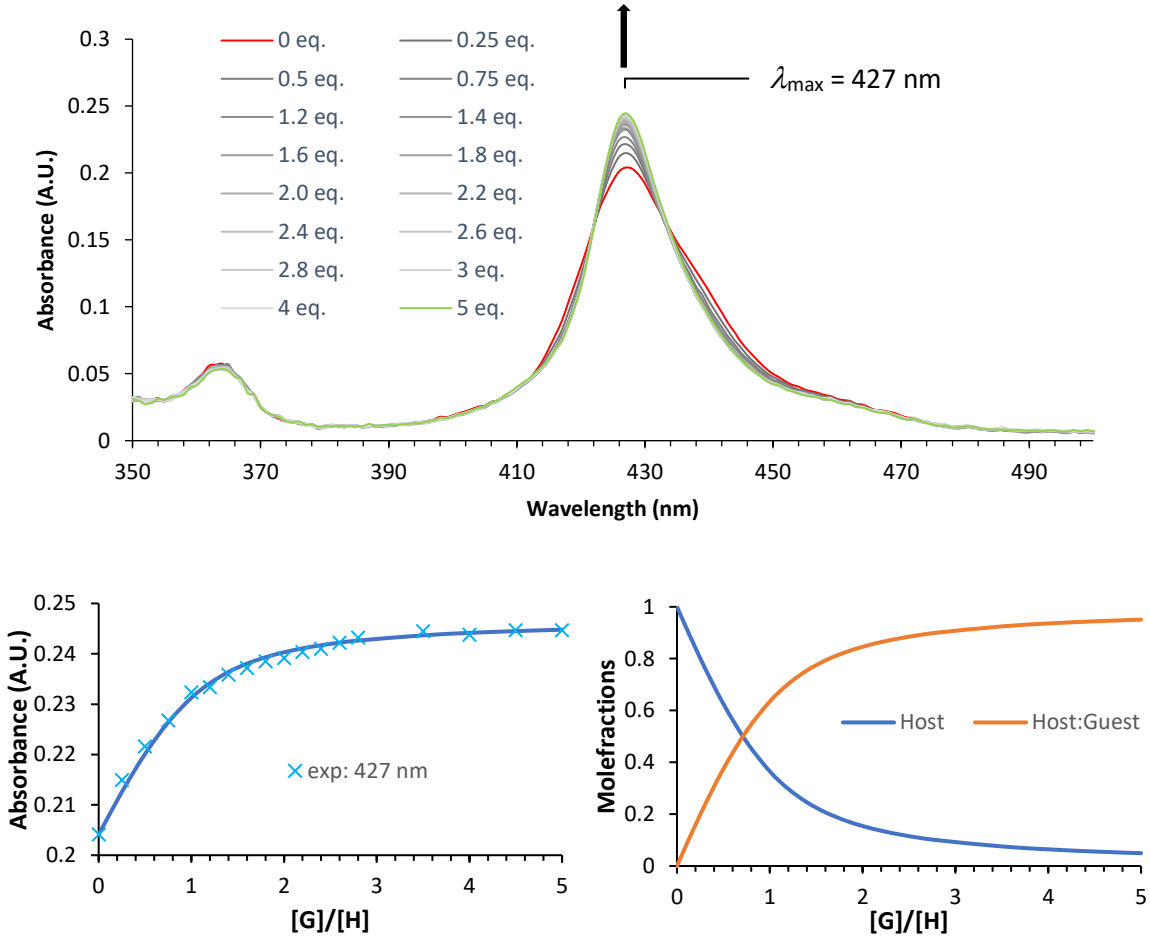

Figure 27. *UV-Vis (CH_2Cl_2, l = 1 cm, 298 K) titration of* ***42·8BArF*** *(c = 0.325 μM) with up to 5 equivalents of DABCO, and the non-linear regression fit of the titration curve with the accompanying calculated speciation diagram.*

6.3. Studies of the allosteric binding of pyrene

Taking advantage of the increased solubility in CD_2Cl_2, the **DABCO@42·8BArF** complex was then assessed for its ability to bind pyrene via NMR titrations (Figure 28). Addition of increasing equivalents of pyrene to a sub millimolar solution of **DABCO@42·8BArF** was seen to lead to increasing upfield shifting of the acridinium protons, with a flattening of the 4/5 and NCH_2 protons of the acridinium. Downfield shifting of the alkene and the allylic methylene protons was also seen, possibly due to their proximity to the amplified magnetic field at the periphery of the aromatic guest. Likewise, the inward-facing *ortho* protons were also increasingly downfield shifted. Interestingly, only a single set of peaks could be seen for the acridinium protons throughout the titration, indicating host-guest exchange between all the

acridinium sites, faster than the NMR time scale. In addition, although the majority of the peaks were seen to shift in one direction throughout the titration, the DABCO protons were seen to initially shift upfield (up to 100 equivalents), before plateauing and then shifting downfield, approaching its original chemical shift. This effect could be due to either an initial stabilisation then destabilisation upon uptake of pyrene guests, or due to increasing anisotropic magnetic field effects from the bound pyrene molecules on the DABCO protons (downfield shift) balanced against the stabilisation of the structure (upfield shift).

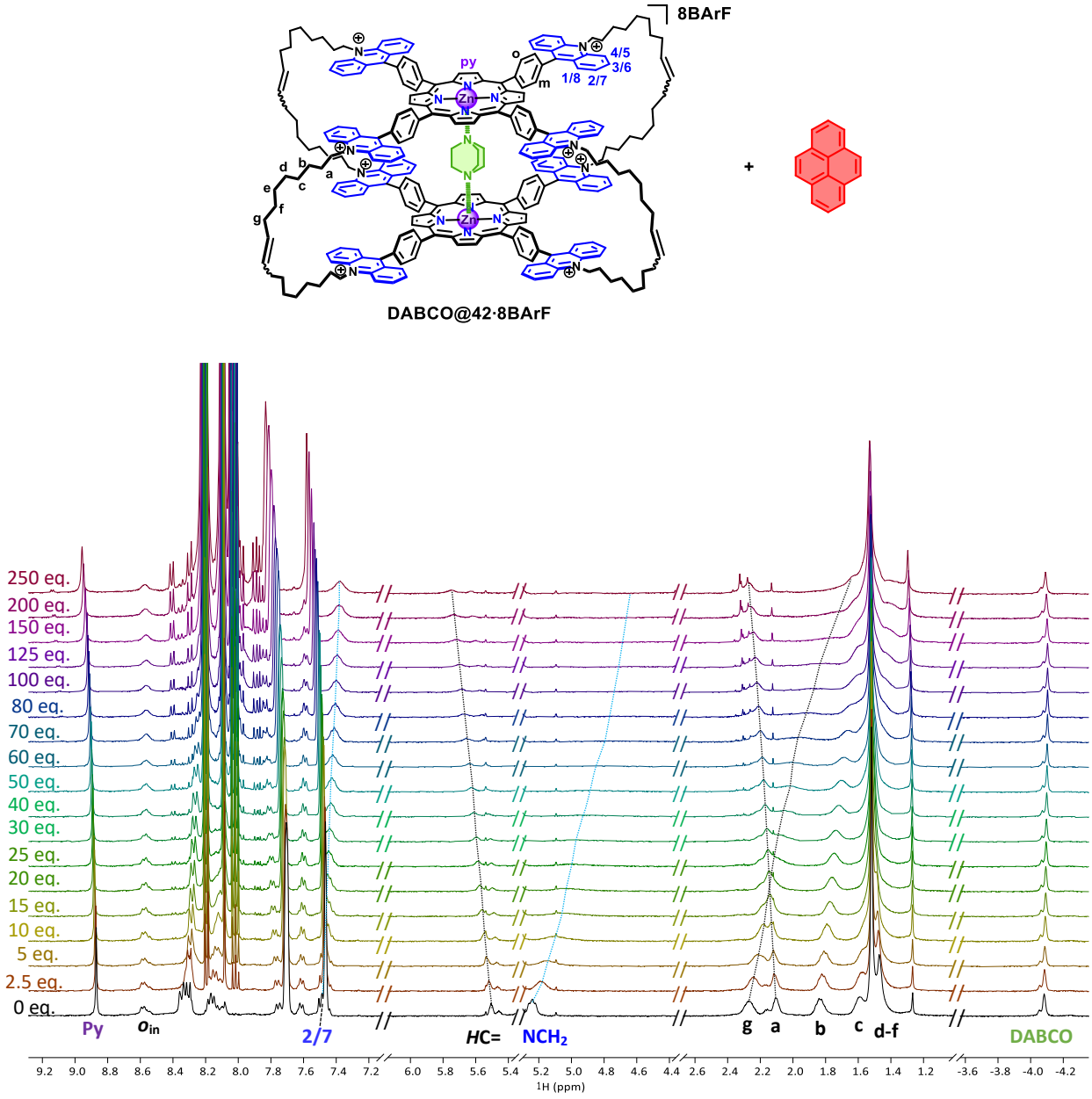

Figure 28. *Stacked ^{1}H NMR (400 MHz, CD_2Cl_2, 0.5 mM, 298 K) spectra, showing the changes in the spectra for* ***DABCO@42·8BArF*** *upon addition of up to 250 equivalents of pyrene.*

The obtained titration curve was not observed to have a sigmoidal shape, commonly seen for positively cooperative systems, [6,7] indicating that positive homotropic cooperativity was not present between the acridinium sites. Instead, a hyperbolic curve was seen for most protons (excluding DABCO), with increasing linearity in the curve at higher equivalents of the guest (Figure 29). The shape of the curve presented some uncertainty in whether there was a presence/lack of cooperativity between the acridinium units (i.e. whether negatively cooperative or non-cooperative). The stoichiometry of the host-guest species formed at the end of the titration could not be determined directly, with continuous variation plots unsuitable due to its unreliability in higher stoichiometry host:guest systems.[8] Due to the complexity of the system and difficulties in the analysis of the titration data, it could not be said directly which binding model was most accurate. Thus, further investigation of the binding of the polyaromatic molecules by the complex is needed, using new methods to ascertain the final stoichiometry.

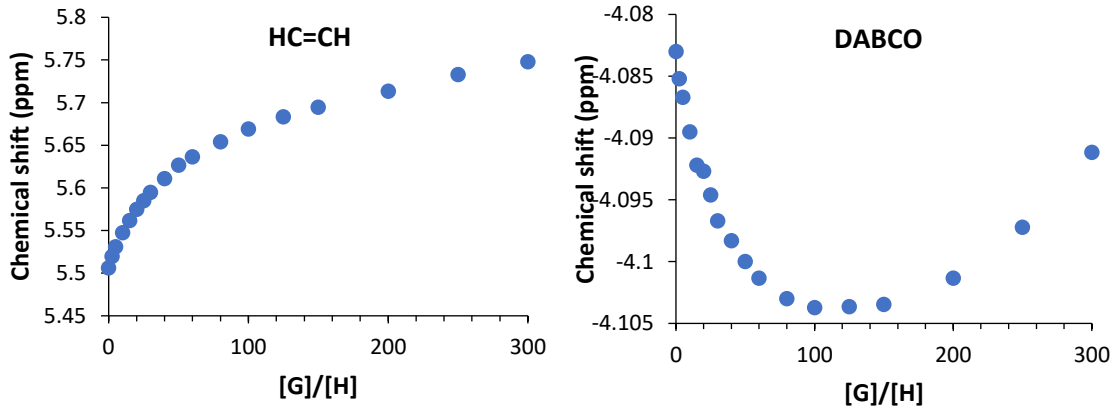

Figure 29. *Titration curves obtained for the alkene and DABCO protons.*

In the absence of the effector DABCO, no significant changes were seen in the ^{1}H NMR spectrum of the cage upon addition of 30 equivalents of pyrene at the same sub-millimolar concentration (Figure 30), in contrast to the upfield shift of approx. 0.3 ppm for the NCH_2 protons seen with the **DABCO@42·8BArF** complex at the same number of equivalents of pyrene. Additionally, no significant shifts were seen for the pyrene proton peaks, indicating little to no interactions taking place between the guest and **42·8BArF**, and that DABCO was an effective effector for realising interaction within the interior of the cage. Thus, it was concluded that an allosteric system had been achieved.

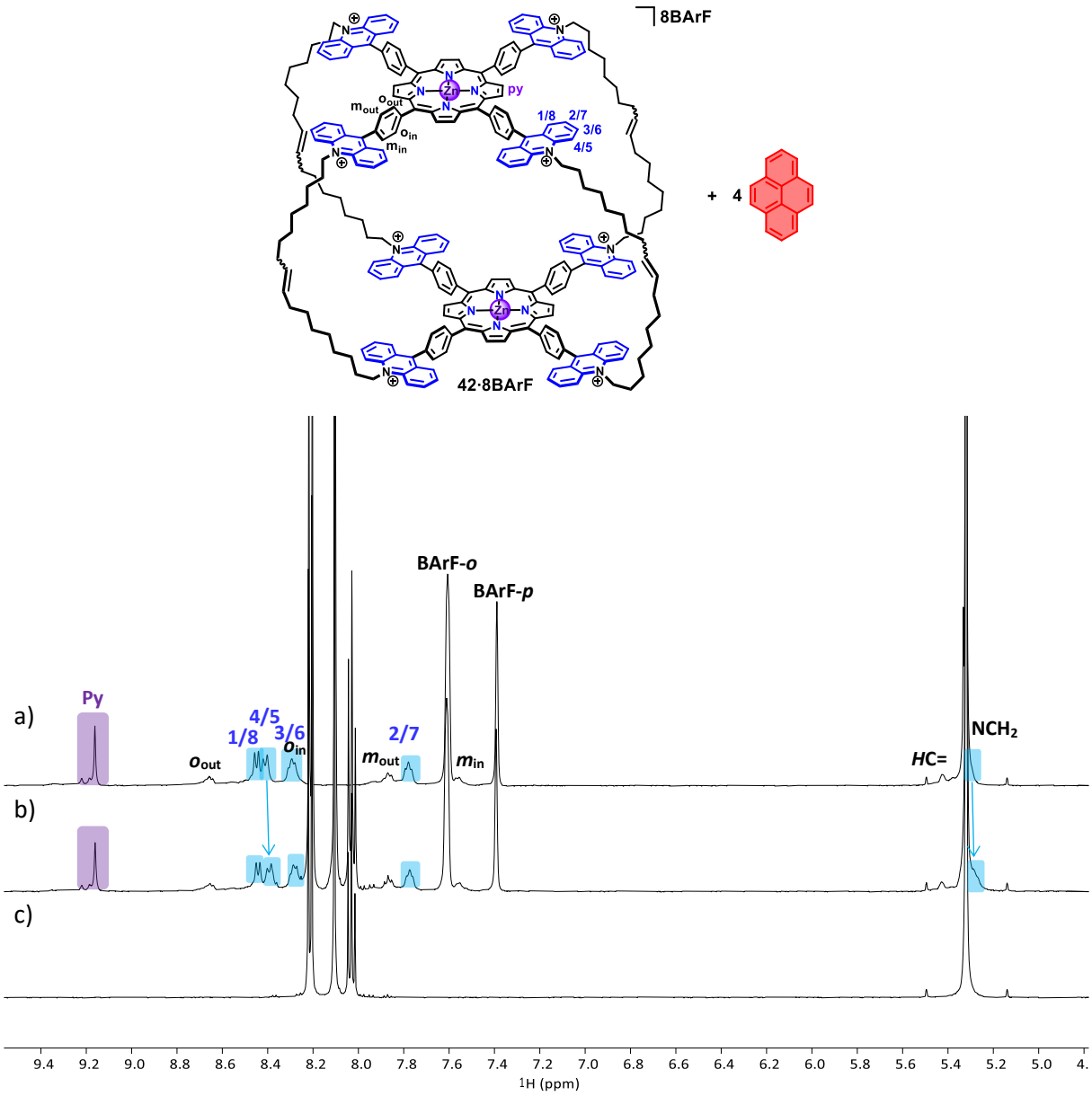

Figure 30. *Stacked ^{1}H NMR (500 MHz, CD_2Cl_2, 298 K) spectra of a) the cage BArF (c = 0.5 mM), b)* ***42·8BArF*** *+ 30 equiv. pyrene. A ^{1}H NMR spectrum of c) pyrene is also included for comparison.*

7. Effect of chemical stimulus in the form of nucleophilic addition

As seen with the tweezer, addition of nucleophiles can drastically alter the properties of the receptor. As such it was expected that due to the presence of more acridinium units, an even more pronounced change in the properties of the cage would be seen upon dearomatisation of the eight acridinium units.

7.1. NMR and mass spectrometry studies

The effects of nucleophilic addition were first explored via NMR spectroscopy, with addition of 8.4 eq. of KOH to a solution of **42·8PF$_6$** in CD_2Cl_2/CD_3CN (5%) leading to very broad peaks, similar to **42·8PF$_6$**. Via evaporation of the solvent and taking up of the resultant solid in CH_2Cl_2/CH_3OH (1:2) exchange of the OH groups to the methoxy group could be afforded, taking advantage of the reversible nature of the C-OH bond. The NMR spectrum of the resultant species was found to also be broad but more easily assigned (Figure 31a), with clear upfield shifts for the NCH_2 protons ($\Delta\delta NCH_2 = -1.5$ ppm). Additionally, the ^{13}C NMR spectrum showed a highly upfield shifted peak for the 9-carbon of the acridane species at 78 ppm ($\Delta\delta C_9 = -85$ ppm, Figure 31b) as seen when the same reaction was performed on **39·2PF$_6$** (Chapter 3, section 5.1). Further characterisation of the cage via DOSY experiments is currently underway, to verify the size and the singularity of the species.

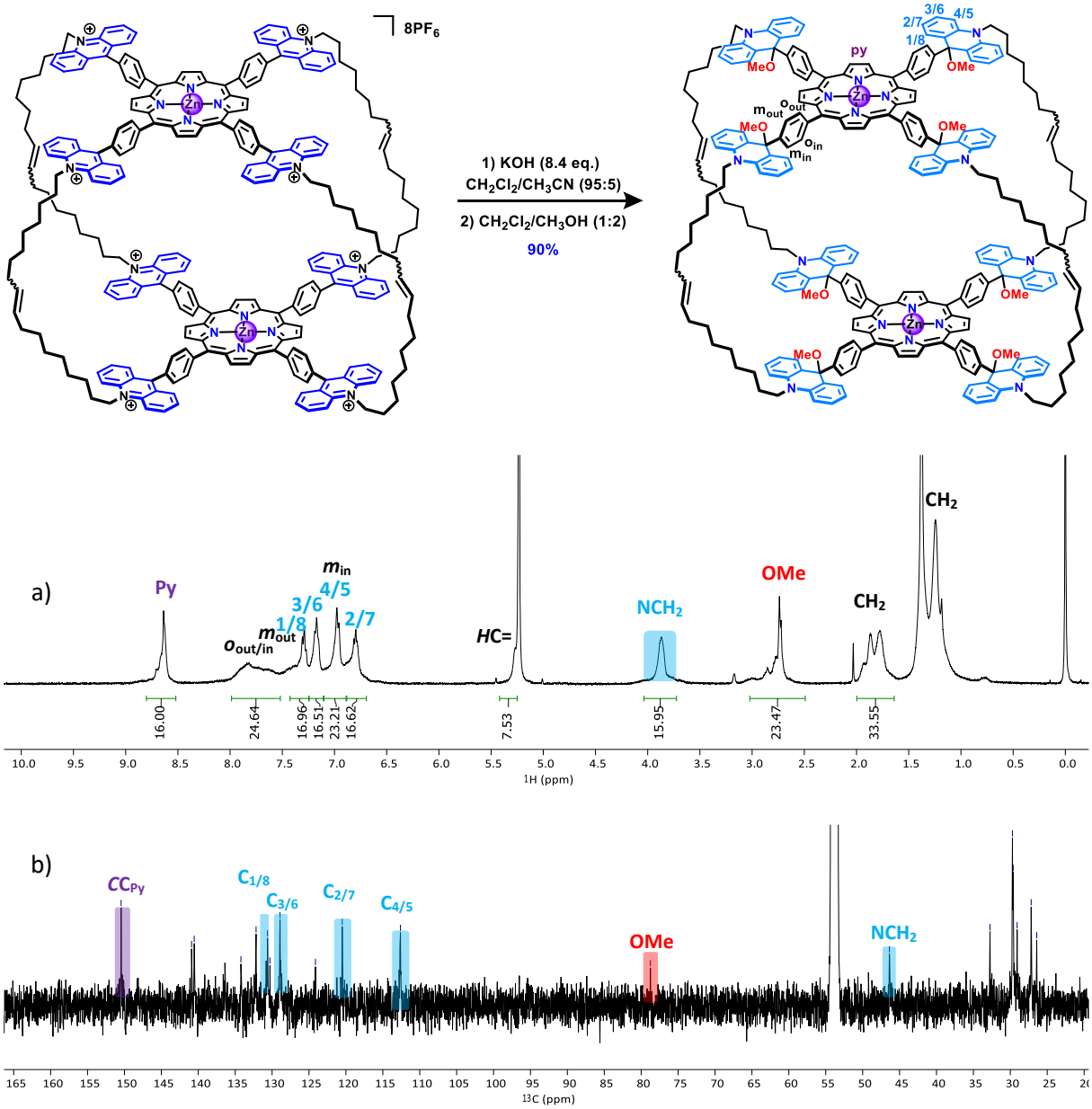

Figure 31. *a) ^{1}H NMR (400 MHz, CD_2Cl_2, 298 K) and b) ^{13}C NMR (125 MHz, CD_2Cl_2, 1.00 mM, 298 K) spectra for the acridane porphyrin cage* ***43*** *(after step 1: R = OH, after step 2: R = OMe).*

Analysis of the cage via ESI mass spectrometry gave a complex spectrum due to the multiple charged and radical species that could be formed as well as the replacement of the OMe groups with ionisation fragments of the solvent (Figure 32). Singly charged derivatives of the cage were not observed, however a number of low intensity 5+, 6+ and 7+ charged species were found. The major mass ion peak was found to be a 6+ species with loss of all methoxy groups and addition of a hydrogen atom ($[M–8OMe+H]^{6+}$ at m/z = 629.31).

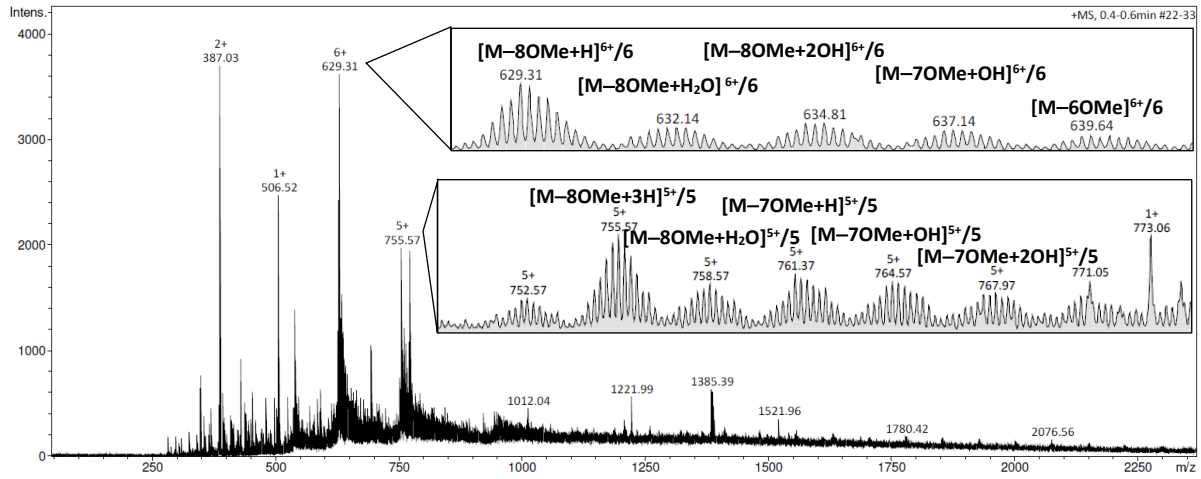

Figure 32. *Mass spectrum (ESI-TOF) obtained for **43**, with zoom insert of the regions m/z = 625 - 645 and 750 - 770.*

7.2. UV-Vis study

To further explore the effects of chemical stimulus, a fatigue study was conducted via UV-Vis spectroscopy, adding 8.4 eq. of TBAOH, followed by TFA to a solution of **42·8PF$_6$** (Figure 33). As with **39·2PF$_6$**, addition of the nucleophile led to flattening of the acridinium transition bands, and the appearance of a new band at around 293 nm. Additionally, the lower energy π–π* acridinium-centred transition band at around 450 nm was flattened, with the broad right-hand shoulder of the Soret band disappearing. Similarly, the Q-band was seen to narrow, most especially for the last peak at 600 nm, which is likely due to the change in nature of the transition for **43** versus **42·8PF$_6$**. In the latter case, the lowest energy transition band is likely due to charge transfer from the HOMO localised on the porphyrin to the octo-degenerate LUMOs localised on the eight acridinium units, as calculated and found (electrochemically) for the bisacridinium porphyrin **35·2PF$_6$** (Chapter 2, section 5). In contrast, for **43** the HOMO and LUMO are likely both localised on the porphyrin units. Additionally, the intensity of the Soret band was seen to increase after addition of TBAOH.

Upon addition of 8.4 equivalents of TFA, the acridinium spectral features were recovered, with the acridinium-centred π–π^* transition bands reappearing, and the Q-band becoming broadened again. The Soret band was not observed to decrease in intensity, however this was ascribed to an anion metathesis from the PF_6^- counter anion to the more strongly

coordinating TFA^- counter anion. Repeat of this cycle nine times, was not seen to lead to any significant loss in conversion or recovery, showing that the acridinium units are robust. Additionally, no demetallation of the Zn(II)-porphyrin units could be observed, consistent with a much more reactive and acid-sensitive acridanol species, compared to the metallo-porphyrin, as was seen in the chemo-switching study of the tweezer **39·2PF$_6$** (Chapter 3, section 5.1.2).

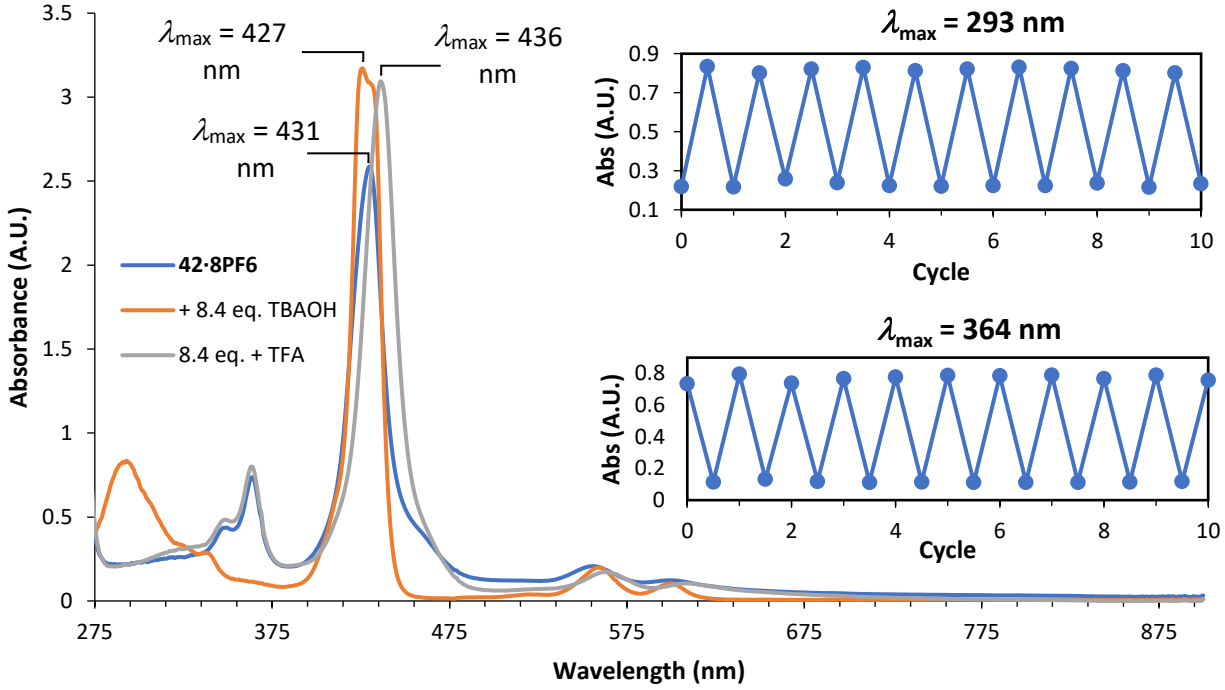

Figure 33. *Overlayed UV-Vis (CH_2Cl_2, l = 0.5 cm, 298 K) spectra, showing the changes in the spectra upon addition of TBAOH (8.4 eq.) to* ***42·8PF$_6$*** *(c = 10.0 μM) followed by addition of TFA (8.4 eq.). The change in absorbance for the acridinium-centred (364 nm) and acridanol-centred (293 nm) bands upon addition of TBAOH followed by TFA are given for 10 cycles.*

7.3. Binding study of the octaacridane porphyrin cage

As the presence of eight acridinium units was expected to lead to a more pronounced response to chemical stimuli, the effects of nucleophiles on the binding ability of the porphyrin unit were next probed.

7.3.1. NMR study of the complexation of biPy

Addition of 8.4 equivalents of KOH in CH_3OH, to a solution of **biPy@42·8PF$_6$** was seen to lead to significant changes to the NMR spectrum (Figure 34). Compared to the **biPy@42·8PF$_6$** spectrum, the peaks of **biPy@43** were observed to be slightly broadened, but significantly less broad than the spectrum of **43**, with more distinct peaks for the phenyl *ortho* protons. Upfield shifts of all protons relative to the **biPy@42·8PF$_6$** were seen, as well as an upfield shift of the pyrrolic protons relative to **43** (by 0.13 ppm). In addition, larger downfield shifts of the acridane protons were seen (by 0.21 ppm). Curiously, peaks for the *beta* protons of biPy were not observed at the chemical shift seen for **biPy@42·8PF$_6$** (4.95 ppm), with possible overlap with nearby peaks.

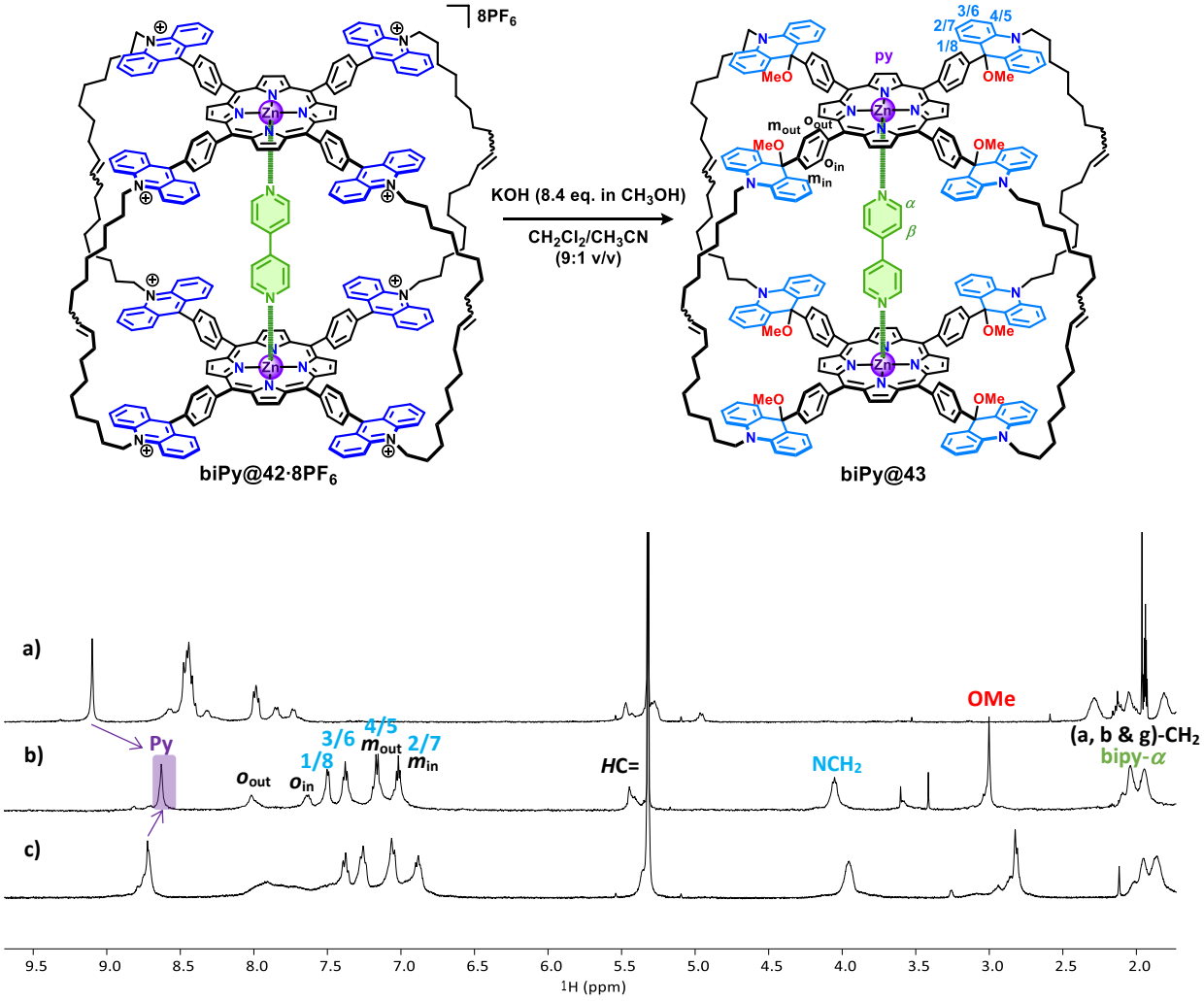

Figure 34. *Stacked ^{1}H NMR (400 MHz, 298 K) spectra of a) the complex* ***biPy@42·8PF$_6$*** *(CD_2Cl_2/CD_3CN (9:1), 1.00 mM), b)* ***biPy@43****, (CD_2Cl_2, 1.00 mM) and c)* ***43****. (CD_2Cl_2, 1.00 mM).*

Further investigation and characterisation of this complex via ^{1}H DOSY NMR experiments are currently underway to confirm complexation of biPy.

7.3.2. UV-Vis study of the complexation of bipy

To ascertain the binding constant, UV-Vis titrations were carried out (Figure 35). Addition of increasing equivalents of biPy, was seen to lead to bathochromic and hyperchromic shifts as seen for **42·8BArF**. The presence of one isosbestic point at 428 nm supported formation of a 1:1 species, thus the data was fit to a 1:1 binding model. It was found that the binding affinity was significantly decreased relative to **42·8BArF** and even to **42·8PF$_6$**, with a binding constant of 1.0 (± 0.2) × 10^6 M^{-1}. This value was 13 times smaller than that obtained for **42·8BArF** and 4 times smaller than that obtained for **42·8PF$_6$**, indicating a significant decrease in the binding ability due to addition of nucleophiles (Table 6). Thus, remote controlled binding of biPy was afforded via chemical stimulus, in a mechanism slightly different to the tweezers **39·2PF$_6$** and **40** where such large differences in the binding affinity were not seen until the addition of electrochemical stimulus.

The difference in behaviour was ascribed to the presence of a larger number of acridinium/acridanol units giving rise to larger cumulative differences in the two cage structures. For example, the loss of the electron withdrawing effect from the acridinium on the porphyrin is larger for the octacationic cage versus the dicationic tweezer. Additionally, the difference in conformational flexibility between the neutral and charged cage may be more pronounced than for the neutral and charged tweezer, which remain highly flexible in either form.

Table 6. *Binding constants obtained via UV-Vis titrations of the cages (**42·8PF$_6$**, **42·8BArF** and **43**) with biPy.*

Species	Guest	Solvent	K_a (L mol^{-1})
42·8PF$_6$	**biPy**	CH_2Cl_2 (0.1% CH_3CN)	4.2 × 10^6
42·8BArF	**biPy**	CH_2Cl_2	1.3 × 10^7
43	**biPy**	CH_2Cl_2	1 × 10^6

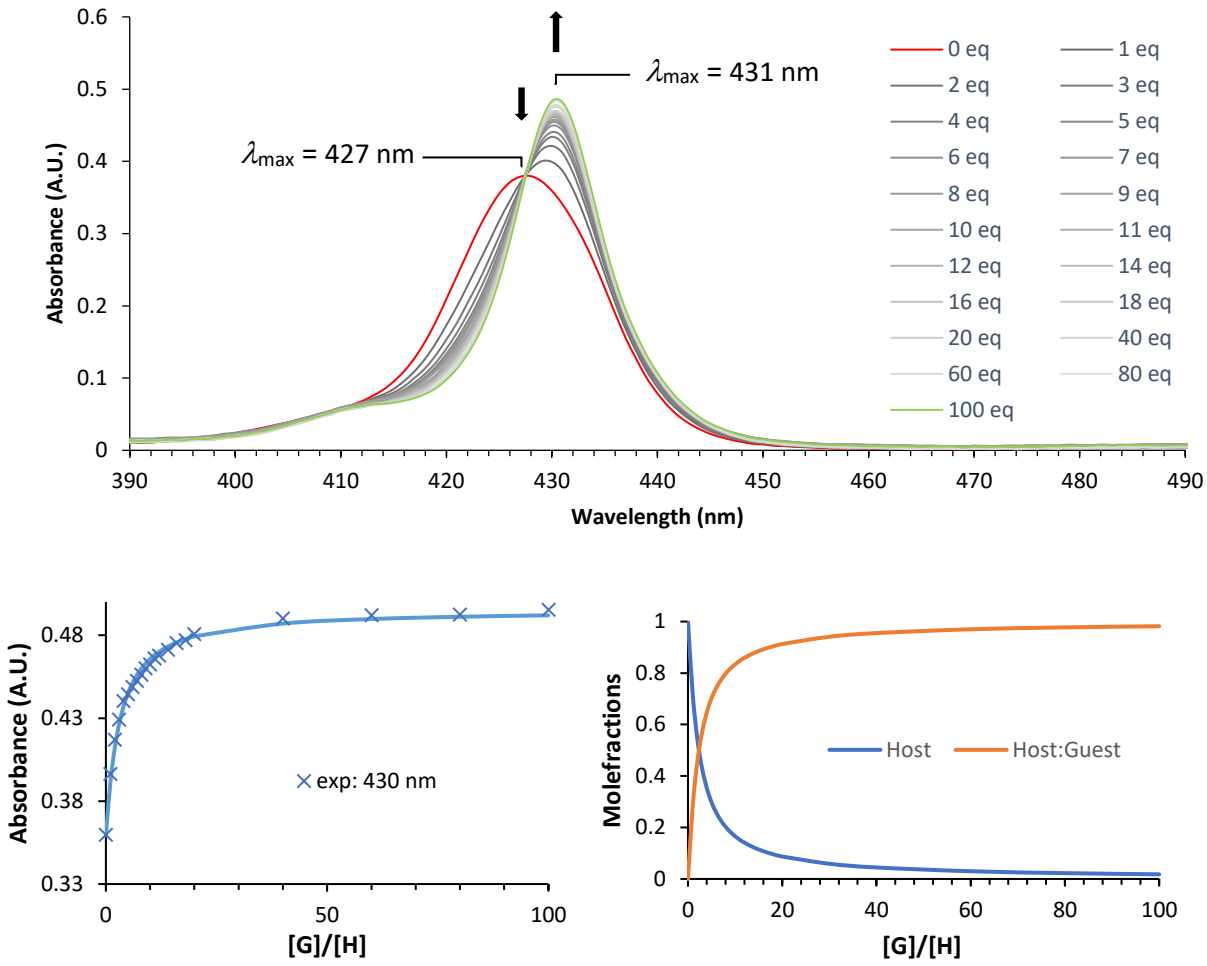

Figure 35. *UV-Vis (CH_2Cl_2, l = 1 cm, 298 K) titration of* ***43*** *(c = 0.475 μM) with up to 100 equivalents of biPy, and the non-linear regression fit of the titration curve with the calculated speciation diagram.*

8. Conclusion

In conclusion, informed by our work in the synthesis of porphyrin-acridinium conjugates, and by the successful synthesis of a porphyrin-acridinium tweezer, an octacationic porphyrin-acridinium cage was synthesised via olefin metathesis, and studied as both a PF_6 and BArF salt. The counter anion was shown to dramatically affect the solubility of the cage, as well as impacting whether parallel offset π–π intramolecular interactions were present between the Zn(II)-porphyrin units.

The cage was shown to be able to ditopically bind both DABCO and biPy to form 1:1 host-guest species. In addition, within the context of allosteric control, the DABCO bound cage complex was shown via ^{1}H NMR spectroscopy to be able to bind aromatic guests. Interestingly, where a strong interaction between the aromatic guest and the cage@DABCO complex was seen, interaction with the cage alone was not indicated. Thus, an allosteric system was successfully developed, with complexation of DABCO by the Zn(II)-porphyrin pre-organising for binding of aromatic guests within the acridinium binding sites.

The effects of chemical stimulus in the form of nucleophiles were examined via NMR and UV-Vis spectroscopy, with switching to the neutral octaacridane porphyrin cage achieved via addition of KOH. The process was found to be reversible via addition of TFA, and the obtaned fatigue cycle showed the switching could be had without major loss of conversion for 10 cycles, representing a robust molecule. Finally, the addition of nucleophiles was found to drastically alter the binding affinity of the cage for biPy, with a lower binding constant compared to both the PF_6 and BArF salt, indicating that addition of nucleophiles could be used as a remote-control for binding of biPy. In totality, the various studies allowed the characterisation of a highly complex, stimuli responsive receptor, showing control of binding affinity at the porphyrin via the acridinium/acridanol, as well as control of the binding affinity at the acridinium site via the porphyrin.

9. References

(1) Wang, H.-W.; Chen, C.-H.; Lim, T.-S.; Huang, S.-L.; Luh, T.-Y. Supramolecular Porphyrin-DABCO Array in Single- and Double-Stranded Polynorbornenes. *Chem. Asian. J.* **2011**, *6* (2), 524–533.

(2) Zhu, B.; Chen, H.; Lin, W.; Ye, Y.; Wu, J.; Li, S. Template-Directed Synthesis of Flexible Porphyrin Nanocage and Nanorings via One-Step Olefin Metathesis. *J. Am. Chem. Soc.* **2014**, *136* (43), 15126–15129.

(3) Taesch, J.; Heitz, V.; Topić, F.; Rissanen, K. Templated Synthesis of a Large and Flexible Covalent Porphyrinic Cage Bearing Orthogonal Recognition Sites. *Chem. Commun.* **2012**, *48* (42), 5118.

(4) Solladié, N.; Aziat, F.; Bouatra, S.; Rein, R. Bis-Porphyrin Tweezers: Rigid or Flexible Linkers for Better Adjustment of the Cavity to Bidentate Bases of Various Size. *J. Porphyr. Phthalocyanines* **2008**, *12* (12), 1250–1260.

(5) Soury, R.; Jabli, M.; Saleh, T. A.; Abdul-Hassan, W. S.; Saint-Aman, E.; Loiseau, F.; Philouze, C.; Nasri, H. Tetrakis(Ethyl-4(4-Butyryl)Oxyphenyl)Porphyrinato Zinc Complexes with 4,4'-Bpyridin: Synthesis, Characterization, and Its Catalytic Degradation of Calmagite. *RSC Adv.* **2018**, *8* (36), 20143–20156.

(6) Shinkai, S.; Ikeda, M.; Sugasaki, A.; Takeuchi, M. Positive Allosteric Systems Designed on Dynamic Supramolecular Scaffolds: Toward Switching and Amplification of Guest Affinity and Selectivity. *Acc. Chem. Res.* **2001**, *34* (6), 494–503.

(7) Lee, C. H.; Yoon, H.; Kim, P.; Cho, S.; Kim, D.; Jang, W. D. An Indolocarbazole-Bridged Macrocyclic Porphyrin Dimer Having Homotropic Allosterism with Inhibitory Control. *Chem. Commun.* **2011**, *47* (14), 4246–4248.

(8) Brynn Hibbert, D.; Thordarson, P. The Death of the Job Plot, Transparency, Open Science and Online Tools, Uncertainty Estimation Methods and Other Developments in Supramolecular Chemistry Data Analysis. *Chem. Commun.* **2016**, *52* (87), 12792–12805.

General conclusions and perspectives

In this project, we first successfully identified an efficient route to synthesis of *meso* substituted porphyrin-acridinium conjugates, using a novel formyl phenyl acridinium reactant. This synthetic route was used to synthesise conjugates with one or two acridinium *meso* substituents. Furthermore, the properties of these novel conjugates were investigated, with photoinduced electron transfer implicated in the observed quenched fluorescence of the bisacridinium porphyrin species.

The synthetic pathway was extended to the synthesis of receptors, with synthesis of both a porphyrin-acridinium tweezer and cage. The capacity of the two receptors to bind differing ditopic ligands (specifically DABCO and 4,4'-bipyridine) was investigated, with binding constants in the range of $10^5 – 10^6$ M^{-1} found for the 1:1 macrocyclic host-guest complexes of the tweezer, and in the range of $10^6 – 10^7$ M^{-1} for the 1:1 complexes of the cage. The ability to pre-organise for binding of polyaromatic guests via ditopic coordination of DABCO was probed in the case of both the cage and the tweezer. For the tweezer, DABCO was found to be a poor effector. However, for the cage DABCO was seen to act as an effective on/off switch for encapsulation of the poly aromatic guest, thus giving rise to a positive heterotropic allosteric control of aromatic guest uptake.

Additionally, the effect of different stimuli on the binding abilities of the two receptors has been explored, with chemical stimulus seen to change the photophysical properties of the receptors due to changes in aromaticity upon nucleophilic addition to the acridinium. For the tweezer, the effects of nucleophilic addition were seen to extend to a change from a photoinduced electron transfer process (seen with the porphyrin-acridinium tweezer) to an energy transfer (for the porphyrin-acridanol tweezer). Finally, the ability to remotely-control the binding of 4,4'-bipyridine at the porphyrin site via nucleophilic addition was evidenced in both receptors, and in the case of the tweezer, shown to proceed via the coupling of redox and chemical stimulus.

As such, the presented studies lead to the conclusion that we have successfully met our aim to synthesise novel receptors, which are able to bind different guests, control binding of guests via an allosteric mechanism and furthermore, respond to multiple

different stimuli, thus having more than one control mechanism for the binding of guests.

Finalisation of the allosteric study is required, specifically in determining the stepwise binding constants for uptake of the aromatic guests. This will thereby establish whether there is any cooperativity between the acridinium binding sites and moreover, whether the cage shows multi-pathway allosteric control. Additionally, the ability to bind different polyaromatic molecules has not yet been fully investigated, with our work focusing on pyrene due to its relatively high solubility. Thus, titration of the hosts with other aromatic species such as perylene, pentacene, coronene etc., should be studied. These studies will also aid in determining the features that most effect the strength of the binding interaction with the receptors.

Further investigations are also underway to complete the stimuli response study of the cage, most especially with regards to the effects of electrochemical stimuli, and whether the effects seen for the tweezer in the binding of 4,4'-bipyridine are similarly seen for the cages. Additionally, photophysical studies on the porphyrin-acridinium and porphyrin-acridanol cage are needed to establish whether similar changes in behaviour are seen upon nucleophilic addition as seen with the tweezer. Furthermore, full studies into the effects of chemical stimulus in the binding of polyaromatic molecules should be completed to confirm whether the acridane species displays no affinity for polyaromatic molecules, and to assess the affect if any on the binding of DABCO, and how this may further impact the binding of polyaromatic molecules.

As this work has been wide-ranging, covering the synthesis of novel porphyrin conjugates, receptors of different architectures and control of molecular encapsulation via different stimuli, many perspectives are opened for further research. For example, to complete the family of receptors, the synthesis of the macrocycle and cryptand structures can also be attempted, with investigations into their properties and encapsulating abilities, and comparison to the tweezer and cage, providing further insight into the impact of the structure on the properties of the cage.

List of molecules

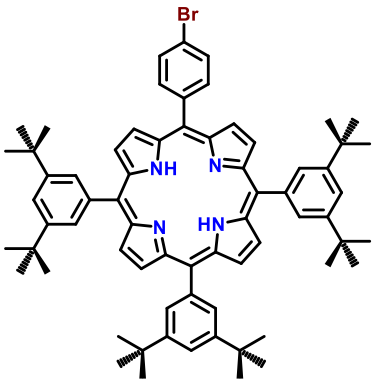

26-2H

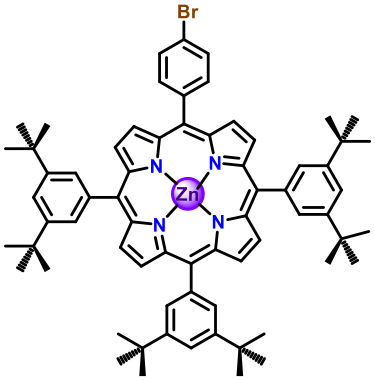

26-Zn

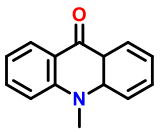

27

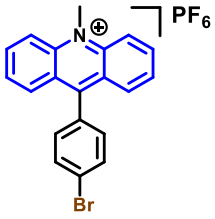

28·PF_6

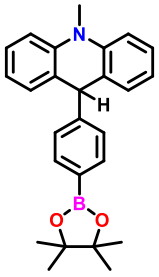

29

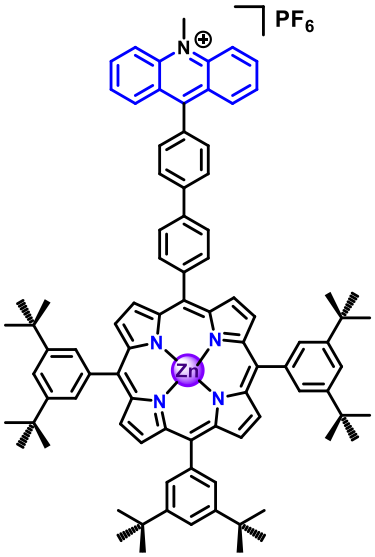

30·PF_6

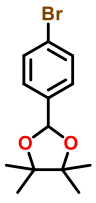

31

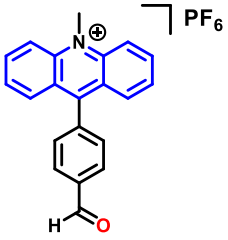

32·PF_6

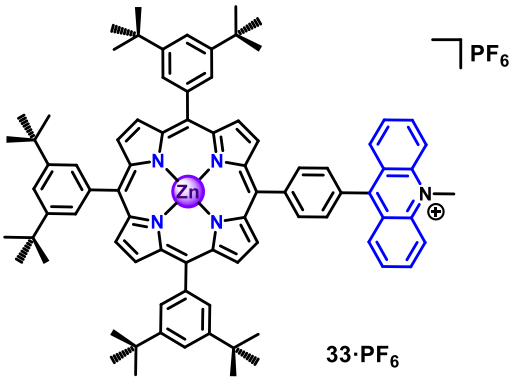

33·PF_6

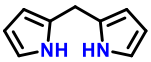

34

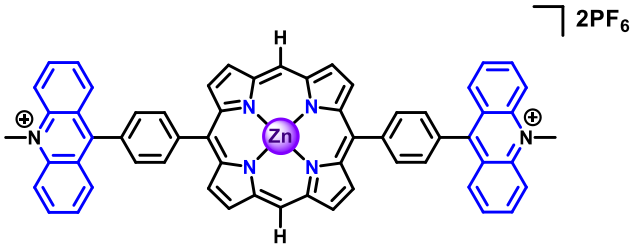

35·2PF$_6$

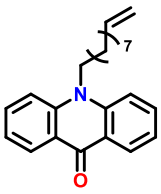

36

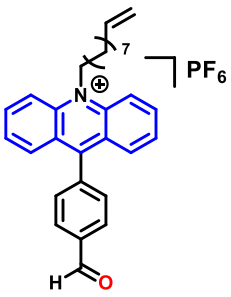

37·PF$_6$

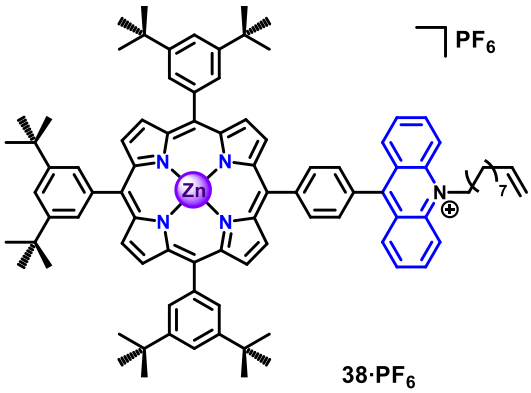

38·PF$_6$

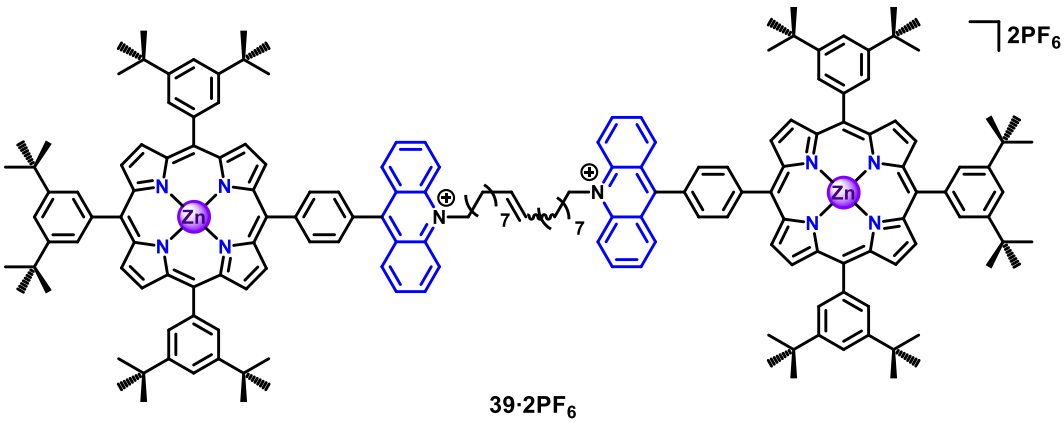

39·2PF$_6$

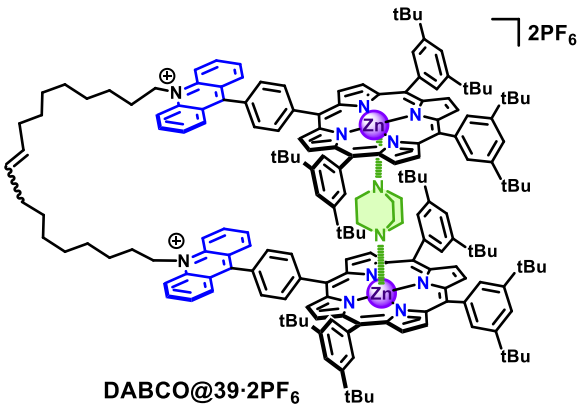

DABCO@39·2PF$_6$

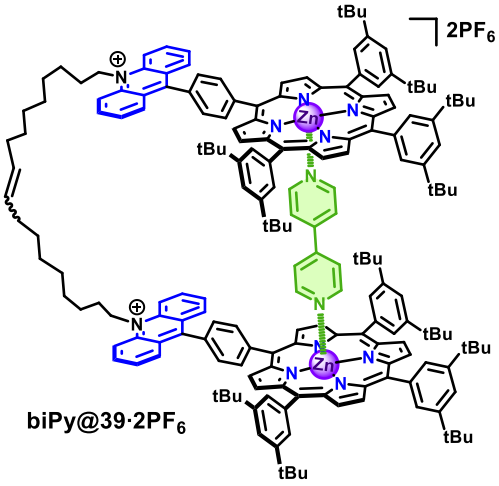

biPy@39·2PF$_6$

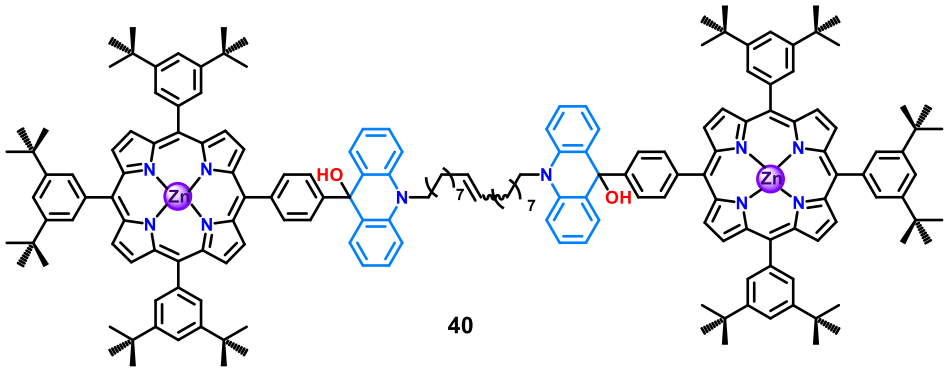

40

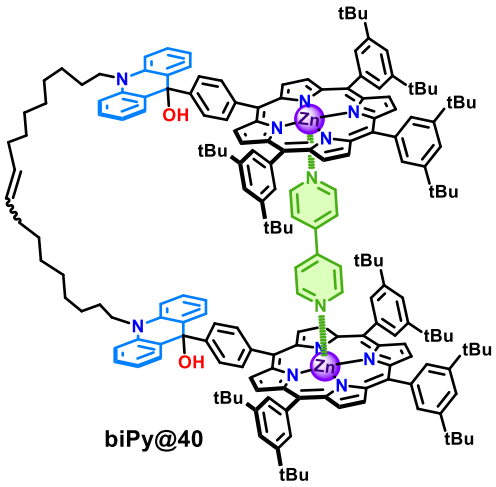

biPy@40

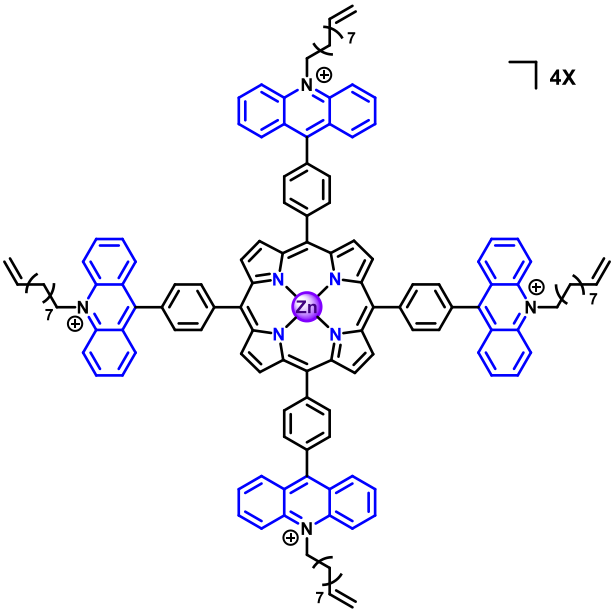

41·4X

where **X** = **PF$_6$** or **BArF**

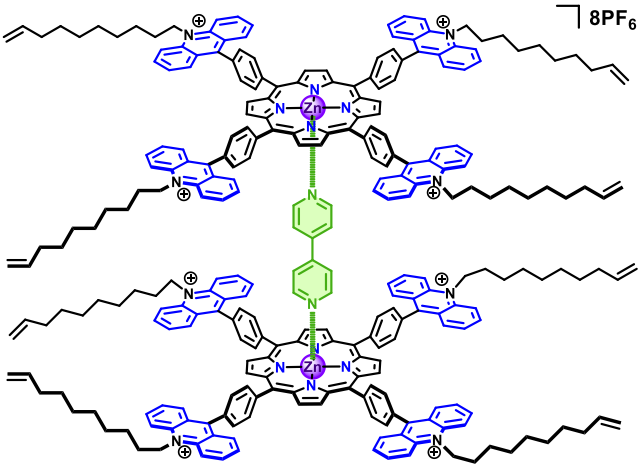

biPy@(41·4PF$_6$)$_2$

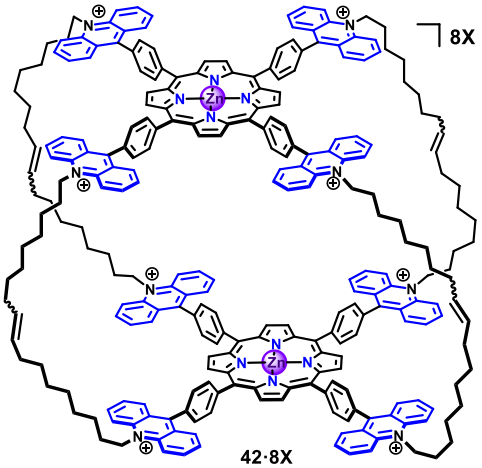

42·8X
where **X** = **PF$_6$** or **BArF**

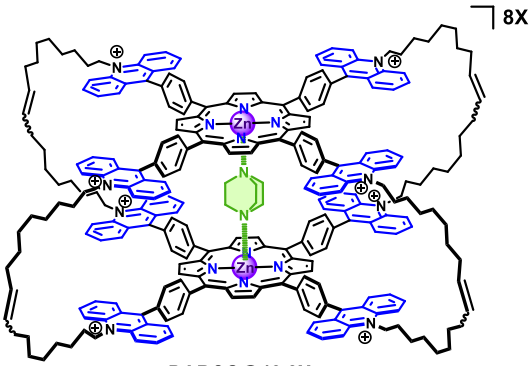

DABCO@42·8X
where **X** = **PF$_6$** or **BArF**

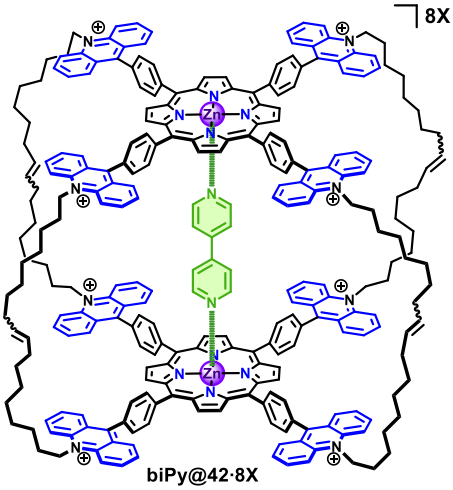

biPy@42·8X
where **X** = **PF$_6$** or **BArF**

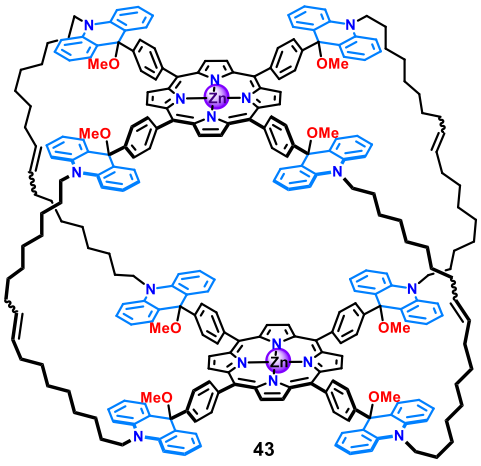

43

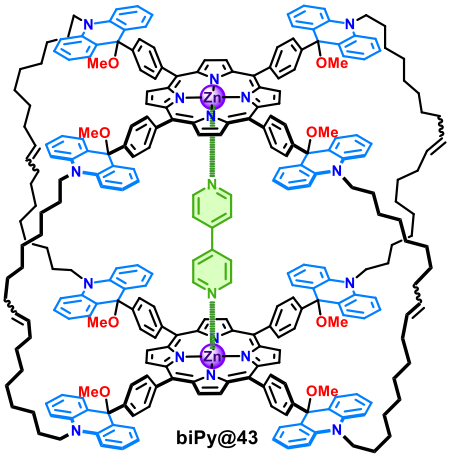

biPy@43

Experimental Section

Materials and methods

All solvents and reagents were acquired from commercial suppliers and used without further purification except in the following cases: Pyrrole was filtered through a plug of alumina before use; anhydrous THF was prepared via distillation over sodium/benzophenone. Where necessary, anhydrous CH_2Cl_2 was prepared via distillation over CaH_2. Analytical reagent grade CH_2Cl_2, stabilised with ethanol, was used for all porphyrin syntheses. Thin layer chromatography was performed on silica gel 60 F254 (Merck), with visualisation under visible light or short wavelength UV lamp.

NMR spectroscopic methods

NMR spectroscopies were carried out on 300, 400, 500 and 600 MHz Bruker Avance III Spectrometers, with residual solvent peaks used as internal references (δH: CD_3CN 1.94 ppm, CD_2Cl_2 5.32 ppm, $CDCl_3$ 7.26ppm; δC: CD_3CN 118.26 ppm, CD_2Cl_2 53.84 ppm, $CDCl_3$ 77.16 ppm). For ^{1}H NMR spectra, chemical shifts are given in ppm, followed by multiplicity (broad singlet (br.s), singlet (s), doublet (d,) triplet (t), doublet of doublet (dd), doublet of triplet (dt), doublet of doublet of doublet (ddd), doublet of quartet (dq), quartet (q), pentet (p), septuplet (sept), multiplet (m)), coupling constants (in Hz) and relative integral. For $^{13}C\{^{1}H\}$, $^{31}P\{^{1}H\}$ and $^{19}F\{^{1}H\}$ NMR spectra, chemical shifts are similarly given in ppm, followed by multiplicity and coupling constant (where relevant). HMBC, HSQC, COSY and NOESY were used to determine and confirm structure, and as aids in spectral assignment.

DOSY experiments were conducted on the 600 MHz Bruker Avance III Spectrometer, equipped with a Bruker BBI probe (developing a pulse field gradient of 5 G cm^{-1} A^{-1}). The diffusion NMR data of the samples (thermostated at 298 K) were acquired using a stimulated echo pulse sequence with bipolar z gradients. The limited Eddy current delay was fixed to 5 ms. For the tweezer receptors, and their respective bipyridine complexes: diffusion time (Δ) = 0.0999 s, and gradient pulse duration (δ) = 2.2 ms. For the complex **DABCO@39·2PF$_6$**: Δ = 0.1199 s, and δ = 1.8 ms. For the cage receptors and their

complexes: Δ = 0.1199 s, and δ = 2.2 ms. A recycling delay (≥ 5 seconds) was also employed between scans. H_2O and CH_3CN were used as reference standards to calibrate the gradient. Sample measurements were recorded in either CD_2Cl_2 (η = 4.353 × 10^{-4} Pa s) or CD_3CN (η = 3.57 × 10^{-4} Pa s). The spectra were then generated using the Dynamics centre module of the Bruker Topspin software package. The Stokes-Einstein equation was used to calculate the hydrodynamic radius (R_h):

$$D = \frac{k_B T}{6\pi\eta R_h}$$

UV-Visible spectroscopic methods

UV-Visible spectra were performed via a Biotek UVIKON XL UV/VIS Spectrophotometer, using quartz cuvettes of 0.1, 0.2, 0.5 or 1 cm path length, with absorbance maxima wavelengths given in nm, and corresponding molar extinction coefficients given in L mol^{-1} cm^{-1}.

Mass spectrometric methods

Accurate mass were obtained by way of high resolution ESI mass spectrometry using a Bruker MicroTOF(II) focus spectrometer.

Electrochemical Methods

Electrochemical experiments were acquired on an EG&G Princeton Applied Research Potentiostat/Galvanostat (Model 273A). Cyclic Voltammetry experiments were performed using a Pt working electrode (0.071 cm^2). The electrode surface was polished routinely with a 0.05 µm alumina-water slurry on a felt surface immediately before use. The counter electrode was a Pt coil and the reference electrode was a saturated calomel electrode (SCE). Samples were prepared in dichloroethane (Acros organics, +99%), dimethylformamide (Fischer, 99.5%) and benzonitrile (Fluka, > 99%), using 0.1 mol L^{-1} tetrabutylammonium hexafluorophosphate ($TBAPF_6$, Sigma Aldrich, +99%) as supporting electrolyte.

5-(4-bromophenyl)-10,15,20-tris(3,5-di-*tert*-butylphenyl)porphyrin (26-2H) [1]

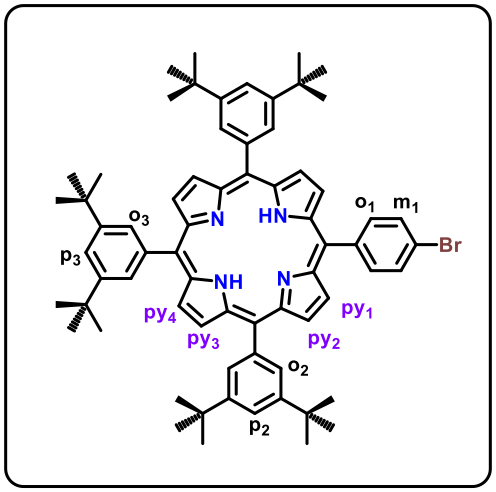

A solution of 4-bromobenzaldehyde (870 mg, 4.7 mmol), pyrrole (1.3 mL, 20 mmol, 4.3 eq.), and 3,5-di-*tert*-butyl-benzaldehyde (4.9 g, 22.4 mmol, 4.8 eq.) dissolved in propionic acid (70 mL) was heated to reflux and stirred overnight. The solvent was evaporated, and the resultant solid taken up in CH_2Cl_2 (100 mL) and washed with a saturated solution of $NaHCO_3$ (1 × 100 mL) and H_2O (3 × 50 mL). The retained organic layer was dried over $MgSO_4$ and the solution filtered through a plug of SiO_2. Following evaporation of the solvent the product was isolated via column chromatography (SiO_2, petroleum ether/CH_2Cl_2, 10:0 to 8:2) giving **26-2H** as a purple solid (337 mg, 7%).

^{1}H NMR (300 MHz, $CDCl_3$, 298 K) δ (ppm) = 8.90 (m, 6H, $H_{py2\text{-}4}$), 8.81 (d, ^3J = 4.8 Hz, 2H, H_{py1}), 8.10 (d, ^3J = 8.4 Hz, 2H, H_{o1}), 8.08 (d, ^4J = 1.9 Hz, 4H, H_{o2}), 8.07 (d, ^4J = 1.9 Hz, 2H, H_{o3}), 7.89 (d, ^3J = 8.4 Hz, 2H, H_{m1}), 7.83 – 7.75 (m, 3H, $H_{p2\text{-}3}$), 1.53 (s, 36H, $(CH_3)_3$), 1.52 (s, 18H, $(CH_3)_3$), −2.72 (s, 2H, N*H*).

UV-Vis: (CH_2Cl_2, 298 K) λ_{max} (nm) = (ε $Lmol^{-1}cm^{-1}$) = 408sh (79 600), 424 (381 000), 519 (16 300), 554 (9 250), 593 (5 430), 650 (5 750).

5-(4-bromophenyl)-10,15,20-tris(3,5-di-*tert*-butylphenyl)porphyrin-Zn(II) (26-Zn) [2]

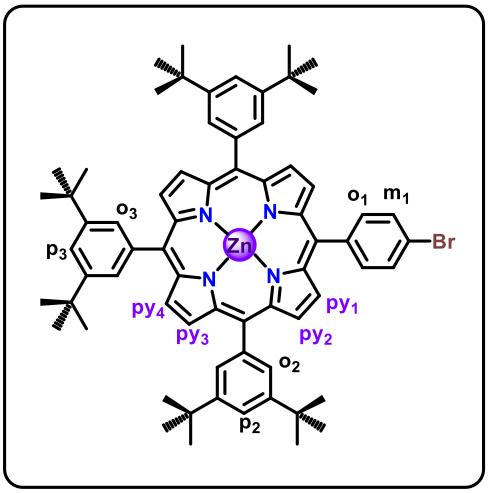

To a solution **26-2H** (237 mg, 0.023 mmol) in CH_2Cl_2 (100 mL) was added a solution of $Zn(OAc)_2{\cdot}2H_2O$ (50.5 mg, 0.023 mmol, 1 eq.) in CH_3OH (10 mL). The mixture was heated to reflux for one hour, before evaporation of the solvent. The resultant solid was taken up in CH_2Cl_2 (100 mL) and washed with H_2O (1 × 50 mL) followed by purification via column chromatography (Al_2O_3, cyclohexane/CH_2Cl_2, 95:5 to 50:50), to give **26-Zn** as a deep pink solid (224 mg, 89%).

^{1}H NMR (300 MHz, $CDCl_3$, 298 K) δ (ppm) = 9.05 – 8.97 (m, 6H, $H_{py2\text{-}4}$), 8.92 (d, ^3J = 4.7 Hz, 2H, H_{py1}), 8.15 – 8.05 (m, 8H, $H_{o1\text{-}3}$), 7.88 (d, ^3J = 8.3 Hz, 2H, H_{m1}), 7.83-7.75 (m, 3H, $H_{p2\text{-}3}$), 1.55-1.51 (m, 54H, $(CH_3)_3$).

UV-Vis: (CH_2Cl_2, 298 K) λ_{max} (nm) = (ε L mol^{-1} cm^{-1}) = 408sh (40 800), 425 (486 000), 552 (18 100), 593 (5 940).

10-Methyl-9(10H)-acridone (27) [3]

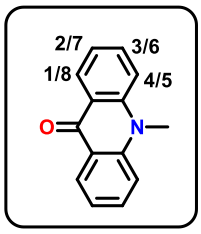

To a solution of 9(10*H*)-acridone (976 mg, 5 mmol) in anhydrous DMF (40 mL) cooled to 0°C, was added 60 wt. % NaH dispersion (500 mg, 12.5 mmol, 2.5 eq.). The solution was stirred for 30 minutes before adding MeI (0.78 mL, 12.5 mmol, 2.5 eq.). The mixture was then heated to 60°C and left to stir overnight, before precipitating from H_2O (500 mL), affording **27** as a pale-yellow precipitate (1.03 g, 98%).

^{1}H NMR (300 MHz, $CDCl_3$, 298 K) δ (ppm) = 8.53 (ddd, ^3J = 8. 0 Hz, ^4J = 1.8 Hz, ^5J = 0.5 Hz, 2H, $H_{1/8}$), 7.73 (ddd, ^3J = 8.7 & 7.0 Hz, ^4J = 1.8 Hz, 2H, $H_{3/6}$), 7.54 (d, ^3J = 8.7 Hz, 2H, $H_{4/5}$), 7.30 (ddd, ^3J = 8.0 & 7.0 Hz, ^4J = 1.0 Hz, 2H, $H_{2/7}$), 3.91 (s, 3H, NCH_3).

9-(4-bromophenyl)-10-methylacridin-10-ium hexafluorophosphate (28·PF_6)

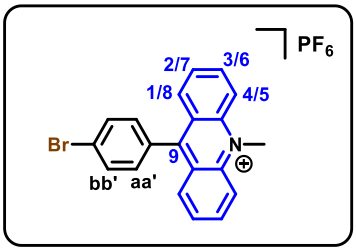

To a solution of 1,4-dibromobenzene (1.13 g, 4.78 mmol) in anhydrous THF (40 mL), cooled to −78°C. was added dropwise 2.5 mol L^{-1} n-BuLi in hexanes (1.91 mL, 4.78 mmol, 1 eq.). The solution was stirred for 30 minutes before addition of **27** (1 g, 4.78 mmol, 1 eq.). The reaction mixture was left to stir overnight at room temperature. 37 wt.% aqueous solution of HCl (15 mL) was added to the resulting solution and left to stir for 30 minutes. The acidified solution was poured slowly into an aqueous solution of KPF_6 (6 g, 150 mL). The resulting precipitate was taken up in CH_3CN (25 mL) and precipitated from Et_2O (500 mL) giving **28·PF_6** as a dark yellow solid (1.73 g, 73%).

^{1}H NMR (500 MHz, CD_3CN, 298 K) δ (ppm) = 8.61 (dt, ^{3}J = 9.3 Hz, $^{4,5}J$ = 0.8 Hz, 2H, $H_{4/5}$), 8.39 (ddd, ^{3}J = 9.3 & 6.7 Hz, ^{4}J = 1.6 Hz, 2H, $H_{3/6}$), 8.03 (ddd, ^{3}J = 8.8 Hz, ^{4}J = 1.6 Hz, ^{5}J = 0.6 Hz, 2H, $H_{1/8}$), 7.93 (d, ^{3}J = 8.6 Hz, 2H, $H_{aa'}$), 7.87 (ddd, ^{3}J = 8.8 & 6.7 Hz, ^{4}J = 0.9 Hz, 2H, $H_{2/7}$) 7.45 (d, ^{3}J = 8.6 Hz, 2H, $H_{bb'}$), 4.84 (s, 3H, NCH_3).

^{13}C{^{1}H} NMR (125 MHz, CD_3CN, 298 K) δ (ppm) = 160.9 (C_9), 142.2 ($CC_{4/5}$), 139.4 ($C_{3/6}$), 132.9 ($CC_{aa'}$), 132.6 ($C_{bb'}$), 132.4 ($C_{1/8}$), 130.6 ($C_{aa'}$), 128.5 ($C_{2/7}$), 126.6 ($CC_{1/8}$), 124.8 (CBr), 119.1 ($C_{4/5}$), 39.4 (NCH_3).

HRMS (ESI-TOF): m/z cald. for $C_{20}H_{15}{}^{79}BrN^{+}$ 348.0382, found 348.0392 ([M–PF_6]$^{+}$, 100%).

10-methyl-9-(4-(4,4,5,5-tetramethyl-1,3,2-dioxaborolan-2-yl)phenyl)-9,10-dihydroacridine (29)

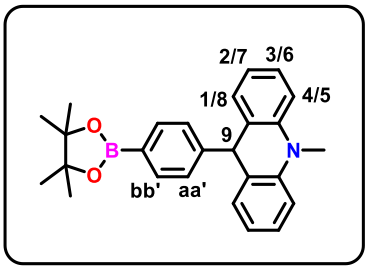

To a solution of **28·PF_6** (400 mg, 0.809 mmol) in anhydrous THF (40 mL) cooled to 0°C, was added $LiAlH_4$ (154 mg, 4.06 mmol, 5 eq.). The resulting mixture was stirred overnight at room temperature, before filtering twice on a plug of SiO_2 (CH_2Cl_2). To a solution of the resulting intermediate in anhydrous degassed DMF (10 mL) was added Bis(pinacolato)diboron (207 mg, 0.814 mmol, 1.01 eq.), Pd(dppf)Cl_2 (26.7 mg, 0.033 mmol, 4 mol%) and KOAc (230 mg, 0.33 mmol, 0.4 eq.). The mixture was stirred overnight at 80°C, and the solvent evaporated. The crude product was purified via column chromatography (SiO_2, CH_2Cl_2), giving **29** as a white solid (322 mg, 81%.).

^{1}H NMR (300 MHz, $CDCl_3$, 298 K) δ (ppm) = 7.72 – 7.62 (m, 2H, $H_{aa'}$), 7.22 (ddd, ^{3}J = 8.5 & 7.2 Hz, ^{4}J = 1.6 Hz, 2H, $H_{3/6}$), 7.16 – 7.11 (m, 4H, $H_{bb'\ \&\ 1/8}$), 6.93 – 6.87 (m, 4H, $H_{4/5\ \&\ 2/7}$), 5.19 (s, 1H, H_9), 3.40 (s, 3H, NCH_3), 1.29 (s, 12H, $C(CH_3)_2$).

5-(9-([1,1'-biphenyl]-4-yl)-10-methylacridin-10-ium))-10,15,20-tris(3,5-di-*tert*-butylphenyl)porphyrin-Zn(II) hexafluorophosphate (30·PF_6)

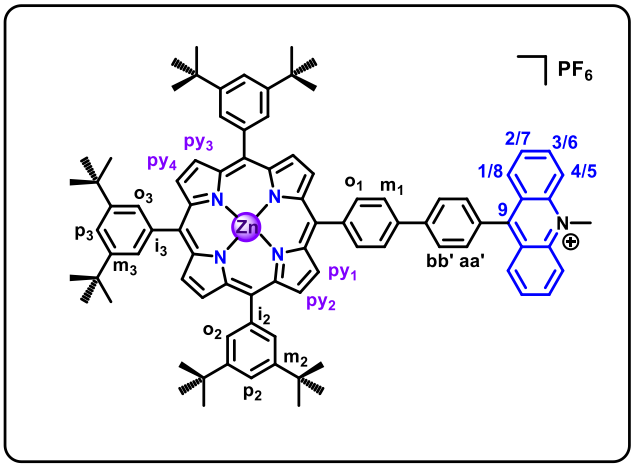

To a solution of **26-Zn** (100 mg, 0.091 mmol) and **29** (40 mg, 0.1 mmol, 1.1 eq.) in degassed anhydrous DMF (10 mL) was added $Pd(PPh_3)_4$ (5 mg, 4.6 µmol, 5 mol %) and K_3PO_4 (58 mg, 0.27 mmol, 3 eq.). The reaction mixture was heated to 80°C and left to stir for 72 hours, before evaporation of the solvent. The crude solid was purified via column chromatography (SiO_2, CH_2Cl_2/petroleum ether, 100:0 to 45:65), to obtain the intermediate as a pink solid. The obtained pink solid was dissolved in CH_2Cl_2 (15 mL) and DDQ (26 mg, 0.114 mmol, 1.25 eq.) added to the solution. The mixture was left to stir overnight before washing with H_2O (3 × 20 mL). The solvent was evaporated to give a solid which was taken up in THF (10 mL) and added dropwise to an aqueous solution of KPF_6 (6 g, 150 ml). The crude product was purified via column chromatography (SiO_2, CH_2Cl_2/CH_3CN, 94:6, R_f = 0.35) giving **30·PF_6** as a deep pink solid (79 mg, 67%).

^{1}H NMR (500 MHz, CD_2Cl_2, 298 K) δ (ppm) = 9.08 (d, ^3J = 4.6 Hz, 2H, H_{py1}), 9.06 (d, ^3J = 4.6 Hz, 2H, H_{py2}), 9.02 (s, 4H, $H_{py3\text{-}4}$), 8.59 (d, ^3J = 9.2 Hz, 2H, $H_{4/5}$), 8.48 – 8.42 (m, 4H, $H_{3/6\ \&\ o1}$), 8.32 (d, ^3J = 8.2 Hz, 2H, $H_{bb'}$), 8.31 (dd, ^3J = 8.6 Hz, ^4J = 1.2 Hz, 3H, $H_{1/8}$), 8.20 (d, ^3J = 8.1 Hz, 2H, H_{m1}), 8.13 (d, ^4J = 1.8 Hz, 4H, H_{o2}), 8.11 (d, ^4J = 1.8 Hz, 2H, H_{o3}), 7.95 (ddd, ^3J = 8.6 & 6.6 Hz, ^4J = 0.6 Hz, 2H, $H_{2/7}$), 7.85 – 7.84 (m, 3H, $H_{p2\&3}$), 7.74 (d, ^3J = 8.2 Hz, 2H, $H_{aa'}$), 4.95 (s, 3H, NCH_3), 1.55 (s, 36H, tBu), 1.54 (s, 18H, tBu).

$^{13}C\{^1H\}$ NMR (125 MHz, CD_2Cl_2, 298 K) δ (ppm) = 162.7 (C_9), 150.9 (CC_{py}), 150.8 (CC_{py}), 150.8 (CC_{py}), 150.3 (CC_{py}), 149.2 (CC_{p2}), 149.1 (CC_{p3}), 143.8 ($CC_{bb'}$), 143.6 (CC_{o1}), 142.12 (CC_{o2}), 142.10 (CC_{o3}), 141.9 ($CC_{4/5}$), 139.8 ($C_{3/6}$), 139.0 ($CC_{aa'}$), 135.6 (C_{o1}), 132.7 (C_{py}), 132.7 (C_{py}), 132.6 (C_{py}), 132.2 (CC_{m1}), 131.9 ($C_{aa'}$), 131.2 ($C_{1/8}$), 130.1 (C_{o2}), 130.0 (C_{o3}), 128.4 ($C_{2/7}$), 128.2 ($C_{bb'}$), 126.6 ($CC_{1/8}$), 125.9 (C_{m1}), 123.1 (C_{meso}), 122.9 (C_{meso}), 121.5 (C_{p2-3}), 120.2 (C_{meso}), 118.4 ($C_{4/5}$), 39.1 (NCH_3), 35.3 ($C(CH_3)_3$), 31.8 (CH_3).

$^{19}F\{^1H\}$ NMR (282 MHz, CD_2Cl_2, 298 K) δ (ppm) = −73.46 (d, $^1J_{P-F}$ = 710.7 Hz).

$^{31}P\{^1H\}$ NMR (121 MHz, CD_2Cl_2, 298 K) δ (ppm) = −144.58 (hept, $^1J_{P-F}$ = 710.7 Hz).

UV-Vis: (CH_2Cl_2, 298 K) λ_{max} (nm) = (ε $Lmol^{-1}cm^{-1}$) = 348 (20 900), 362 (30 200), 408sh (50 100), 426 (541 000), 554 (21 600), 596 (8 260).

HRMS (ESI-TOF): m/z cald. for $C_{88}H_{90}N_5Zn^+$ 1280.6482, found 1280.6458 ($[M-PF_6]^+$, 100%).

2-(4-bromophenyl)-4,4,5,5-tetramethyl-1,3-dioxolane (31) [4]

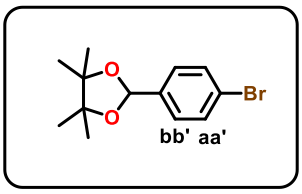

To a solution of 4-bromobenzaldehyde (10.0 g, 54.0 mmol, 1 eq.), and 2,3-dimethyl-2,3-butanediol (7.03 g, 59.5 mmol, 1.1 eq.) in toluene (150 mL), para-tosylic acid monohydrate (274 mg, 1.44 mmol, 2.6 mol%) was added. After Dean-Stark extraction for 10 hours, the reaction mixture was washed with a saturated aqueous solution of Na_2CO_3 (2 × 100 mL) and the aqueous layer extracted using ethyl acetate (3 × 100 mL). The organic layers were combined and dried ($MgSO_4$) before evaporation of the solvents. The crude product was purified by column chromatography (SiO_2, petroleum

ether/ethyl acetate, 9:1, R_f = 0.62), giving the desired product **31** as colourless crystals (13.6 g, 88%).

^{1}H NMR (500 MHz, $CDCl_3$, 298 K) δ (ppm) = 7.49 (d, ^3J = 8.5 Hz, 2H, $H_{aa'}$), 7.36 (d, ^3J = 8.5 Hz, 2H, $H_{bb'}$), 5.93 (s, 1H, O_2CH), 1.31 (s, 6H, CH_3), 1.24 (s, 6H, CH_3).

^{13}C{^{1}H} NMR (125 MHz, $CDCl_3$, 298 K) δ (ppm) = 139.1 ($CC_{bb'}$), 131.5 ($C_{aa'}$), 128.1 ($C_{bb'}$), 122.7 ($CC_{aa'}$), 99.3 (O_2CH), 83.0 ($(CH_3)_2C$), 24.4 (CH_3), 22.3 (CH_3).

9-(4-formylphenyl)-10-methylacridin-10-ium hexafluorophosphate (32·PF$_6$)

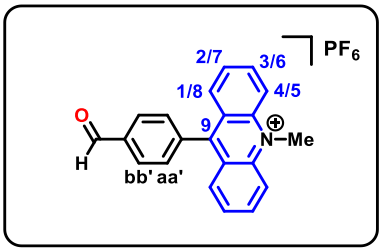

To a solution of **31** (1.28 g, 4.50 mmol, 1.2 eq.) in anhydrous THF (50 mL) at −78°C, was added dropwise 2.5 mol L^{-1} n-BuLi in hexanes (1.50 mL, 3.75 mmol, 1 eq.). After stirring for one hour, **27** (792 mg, 3.75 mmol, 1 eq.) was added. The resulting mixture was stirred for an additional 16 hours at room temperature. 37 wt.% aqueous solution HCl (50 mL) was added dropwise, and the solution left to stir for 30 minutes, after which it was added dropwise to an aqueous solution of KPF_6 (6.00 g, 150 mL). The resulting solid was dissolved in CH_3CN (20 mL) and precipitated from Et_2O (500 mL) to give **32·PF$_6$** as a yellow solid (1.25 g, 78%).

^{1}H NMR (500 MHz, CD_3CN, 298 K) δ (ppm) = 10.25 (s, 1H, CHO), 8.63 (d, ^3J = 9.3 Hz, 2H, $H_{4/5}$), 8.40 (ddd, ^3J = 9.3 & 6.7 Hz, ^4J = 1.5 Hz, 2H, $H_{3/6}$), 8.28 – 8.22 (m, 2H, $H_{bb'}$), 7.97 (dd, ^3J = 8.7 Hz, ^4J = 1.5 Hz, 2H, $H_{1/8}$), 7.86 (ddd, ^3J = 8.7 & 6.7 Hz, ^4J = 1.0 Hz, 2H, $H_{2/7}$), 7.76 – 7.70 (m, 2H, $H_{aa'}$), 4.86 (s, 3H, NCH_3).

$^{13}C\{^1H\}$ NMR (125 MHz, CD_3CN, 298 K) δ (ppm) = 193.3 (*C*HO), 160.9 (C_9), 142.5 ($CC_{4/5}$), 139.9 ($C_{3/6}$), 139.8 ($CC_{aa'}$), 138.5 ($CC_{bb'}$), 131.6 ($C_{bb'}$), 130.8 ($C_{1/8}$), 130.6 ($C_{bb'}$), 129.0 ($C_{2/7}$), 126.8 ($CC_{1/8}$), 119.5 ($C_{4/5}$), 39.8 (NCH_3).

$^{31}P\{^1H\}$ NMR (121 MHz, CD_3CN, 298 K) δ (ppm) = −144.56 (hept, $^1J_{P\text{-}F}$ = 712.6 Hz).

$^{19}F\{^1H\}$ NMR (282 MHz, CD_3CN, 298 K) δ (ppm) = −73.41 (d, $^1J_{P\text{-}F}$ = 712.6 Hz).

HRMS (ESI-TOF): m/z cald. for $C_{21}H_{16}NO^+$ 298.1226, found 298.1211 ([M−PF_6]$^+$, 100%).

5-(10-methyl-9-phenylacridin-10-ium)-10,15,20-tris(3,5-di-*tert*-butylphenyl)porphyrin-Zn(II) hexafluorophosphate (33·PF_6)

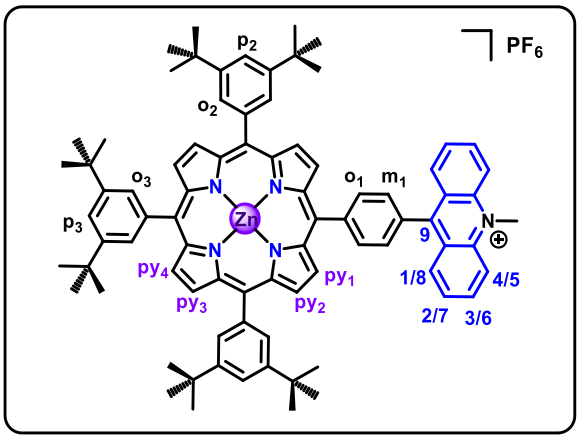

To a solution of **32·PF_6** (227 mg, 0.625 mmol), 3,5-di-*tert*-butyl-benzaldehyde (409 mg, 1.88 mmol, 3 eq.) and pyrrole (0.17 mL, 2.5 mmol, 4 eq.) in degassed CH_2Cl_2 (250 mL), was added TFA (60 μL, 0.75 mmol, 1.2 eq.). The solution was stirred in the dark for three hours followed by addition of DDQ (426 mg, 1.88 mmol, 3 eq.) to the solution, and left to stir for another hour. The mixture was then neutralised with Et_3N (2 mL) and the solvent evaporated, to give a crude solid which was redissolved in CH_3OH (50 mL) and $Zn(OAc)_2{\cdot}2H_2O$ (137 mg, 0.625 mmol, 1 eq.) added. The solution was heated to reflux for one hour, with completion of the metalation assessed via UV-Vis spectroscopy. The solvent was then reduced and diluted with CH_2Cl_2 (100 mL) and washed with H_2O (3 × 100 mL). The solvent was once more evaporated, redissolved in petroleum ether and

filtered, before purification via column chromatography (SiO_2, CH_2Cl_2/CH_3CN, 99:1 to 95:5, R_f = 0.44), giving **33·PF$_6$** as a purple solid (101 mg, 12%).

^{1}H NMR (500 MHz, CD_2Cl_2, 298 K) δ (ppm) = 9.17 (d, ^3J = 4.6 Hz, 2H, H_{py1}), 9.14 (d, ^3J = 4.6 Hz, 2H, H_{py2}), 9.05 (d, ^3J = 4.5 Hz, 2H, $H_{py3/4}$), 9.04 (d, ^3J = 4.5 Hz, 2H, $H_{py3/4}$), 8.67 (d, ^3J = 9.2 Hz, 2H, $H_{4/5}$), 8.65 (d, ^3J = 8.2 Hz, 2H, H_{o1}), 8.61 (dd, ^3J = 8.6 Hz, ^4J = 1.4 Hz, 2H, $H_{1/8}$), 8.53 (ddd, ^3J = 9.2 & 6.7 Hz, ^4J = 1.4 Hz, 2H, $H_{3/6}$), 8.15 (d, ^4J = 1.8 Hz, 4H, H_{o2}), 8.12 (d, ^4J = 1.9 Hz, 2H, H_{o3}), 8.10 (ddd, ^3J = 8.6 & 6.7 Hz, ^4J = 0.9 Hz, 2H, $H_{2/7}$), 7.94 (d, ^3J = 8.2 Hz, 2H, H_{m1}), 7.88 (t, ^4J = 1.8 Hz, 2H, H_{p2}), 7.87 (t, ^4J = 1.8 Hz, 1H, H_{p3}), 5.01 (s, 3H, NCH_3), 1.57 (s, 36H, tBu), 1.55 (s, 18H, tBu).

^{13}C{^{1}H} NMR (125 MHz, CD_2Cl_2, 298 K) δ (ppm) = 162.8 (C_9), 151.1 (CC_{py}), 151.0 (CC_{py}), 150.8 (CC_{py}), 149.9 (CC_{py}), 149.2 (CC_{p3}), 149.2 (CC_{p3}), 146.1 (CC_{o1}), 142.04 ($CC_{o2\text{-}3}$), 142.01 ($CC_{4/5}$), 139.9 ($C_{3/6}$), 135.1 (C_{o1}), 133.0(C_{py}), 132.9 (C_{py}), 132.7 (C_{py}), 132.3 (CC_{m1}), 131.6 (C_{py}), 131.3 ($C_{1/8}$), 130.2 (C_{o2}), 130.0 (C_{o3}), 128.8 (C_{m1}), 128.7 ($C_{2/7}$), 126.8 ($CC_{1/8}$), 123.5 (C_{meso}), 123.1 (C_{meso}), 121.6 (C_{p3}), 121.5 (C_{p2}), 118.9 (C_{meso}), 118.6 ($C_{4/5}$), 39.3 (NCH_3), 35.4 ($C(CH_3)_3$), 35.3 ($C(CH_3)_3$), 31.9 (CH_3) 31.8 (CH_3).

^{19}F{^{1}H} NMR (282 MHz, CD_2Cl_2, 298 K) δ (ppm) = −73.41 (d, $^1J_{P\text{-}F}$ = 710.8 Hz).

^{31}P{^{1}H} NMR (121 MHz, CD_2Cl_2, 298 K) δ (ppm) = −144.56 (hept, $^1J_{P\text{-}F}$ = 710.8 Hz).

UV-Vis (CH_2Cl_2, 298 K) λ_{max} (nm) = (ε Lmol^{-1}cm^{-1}) = 362 (34 300), 406sh (48 800) 426 (521 000), 553 (21 900), 594 (8 100).

HRMS (ESI-TOF): m/z cald. for $C_{82}H_{86}N_5Zn^+$ 1204.6169, found 1204.1680 ([M−PF$_6$]$^+$, 100%).

UV-Vis Titrations:

For the UV-Vis titration with biPy, two solutions were prepared:

Host Solution: **33·PF$_6$** (0.1338 mg, 99.0 nmol) in CH_2Cl_2 (20 mL)

Guest Solution: biPy (193.2 mg, 1.24 mmol) in CH_2Cl_2 (5 mL)

1 mL of the host solution was added to a cuvette (l = 0.5 cm) and small aliquots of the guest solution added to the solution, with UV-Vis spectra recorded after each addition. The absorption values (at wavelengths 415 - 432 nm) for each recorded spectrum were compiled in an excel file, the data corrected for dilution (< 5% dilution of initial concentration at end point of titration)) and the data analysed using the BindFit titration program (http://supramolecular.org). Fitting to a 1:1 binding model was observed to be most accurate, with a value of 3.85 (± 0.15) × 10^3 L mol^{-1} obtained.

For the UV-Vis titration with DABCO, two solutions were prepared:
Host Solution: **33·PF_6** (54.1 μg, 40 nmol) in CH_2Cl_2 (20 mL)
Guest Solution: DABCO (4.49 mg, 80.0 μmol) in CH_2Cl_2 (10 mL)

Small aliquots of the guest solution were added to the host solution (2 mL in a 1 cm quartz cuvette), and UV-Vis spectra recorded after each addition. The absorption values (at wavelengths 425 - 435 nm) for each recorded spectrum were compiled in an excel file, corrected for dilution (< 3% dilution of initial concentration at end point of titration) and the data analysed using the BindFit titration program (http://supramolecular.org). Fitting to a 1:1 binding model was observed to be most accurate, with a value of K_a = 1.06 (± 0.03) × 10^5 L mol^{-1} obtained.

---

di(1H-pyrrol-2-yl)methane (34) [5]

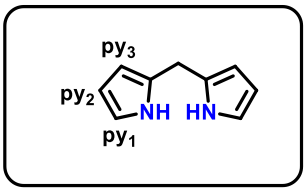

To a solution of paraformaldehyde (649 mg, 21.6 mmol) in degassed pyrrole (150 mL, 2.16 mol, 100 eq.) was added $InCl_3·4H_2O$ (635 mg, 2.16 mmol, 0.1 eq.). The resulting mixture was stirred at 55°C for 2.5 hours. The mixture was allowed to cool to room temperature, pulverised NaOH (4.32 g, 0.108 mol, 5 eq.) added and stirred for a further hour. The mixture was filtered through celite and excess pyrrole recovered via rotary

evaporation, giving a brown oil which was washed with petroleum ether/EtOAc (8:2, 5 × 50 mL), filtered and the solvent evaporated. The crude product was purified via column chromatography (SiO_2, CH_2Cl_2/petroleum ether/EtOAc 2:7:1, R_f = 0.40) giving **34** as an off-white solid (1.83 g, 58%).

^{1}H NMR (300 MHz, $CDCl_3$, 298 K) δ (ppm) = 7.89 (br.s, 2H, N*H*), 6.71– 6.63 (m, H_{py1}), 6.15 (dd, ^3J = 5.8 Hz, ^4J = 2.7 Hz, 2H, H_{py3}), 6.09 – 5.99 (m, H_{py2}), 3.99 (s, 2H, CH_2).

5,15-bis(10-methyl-9-phenylacridin-10-ium)porphyrin-Zn(II) hexafluorophosphate (35·2PF$_6$)

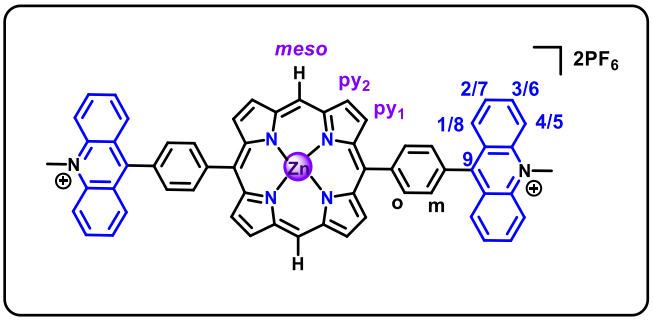

To a solution of **32·PF$_6$** (554 mg, 1.25 mmol, 1 eq.) and **34** (183 mg, 1.25 mmol, 1 eq.) in degassed CH_2Cl_2 (250 mL) was added TFA (60.0 μL, 0.75 mmol, 0.6 eq.). The solution was left to stir in the dark for four hours, before neutralising with Et_3N (2 mL). Following removal of the solvent, the resultant solid was taken up in CH_3CN (100 mL) and DDQ (426 mg, 1.88 mmol, 1.5 eq.) added to the solution. After stirring for one hour, purification was carried out via column chromatography (SiO_2, acetone/aq. KPF_6 soln., 100:0 to 95:5, R_f = 0.36) giving a purple solid. The solid was re-dissolved in CH_3CN (50 mL) and a solution of $Zn(OAc)_2{\cdot}2H_2O$ (137 mg, 0.625 mmol, 0.5 eq.) in CH_3OH (10 mL) added. The mixture was heated to reflux for one hour, before evaporating the solvent. The resulting crude solid was triturated with CH_3OH (50 mL), and then taken up in CH_3CN (50 mL) and precipitated from Et_2O (250 mL) to give **35·2PF$_6$** as a dark purple solid (214 mg, 29%.).

^{1}H NMR (500 MHz, CD_3CN, 298 K) δ (ppm) = 10.49 (s, 2H, H_{meso}), 9.65 (d, ^{3}J = 4.4 Hz, 4H, H_{py1}), 9.40 (d, ^{3}J = 4.4 Hz, 4H, H_{py2}), 8.72 (d, ^{3}J = 9.2 Hz, 4H, $H_{4/5}$), 8.69 – 8.63 (m, 8H, $H_{1/8\ \&\ o}$), 8.53 (ddd, ^{3}J = 9.2 & 6.5 Hz, ^{4}J = 1.4 Hz, 4H, $H_{3/6}$), 8.13 (ddd, ^{3}J = 8.8 & 6.5 Hz, ^{4}J = 0.8 Hz, 4H, $H_{2/7}$), 7.99 (d, ^{3}J = 8.0 HZ, 4H, H_m), 4.93 (s, 6H, NCH_3).

^{13}C{^{1}H} NMR (125 MHz, CD_3CN) δ (ppm) = 162.9 (C_9), 150.6 (CC_{Py}), 146.0 (CC_o), 142.7 ($CC_{4/5}$), 139.8 ($C_{3/6}$), 135.6 (C_o), 133.3 (CC_m), 133.2 (C_{Py}), 133.1 (C_{Py}), 131.7 ($C_{1/8}$), 129.3 (C_m), 128.9 ($C_{2/7}$), 127.3 ($CC_{1/8}$), 119.4 ($C_{4/5}$), 107.2 (C_{meso}), 39.7 (NCH_3).

^{31}P{^{1}H} NMR (121 MHz, CD_3CN) δ (ppm) = −144.64 (hept, $^{1}J_{P\text{-}F}$ = 706 Hz).

^{19}F{^{1}H} NMR (282 MHz, CD_3CN) δ (ppm) = −72.97 (d, $^{1}J_{P\text{-}F}$ = 706 Hz).

UV-Vis: (CH_3CN, 298 K) λ_{max}(nm) = 346 (ε L mol^{-1}cm^{-1} 24 300), 362 (38 900), 394sh (36 800), 411 (293 000), 454sh (18 100), 545 (16 100), 586 (5 900).

HRMS (ESI-TOF): m/z cald. for $C_{60}H_{40}N_6Zn^{2+}$ 454.1297, found 454.1268 ($[M-2PF_6]^{2+}$, 100%).

10-(dec-9-en-1-yl)acridin-9(10H)-one (36) [6]

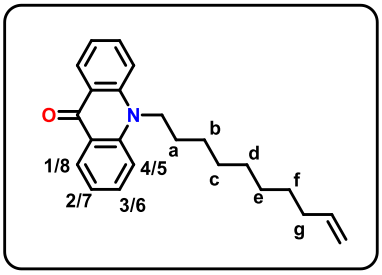

To a solution of 9(10*H*)-acridanone (780 mg, 4 mmol) in anhydrous DMF, cooled to 0°C was added 60% NaH dispersion (240 mg, 6 mmol, 1.5 eq.). The mixture was stirred for 30 minutes before addition of 1-(10)bromohex-1-ene (1.20 mL, 6 mmol, 1.5 eq.). The mixture was then heated to 60°C and left to stir overnight, before quenching with H_2O (500 mL), then extracted using Et_2O (3 × 100 mL). Evaporation of the solvent gave an

orange oil which was purified via column chromatography (SiO_2, CH_2Cl_2/acetone, 100:0 to 99:1, R_f = 0.36), giving **36** as a pale-yellow solid (934 mg, 70%).

^{1}H NMR (500 MHz, $CDCl_3$, 298 K) δ (ppm) = 8.60 (dd, ^3J = 8.0 Hz, ^4J = 1.8 Hz, 2H, $H_{1/8}$), 7.74 (ddd, ^3J = 8.7 & 7.0 Hz, ^4J = 1.8 Hz, 2H, $H_{3/6}$), 7.51 (d, ^3J = 8.7 Hz, 2H, $H_{4/5}$), 7.30 (ddd, ^3J = 8.0 & 7.0 Hz, ^4J = 0.9 Hz, 2H, $H_{2/7}$), 5.82 (ddt, ^3J = 17.0, 10.2 & 6.7 Hz, 1H, *H*C=), 5.01 (dq, ^3J = 17.0, $^{2,4}J$ = 2.2 Hz, 1H, =CHH_{trans}), 4.95 (ddt, ^3J = 10.2 Hz, ^2J = 2.2 Hz, ^4J = 1.3 Hz, 1H, =CH_{cis}H), 4.38 – 4.31 (m, 2H, NCH_2), 2.06 (q, ^3J = 6.7 Hz, 2H, g-CH_2), 2.00 – 1.90 (m, 2H, a-CH_2), 1.58 – 1.52 (m, 2H, b-CH_2), 1.50 – 1.42 (m, 2H, c-CH_2), 1.41 – 1.30 (m, 4H, (d-f)-CH_2).

^{13}C{^{1}H} NMR (125 MHz, $CDCl_3$, 298 K) δ (ppm) = 178.2 (*C*O), 141.9 ($CC_{4/5}$), 139.2 (=*C*H), 134.0 ($C_{3/6}$), 128.2 ($C_{1/8}$), 122.6 ($CC_{1/8}$), 121.4 ($C_{2/7}$), 114.7 ($C_{4/5}$), 114.4 (H_2C=), 46.4 (N*C*H$_2$), 33.9 (g-*C*H$_2$), 29.6 (c-*C*H$_2$), 29.5 (d/e/f-*C*H$_2$), 29.2 (d/e/f-*C*H$_2$), 29.0 (d/e/f-*C*H$_2$), 27.3 (a-*C*H$_2$), 27.1 (b-*C*H$_2$).

10-(dec-9-en-1-yl)-9-(4-formylphenyl)acridin-10-ium (37·PF$_6$)

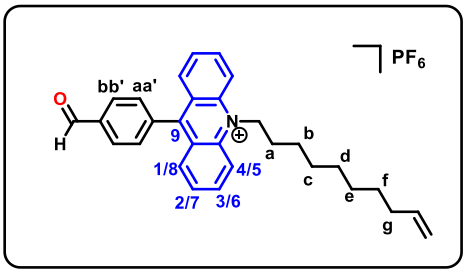

To a solution of **31** (770 mg, 2.7 mmol, 1.2 eq.) in anhydrous THF (30 mL), cooled to –78°C, was added 2.5 mol L^{-1} n-BuLi in hexanes (0.9 mL, 2.25 mmol, 1 eq.). The solution was stirred for one hour before addition of **36** (750 mg, 2.25 mmol, 1 eq.), and the resulting mixture stirred for an additional 16 hours at room temperature. 37 wt.% aqueous solution of HCl (30 mL) was added and the solution left to stir for 30 minutes, after which it was added dropwise to an aqueous solution of KPF_6 (6 g, 150 mL), giving a yellow oil which was isolated via extraction using CH_2Cl_2 (3 × 100 mL). The organic layer was then washed with H_2O (3 × 100 mL). The solvent was evaporated, and the resultant

residue taken up in minimal CH_3CN (10 mL) and precipitated from Et_2O (500 mL) to give **37·PF$_6$** as a yellow solid (0.829 g, 65%).

^{1}H NMR (500 MHz, CD_2Cl_2, 298 K) δ (ppm) = 10.25 (s, 1H, C*H*O), 8.48 (d, ^3J = 9.3 Hz, 2H, $H_{4/5}$), 8.43 (ddd, ^3J = 9.3 & 6.6 Hz, ^4J = 1.5 Hz, 2H, $H_{3/6}$), 8.24 (d, ^3J = 8.2 Hz, 2H, $H_{bb'}$), 7.98 (dd, ^3J = 8.8 Hz, ^4J = 1.5 Hz, 2H, $H_{1/8}$), 7.87 (ddd, ^3J = 8.8 & 6.6 Hz, ^4J = 1.1 Hz, 2H, $H_{2/7}$), 7.70 (d, ^3J = 8.2 Hz, 2H, $H_{aa'}$), 5.84 (ddt, ^3J = 17.0, 10.2 & 6.7 Hz, 1H, *H*C=), 5.38 – 5.31 (m, 2H, NCH_2), 5.01 (dq, ^3J = 17.0 Hz, $^{2,4}J$ = 1.7 Hz, 1H, =CHH_{trans}), 4.94 (ddt, ^3J = 10.2 Hz, ^2J = 2.4 Hz, ^4J = 1.2 Hz, 1H, =CH_{cis}H), 2.33 – 2.22 (m, 2H, a-CH_2), 2.14 – 2.03 (m, 2H, g-CH_2), 1.78 (p, ^3J = 7.6 Hz, 2H, b-CH_2), 1.57 – 1.49 (m, 2H, c-CH_2), 1.46 – 1.37 (m, 6H, (d - f)-CH_2).

^{13}C{^{1}H} NMR (125 MHz, CD_2Cl_2, 298 K) δ (ppm) = 191.7 (*C*HO), 160.7 (C_9), 141.0 ($CC_{4/5}$), 140.0 ($C_{3/6}$), 139.6 ($CC_{aa'}$), 138.9 (=*C*H), 138.1 (*C*CHO), 131.0 ($C_{bb'}$), 130.8 ($C_{1/8}$), 130.4 ($C_{aa'}$), 128.7 ($C_{2/7}$), 126.4 ($CC_{1/8}$), 118.2 ($C_{4/5}$), 114.4 (H_2C=), 52.0 (NCH_2), 34.1 (g-CH_2), 29.7 (c-CH_2), 29.6 (d/e/f-CH_2), 29.4 (d/e/f-CH_2), 29.3 (d/e/f-CH_2), 29.2 (a-CH_2), 27.3 (b-CH_2).

^{19}F{^{1}H} NMR (282 MHz, CD_2Cl_2, 298 K) δ (ppm) = −73.58 (d, $^1J_{P\text{-}F}$ = 711 Hz).

^{31}P{^{1}H} NMR (121 MHz, CD_2Cl_2, 298 K) δ (ppm) = −144.78 (hept, $^1J_{P\text{-}F}$ = 711 Hz).

HRMS (ESI-TOF): m/z cald. for $C_{30}H_{32}NO^+$ 422.2499, found 422.2478 ([M−PF_6]$^+$, 100%).

5-((10-dec-9-en-1-yl)-9-phenylacridin-10-ium)-10,15,20-tris(3,5-di-*tert*-butylphenyl)porphyrin-Zn(II) hexafluorophosphate (38·PF_6)

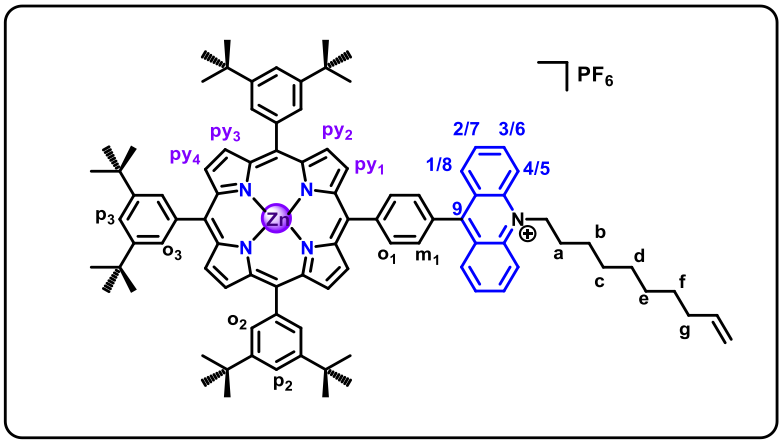

To a solution of **37·PF_6** (284 mg, 0.5 mmol), 3,5-di-*tert*-butylbenzaldehyde (328 mg, 1.5 mmol, 3 eq.) and pyrrole (0.139 mL, 2 mmol, 4 eq.) in degassed CH_2Cl_2 (120 mL) was added TFA (0.23 mL, 3 mmol, 6 eq.). The solution was stirred in the dark for three hours before neutralising with Et_3N (4 mL) and evaporating the solvent. The resultant solid was taken up in CH_2Cl_2 (100 mL) and DDQ (342 mg, 1.5 mmol, 3 eq.) added, before stirring for a further hour. To the mixture was added acetone (25 mL) and the solution filtered through a plug of SiO_2. The solvent was evaporated, and the resultant solid taken up in CH_2Cl_2 (100mL). $Zn(OAc)_2{\cdot}2H_2O$ (110 mg, 0.5 mmol, 1 eq.) in CH_3OH (10 mL) was added to the solution, which was then heated to reflux for one hour, The solvent was evaporated, and purification carried out via column chromatography (SiO_2, CH_2Cl_2/acetone, 98:2, R_f = 0.36) followed by crystallisation from acetone/petroleum ether (1:4), giving **38·PF_6** as a purple crystalline solid (92 mg, 12%).

^{1}H NMR (500 MHz, CD_2Cl_2, 298 K) δ (ppm) = 9.15 (d, ^3J = 4.7 Hz, 2H, H_{py1}), 9.13 (d, ^3J = 4.7 Hz, 2H, H_{py2}), 9.05 (d, ^3J = 4.6 Hz, 2H, $H_{py3/4}$), 9.03 (d, ^3J = 4.6 Hz, 2H, $H_{py3/4}$), 8.64 (d, ^3J = 8.1 Hz, 2H, H_{o1}), 8.61 (dd, ^3J = 8.5 Hz, ^4J = 1.4 Hz, 2H, $H_{1/8}$), 8.57 (d, ^3J = 9.1 Hz, 2H, $H_{4/5}$), 8.54 (ddd, ^3J = 9.1 & 6.2 Hz, ^4J = 1.4 Hz, 2H, $H_{3/6}$), 8.14 (d, ^4J = 1.8 Hz, 4H, H_{o2}), 8.11 (d, ^4J = 1.8 Hz, 2H, H_{o3}), 8.10 (ddd, ^3J = 8.5 & 6.2 Hz, ^4J = 0.9 Hz, 2H, $H_{2/7}$), 7.93 (d, ^3J = 8.1 Hz, 2H, H_{m1}), 7.87 (t, ^4J = 1.9 Hz, 2H, H_{p2}), 7.86 (t, ^4J = 1.9 Hz, 1H, H_{p3}), 5.87 (ddt, ^3J = 17.0, 10.2 & 6.6 Hz, 1H, *H*C=), 5.45 – 5.38 (m, 2H, NCH_2), 5.03 (dq, ^3J = 17.0 Hz, $^{2,4}J$ = 1.7 Hz,

1H, =CHH_{trans}), 4.96 (ddt, ^{3}J = 10.2 Hz, ^{2}J = 2.3 Hz, ^{4}J = 1.3 Hz, 1H, =CH_{cis}H), 2.37 (p, ^{3}J = 8.5 Hz, 2H, a-CH_2), 2.09 (q, ^{3}J = 6.6 Hz, 2H, g-CH_2), 1.85 (p, ^{3}J = 7.5 Hz, 2H, b-CH_2), 1.63 – 1.57 (m, 2H, c-CH_2), 1.56 – 1.54 (m, 54H, tBu), 1.49 – 1.38 (m, 6H, (d-f)-CH_2).

^{13}C{^{1}H} NMR (125 MHz, CD_2Cl_2, 298 K) δ (ppm) = 162.8 (C_9), 151.1 (CC_{py}), 151.0 (CC_{py}) 150.8 (CC_{py}), 149.9 (CC_{py}), 149.22 (CC_{p2}), 149.17 (CC_{p3}), 146.2 (CC_{o1}), 142.1 (CC_{o2}), 142.0 (CC_{o3}), 141.2 ($CC_{4/5}$), 140.1 ($C_{3/6}$), 139.6 (=CH), 135.2 (C_{o1}), 133.0 (C_{py}), 132.9 (C_{py}), 132.7 (C_{py}), 132.3 (CC_{m1}) 131.6 (C_{py}) 131.5 ($C_{1/8}$), 130.2 (C_{o2}), 130.0 (C_{o3}), 128.8 (C_{m1}), 128.7 ($C_{2/7}$), 126.9 ($CC_{1/8}$), 123.5 (C_{meso}), 123.1 (C_{meso}), 121.5 (C_{p2-3}), 118.9 (C_{meso}), 118.2 ($C_{4/5}$), 114.4 (H_2C=), 51.7 (NCH_2), 35.4 ($C(CH_3)_3$), 35.3 ($C(CH_3)_3$), 34.2 (g-CH_2), 31.9 (CH_3), 29.8 (c-CH_2), 29.7 (d/e/f-CH_2), 29.41 (d/e/f-CH_2), 29.38 (d/e/f-CH_2), 29.3 (a-CH_2), 27.2 (b-CH_2).

^{19}F{^{1}H} NMR (470 MHz, CD_2Cl_2, 298 K) δ (ppm) = –73.47 (d, $^{1}J_{P\text{-}F}$ = 711 Hz).

^{31}P{^{1}H} NMR (202 MHz, CD_2Cl_2, 298 K) δ (ppm) = –144.39 (hept, $^{1}J_{P\text{-}F}$ = 711 Hz).

UV-Vis: (CH_2Cl_2, 298 K) λ_{max}(nm) = 347 (ε Lmol^{-1}cm^{-1} 22 500), 363 (27 400), 409sh (42 200), 426 (378 500), 553 (18 000), 795 (7 600).

HRMS (ESI-TOF): m/z cald. for $C_{91}H_{102}N_5Zn^+$ 1328.7421, found 1328.7402 ([M–PF_6]$^+$, 100%); m/z cald. for $C_{91}H_{102}N_5Zn^{2+}$ 664.370784, found 664.371148 ([M–PF_6]$^{2+}$, 35%).

Porphyrin-acridinium tweezer (39·2PF$_6$)

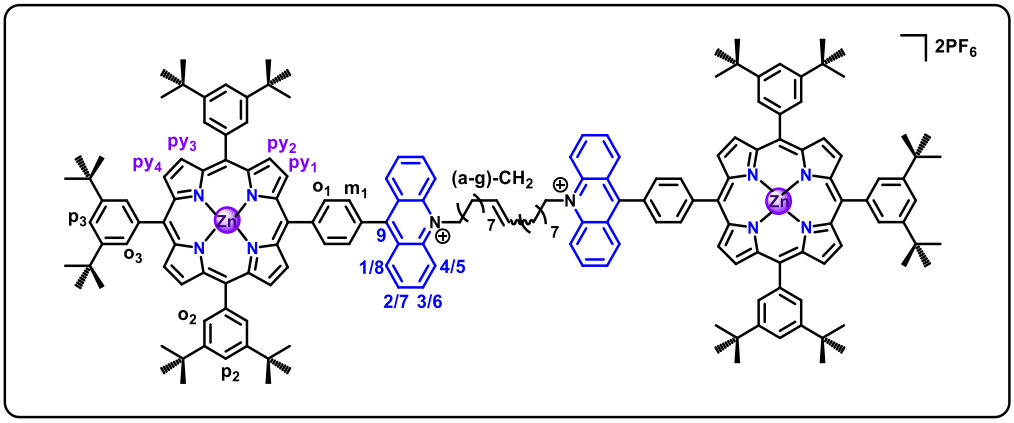

To a solution of **38·PF$_6$** (60 mg, 40.6 μmol) in anhydrous degassed CH_2Cl_2 (10 mL), was added Grubbs (I) Catalyst (3.72 mg, 4.52 μmol, 10 mol%). The resultant solution was stirred in the dark for 16 hrs, before washing with brine (1 × 10 mL), and H_2O (3 × 10 mL). Following removal of the solvent, the resultant solid was purified via column chromatography (SiO_2, CH_2Cl_2/CH_3CN, 99:1 to 97:3, R_f = 0.26), to give **39·2PF$_6$** as a purple crystalline solid (45.8 mg, 77%).

^{1}H NMR (500 MHz, CD_2Cl_2, 298 K) δ (ppm) = 9.16 (d, ^3J = 4.6 Hz, 4H, H_{py1}), 9.12 (d, ^3J = 4.6 Hz, 4H, H_{py2}), 9.03 (s, 8H, H_{py3-4}), 8.66 (d, ^3J = 8.0 Hz, 4H, H_{o1}), 8.61 – 8.57 (m, 12H, $H_{1/8,\ 4/5\ \&\ o1}$), 8.54 (ddd, ^3J = 9.2 & 6.4 Hz, ^4J = 1.5 Hz, 4H, $H_{3/6}$), 8.13 (d, ^4J = 1.8 Hz, 8H, H_{o2}), 8.12 – 8.06 (m, 8H, $H_{2/7\ \&\ o3}$), 7.92 (d, ^3J = 8.0 Hz, 4H, H_{m1}), 7.87 (t, ^4J = 1.9 Hz, 4H, H_{p2}), 7.86 (d, ^4J = 1.8 Hz, 1H, H_{p3}), 5.53 – 5.47 (m, 2H, =C*H*), 5.46 – 5.39 (m, 4H, NCH_2), 2.44 – 2.31 (m, 4H, a-CH_2), 2.11 – 2.05 (m, 4H, g-CH_2), 1.86 (p, ^3J = 8.2 Hz, 4H, b-CH_2), 1.62 (p, ^3J = 7.0 Hz, 4H, c-CH_2), 1.56-1.54 (m, 108H, tBu), 1.48 – 1.41 (m, 12H, (d-f)-CH_2).

^{13}C{^{1}H} NMR (125 MHz, CD_2Cl_2, 298 K) δ (ppm) = 162.7 (C_9), 151.0 (CC_{py}), 150.9 (CC_{py}), 150.8 (CC_{py}), 149.9 (CC_{py}), 149.2 (CC_{p2-3}), 146.1 (CC_{o1}), 142.03 (CC_{o2-3}), 141.2 ($CC_{4/5}$), 140.0 ($C_{3/6}$), 135.1 (C_{o1}), 133.0 (C_{py}), 132.8 (C_{py}), 132.7 (C_{py}), 132.3 (C_{py}), 131.6 ($C_{1/8}$), 130.8 (H*C*=), 130.3 (C_{o2}), 130.2 (C_{o3}), 130.0 (CC_{m1}), 128.8 ($C_{2/7}$), 128.7 (C_{m1}),126.9 ($CC_{1/8}$), 123.4 (C_{meso}), 123.1 (C_{meso}), 121.5 (C_{p2-3}), 118.9 (C_{meso}) 118.2 ($C_{4/5}$), 51.7 (NCH_2), 35.33 ($C(CH_3)_3$), 35.31 ($C(CH_3)_3$), 32.9 (g-CH_2), 31.8 (CH_3), 30.0 (c-CH_2), 29.8 (d/e/f-CH_2), 29.7 (d/e/f-CH_2), 29.3 (a-CH_2), 27.2 (b-CH_2).

$^{19}F\{^{1}H\}$ NMR (282 MHz, CD_2Cl_2, 298 K) δ (ppm) = –73.38 (d, $^{1}J_{P\text{-}F}$ = 711 Hz).

$^{31}P\{^{1}H\}$ NMR (202 MHz, CD_2Cl_2, 298 K) δ (ppm) = –144.34 (hept, $^{1}J_{P\text{-}F}$ = 711 Hz).

UV-Vis: (CH_2Cl_2, 298 K) λ_{max}(nm) = 347 (ε $Lmol^{-1}cm^{-1}$ 44 200), 364 (62 600), 426 (925 000), 554 (39 700), 596 (15 400).

HRMS (ESI-TOF): m/z cald. for $C_{180}H_{200}N_{10}Zn_2^{2+}$ 1314.7243, found 1314.7265 ($[M–2PF_6]^{2+}$, 100%).

(Porphyrin-acridinium tweezer)@DABCO complex (DABCO@39·2PF$_6$)

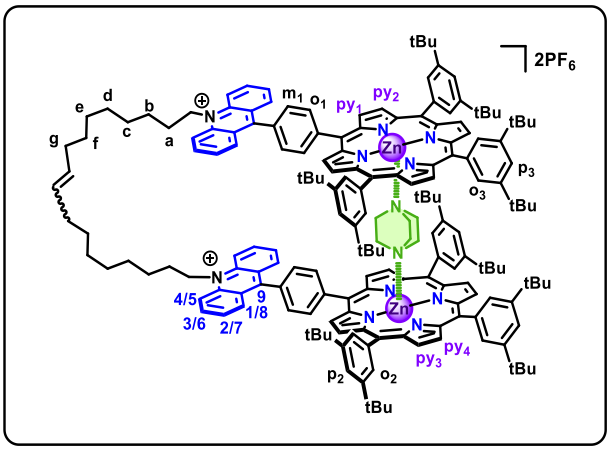

To a solution of **39·2PF$_6$** (2.34 mg, 0.8 μmol) in CD_2Cl_2 (0.7 mL) was added a solution of DABCO (89.7 μg, 0.8 μmol) in CD_2Cl_2 (0.1 mL). The mixture was manually stirred, and formation of the **DABCO@39·2PF$_6$** complex assessed via ^{1}H NMR spectroscopy.

^{1}H NMR (500 MHz, CD_2Cl_2, 298 K) δ (ppm) = 8.71 (d, ^{3}J = 4.5 Hz, 4H, H_{py1}), 8.69 (d, ^{3}J = 4.5 Hz, 4H, H_{py2}), 8.62 (s, 8H, $H_{py3\text{-}4}$), 8.42 – 8.34 (m, 12H, $H_{1/8,\ 4/5\ \&\ 3/6}$), 8.22 (br. s, 4H, H_{o1}), 7.96 – 7.88 (m, 4H, $H_{2/7}$), 7.75 (t, ^{4}J = 1.8 Hz, 4H, H_{p2}), 7.73 (t, ^{4}J = 1.9 Hz, 2H, H_{p3}), 7.71 – 7.65 (m, 12H, $H_{o2\text{-}3}$), 5.53 – 5.43 (m, 2H, *HC=CH*), 5.28-5.20 (m, 4H, NCH_2), 2.34 – 2.30 (m, 4H, a-CH_2), 2.19 – 2.08 (m, 4H, g-CH_2), 1.84 – 1.79 (m, 4H, b-CH_2), 1.67 – 1.58 (m, 4H, c-CH_2), 1.48 – 1.43 (m, 120H, tBu & (d-f)-C*H*$_2$), –4.56 (s, 12H, H_{DABCO}).

$^{13}C\{^1H\}$ NMR (125 MHz, CD_2Cl_2, 298 K) δ (ppm) = 150.5 (CC_{py}), 150.3 (CC_{py}), 150.2 (CC_{py}), 149.3 (CC_{py}), 148.9 ($CC_{p2\text{-}3}$), 145.9 (CC_{o1}), 142.3 ($CC_{4/5}$), 142.11 ($CC_{o2\text{-}3}$), 142.05 ($CC_{o2\text{-}3}$), 141.1 ($C_{3/6}$), 133.8 ($C_{bb'}$), 132.3 (C_{py}), 132.24 (C_{py}), 132.16 (C_{py}), 131.5 ($C_{1/8}$), 131.0 (CC_{m1}), 130.8 (C=C), 130.5 ($C_{o2\text{-}3}$), 128.1 ($C_{2/7}$), 128.0 (C_{m1}), 127.2 ($CC_{1/8}$), 122.1 (C_{meso}),121.2 (C_{p2}), 121.2 (C_{p3}), 120.8 (C_{meso}), 117.8 ($C_{4/5}$), 51.4 (NCH_2), 34.8 ($C(CH_3)_3$), 32.6 (g-CH_2), 31.9 (CH_3), 29.9 (c-CH_2), 29.6 (d/e/f-CH_2), 29.3 (d/e/f-CH_2), 29.2 (d/e/f-CH_2), 28.8 (a-CH_2), 27.5 (b-CH_2).

$^{19}F\{^1H\}$ NMR (470 MHz, CD_2Cl_2, 298 K) δ (ppm) = −73.88 (d, $^1J_{P\text{-}F}$ = 711.7 Hz).

$^{31}P\{^1H\}$ NMR (202 MHz, CD_2Cl_2, 298 K) δ (ppm) = −144.92 (hept, $^1J_{P\text{-}F}$ = 711.6 Hz).

UV-Vis titration:

Host Solution: **39·2PF$_6$** (58.5 μg, 20 nmol) in CH_2Cl_2 (20 mL).

Guest Solution: DABCO (8.97 mg, 80.0 μmol) in CH_2Cl_2 (10 mL).

2 mL of the host solution was added to a 1 cm cuvette, and small aliquots of the guest solution added directly to the cuvette, with UV-Vis spectra recorded after each addition. The absorption values (at wavelengths 420 - 435 nm) for each recorded spectrum were compiled in an excel file, corrected for dilution (< 3% dilution of initial concentration at end point of titration) and the data analysed using the BindFit titration program (http://supramolecular.org). Fitting to a 1:2 binding model was observed to be most accurate, with values of K_{11} = 2.0 (± 0.3) × 10^6 L mol^{-1} and K_{12} = 6.0 (± 0.7) × 10^3 L mol^{-1} obtained.

(Porphyrin-acridinium tweezer)@4,4'-bipyridine complex (biPy@39·2PF$_6$)

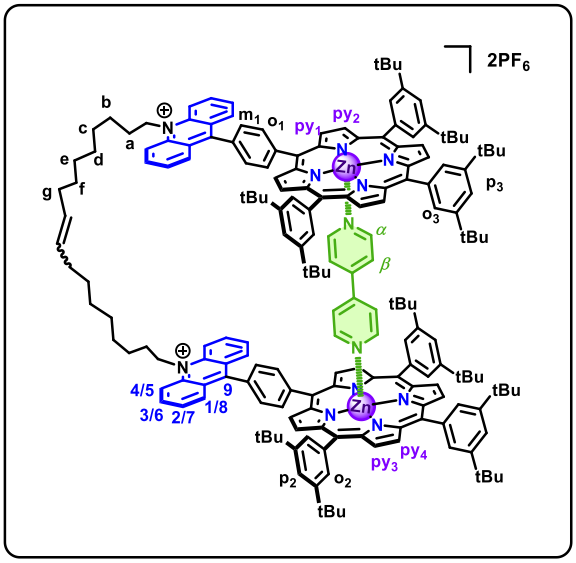

To a solution of **39·2PF$_6$** (3.33 mg, 1.14 μmol) in CD_2Cl_2 (0.55 mL) was added a solution of 4,4'-bipyridine (0.178 mg, 1.14 μmol) in CD_2Cl_2 (50 μL). The mixture was manually stirred, and formation of the **biPy @39·2PF$_6$** complex assessed via ^{1}H NMR spectroscopy.

^{1}H NMR (500 MHz, CD_2Cl_2, 298 K) δ (ppm) = 8.90 (d, ^3J = 4.5 Hz, 4H, H_{py1}), 8.87 (d, ^3J = 4.5 Hz, 4H, H_{py2}), 8.83 – 8.78 (m, 8H, H_{py3-4}), 8.48 – 8.41 (m, 12H $H_{1/8,\ 4/5\ \&\ 3/6}$), 8.39 (s, 4H, H_{o1}), 8.00 – 7.93 (m, 4H, $H_{2/7}$), 7.92 (d, ^4J = 1.9 Hz, 12H, H_{o2-3}), 7.78 – 7.74 (m,10H, $H_{p2-3\ \&\ m1}$), 5.51 – 5.43 (m, 2H, =C*H*), 5.32 – 5.26 (m, 4H, NCH_2), 4.94 (d, ^3J = 6.3 Hz, 4H, $H_{bipy-\beta}$), 2.35 – 2.30 (m, 8H, $H_{bipy-\alpha}$ & a-CH_2), 2.09 – 2.05 (m, 4H, g-CH_2), 1.87 – 1.77 (m, 4H, b-CH_2), 1.66 – 1.58 (m, 4H, c-CH_2), 1.49 – 1.42 (m, 120H, tBu & (d-f)-CH_2).

^{13}C{^{1}H} NMR (125 MHz, CD_2Cl_2, 298 K) δ (ppm) = 150.7 (CC_{py}), 150.5 (CC_{py}), 150.4(CC_{py}), 149.5 (CC_{py}), 148.8 (CC_{p2-3}), 146.3 (CC_{o1}), 143.7 ($C_{bipy-\alpha}$), 142.4 (CC_{o2-3}), 141.1 ($CC_{4/5}$), 139.7 ($C_{3/6}$), 132.5 (C_{py}), 132.4 (C_{py}), 132.3 (C_{py}), 131.6 ($C_{1/8}$), 131.2 (CC_{m1}), 130.7 (C=C), 130.1 (C_{o2-3}), 129.9 ($C_{2/7}$), 128.4 (C_{m1}), 126.9 ($CC_{1/8}$), 122.5 (C_{meso}), 121.1 (C_{p2-3}), 120.2 ($C_{bipy-\beta}$), 118.3 (C_{meso}), 117.9 ($C_{4/5}$), 51.7 (NCH_2), 35.2 ($C(CH_3)_3$), 32.9 (g-CH_2), 31.8 (CH_3), 30.1 (c-CH_2), 29.7 (d/e/f-CH_2), 29.6 (d/e/f-CH_2), 29.4 (d/e/f-CH_2), 29.0 (a-CH_2), 27.5 (b-CH_2).

^{19}F{^{1}H} NMR (470 MHz, CD_2Cl_2, 298 K) δ (ppm) = –73.65 (d, $^1J_{P-F}$ = 711.3 Hz).

$^{31}P\{^{1}H\}$ NMR (202 MHz, CD_2Cl_2, 298 K) δ (ppm) = –144.67 (hept, $^{1}J_{P\text{-}F}$ = 711.3 Hz).

UV-Vis titration:

Host Solution: **39·2PF$_6$** (30.9 μg, 10.6 nmol) in CH_2Cl_2(20 mL)

Guest Solution: 4,4'-bipyridine (3.1 mg, 19.8 μmol) in CH_2Cl_2 (5 mL)

Small aliquots of the guest solution were added to the host solution (0.15 mL in a 0.1 cm cuvette) with the host concentration kept constant, and UV-Vis spectra recorded after each addition. The absorption values (at wavelengths 415-435 nm) for each recorded spectra were compiled in an excel file and the data analysed using the BindFit titration program (http://supramolecular.org). Fitting to a 1:2 binding model was observed to be most accurate, with averaged values of K_{11} = 1.8 (± 0.1) × 10^5 L mol^{-1} and K_{12} = 799 (± 130) L mol^{-1} obtained.

Porphyrin-acridanol tweezer (40)

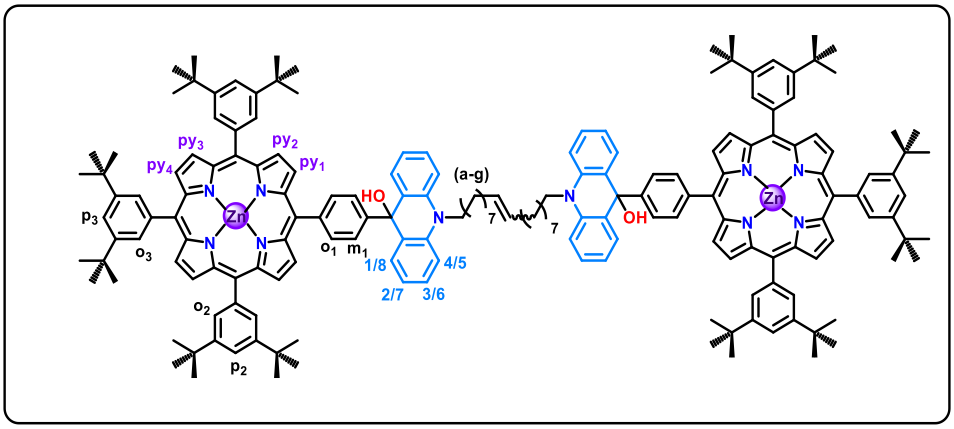

To a solution of tweezer **39·2PF$_6$** (22.5 mg, 7.69 μmol, 1 eq.) in CH_2Cl_2 (4 mL), was added an aliquot of 40 wt. % TBAOH in Methanol (12.1 μL, 16.9 μmol, 2.2 eq.). After 30 minutes stirring in the dark, the solution was washed with H_2O (3 × 10 mL) the solvent evaporated and the solid triturated with methanol. The desired product **40** was obtained as a purple solid (18 mg. 88%).

^{1}H NMR (500 MHz, CD_2Cl_2, 298 K) δ (ppm) = 8.95 – 8.89 (m, 8H, $H_{py3\text{-}4}$), 8.89 (d, ^{3}J = 4.7 Hz, 4H, $H_{py1/2}$), 8.85 (d, ^{3}J = 4.7 Hz, 4H, $H_{py1/2}$), 8.10 – 8.05 (m, 16H, $H_{o1\text{-}3}$), 7.82 (s, 6H, $H_{p2\text{-}}$

$_3$), 7.69 (d, ^3J = 8.1 Hz, 4H, H_{m1}), 7.61 (dd, ^3J = 7.7 Hz, ^{4}J = 1.7 Hz, 4H, $H_{1/8}$), 7.38 (t, ^3J = 8.1 Hz, 4H, $H_{3/6}$), 7.17 (d, ^3J = 8.5 Hz, 4H, $H_{4/5}$), 7.07 (t, ^3J = 7.7 Hz, 4H, $H_{2/7}$), 5.37 – 5.33 (m, 2H, =C*H*), 4.09 – 4.02 (m, 4H, NCH_2), 2.03 – 1.98 (m, 4H, a-CH_2), 1.95 – 1.91 (m, 8H, (b&g)-CH_2), 1.65 – 1.54 (m, 16H, (c-f)-CH_2). 1.53 – 1.49 (m, 108H, tBu).

^{13}C{^{1}H} NMR (125 MHz CD_2Cl_2, 298 K) δ (ppm) = 150.7 (CC$_{py}$), 150.6 (CC$_{py}$), 150.4 (CC$_{py}$) 149.0 (CC$_{p2-3}$), 142.1 (CC$_{o2-3}$), 141.0 (CC$_{o1}$), 140.6 (CC$_{4/5}$), 134.2(C_{o1}), 132.5 (C_{py}), 132.4 (C_{py}), 132.2 (C_{py}), 130.7 (C=C), 130.6 ($C_{1/8}$), 130.1 (C$_{o2-3}$), 129.9 (CC$_{m1}$), 129.0 ($C_{3/6}$), 124.7 (CC$_{1/8}$), 124.3 (C$_{m1}$), 122.3 (C$_{meso}$), 121.1 (C_{p2-3}), 120.5 ($C_{2/7}$), 112.8($C_{4/5}$), 78.8 (COH), 46.5 (NCH$_2$), 35.3 (C(CH$_3$)), 32.9 (g-CH$_2$), 31.8 (CH$_3$), 30.0 (c/d/e/f-CH$_2$), 29.9 (c/d/e/f-CH$_2$), 29.8 (c/d/e/f-CH$_2$), 29.5 (c/d/e/f-CH$_2$), 27.6 (c/d/e/f-CH$_2$), 27.3 (a-CH$_2$), 26.5 (b-CH$_2$).

UV-Vis (CH_2Cl_2, 298 K) λ_{max} (nm) = 407sh (ε L mol^{-1} cm^{-1} 78 300), 426 (863 000), 552 (36 100), 592 (15 100).

MS (ESI-TOF): m/z cald. for $C_{180}H_{200}N_{10}Zn_2^{2+}$ 1314.73, found 1314.73 ([M–2OH]$^{2+}$, 100%); m/z cald. for $C_{180}H_{201}N_{10}Zn_2^{3+}$ 876.82, found 876.82 ([M–2OH+H]$^{3+}$, 10%); m/z cald. for $C_{181}H_{203}N_{10}Zn_2O^+$ 2660.47, found 2660.46 ([M–2OH+OCH$_3$]$^{2+}$, 5%).

(Porphyrin-acridanol tweezer)@4,4-bipyridine complex (biPy@40)

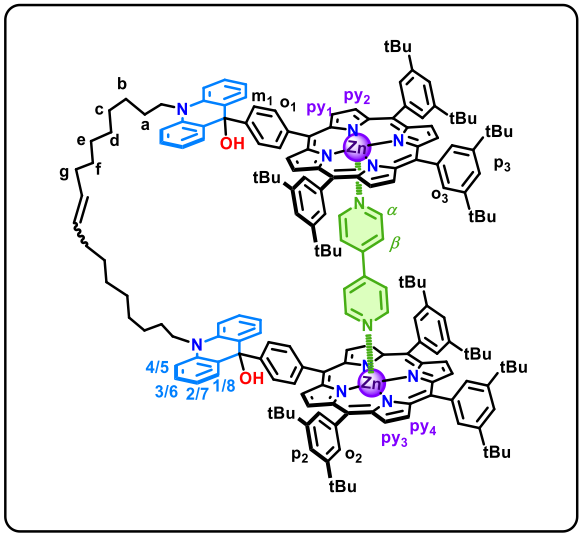

To a solution of **40** (3.24 mg, 1.22 μmol) in CD_2Cl_2 (0.55 mL) was added a solution of 4,4'-bipyridine (0.19 mg, 1.22 μmol) in CD_2Cl_2 (50 μL). The mixture was manually stirred, and formation of the **biPy@40** complex assessed via ^{1}H NMR spectroscopy.

^{1}H NMR (500 MHz, CD_2Cl_2, 298 K) δ (ppm) = 8.76 (s, 8H, H_{py3-4}), 8.73 (d, ^3J = 4.5 Hz, 4H, $H_{py1/2}$), 8.72 (d, ^3J = 4.5 Hz, 4H, $H_{py1/2}$), 7.94 – 7.86 (m, 16H, H_{o1-3}), 7.73 (s, 6H, H_{p2-3}), 7.64 – 7.53 (m, 8H, $H_{m1\ \&\ 1/8}$), 7.38 (t, ^3J = 7.8 Hz, 4H, $H_{3/6}$), 7.17 (d, ^3J = 8.3 Hz, 4H, $H_{4/5}$), 7.03 (t, ^3J = 7.3 Hz, 4H, $H_{2/7}$), 5.43 – 5.38 (m, 2H, *H*C=), 4.86 (d, ^3J = 6.0 Hz, 4H, $H_{bipy\text{-}\beta}$), 4.10 – 4.02 (m, 4H, NC*H*$_2$), 2.34 (s, 4H, $H_{bipy\text{-}\alpha}$), 2.10 – 1.92 (m, 8H, (a&g)-C*H*$_2$), 1.50 (m, 8H, (b&c)-CH_2), 1.43 (s, 108H, CH_3), 1.41 – 1.35 (m, 12H, (d-f)-C*H*$_2$).

^{13}C{^{1}H} NMR (125 MHz CD_2Cl_2, 298 K) *δ* (ppm) = 150.3 (*C*C_{Py}), 150.1 (*C*C_{Py}), 148.7 (*C*C_{p2-3}), 144.0 (*C*C_{o1}), 143.8($C_{bipy\text{-}\alpha}$), 142.5(*C*C_{o2-3}), 140.6(*C*$C_{4/5}$), 134.3(C_{o1}), 132.0 (C_{Py}), 131.8 (C_{Py}), 130.8(C=C), 130.6 ($C_{1/8}$), 130.1 (C_{o2-3}), 129.9 (*C*C_{m1}), 129.0 ($C_{3/6}$), 124.3 (*C*$C_{1/8}$ & C_m), 122.1 (C_{meso}), 120.9 (C_{p2-3}), 120.5 ($C_{2/7}$), 120.1 ($C_{biPy\text{-}\beta}$), 112.7 ($C_{4/5}$), 78.8 (*C*OH), 46.4 (NCH_2), 35.2 (*C*$(CH_3)_3$), 32.8 (g-CH_2), 31.8 (CH_2), 31.7 (CH_3), 29.8 (c/d/e/f-CH_2), 29.7 (c/d/e/f-CH_2), 29.6 (c/d/e/f-CH_2), 29.0 (c/d/e/f-CH_2), 27.1 (a-CH_2), 26.4 (b-CH_2).

UV-Vis titration:

Host Solution: **40** (30.6 μg, 11.5 nmol) in CH_2Cl_2 (20 mL).

Guest Solution: 4,4'-bipyridine (3.3 mg, 21.1 μmol) in CH_2Cl_2 (5 mL).

Small aliquots of the guest solution were added to the host solution (0.15 mL in a 0.1 cm cuvette) with the host concentration kept constant, and UV-Vis spectra recorded after each addition. The absorption values (at wavelengths 415-435 nm) for each recorded spectrum were compiled in an excel file and the data analysed using the BindFit titration program (http://supramolecular.org). Fitting to a 1:2 binding model was observed to be most accurate, with averaged values of K_{11} = 1.4 (± 0.3) × 10^5 L mol^{-1} and K_{12} = 870 (± 200) L mol^{-1} obtained.

Determination of binding constants for oxidised species ($K_{a\text{-}Ox}$)

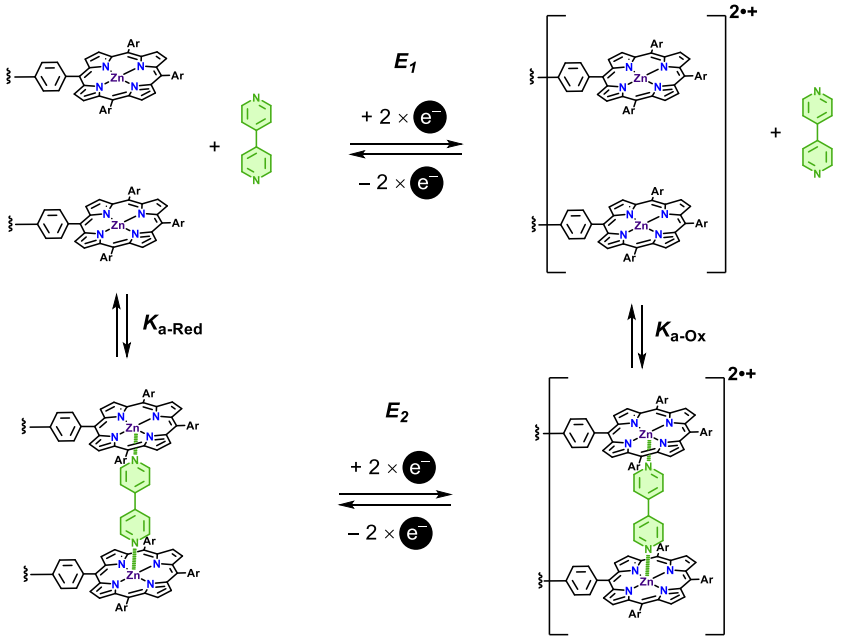

Given the Nernst equation(s):

1) $E_1 = E_1^0 + \frac{RT}{nF}\ln\left(\frac{[M^0]}{[M^{2\cdot+}]}\right)$

2) $E_2 = E_2^0 + \frac{RT}{nF}\ln\left(\frac{[c^0]}{[c^{2\cdot+}]}\right)$

And defining the binding constant(s) as:

3) $K_{a-Red} = \frac{[c^0]}{[M^0][biPy]}$

4) $K_{a-Ox} = \frac{[c^{2\cdot+}]}{[M^{2\cdot+}][biPy]}$

The following equations can be obtained:

5)

a) $E_1 - E_2 = E_1^0 - E_2^0 + \frac{RT}{nF}\ln\left(\frac{[M^0][c^{2\cdot+}]}{[M^{2\cdot+}][c^0]}\right)$

b) $E_1 - E_2 = E_1^0 - E_2^0 + \frac{RT}{nF}\ln\left(\frac{K_{a-Ox}}{K_{a-Red}}\right)$

Assuming that the system is in thermodynamic equilibrium:

$$E_1 = E_2$$

Equation (5b) can be rearranged to give:

$$K_{a-Ox} = K_{a-Red} \exp\left(\frac{nF}{RT} \times (E_2^0 - E_1^0)\right.$$

For **biPy@39·2PF$_6$**: $K_{a\text{-}Red}$ = 1.8 ×10^5 L mol^{-1} and $\Delta E_{1/2}$ = −57 mV

For **biPy@40:** $K_{a\text{-}Red}$ = 1.4 ×10^5 L mol^{-1} and $\Delta E_{1/2}$ = −19 mV

n = 2; F = 96485 C mol^{-1}; R = 8.3144621 J mol^{-1} K^{-1}; T = 293 K

Tetrakis(10-decenyl-9-phenylacridin-10-ium)porphyrin-Zn(II) hexafluorophosphate (41·4PF$_6$)

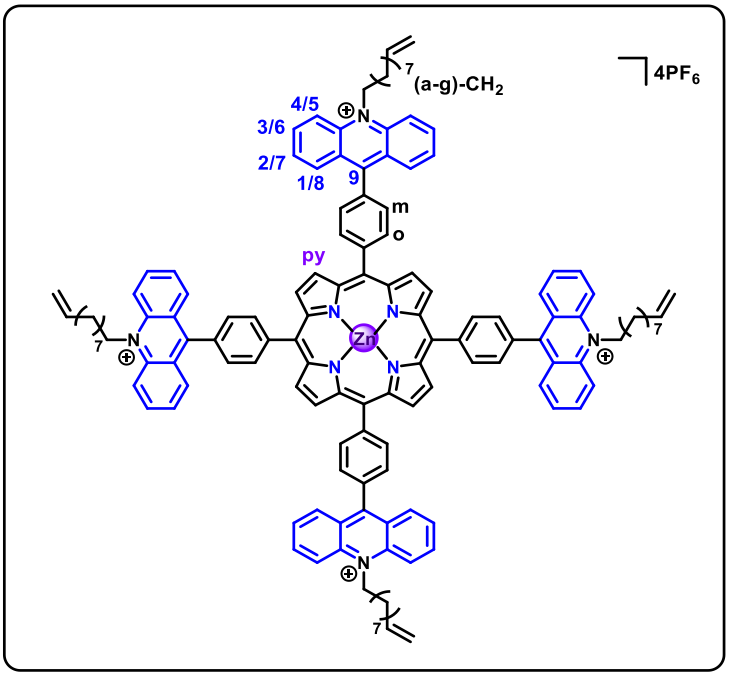

To a solution of **37·PF$_6$** (454 mg, 0.8 mmol) and pyrrole (55.5 μL, 0.8 mmol, 1 eq.) in degassed CH_2Cl_2 (50 mL) was added TFA (95.7 μL, 1.25 mmol, 1.2 eq.). The mixture was stirred in the dark for four hours before addition of DDQ (136 mg, 0.6 mmol, 0.75 eq.), then left to stir for an additional hour. The solution was then neutralised with Et_3N (1 mL), and the resultant mixture filtered through a short plug of SiO_2 (CH_2Cl_2/CH_3OH, 95:5). After removal of the solvent, purification was carried out via column chromatography (SiO_2, CH_2Cl_2/CH_3OH, 96:4, R_f = 0.39), followed by recrystallisation from CH_3CN/$CHCl_3$ (1:10 v/v) giving a purple precipitate. The precipitate was isolated then dissolved in CH_2Cl_2 (50 mL), and a solution of $Zn(OAc)_2{\cdot}2H_2O$ (17.6 mg, 0.08 mmol, 0.1 eq.) in CH_3OH (5 mL) added. The resultant mixture was heated to reflux for one hour, then extracted with H_2O (3×50 mL). The retained organic layer was evaporated and the resultant solid triturated with $CHCl_3$, then further purified via column chromatography (SiO_2, CH_2Cl_2/0.02 M methanolic KPF_6 soln./CH_3CN 80:5:15, R_f = 0.81). The relevant fractions were combined and extracted with H_2O (3 × 100 mL), retaining the organic fraction and evaporating the solvent to give **41·4PF$_6$** as a purple solid (171 mg, 34%).

^{1}H NMR (500 MHz, CD_2Cl_2, 298 K) δ (ppm) = 9.39 (s, 8H, H_{py}), 8.72 (d, ^{3}J = 7.5 Hz, 8H, H_o), 8.66 (d, ^{3}J = 8.5 Hz, 8H, $H_{1/8}$), 8.56 – 8.52 (m, 16H, $H_{3/6\ \&\ 4/5}$), 8.16 (ddd, ^{3}J = 8.0 & 4.8 Hz, ^{4}J = 2.5 Hz, 8H, $H_{2/7}$), 8.00 (d, ^{3}J = 7.5 Hz, 8H, H_m), 5.87 (ddt, ^{3}J = 16.9, 10.2 & 6.6 Hz, 4H, *H*C =), 5.43 – 5.36 (m, 8H, NCH_2), 5.04 (dq, ^{3}J = 17.1 Hz, $^{2,4}J$ = 1.7 Hz, 4H, =CHH_{trans}), 4.97 (ddt, ^{3}J = 10.2 Hz, ^{2}J = 2.3 Hz, ^{4}J = 1.3 Hz, 4H, =CH_{cis}H), 2.38 (p, ^{3}J = 8.0 Hz, 8H, a-CH_2), 2.11 (q, ^{3}J = 6.6 Hz, 8H, g-CH_2), 1.85 (p, ^{3}J = 7.6 Hz, 8H, b-CH_2), 1.62 (p, ^{3}J = 7.3 Hz, 8H, c-CH_2), 1.49 – 1.41 (m, 24H, (d-f)-CH_2).

^{13}C{^{1}H} NMR (125 MHz, CD_2Cl_2, 298 K) δ (ppm) = 162.8 (C_9), 150.6 (*C*C_{py}), 145.8 (*C*C_o), 141.1 (*C*$C_{4/5}$), 140.1 ($C_{3/6}$), 139.6 (=*C*H), 135.4 (C_o), 132.9 (C_{py}), 132.6 (*C*C_m), 131.7 ($C_{1/8}$), 128.9 (C_m), 128.8 ($C_{2/7}$), 126.9 (*C*$C_{1/8}$), 120.4 (C_{meso}), 117.9 ($C_{4/5}$), 114.4 (H_2C=), 51.7 (NCH_2), 34.2 (g-CH_2), 29.8 (c-CH_2), 29.7 (d/e/f-CH_2), 29.4 (d/e/f-CH_2), 29.3 (a-CH_2), 27.3 (b-CH_2).

^{19}F{^{1}H} NMR (470 MHz, CD_2Cl_2, 298 K) δ (ppm) = –73.33 (d, ^{1}J = 711 Hz).

^{31}P{^{1}H} NMR (202 MHz, CD_2Cl_2, 298 K) δ (ppm) = –144.40 (hept, ^{1}J = 711 Hz).

UV-Vis (CH_2Cl_2, 298 K) λ_{max} (nm) = 348 (ε $Lmol^{-1}cm^{-1}$ 47 700), 364 (87 200), 427 (361 000), 556 (21 600), 603 (10 200).

HRMS (ESI-TOF): m/z cald. for $C_{136}H_{132}N_8Zn^{4+}$ 485.2461, found 485.2474 ($[M–4PF_6]^{4+}$, 100%).

Tetrakis(10-decenyl-9-phenylacridin-10-ium)porphyrin-Zn(II) tetrakis[3,5-bis(trifluoromethyl)phenyl]borate (41·4BArF)

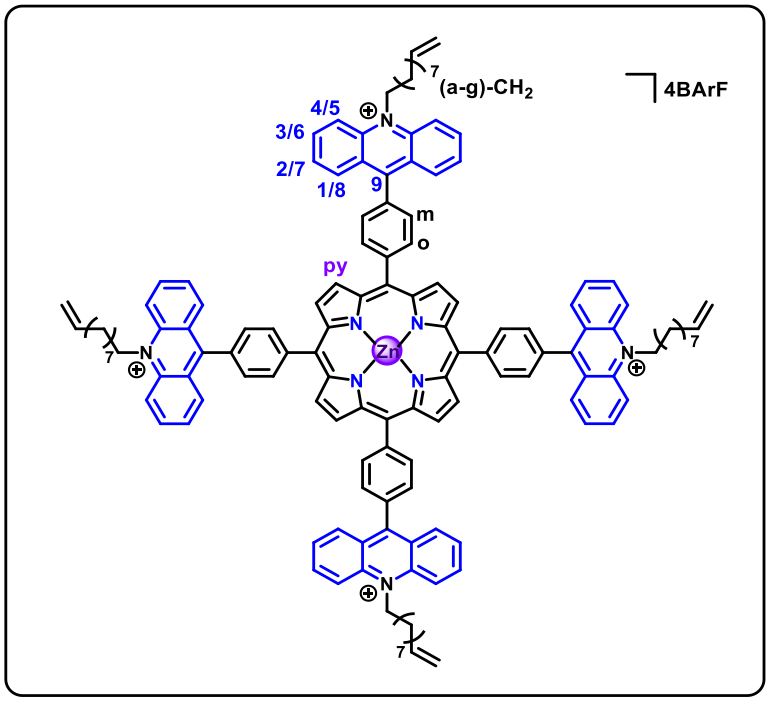

To a solution **41·4PF$_6$** (40.0 mg, 15.8 μmol) of in CH_2Cl_2 was added NaBArF (56.0 mg, 63.3 μmol, 4 eq.), and the mixture left to stir overnight. The resultant solution was washed with H_2O (3 × 100 mL), with the organic fraction retained and dried, giving the product as a purple solid (85.3 mg, quant.)

^{1}H NMR (500 MHz, CD_2Cl_2, 298 K) δ (ppm) = 9.35 (s, 8H, H_{Py}), 8.70 (d, ^3J = 7.6 Hz, 8H, H_o), 8.61 (dd, ^3J = 8.7, ^4J = 1.5 Hz, 8H, $H_{1/8}$), 8.49 (d, ^3J = 9.2 Hz, 8H, $H_{4/5}$), 8.43 (ddd, ^3J = 9.2 & 6.4 Hz, ^4J = 1.5 Hz, 8H, $H_{3/6}$), 8.01 – 7.88 (m, 16H, $H_{2/7\ \&\ m}$), 7.69 – 7.65 (m, 32H, $H_{BArF\text{-}o}$), 7.48 (s, 16H, $H_{BArF\text{-}p}$), 5.87 (ddt, ^3J = 16.9, 10.2 & 6.8 Hz, 4H, *H*C=), 5.40 – 5.34 (m, 8H, NCH_2), 5.04 (dq, ^3J = 17.1 Hz, $^{2,4}J$ = 1.7 Hz, 4H, =CHH_{trans}), 4.96 (ddt, ^3J = 10.1 Hz, ^2J = 2.3 Hz, ^4J = 1.2 Hz, 4H, =CH_{cis}H), 2.37 (p, ^3J = 8.3 Hz, 8H, a-CH_2), 2.11 (q, ^3J = 6.8 Hz, 8H, g-CH_2), 1.85 (p, ^3J = 7.7 Hz, 8H, b-CH_2), 1.61 (p, ^3J = 7.0 Hz, 8H, c-CH_2), 1.51 – 1.38 (m, 24H, (d-f)-CH_2).

^{13}C{^{1}H} NMR (125 MHz, CD_2Cl_2, 298 K) δ (ppm) = 163.0 (C_9), 162.1 (q, $^1J_{C\text{-}B}$ = 49.9 Hz, CB_{BArF}), 150.8 (CC_{py}), 145.9 (CC_o), 141.1 ($CC_{4/5}$), 140.2 ($C_{3/6}$), 139.5 (H*C*=), 135.4 (C_o), 135.2

($C_{BArF\ -o}$), 132.8 (C_{py}), 132.5 (*C*C_m), 131.7 ($C_{1/8}$), 129.3 (qq, $^2J_{C\text{-}F}$ = 31.4 Hz, $^4J_{C\text{-}F}$ = 2.8 Hz, $C_{BArF\text{-}m}$), 128.9 (C_m), 128.8 ($C_{2/7}$), 126.9 (*C*$C_{1/8}$), 124.9 (q, $^1J_{C\text{-}F}$ = 272.5 Hz, $CF_{3\text{-}BArF}$), 120.6 (C_{meso}), 117.9 – 117.8 (m, $C_{BArF\text{-}p}$ & $C_{4/5}$), 114.5 (=*C*H_2), 51.9 (N*C*H_2), 34.1 (s, g-*C*H_2), 29.8 (c-CH_2), 29.6 (d/e/f-CH_2), 29.4 (d/e/f-CH_2), 29.3 (d/e/f/a-CH_2), 29.2 (a-CH_2), 27.4 (b-*C*H_2).

^{19}F{^{1}H} NMR (470 MHz, CD_2Cl_2, 298 K) δ (ppm) = –62.84 (s).

UV-Vis (CH_2Cl_2, 298 K) λ_{max} (nm) = 349 (ε $Lmol^{-1}cm^{-1}$ 45 500), 364 (82 200), 427 (338 000), 556 (18 800), 603 (9590).

(Tetrakis(10-decenyl-9-phenylacridin-10-ium)porphyrin-Zn(II) hexafluorophosphate)$_2$@4,4'-bipyridine (biPy@(41·4PF$_6$)$_2$)

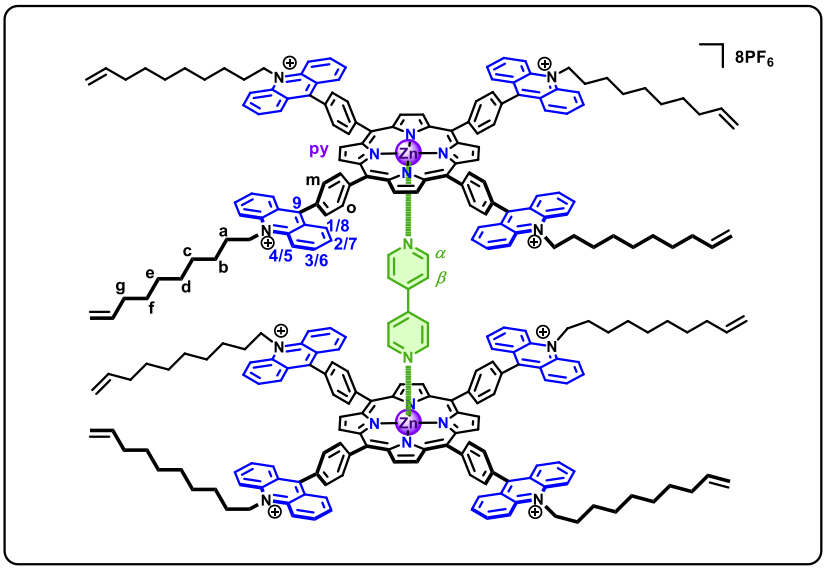

To a solution of **41·4PF$_6$** (2.08 mg, 0.825 μmol) in CD_2Cl_2 (0.5 mL) was added an aliquot of 4,4'-bipyridine (64.5 μg, 0.413 μmol, 0.5 eq.) in CD_2Cl_2 (50 μL), and the resultant solution manually stirred.

^{1}H NMR (500 MHz, CD_2Cl_2, 298 K) δ (ppm) = 9.20 (s, 16H, H_{py}), 8.58 – 8.53 (m, 16H, $H_{o\ \&\ 1/8}$), 8.51 – 8.45 (m, 16H, $H_{3/6\ \&\ 4/5}$), 8.09 – 8.04 (m, 16H, $H_{2/7}$), 7.88 (d, ^3J = 7.3 Hz, 16H, H_m), 5.88 (ddt, ^3J = 17.0, 10.2 & 6.8 Hz, 8H, *H*C=), 5.38 – 5.33 (m, 16H, NCH_2), 5.12 (br. s, 4H, $H_{biPy\text{-}\beta}$), 5.05 (dq, ^3J = 17.0 Hz, $^{2,4}J$ = 1.7 Hz, 8H, =CHH_{trans}), 4.97 (ddt, ^3J = 10.2 Hz, ^2J =

2.3 Hz, ^{4}J = 1.2 Hz, 8H, =CH_{cis}H), 2.49 (br. s, 4H, $H_{biPy\text{-}\alpha}$), 2.34 (p, ^{3}J = 8.2 Hz, 16H, a-CH_2), 2.11 (q, ^{3}J = 6.8 Hz, 16H, g-CH_2), 1.84 (p, ^{3}J = 7.6 Hz, 16H, b-CH_2), 1.60 (p, ^{3}J = 7.1 Hz, 16H, c-CH_2), 1.52 – 1.39 (m, 48H, (d-f)-CH_2).

$^{13}C\{^{1}H\}$ NMR (125 MHz, CD_2Cl_2) δ (ppm) = 162.8 (C_9), 150.5 (CC_{py}), 145.8 (CC_o), 141.1 ($CC_{4/5}$), 140.0 ($C_{3/6}$), 139.6 (HC=), 135.4 (C_o), 132.7 (CC_m), 132.4 (C_{py}), 131.7 ($C_{1/8}$), 128.8 (C_m) 128.7 ($C_{2/7}$), 126.9 ($CC_{1/8}$), 120.2 ($C_{bipy\text{-}\beta}$), 118.6 (C_{meso}), 118.0 ($C_{4/5}$), 114.4 (H_2C=), 51.7 (NCH_2), 34.2 (g-CH_2), 29.8 (c-CH_2), 29.6 (d/e/f-CH_2), 29.4 (d/e/f-CH_2), 29.3 (a-CH_2), 27.3 (b-CH_2).

$^{19}F\{^{1}H\}$ NMR (470 MHz, CD_2Cl_2, 298 K) δ (ppm) = –73.45 (d, $^{1}J_{P\text{-}F}$ = 711 Hz).

$^{31}P\{^{1}H\}$ NMR (202 MHz, CD_2Cl_2, 298 K) δ (ppm) = –144.47 (hept, $^{1}J_{P\text{-}F}$ = 711 Hz).

Porphyrin-acridinium cage hexafluorophosphate (42·8PF_6)

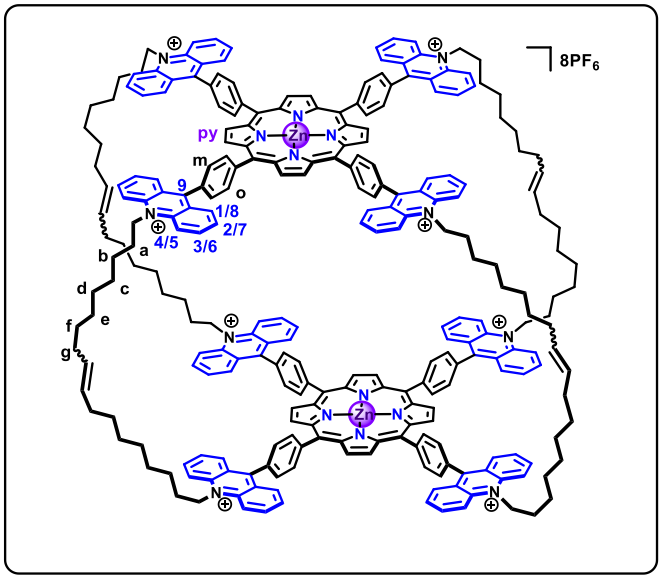

To a degassed solution of **41·4PF_6** (150.0 mg, 59.4 μmol) and 4,4'-bipyridine (4.64 mg, 29.7 μmol) in CH_2Cl_2 (120 mL) was added Grubbs (I) Catalyst (12.2 mg, 14.9 μmol, 20 mol%), and the resulting solution left to stir for 16 hrs, after which a second load of catalyst was added (12.2 mg, 14.91 μmol, 20 mol%), and the solution left to stir for an additional eight hours before opening the solution to air to quench the catalyst. The

solution was evaporated and triturated with $CHCl_3$, then taken up in a 0.04 M KPF_6 CH_3CN solution (10 mL) and filtered over a plug of SiO_2, removing the template. Purification via column chromatography (SiO_2, CH_2Cl_2/0.02 M methanolic KPF_6 soln./CH_3CN 80:5:15, R_f = 0.48), then gave the product as a purple solid (71.2 mg, 49%).

^{1}H NMR (400 MHz, CD_2Cl_2, 298 K) δ (ppm) = 9.39 (br. s, 16H, H_{py}), 8.71 – 7.78 (m, 96H, $H_{1-8,\,o\,\&\,m}$), 5.47 – 5.37 (m, 8H, *H*C=), 5.26 – 4.98 (m, 16H, NCH_2), 2.38 – 2.27 (m, 16H, a-CH_2), 2.04 – 2.00 (m, 16H, g-CH_2), 1.85 – 1.80 (m, 16H, b-CH_2), 1.61 – 1.55 (m, 16H, c-CH_2), 1.46 – 1.08 (m, 48H, (d-f)-CH_2).

^{19}F{^{1}H} NMR (470 MHz, CD_2Cl_2) δ (ppm) = −73.16 (d, $^1J_{P\text{-}F}$ = 711.3 Hz).

^{31}P{^{1}H} NMR (202 MHz, CD_2Cl_2) δ (ppm) = −144.36 (hept, $^1J_{P\text{-}F}$ = 711.3 Hz).

UV-Vis: (CH_2Cl_2, 298 K) λ_{max} (nm) = 348 (ε $Lmol^{-1}cm^{-1}$ 93 000), 364 (169 000), 431 (558 000), 559 (38 600), 603 (22 900).

UV-Vis: (CH_3CN, 298 K) λ_{max} (nm) = 347 (ε $Lmol^{-1}cm^{-1}$ 91 300), 363 (144 000), 439 (573 000), 570 (31 100), 615 (26 100).

HRMS (ESI-TOF): m/z cald. for $C_{264}H_{248}N_{16}Zn_2^{7+}$ 538.549177, found 538.549151 ($[M^{\cdot}-8PF_6]^{7+}$, 100%); m/z cald. for $C_{264}H_{248}N_{16}Zn_2^{8+}$ 471.2305, found 471.2323 ($[M-8PF_6]^{8+}$, 60%); m/z cald. for $C_{264}H_{248}F_6N_{16}PZn_2^{7+}$ 559.2583, found 559.2617 ($[M-7PF_6]^{7+}$, 25%).

(Porphyrin-acridinium cage)@DABCCO complex hexafluorophosphate

(DABCO@42·8PF$_6$))

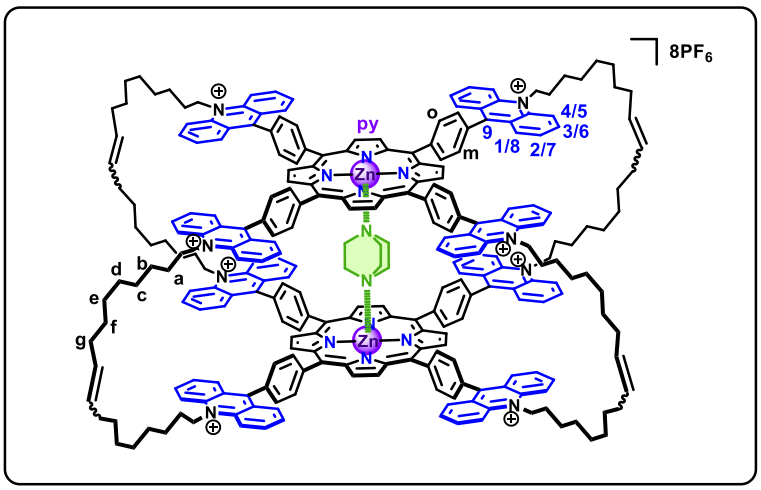

To a solution of **42·8PF$_6$** (2.71 mg, 0.55 μmol) in CD_3CN (0.5 mL) was added a solution of DABCO (61.7 μg, 0.55 μmol) in CD_3CN (50 μL), and the resulting solution manually stirred.

^{1}H NMR (500 MHz, CD_3CN, 298 K) δ (ppm) = 9.00 (s, 16H, H_{py}), 8.60 (d, ^3J = 8.9 Hz, 16H, $H_{4/5}$), 8.45 – 8.39 (m, 32H, $H_{1/8\ \&\ 3/6}$), 8.38 – 8.28 (m, 16H, H_o), 7.96 (t, ^3J = 7.0 Hz, 16H, $H_{2/7}$), 7.81 – 7.71 (m, 16H, H_m), 5.55 – 5.48 (m, 8H, =C*H*), 5.36 – 5.28 (m, 16H, NCH_2), 2.28 – 2.24 (m, 16H, (a&g)-CH_2), 1.88 (p, ^3J = 6.8 Hz, 16H, b-CH_2), 1.60 – 1.46 (m, 16H, c-CH_2), 1.57 – 1.47 (m, 64H, (d-f)-CH_2), −4.59 – −4.78 (m, 12H, H_{DABCO}).

^{13}C{^{1}H} NMR (125 MHz, CD_3CN, 298 K) δ (ppm) = 162.6 (C_9), 150.6 (CC_{py}), 145.6 (CC_o), 141.7 ($CC_{4/5}$), 140.0 ($C_{3/6}$), 135.3 (C_o), 133.5 (CC_m), 132.9 (C_{py}), 131.7 (=*C*H), 131.6 ($C_{1/8}$), 128.8 ($C_{2/7}$), 128.5 (C_m), 127.4 ($CC_{1/8}$), 120.5 (C_{meso}), 119.1 ($C_{4/5}$), 52.1 (NCH_2), 32.8 (g-CH_2), 30.4 (c-CH_2), 30.0 (d/e/f-CH_2), 29.7 (d/e/f-CH_2), 29.6 (d/e/f-CH_2), 29.5 (a-CH_2), 27.6 (b-CH_2).

^{19}F{^{1}H} NMR (282 MHz, CD_3CN, 298 K) δ (ppm) = −72.89 (d, $^1J_{P\text{-}F}$ = 707.3 Hz).

^{31}P{^{1}H} NMR (121 MHz, CD_3CN, 298 K) δ (ppm) = −144.69 (hept, $^1J_{P\text{-}F}$ = 707.3 Hz).

For the UV-Vis titration two solutions were prepared:

Host Solution: **42·8PF$_6$** (99.0 μg, 20.1 nmol) in CH_3CN (20 mL)

Guest Solution: DABCO (0.113 mg, 1.00 μmol) in CH_3CN (5 mL)

Small aliquots of the guest solution were added to the host solution, and UV-Vis spectra recorded after each addition. The absorption values (at wavelengths 420 - 440 nm) for each recorded spectrum were compiled in an excel file, corrected for dilution and the data analysed using the BindFit titration program (http://supramolecular.org). Fitting to a 1:1 binding model was observed to be most accurate, with an averaged value of K_a = 4.5 (± 0.2) × 10^5 L mol^{-1} obtained.

(Porphyrin-acridinium cage)@biPy complex hexafluorophosphate (biPy@42·8PF$_6$)

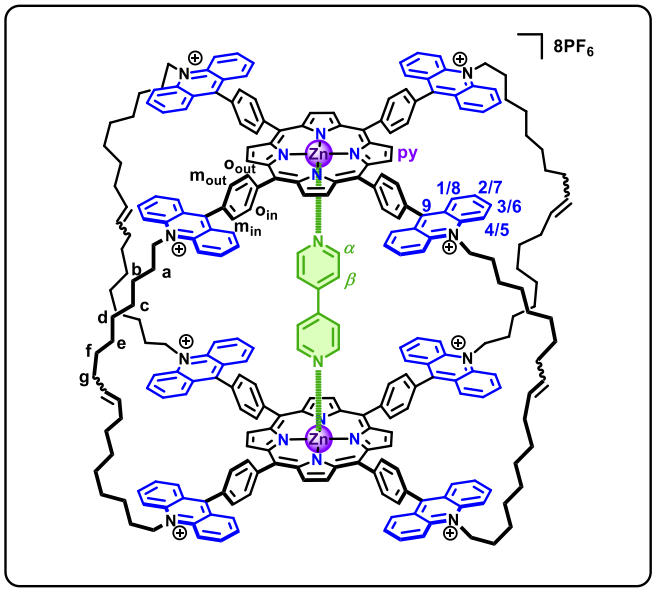

A solution of 4,4'-bipyridine (85.9 μg, 0.55 μmol) in CH_3CN (0.1 mL) was added to **42·8PF$_6$** (2.71 mg, 0.55 μmol) and the mixture dried under vacuum. The solid was then dissolved in CD_2Cl_2/CD_3CN (0.55 mL, 9:1 v/v) and manually stirred.

^{1}H NMR (500 MHz, CD_2Cl_2/CD_3CN (9:1), 298 K) δ (ppm) = 9.10 (s, 16H, H_{py}), 8.62 – 8.54 (m, 8H, $H_{o\text{-}out}$), 8.49 – 8.39 (m, 48H, $H_{1/8,\ 3/6\ \&\ 4/5}$), 8.34 – 8.25 (m, 8H, $H_{o\text{-}in}$), 7.98 (dd, ^3J = 8.5 & 5.7 Hz, 16H, $H_{2/7}$), 7.89 – 7.81 (m, 8H, $H_{m\text{-}out}$), 7.78 – 7.68 (m, 8H, $H_{m\text{-}in}$), 5.48 – 5.41

(m, 8H, =C*H*), 5.30 – 5.22 (m, 16H, NCH_2), 4.95 (d, ^3J = 7.0 Hz, 4H, $H_{biPy\text{-}\beta}$), 2.32 – 2.23 (m, 16H, a-CH_2), 2.08 – 2.01 (m, 20H, $H_{biPy\text{-}\alpha}$ & g-CH_2), 1.83 – 1.78 (m, 16H, b-CH_2), 1.59 – 1.54 (m, 16H, c-CH_2), 1.47 – 1.39 (m, 48H, (d-f)-CH_2).

$^{13}C\{^1H\}$ NMR (125 MHz, CD_2Cl_2/CD_3CN (9:1), 298 K) δ (ppm) = 162.5 (C_9), 150.2 (CC_{py}), 145.6 (CC_o), 143.3 ($C_{bipy\text{-}\alpha}$), 141.0 ($CC_{4/5}$), 139.7 ($C_{3/6}$), 135.2 ($C_{o\text{-}in}$), 134.5 ($C_{o\text{-}out}$), 132.4 (C_{py}), 132.2 (CC_m), 131.4 ($C_{1/8}$), 130.6 (=*C*H), 128.6 ($C_{m\text{-}in}$), 128.4 ($C_{2/7}$), 128.3 ($C_{m\text{-}out}$), 126.7 ($CC_{1/8}$), 120.1 (C_{meso}), 119.9 ($C_{bipy\text{-}\beta}$), 117.9 ($C_{4/5}$), 51.6 (N*C*H_2), 32.8 (g-CH_2), 29.9 (c-CH_2), 29.5 (d/e/f-CH_2), 29.3 (d/e/f-CH_2), 29.0 (a-CH_2), 27.2 (b-CH_2).

$^{19}F\{^1H\}$ NMR (282 MHz, CD_2Cl_2/CD_3CN (9:1), 298 K) δ (ppm) = –73.31 (d, $^1J_{P\text{-}F}$ = 711.2 Hz).

$^{31}P\{^1H\}$ NMR (121 MHz, CD_2Cl_2/CD_3CN (9:1), 298 K) δ (ppm) = –144.71 (hept, $^1J_{P\text{-}F}$ = 711.2 Hz).

UV-Vis titration:

Host Solution: **42·8PF_6** (99.0 μg, 20.1 nmol) in CH_2Cl_2 [0.1% CH_3CN] (20 mL).

Guest Solution: biPy (0.624 mg, 4.00 μmol) in CH_2Cl_2 [0.1% CH_3CN] (10 mL).

Small aliquots of the guest solution were added to the host solution (2 mL in a 1 cm cuvette), and UV-Vis spectra recorded after each addition. The absorption values (at wavelengths 423 – 435 nm) for each recorded spectrum were compiled in an excel file, corrected for dilution (< 3% dilution of initial concentration at end point of titration) and the data analysed using the BindFit titration program (http://supramolecular.org). Fitting to a 1:1 binding model was observed to be most accurate, with an averaged value of K_a = 4.2 (± 0.7) × 10^6 L mol^{-1} obtained.

Porphyrin-acridinium cage tetrakis[3,5-bis(trifluoromethyl)phenyl]borate (42·8BArF)

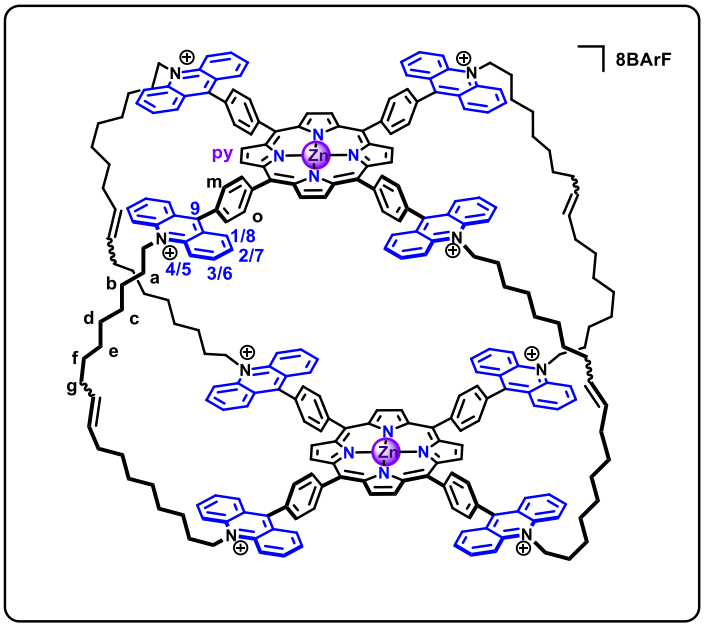

To a suspension of **42·8PF$_6$** (13.96 mg, 2.83 μmoles) in CH_2Cl_2 (5 mL) was added NaBArF (20.05 mg, 22.63 μmoles), and the mixture left to stir overnight. The resultant solution was then extracted with H_2O (3 × 10 mL) and the retained organic fraction evaporated to dryness, giving the product as a purple solid (30.2 mg, quant.).

^{1}H NMR (500 MHz, CD_2Cl_2, 298 K) δ (ppm) = 9.16 (s, 16H, H_{py}), 8.72 – 8.61 (m, 8H, $H_{o\text{-}out}$), 8.45 (d, ^3J = 8.4 Hz, 16H, $H_{1/8}$), 8.41 (d, ^3J = 8.9 Hz, 16H, $H_{4/5}$), 8.37 – 8.17 (m, 24H, $H_{3/6\ \&\ o\text{-}in}$), 7.92 – 7.84 (m, 8H, $H_{m\text{-}out}$), 7.84 – 7.74 (m, 16H, $H_{2/7}$), 7.70 – 7.58 (m, 64H, $H_{BArF\text{-}o}$), 7.59 – 7.53 (m, 8H, $H_{m\text{-}in}$), 7.39 (s, 32H, $H_{BArF\text{-}p}$), 5.42 (s, 8H, *H*C=), 2.36 – 2.20 (m, 16H, a-CH_2), 2.10 – 1.93 (m, 16H, g-CH_2), 1.87 – 1.72 (m, 16H, b-CH_2), 1.60 – 1.50 (m, 16H, c-CH_2), 1.44 – 1.31 (m, 48H, (d-f)-CH_2).

^{13}C{^{1}H} NMR (125 MHz, CD_2Cl_2, 298 K) δ (ppm) = 162.9 (C_9), 162.0 (q, $^1J_{C\text{-}B}$ = 49.8 Hz), 150.6 (*C*C_{py}), 145.7 (*C*C_o), 141.0 (*C*$C_{4/5}$), 140.0 ($C_{3/6}$), 135.1 ($C_{BArF\text{-}o}$), 134.6 ($C_{o\text{-}in}$), 133.2 ($C_{o\text{-}out}$), 132.6 (C_{py}), 132.3 (*C*C_m), 131.6 ($C_{1/8}$), 130.7 (=CH), 129.2 (qq, $^2J_{C\text{-}F}$ = 31.6 Hz, $^4J_{C\text{-}F}$ = 3.0 Hz, $C_{BArF\text{-}m}$), 128.8 ($C_{m\text{-}in}$), 128.6 ($C_{m\text{-}out}$), 128.5 ($C_{2/7}$), 126.8 (*C*$C_{1/8}$), 124.8 (q, $^1J_{C\text{-}F}$ = 272.3 Hz, $CF_{3\text{-}BArF}$), 120.3 (C_{meso}), 117.9 – 117.6 (m, $C_{BArF\text{-}p}$ & $C_{4/5}$), 33.0 (g-CH_2), 30.1 (d/e/f-CH_2), 29.8 (d/e/f-CH_2), 29.7 (d/e/f-CH_2), 29.5 (c-CH_2), 29.2 (a-CH_2), 27.3 (b-CH_2).

$^{19}F\{^{1}H\}$ NMR (470 MHz, CD_2Cl_2, 298 K) δ (ppm) = – 62.89 (s).

UV-Vis: (CH_2Cl_2, 298 K) λ_{max} (nm) = 348 (ε $Lmol^{-1}cm^{-1}$ 102 000), 363 (181 000), 426 (671 000), 556 (38 700), 603 (18 500).

HR-MS(ESI-TOF): m/z cald. for $C_{264}H_{248}N_{16}Zn_2^{7+}$ 538.549177, found 538.549807 ($[M^{\cdot}-8BArF]^{7+}$, 100%); m/z cald. for $C_{264}H_{248}N_{16}Zn_2^{8+}$ 471.230461, found 471.233478 ($[M-8BArF]^{8+}$, 60%); m/z cald. for $C_{296}H_{260}BF_{24}N_{16}Zn_2^{7+}$ 661.844160, found 661.845437 ($[M-7BArF]^{7+}$, 30%).

(Porphyrin-acridinium cage)@DABCO complex tetrakis[3,5-bis(trifluoromethyl)phenyl]borate (DABCO@42·8BArF)

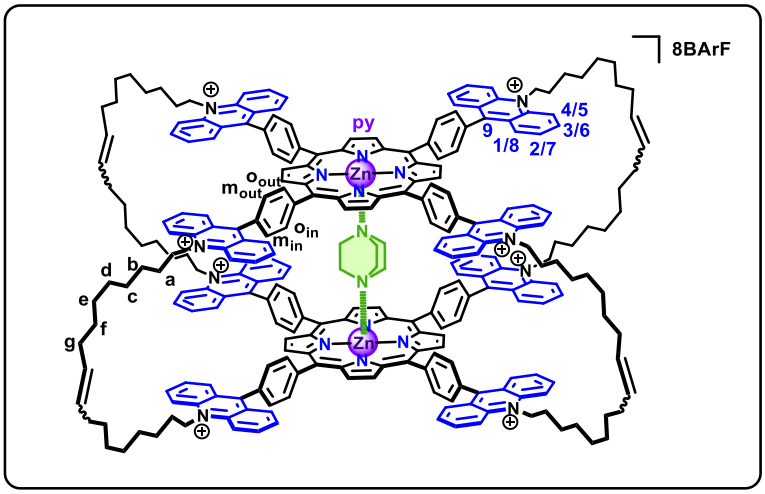

To a solution of **42·8BArF** (5.87 mg, 0.55 μmol) in CD_2Cl_2 (0.5 mL) was added a solution of DABCO (61.7 μg, 0.55 μmol) in CD_2Cl_2 (50 μL). The resulting solution was manually stirred, and an NMR recorded.

^{1}H NMR (500 MHz, CD_2Cl_2, 298 K) δ (ppm) = 8.87 (s, 16H, H_{py}), 8.58 (d, ^{3}J = 7.4 Hz, 8H, $H_{o\text{-}in}$), 8.35 (d, ^{3}J = 9.0 Hz, 16H, $H_{4/5}$), 8.31 (d, ^{3}J = 8.4 Hz, 16H, $H_{1/8}$), 8.19 – 8.14 (m, 16H, $H_{3/6}$), 8.09 (d, ^{3}J = 7.1 Hz, 8H, $H_{o\text{-}out}$), 7.76 (d, ^{3}J = 7.4 Hz, 8H, $H_{m\text{-}in}$), 7.70 (s, 64H, $H_{BArF\text{-}o}$), 7.61 (d, ^{3}J = 7.1 Hz, 8H, $H_{m\text{-}out}$), 7.51 – 7.47 (m, 48H, $H_{BArF\text{-}p\ \&\ 2/7}$), 5.53 – 5.44 (m, 8H, HC=), 5.29 – 5.21 (m, 16H, NCH_2), 2.31 – 2.24 (m, 16H, a-CH_2), 2.12 – 2.07 (m, 16H, g-CH_2), 1.86

– 1.81 (m, 16H, b-CH_2), 1.62 – 1.58 (m, 16H, c-CH_2), 1.49 – 1.40 (m, 48H, (d-f)-CH_2), –4.09 (s, 12H, H_{DABCO}).

$^{13}C\{^1H\}$ NMR (125 MHz, CD_2Cl_2, 298 K) δ (ppm) = 162.8 (C_9), 162.1 (q, $^1J_{C\text{-}B}$ = 49.5 Hz, *C*B_{BArF}), 150.4 (*C*C_{Py}), 145.8 (*C*C_o), 140.9 (*C*$C_{4/5}$), 139.9 ($C_{3/6}$), 135.3 ($C_{o\text{-}out}$), 135.2 ($C_{BArF\text{-}o}$), 134.0 ($C_{o\text{-}in}$), 132.1 (*C*C_m), 132.0 (C_{Py}), 131.2 ($C_{1/8}$), 129.3 (qq, $^2J_{C\text{-}F}$ = 31.6 Hz, $^4J_{C\text{-}F}$ = 2.9 Hz, $C_{BArF\text{-}m}$), 128.3 ($C_{m\text{-}out}$), 128.3 ($C_{2/7}$), 127.8 ($C_{m\text{-}in}$) 126.7 (*C*$C_{1/8}$), 124.9 (q, $^1J_{C\text{-}F}$ = 272.4 Hz, $CF_{3\text{-}BArF}$), 119.8 (C_{meso}), 118.0 – 117.7 (m, $C_{BArF\text{-}p}$), 117.6 ($C_{4/5}$) 51.9 (NCH_2), 37.0 (C_{DABCO}), 33.1 (g-CH_2), 29.9 (c/d/e/f-CH_2), 29.8 (c/d/e/f-CH_2), 29.6 (c/d/e/f-CH_2), 29.3 (c/d/e/f-CH_2), 29.2 (a-CH_2), 27.7 (b-CH_2).

$^{19}F\{^1H\}$ NMR (470 MHz, CD_2Cl_2, 298 K) δ (ppm) = – 62.75 (s).

UV-Vis titration:

Host Solution: **42·8BArF** (34.7 μg, 3.25 nmol) in CH_2Cl_2 (10 mL).

Guest Solution: DABCO (58.3 μg, 520 nmol) in CH_2Cl_2 (10 mL).

Small aliquots of the guest solution were added to the host solution (2 mL in a 1 cm cuvette), and UV-Vis spectra recorded after each addition. The absorption values (at wavelength 425-435 nm) for each recorded spectrum were compiled in an excel file, corrected for dilution (< 3% dilution of initial concentration at end point of titration) and the data analysed using the BindFit titration program (http://supramolecular.org). Fitting to a 1:1 binding model was observed to be the most accurate, with a value of 1.2 (± 0.2) × 10^7 L mol^{-1} obtained.

Porphyrin-acridinium cage@biPy complex tetrakis[3,5-bis(trifluoromethyl)phenyl]borate (biPy@42·8BArF)

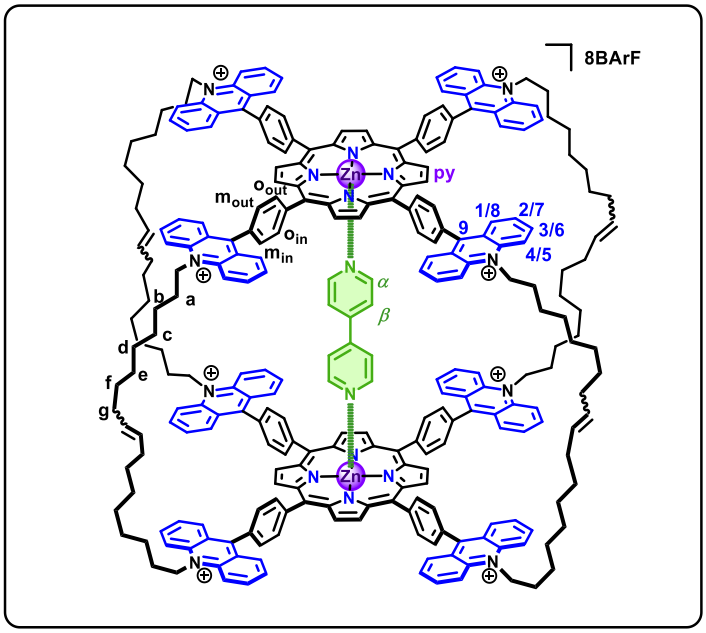

To a solution of cage **42·8BArF** (5.87 mg, 0.55 μmol) in CD_2Cl_2 (0.5 mL) was added a solution of 4,4'-bipyridine (85.9 μg, 0.55 μmol) in CD_2Cl_2 (50 μL), and the resulting solution manually stirred.

^{1}H NMR (500 MHz, CD_2Cl_2, 298 K) δ (ppm) = 9.07 (s, 16H, H_{py}), 8.49 (d, ^3J = 6.6 Hz, 8H, $H_{o\text{-}out}$), 8.44 – 8.36 (m, 42H, $H_{4/5,\ 1/8,\ o\text{-}in}$), 8.30 – 8.23 (m, 16H, $H_{3/6}$), 7.78 (d, ^3J = 6.6 Hz, 8H, $H_{m\text{-}out}$), 7.71 – 7.66 (m, 16H, $H_{2/7}$), 7.63 (s, 64H, $H_{BArF\text{-}o}$), 7.59 (d, ^3J = 7.0 Hz, 8H, $H_{m\text{-}in}$), 7.42 (s, 32H, $H_{BArF\text{-}p}$), 5.49 – 5.39 (m, 8H, HC=), 5.31 – 5.25 (m, 16H, NCH_2), 4.89 (d, ^3J = 5.6 Hz, 4H, $H_{bipy\text{-}\beta}$), 2.39 (br. s, 4H, $H_{bipy\text{-}\alpha}$), 2.34 – 2.26 (m, 16H, a-CH_2), 2.13 – 2.00 (m, 16H, g-CH_2), 1.85 – 1.77 (m, 16H, b-CH_2), 1.61 – 1.55 (m, 16H, c-CH_2), 1.47 – 1.38 (m, 48H, (d-f)-CH_2).

^{13}C{^{1}H} NMR (125 MHz, CD_2Cl_2, 298 K) δ (ppm) = 163.0 (C_9), 162.1 (q, $^1J_{C\text{-}B}$ = 49.9 Hz, $CB_{\text{-}BArF}$),150.4 (CC_{Py}), 143.7 ($C_{bipy\text{-}\alpha}$), 140.9 ($CC_{4/5}$), 140.0 ($C_{3/6}$), 135.4 ($C_{o\text{-}out}$), 135.3 ($C_{o\text{-}in}$), 135.0 ($C_{BArF\text{-}o}$), 132.2 (C_{py}), 132.0 (CC_m), 131.5 ($C_{1/8}$), 130.6 (C=C), 129.1 (q, $^2J_{C\text{-}F}$ = 31.7 Hz, $C_{BArF\text{-}m}$), 128.4 ($C_{m\text{-}in\&out}$), 128.2 ($C_{2/7}$), 126.7 ($CC_{1/8}$), 124.8 (q, $^1J_{C\text{-}F}$ = 272.2 Hz, $CF_{3\text{-}BArF}$),

120.1 ($C_{bipy\text{-}\beta}$), 117.8 ($C_{BArF\text{-}p}$), 117.6 ($C_{4/5}$), 51.7 (NCH_2), 33.0 (g-CH_2), 29.8 (c/d/e/f-CH_2), 29.6 (c/d/e/f-CH_2), 29.5 (c/d/e/f-CH_2), 29.0 (a-CH_2), 27.4 (b-CH_2).

$^{19}F\{^1H\}$ NMR (470 MHz, CD_2Cl_2, 298 K) δ (ppm) = –62.83 (s).

UV-Vis titration:

Host Solution: **42·8BArF** (160 μg, 15.0 nmol) in CH_2Cl_2 (20 mL).

Guest Solution: **biPy** (93.7 μg, 600 nmol) in CH_2Cl_2 (20 mL).

Small aliquots of the guest solution were added to the host solution (2 mL in a 1 cm cuvette), and UV-Vis spectra recorded after each addition. The absorption values (at wavelength 425-435 nm) for each recorded spectrum were compiled in an excel file, corrected for dilution (< 3% dilution of initial concentration at end point of titration) and the data analysed using the BindFit titration program (http://supramolecular.org). Fitting to a 1:1 binding model was observed to be the most accurate, with a value of 1.3 (± 0.2) × 10^7 L mol^{-1} obtained.

Porphyrin acridane cage (43)

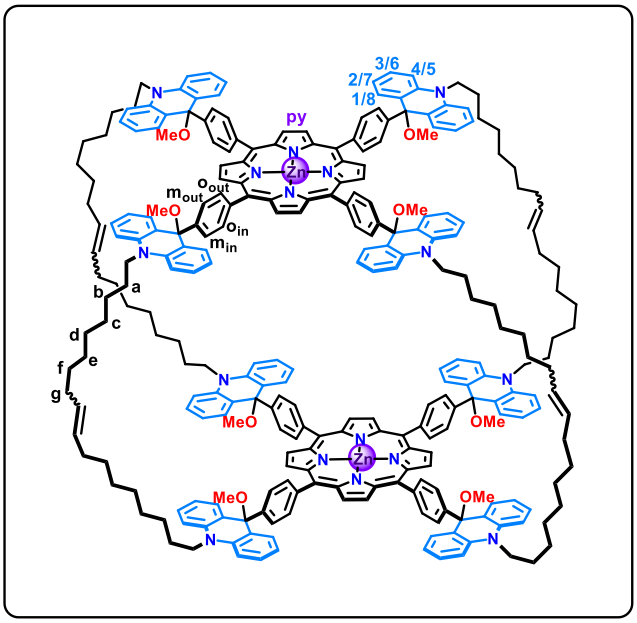

To a solution of the **42·8PF$_6$** (3.95 mg, 0.8 μmol) in CH_2Cl_2/CH_3CN (2 mL, 95:5 v/v) was added a methanolic (0.2 mL) solution of KOH (0.404 mg, 7.2 μmol, 9 eq.). The resultant solution was stirred for one minute, and conversion assessed via UV-Vis spectroscopy. The solution was then diluted with CH_2Cl_2 (20 mL) and an extraction carried out using H_2O (3 × 20 mL), retaining the organic fraction, which was then evaporated to dryness. The solid was then dissolved in CH_2Cl_2 (1 mL), and CH_3OH (2 mL) added, then the left to sit overnight, giving the product **43** as a purple precipitate (2.90 mg, 90%.)

^{1}H NMR (500 MHz, CD_2Cl_2, 298 K) δ (ppm) = 8.80 – 8.52 (m, 16H, H_{Py}), 8.01 – 7.53 (m, 24H, $H_{o\ \&\ m\text{-}out}$), 7.29 (d, ^3J = 8.1 Hz, 16H, $H_{1/8}$), 7.18 (d, ^3J = 8.0 Hz, 16H, $H_{3/6}$), 7.08 – 6.90 (m, 24H, $H_{4/5\ \&\ m\text{-}in}$), 6.88 – 6.69 (m, 16H, $H_{2/7}$), 5.28 (s, 8H, HC=), 3.88 (s, 16H, NCH_2), 2.00 – 1.55 (m, 32H, (g&a)-CH_2), 1.36 – 0.90 (m, 80H, (b-f)-CH_2).

^{13}C{^{1}H} NMR (125 MHz, CD_2Cl_2, 298 K) δ (ppm) = 150.5 (CC_{Py}), 140.9 (CC_o), 140.5 ($CC_{4/5}$), 134.2 (C_o), 132.2 (C_{Py}), 130.8 (HC=), 130.6 ($C_{1/8}$), 130.3 (CC_m), 128.9 ($C_{3/6}$), 124.1 ($CC_{1/8}$ & C_m), 120.5 ($C_{2/7}$), 112.6 ($C_{4/5}$), 78.8 (*C*OMe), 50.9 (OMe), 46.4 (NCH_2), 32.8 (g-CH_2), 29.7 (c/d/e/f-CH_2), 29.6 (c/d/e/f-CH_2), 29.1 (c/d/e/f-CH_2), 27.2 (a-CH_2), 26.4 (b-CH_2).

UV-Vis (CH_2Cl_2, 298 K) λmax (nm) = 294 (ε $Lmol^{-1}cm^{-1}$ 180 000), 427 (804 000), 557 (38 900), 600 (18 500).

MS (ESI-TOF): m/z cald. for $C_{264}H_{249}N_{16}Zn_2^{6+}$ 628.48, found 628.47 ($[M^{\cdot}-8OMe+H]^{6+}$, 100%).

(Porphyrin acridane cage)@biPy complex (biPy@43)

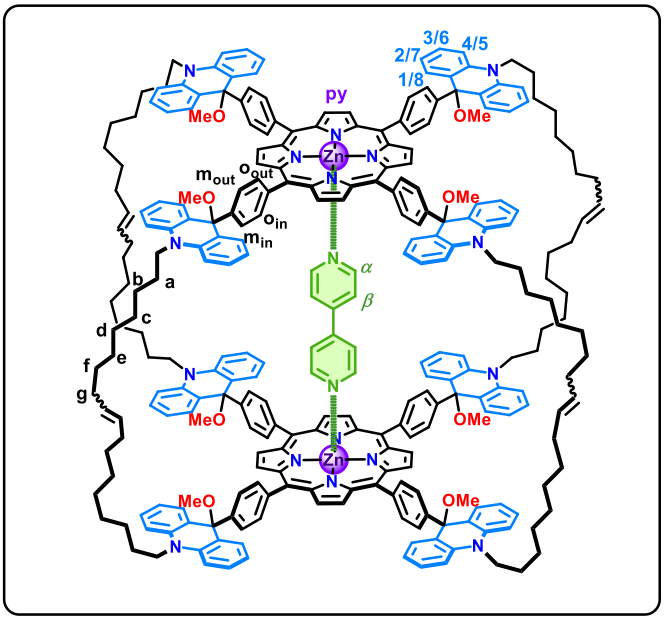

To a solution of **42·8PF$_6$** (2.71 mg, 0.55 μmol) in CD_2Cl_2/CD_3CN 9:1 (0.5 mL) was added biPy (85.9 μg, 0.55 μmol, 1 eq.). The resultant solution was manually stirred then an aliquot of KOH (0.259 mg, 4.62 μmol, 8.4 eq.) in CH_3OH (10 μL) added, and manually stirred once more. The resulting solution was evaporated and triturated with H_2O to remove residual salts, dried under vacuum, then re-dissolved in CD_2Cl_2 (0.55 mL).

^{1}H NMR (500 MHz, CD_2Cl_2, 298 K) δ (ppm) = 8.63 (s, 16H, H_{py}), 8.11 – 7.93 (m, 8H, $H_{o\text{-}out}$), 7.70 – 7.59 (m, 8H, $H_{o\text{-}in}$), 7.50 (d, ^3J = 7.8 Hz, 16H, $H_{1/8}$), 7.43 – 7.31 (m, 16H, $H_{3/6}$), 7.26 – 7.10 (m, 24H, $H_{4/5\&\ m\text{-}out}$), 7.09 – 6.88 (m, 24H, $H_{2/7\ \&\ m\text{-}in}$), 5.49 – 5.38 (m, 8H, *H*C=), 4.16 – 3.92 (m, 16H, NCH_2), 3.00 (s, 24H, OMe), 2.16 – 1.82 (m, 52H,$H_{biPy\text{-}\alpha}$ & (a, b & g)-CH_2), 1.61 – 1.47 (m, 64H, (c-f)-CH_2).

For the UV-Vis titration, two solutions were prepared:

Host Solution: **43** (38.2 μg, 9.51 nmol) in CH_2Cl_2 (20 mL).

Guest Solution: **biPy** (5.94 mg, 38.0 μmol) in CH_2Cl_2 (10 mL).

Small aliquots of the guest solution were added to the host solution (2 mL in a 1 cm cuvette), and UV-Vis spectra recorded after each addition. The absorption values (at wavelength 425 – 435 nm) for each recorded spectrum were compiled in an excel file, corrected for dilution (< 3% dilution of initial concentration at end point of titration) and the data analysed using the BindFit titration program (http://supramolecular.org). Fitting to a 1:1 binding model was observed to be the most accurate, with an averaged value of K_a = 1.0 (± 0.2) × 10^6 L mol^{-1} obtained.

Crystallographic data of **41·4PF$_6$**

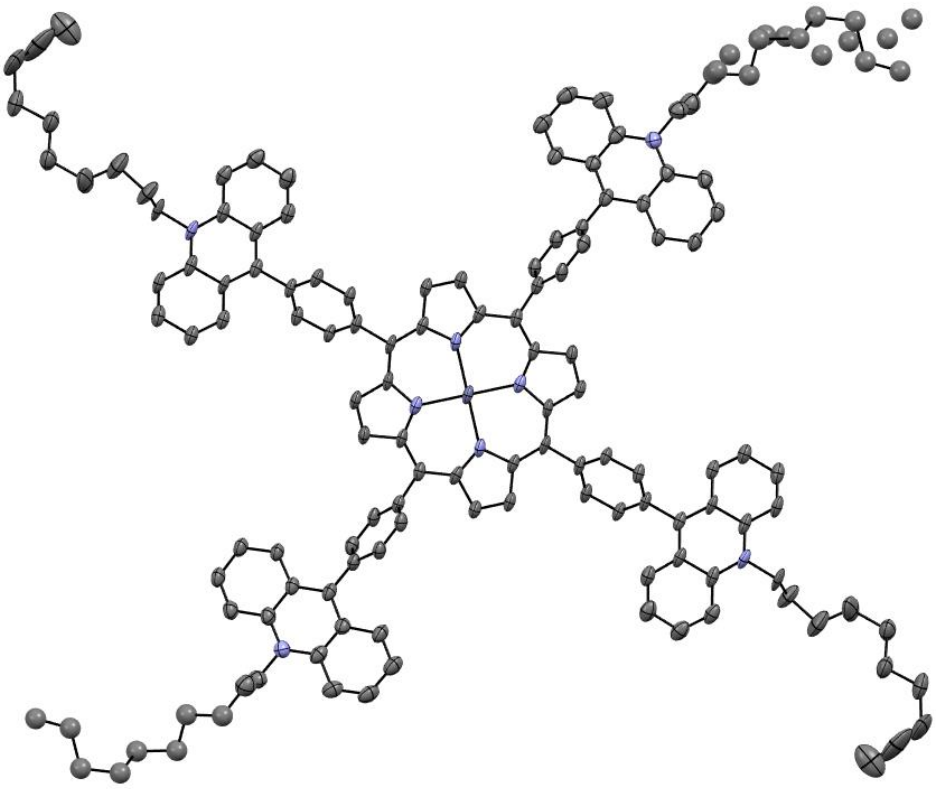

*Structure of **41·4PF$_6$** in ORTEP style. Ellipsoids are drawn at 30% probability. For clarity, hydrogen atoms, solvent molecules and counter anions are omitted. Crystals were prepared via vapour diffusion of Et_2O into a solution of **41·4PF$_6$** in minimal CH_3CN.*

Bond precision	C-C = 0.0114 Å	
Wavelength =	1.54178	
Cell:	a = 10.2918(4) Å	alpha = 92.813(2)°
	b = 17.8609(6) Å	beta = 97.943(2)°
	c = 18.9082(7) Å	gamma = 103.704(2)°
Temperature:	120 K	

	Calculated	Reported
Volume	3332.3(2) Å	3332.3(2) Å
Space group	P $\bar{1}$	P $\bar{1}$
Hall group	-P 1	-P 1
Moiety formula	C136 H132 N8 Zn, 4(F6 P), 3(C2 H3 N) C136 H132 N8 Zn, 4(F6 P), 3(C2 H3 N)	
Sum formula	C142 H141 F24 N11 P4 Zn C142 H141 F24 N11 P4 Zn	
***M*$_r$**	2646.93	2646.90
ρ_{cald} (g cm^{-3})	1.319	1.319
Z	1	1
Mu (mm^{-1})	1.456	1.456
F000	1376.0	1376.0
F000'	1380.09	
h, k, l$_{max}$	12, 21, 22	12, 21, 22
N$_{ref}$	11998	11834
T$_{min}$, T$_{max}$	0.840, 0.865	0.589, 0.753
T$_{min'}$	0.747	
Correction method	T Limits: T$_{min}$=0.589 T$_{max}$=0.753	
AbsCorr	= MULTI-SCAN	
Data completeness =	0.986	
Theta(max)	= 67.455	
R(reflections) =	0.1356(7423)	
wR$_2$(reflections) =	0.4169(11834)	
S =	1.530	
N$_{par}$ =	798	

:

References

(1) Nöll, G.; Daub, J.; Lutz, M.; Rurack, K. Synthesis, Spectroscopic Properties, and Electropolymerization of Azulene Dyads. *J. Org. Chem.* **2011**, *76* (12), 4859–4873.

(2) Umeyama, T.; Hanaoka, T.; Baek, J.; Higashino, T.; Abou-Chahine, F.; Tkachenko, N. V.; Imahori, H. Remarkable Dependence of Exciplex Decay Rate on Through-Space Separation Distance between Porphyrin and Chemically Converted Graphene. *J. Phys. Chem. C* **2016**, *120* (49), 28337–28344.

(3) Gosset, A.; Xu, Z.; Maurel, F.; Chamoreau, L.-M.; Nowak, S.; Vives, G.; Perruchot, C.; Heitz, V.; Jacquot de Rouville, H.-P. A Chemically-Responsive Bis-Acridinium Receptor. *New J. Chem.* **2018**, *42* (6), 4728–4734.

(4) Yi, H.; Niu, L.; Wang, S.; Liu, T.; Singh, A. K.; Lei, A. Visible-Light-Induced Acetalization of Aldehydes with Alcohols. *Org. Lett.* **2017**, *19* (1), 122–125.

(5) Nowak-Król, A.; Plamont, R.; Canard, G.; Edzang, J. A.; Gryko, D. T.; Balaban, T. S. An Efficient Synthesis of Porphyrins with Different Meso Substituents That Avoids Scrambling in Aqueous Media. *Chem. Eur. J.* **2015**, *21* (4), 1488–1498.

(6) Hu, J.; Ward, J. S.; Chaumont, A.; Rissanen, K.; Vincent, J.; Heitz, V.; Jacquot de Rouville, H.-P. A Bis-Acridinium Macrocycle as Multi-Responsive Receptor and Selective Phase-Transfer Agent of Perylene. *Angew. Chem. Int. Ed.* **2020**, *59* (51), 23206–23212.

Résumé de Thèse

Les porphyrines sont des unités de reconnaissance intéressantes en chimie hôte-invité en vertu de leur capacité à former des interactions π-π ou métal-ligand, de leur possible fonctionnalisation en positions β ou méso, de leurs propriétés optiques ainsi que de leur réponse à des stimuli. Ainsi, les unités porphyrines ont été incorporées dans des hôtes supramoléculaires. Le développement de la chimie hôte-invité a conduit à l'élaboration de systèmes ayant des applications dans des domaines liés à la détection, à la catalyse commutable et à la vectorisation de médicaments. Cependant, une méthode de contrôle est nécessaire afin de réaliser des systèmes pour de telles applications. Ceci peut se faire par l'intermédiaire d'un stimulus lumineux, chimique ou rédox.

La lumière est un stimulus non-invasif, rapide offrant une haute-sensitivité (Figure 1). Les caractéristiques de la lumière ont été utilisées par le groupe d'Aida pour contrôler le mouvement d'une pince moléculaire (**2**) incorporant deux unités porphyriniques reliées par un espaceur azobenzène.[1] Dans cet exemple, un ligand ditopique joue le rôle d'invité. Le changement de conformation de l'hôte porphyrinique induit un changement des propriétés chiroptiques de l'invité. Un second exemple reporté par le groupe de Nolte a démontré la possibilité de photo-contrôler l'association entre un invité viologène et un hôte porphyrinique comportant des rotors de type Feringa (**3**).[2]

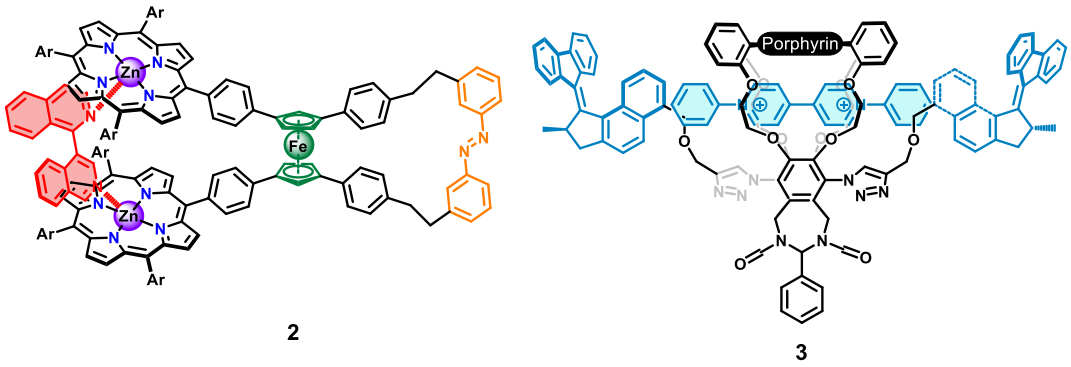

Figure 1. *Structures des deux hôtes photosensibles : du groupe d'Aida (**2**)*[1] *et du groupe de Nolte (**3**).*[2]

De même, un stimulus électrochimique peut être utilisé pour contrôler l'affinité entre un invité et des hôtes porphyriniques (Figure 2). Le groupe de Bucher a montré qu'il était possible d'entraver ou de favoriser l'interaction entre un ligand ditopique (DABCO) et

une pince moléculaire porphyrine fonctionnalisée par des unités viologènes (**4**).[3] A son état natif, le récepteur **3** n'interagit pas avec le DABCO. Une fois les viologènes réduits, la formation d'un π-dimère intramoléculaire permet le rapprochement des porphyrines conduisant à la formation du complexe hôte-invité. Le groupe de Weiss a exploité les propriétés rédox intrinsèques des porphyrines de leur pince moléculaire (**5**) pour moduler la coordination du DABCO (monotopique vs ditopique).[4] De manière analogue le groupe de Lipke a réduit les unités porphyrines de l'hôte (**6**) pour relarguer un invité cationique.[5]

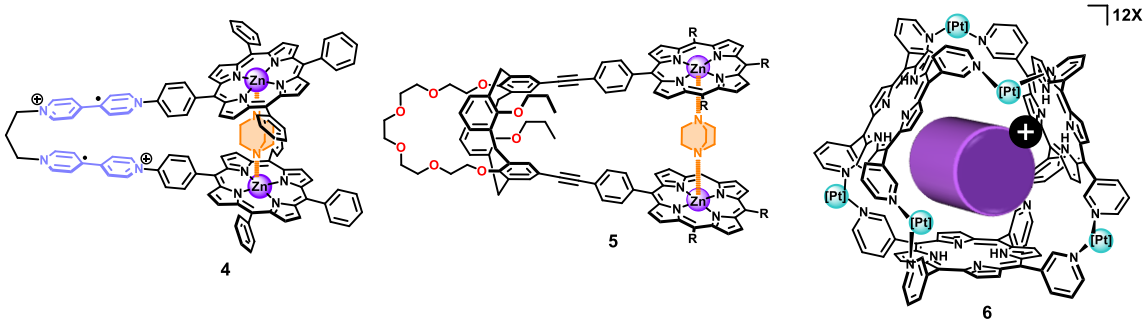

Figure 2. *Structures des hôtes rédox commutables avec leurs invités respectifs : du groupe de Bucher (**4**),[3] du groupe de Weiss (**5**)[4] et du groupe de Lipke (**6**).[5]*

L'utilisation d'un stimulus chimique dans des systèmes hôte-invité peut prendre deux aspects. Le premier aspect concerne la modification chimique de l'hôte comme dans les travaux du groupe de Shionoya (Figure 3). Ils ont utilisé plusieurs stimuli chimiques différents pour changer la conformation et donc les capacités d'interaction de leur hôte porphyrine **7**.[6] Sous sa forme bol (**7-bowl**), le récepteur **7** peut être converti réversiblement en sa forme **7-capsule** par addition d'aryl sulfonamide ou d'adamantane. Pour chacun des invités, l'hôte **7** prend la géométrie la plus adaptée pour maximiser les interactions.

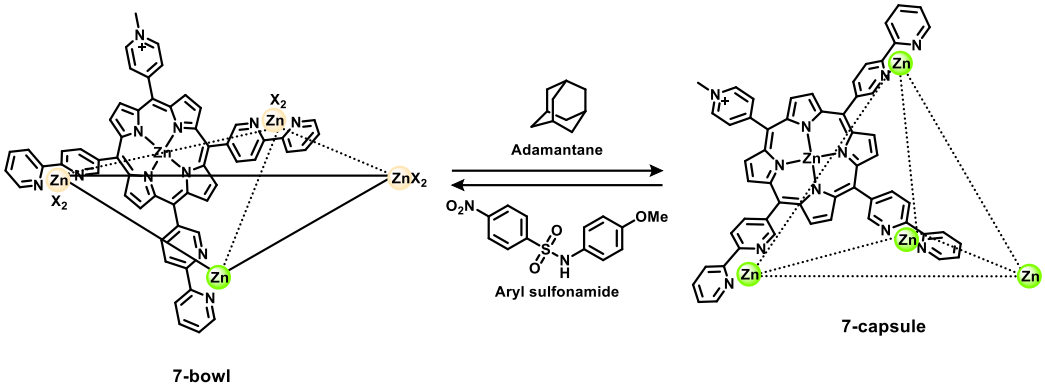

Figure 3. *Structure de l'hôte **7** du groupe Shionoya sous ses deux formes **7**-bowl et **7**-capsule lors de l'addition d'invités.*[6]

La seconde utilisation d'un stimulus chimique peut être observée chez des hôtes multivalents, c'est-à-dire composés de plusieurs sites de reconnaissance. Dans ce cas, une coopérativité entre les sites d'interaction est nécessaire selon un mécanisme de contrôle allostérique. Il s'agit d'un processus de contrôle commun observé dans la nature (plus particulièrement dans l'action des enzymes et des protéines). Il est décrit par les changements conformationnels et/ou électroniques d'une macromolécule par une première molécule invitée effectrice. Ce changement a un impact sur l'activité biologique par modification des interactions de la macromolécule avec un ou plusieurs invités secondaires sur un site séparé et distinct. Lorsque l'interaction avec l'invité secondaire est inhibée en raison de la liaison de l'effecteur, le contrôle allostérique est dit négatif. Inversement lorsque l'invité voit son affinité pour la macromolécule augmentée, l'allostérie est qualifiée de positive. De plus, le processus de régulation allostérique est hétérotrope quand l'effecteur et l'invité ne sont pas la même espèce chimique ou homotrope quand l'effecteur et l'invité sont la même espèce.

Des exemples de systèmes allostériques synthétiques ont été décrits à la fin des années 1970 par le groupe de J. Rebek Jr. et ses collègues.[7] Depuis, des récepteurs allostériques artificiels ont été synthétisés et exploitent différents motifs de reconnaissance afin d'interagir avec un large éventail d'invités. En raison de leur robustesse, les porphyrines ont été bien utilisées en association à différents motifs de reconnaissance orthogonaux. Ces systèmes ont été exploités pour créer des effets allostériques de grande amplitude (Figure 4). Par exemple, une forte augmentation de l'affinité d'un hôte porphyrine **10**

pour un invité tritopique a été observée par Shinkai et son groupe. Lors de l'interaction d'ions Na^+ avec les calixarènes du récepteur **9**, l'association avec le ligand tritopique a été augmentée de trois ordres de grandeur.[8] De manière analogue, la cage auto-assemblée **10** du groupe Ballester[9] n'est capable de se former et d'encapsuler un invité polyaromatique qu'après coordination de trois ligand DABCO.

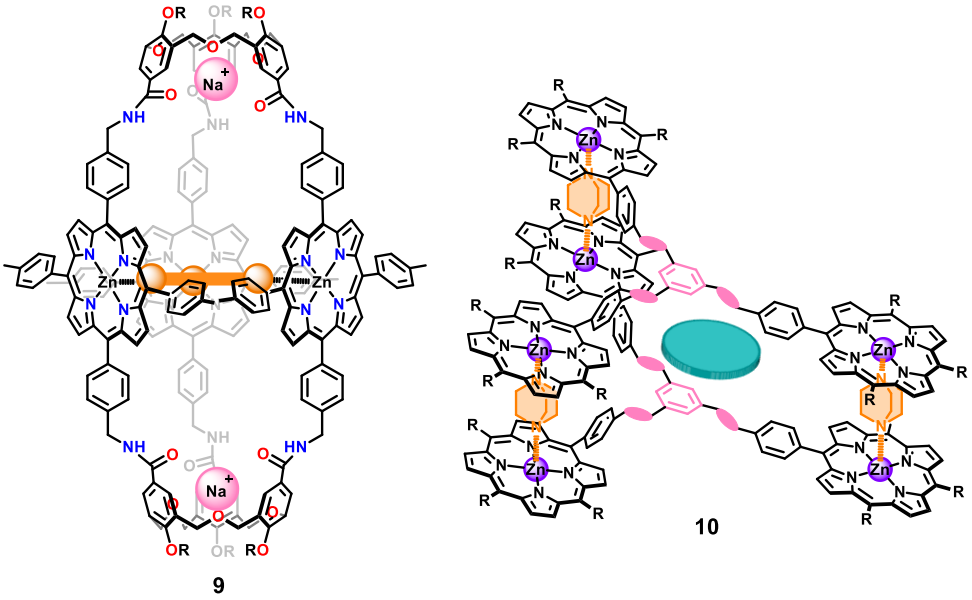

Figure 4. *Représentation des structures hôte-invité formées par les deux récepteurs du groupe Shinkai (**9**)*[8] *et Ballester (**10**).*[9]

La conception de systèmes synthétiques présentant une régulation allostérique à voies multiples est un défi. Ceci est représenté par les travaux du groupe Jang avec leurs récepteurs porphyrinique pontés (**11** et **12**) par des espaceurs biindole (Figure 5).[10,11] En effet, la complexation des ions chlorures au sein de l'espaceur modifie la constante d'association entre les unités porphyrines et du DABCO et inversement. Ce type de régulation allostérique est couramment observée dans la nature comme dans le cas de l'hémoglobine.

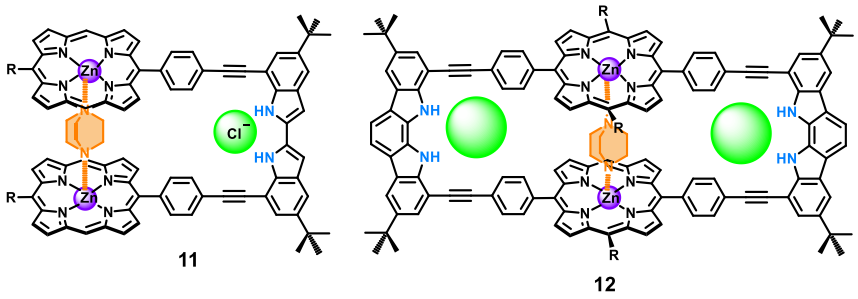

*Figure 5. Représentations des structures hôte-invité formées par les deux récepteurs biindole-porphyrine (**11**) et (**12**) du groupe Jang.* [10,11]

Des exemples d'hôtes synthétiques affichant une translation multidirectionnelle des événements de liaison ont été réalisés par le groupe de Shinkai (**13**).[12,13] Leur récepteur est composé de complexes de type double-decker de Ce(IV) fonctionnalisé par des unités pyridyles. L'interaction d'un premier ligand dicarboxylate avec deux des unités pyridines rigidifie la structure de la molécule augmentant ainsi l'interaction avec d'autres ligands dicarboxylates. Notre propre groupe de recherche a également décrit une cage covalente à base de porphyrine (**15**) possédant des triazoles intégrés dans les espaceurs. L'espace de la cavité de ce récepteur s'ouvre après coordination d'ions Ag^+ jouant le rôle d'effecteur ce qui permet la coordination du ligand pyrazine entre les porphyrines.[14,15]

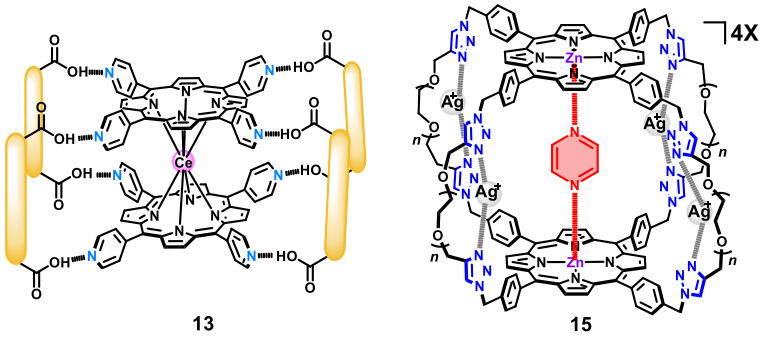

*Figure 6. Structures des hôtes allostériques multidirectionnels, les doubles étages de porphyrine de Ce(IV) (**13**) du groupe*[12,13] *Shinkai et la cage de porphyrine du groupe Heitz (**15**).*[14,15]

Les travaux du groupe de Mirkin ont mis en évidence l'action du récepteur **16** à base de porphyrines macrocycliques dans un contrôle allostérique en catalyse (Figure 7).[16] Les centres métalliques Rh périphériques interagissent avec des ions chlorures ce qui ouvre la cavité du récepteur permettant ainsi la catalyse. De plus, le groupe de Schmittel a

exploité à la fois le contrôle allostérique et la capacité de photosensibilisation des unités de porphyrine pour fournir un photocatalyseur allostérique **18**.[17]

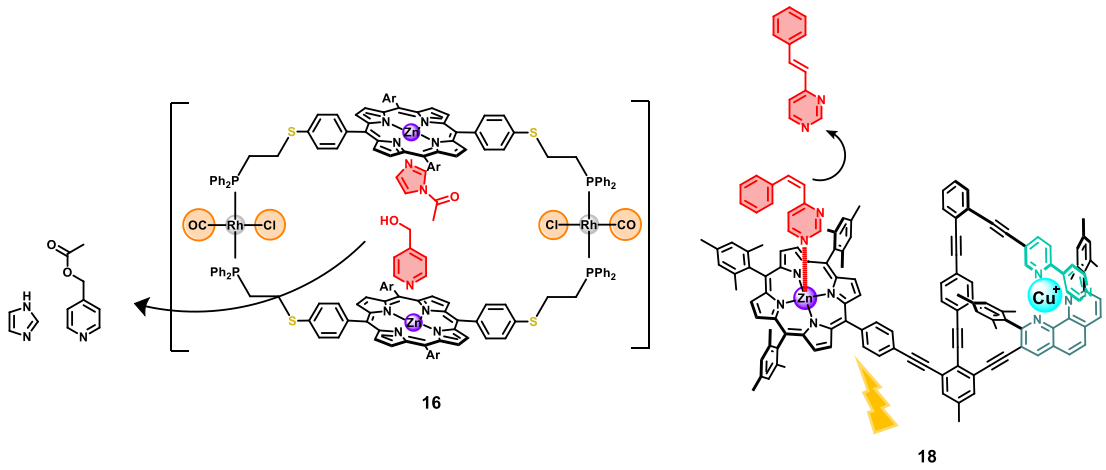

Figure 7. *Représentations de la réponse aux stimuli des récepteurs allostériques catalytiques du macrocycle **16** du groupe Mirkin[16] et **18** du groupe Schmittel[17]sous leurs formes activées.*

Le développement de systèmes présentant plusieurs moyens de contrôle (multi-réponse, c'est-à-dire sensibles à plusieurs stimuli sensibles) reste un défi et élargit les domaines d'applications possibles. A cette fin, la combinaison de motifs porphyrines et acridiniums ouvre le champ des possibles. Les noyaux acridiniums sont connus pour avoir une nature multi-réponse (commutation chimiochromique, photochromique et rédox) et peuvent interagir avec des invités riches en électrons par interactions π-donor/π-acceptor. En effet, les travaux pionniers du groupe Lehn (**19**) ont montré que des récepteurs acridinium pouvaient encapsuler des invités polyaromatiques riches via des interactions π-donor/π-acceptor (Figure 8).[18,19] Les propriétés de reconnaissance et la nature commutable du noyau acridinium ont été utilisées par le groupe de Yoshizawa (**20**) et par notre groupe de recherche (**21**) pour permettre une capture et un relargage de substrats aromatiques.[19,20]

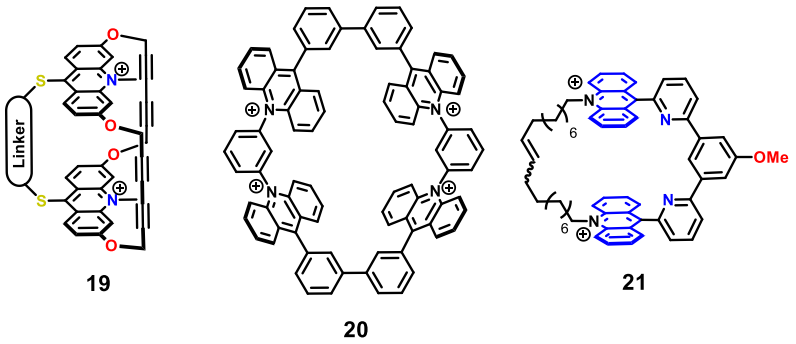

Figure 8. *Structures des récepteurs macrocycliques acridinium du groupe de Lehn (**19**),* [18] *du groupe de Yoshizawa (**20**)* [20] *et de notre groupe de recherche (**21**).* [19]

L'utilisation d'unités porphyrines avec des fragments acridinium dans des systèmes hôte-invité a été limitée à l'encapsulation d'acridines protonées (**AcrH**) dans des récepteurs porphyrines, tels que ceux du groupe de Fukuzumi (**22**) et de Rath & Chaudhary (**23**) (Figure 9).[21,22] Cependant, les unités de reconnaissance acridinium et porphyrine n'ont pas été utilisées en tant qu'unités de reconnaissance orthogonales en chimie supramoléculaire. Ceci implique un attachement covalent de ces deux fragments. Cette fonctionnalisation se limite aux travaux du groupe de Fukuzumi sur une triade composée d'un conjugué acridinium-porphyrine (**24**) mais ce système n'a été utilisé que comme détecteur de fluorescence du superoxyde et non pour la reconnaissance supramoléculaire.[23]

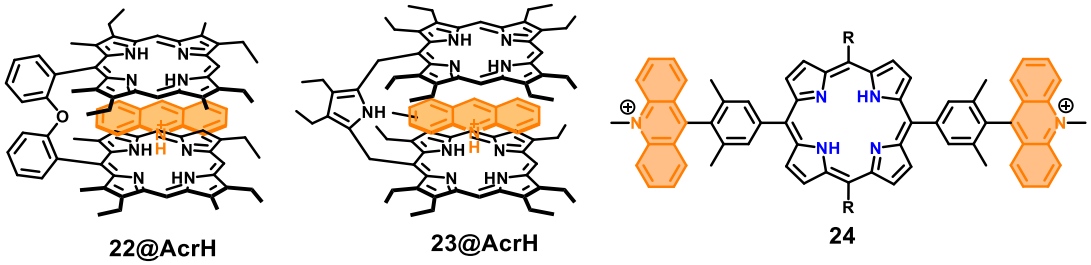

Figure 9. *Structures des systèmes porphyrine/acridinium publiés.* [21–23]

Ce projet porte sur la conception, la synthèse et l'étude de nanorécepteurs porphyrine-acridinium répondant à différents stimuli. En effet, les métalloporphyrines peuvent former des liaisons de coordination de type métal-ligand pour la reconnaissance de ligand ditopique et les acridiniums peuvent former des interactions π-donneur/π-accepteur pour la reconnaissance de polyaromatique. De manière interessante, la distance entre les deux noyaux porphyriniques après coordination à du DABCO

correspondant à la distance optimum pour des interactions π, c'est-à-dire 7 Å (Figure 10). Afin de sonder la faisabilité de ce projet, nous avons d'abord cherché à synthétiser de nouveaux conjugués porphyrine-acridinium en un nombre limité d'étapes avec des rendements relativement élevés.

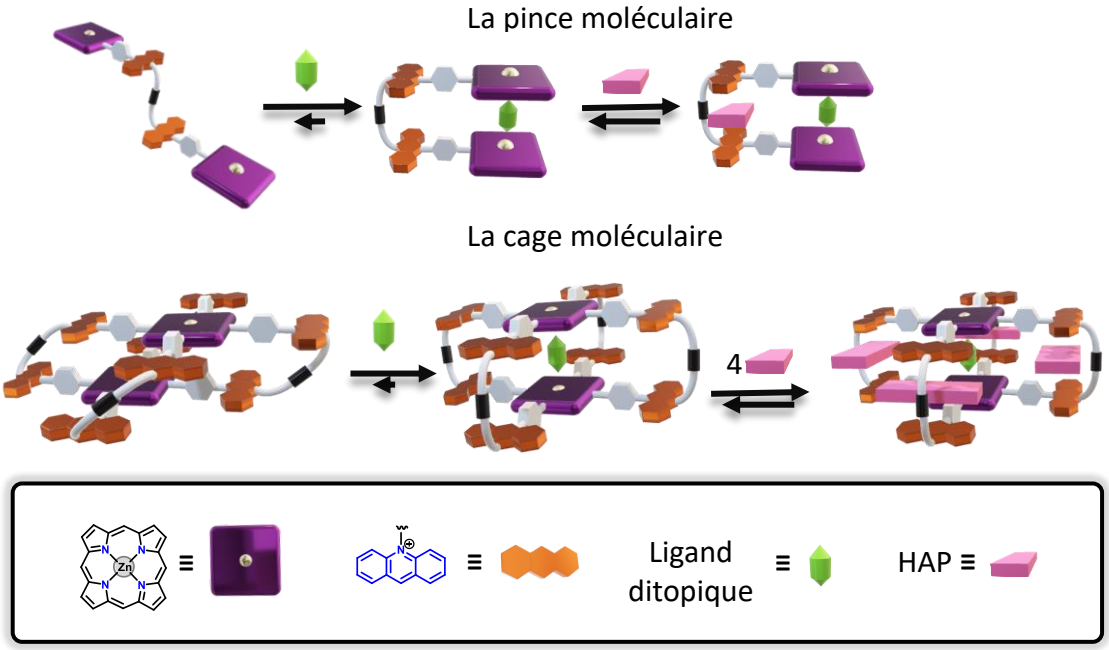

Figure 10. *Illustration 3D du mécanisme par lequel un contrôle allostérique positif de la liaison de l'invité polyaromatique est assuré.*

Trois voies de synthèse ont été identifiées pour la synthèse des conjugués acridinium-porphyrines. Basé sur les travaux du groupe d'Hirel, la première voie de synthèse implique l'attachement par réaction d'une espèce de porphyrine aryle lithiée (formée à partir de la porphyrine bromée correspondante **26-2H/26-Zn**) avec une acridone N-méthylée (**27**, Figure 11). Cependant, les tentatives par cette voie se sont avérées infructueuses car les réactifs ont été récupérés suggérant que l'espèce lithiée n'a pas été formée.

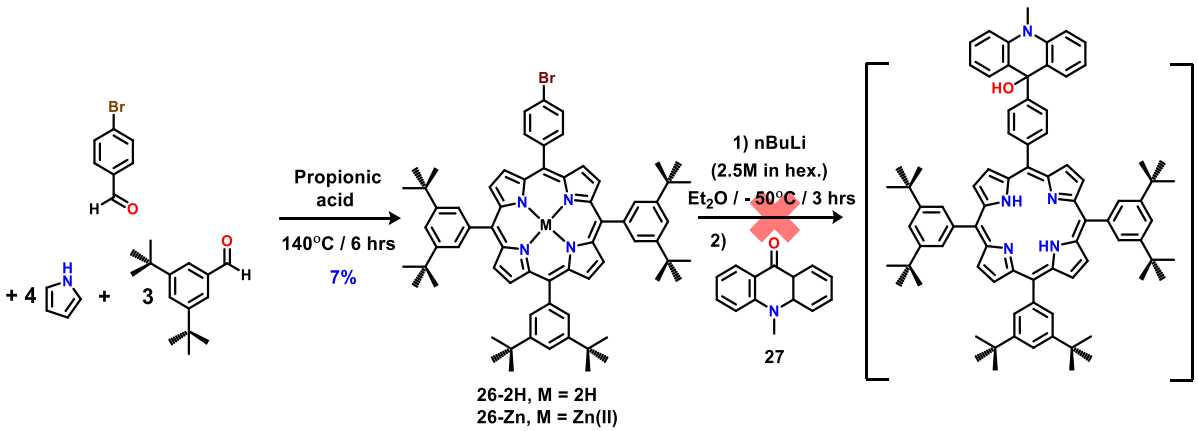

Figure 11. *Schéma réactionnel proposé pour la première voie explorée dans la synthèse de conjugués de porphyrine et d'acridinium.*

La deuxième voie explorée vise à synthétiser des conjugués acridinium-porphyrine via un couplage au palladium (Figure 12). Cette stratégie implique la formation d'un hydroacridane fonctionnalisé par un ester boronique (**29**) par des raisons de purification. Cette espèce a été mise en réaction avec la porphyrine **26-Zn** pour former un intermédiaire acridane-porphyrine qui a ensuite été oxydé pour former l'espèce acridinium-porphyrine (**30·PF$_6$**). Le rendement final de cette réaction est de 67%. Cependant, cette voie de synthèse n'a pas été retenue en raison de l'instabilité des intermédiaires acridanes qui se réoxydent sous air ainsi que de la formation d'un espaceur biphényle qui est moins rigide que l'espaceur phénylène envisagé originalement.

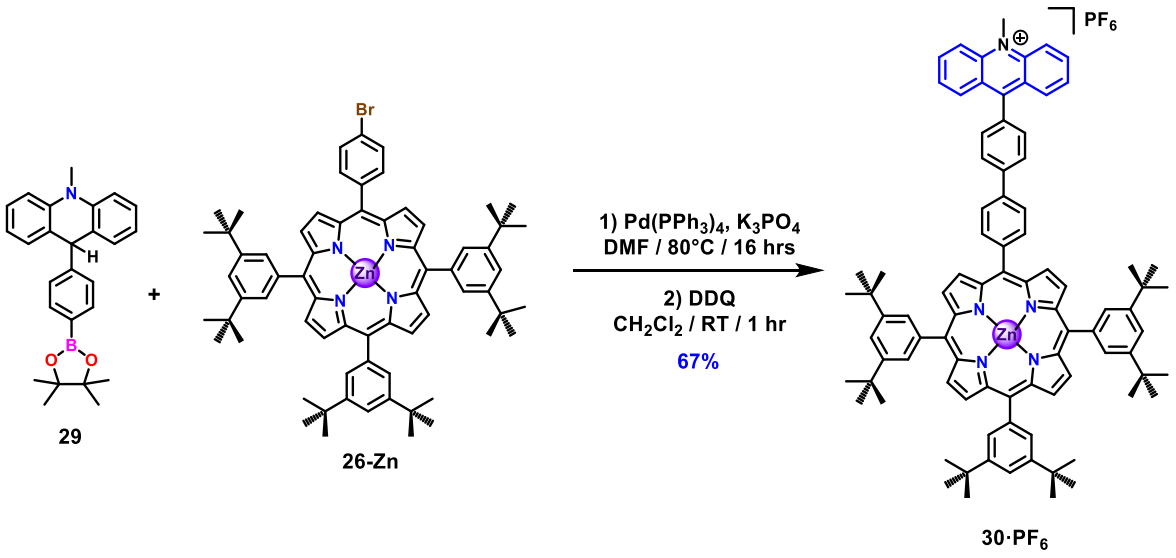

Figure 12. *Synthèse de **30·PF $_6$** via un couplage catalysé au palladium en utilisant l'ester boronique d'acridane **29** et la bromo-aryl porphyrine-Zn(II) **26-Zn**.*

Enfin, nous nous sommes tournés vers une troisième voie de synthèse (Figure 13). Elle fait intervenir un acridinium fonctionnalisé par un formyle (**32·PF$_6$**). Cet intermédiaire de synthèse est stable à l'air. Ce réactif clé est synthétisé via un échange métal-halogène en utilisant des synthons bon marché et disponibles dans le commerce. La réaction du 4-bromobenzaldéhyde en présence de BuLi sur l'acridone **31** permet la formation de l'acridinium **32·PF$_6$**. Ce composé peut être ainsi obtenu à l'échelle du gramme avec un rendement de 78%.

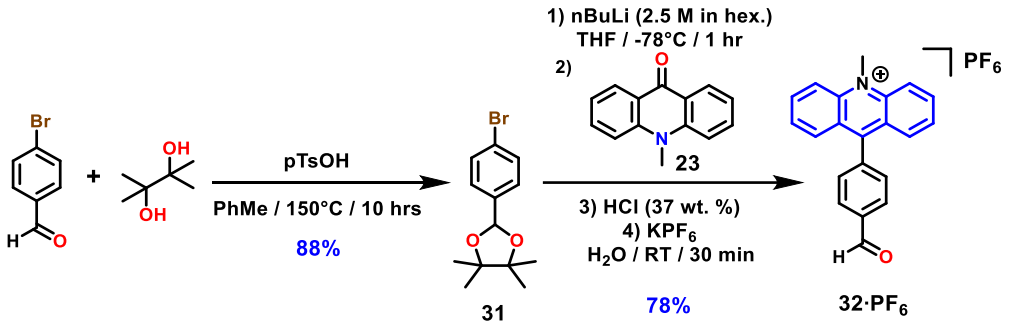

Figure 13. *Synthèse du formyle phényl acridinium (**32·PF$_6$**) par réaction d'un échange bromo lithium d'un bromo benzaldéhyde protégé (**31**).*

Ce nouveau réactif a d'abord été utilisé pour synthétiser une porphyrine AB$_3$ dans des conditions de Lindsey (Figure 14). La réaction entre le pyrrole, le 3,5-di-tert-butyl-benzaldéhyde et l'acridinium **32·PF$_6$** en conditions acides, suivi d'une oxydation DDQ et d'une métallation avec Zn^{2+} a permis d'obtenir le conjugué **33·PF$_6$** avec un rendement de 12%.

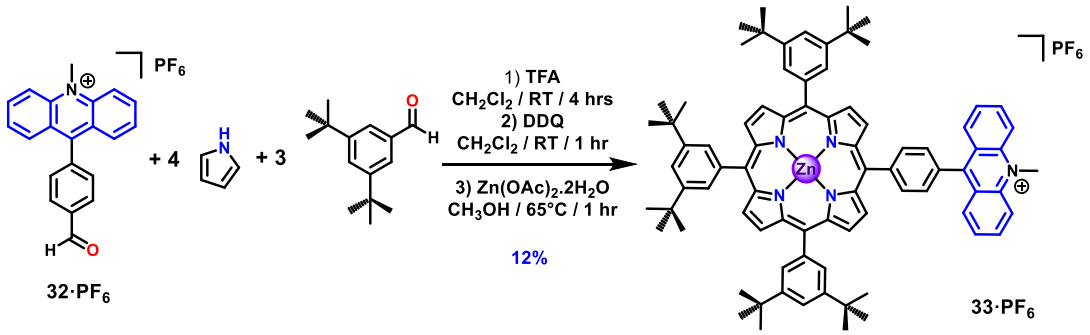

Figure 14. *Synthèse du conjugué monoacridinium porphyrine (**33·PF$_6$**), par condensation de porphyrine à partir de **32·PF$_6$**.*

La flexibilité de cette voie de synthèse permet la synthèse directe d'un certain nombre de conjugués différents. Ainsi en faisant réagir l'acridinium **32·PF$_6$** avec du 2,2'-

dipyrrométhane (dans des conditions de Lindsey), la synthèse d'une porphyrine de bisacridinium **35·2PF$_6$** a été réalisée avec un rendement de 29% (Figure 15).

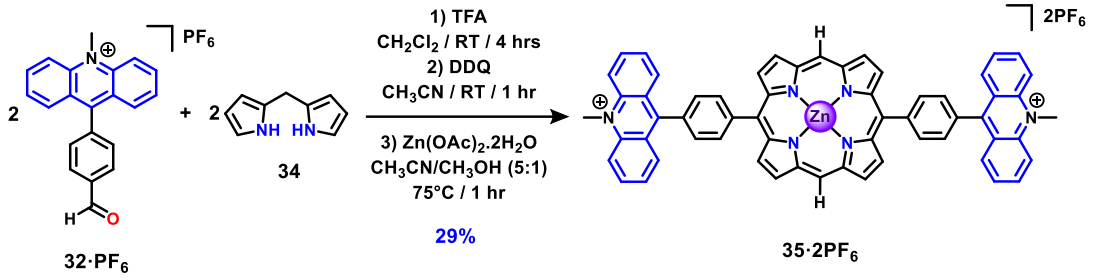

Figure 15. *Synthèse du conjugué bisacridinium porphyrine **35·2PF$_6$** par condensation de porphyrine à partir de **32·PF$_6$** et de 2,2'-dipyrrométhane.*

Ainsi, la synthèse par condensation de porphyrine est la voie la plus efficace pour former des conjugués acridinium-porphyrine. Cette voie de synthèse permet l'utilisation de réactifs stables et permet de modifier facilement les conditions de réaction pour l'obtention de différentes structures (A_3B, A_2B_2, A_4 par exemple).

Afin de sonder les propriétés de ces conjugués, des études ont été menées en collaboration avec le Dr Barbara Ventura et Daniel Sánchez-Resa à l'ISOF-Bologne (études photophysiques) et le Dr Christophe Gourlaouen (études computationnelles) sur le composé **35·2PF$_6$**. Les résultats de cette étude ont été récemment publiés.[24] Pour ce composé, les deux orbitales moléculaires vacantes les plus basses en énergie (LUMO) sont dégénérées et localisées sur les unités acridiniums tandis que les deux orbitales moléculaires occupées les plus hautes en énergie (HOMO) sont dégénérées et localisées sur la porphyrine. Dans l'étude électrochimique du conjugué **35·2PF$_6$**, il a été constaté que l'espèce se comportait d'une manière quelque peu différente de ce qui est couramment observé pour une espèce de porphyrine. Bien qu'une réduction réversible des deux unités d'acridinium soit observée au même potentiel, l'unité de porphyrine est oxydée à deux électrons de manière irréversible. En utilisant les données, un écart HOMO-LUMO de 1,4 eV a été calculé. Les propriétés photophysiques du conjugué **35·2PF$_6$** ont également été sondées, avec une extinction quasi quantitative de la fluorescence des unités porphyrine et acridinium. En utilisant la spectroscopie d'absorption transitoire, le piégeage de luminescence s'est avérée être due à un transfert d'électron photo-induit.

Enfin, le conjugué **35·2PF$_6$** a été évalué comme composé modèle dans un contrôle allostérique positif impliquant la coordination du DABCO, jouant le rôle d'effecteur, et pour l'interaction de molécules invitées polyaromatiques jouant le rôle d'invités secondaires. Suivi par spectroscopie RMN ^{1}H, il a été montré que le conjugué forme un complexe sandwich en présence de DABCO (0,5 éq.) (**DABCO@(35·2PF$_6$)**) et ce complexe a montré des interactions avec le pyrène (Figure 16). En l'absence de DABCO, le conjugué **35·2PF$_6$** isolé n'interagit pas avec le pyrène confirmant ainsi notre hypothèse selon laquelle le DABCO est nécessaire pour pré-organiser les noyaux acridiniums et ainsi complexer le pyrène.

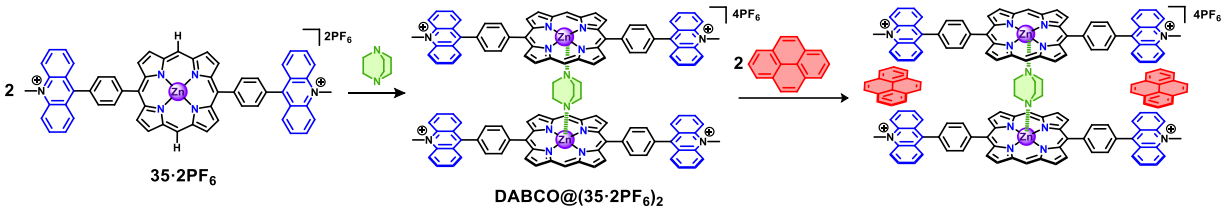

Figure 16. *Complexes formés lors de l'addition de DABCO (0,5 équivalent), suivi de pyrène (1 équivalent) à une solution de* ***35·2PF$_6$*** *dans CD_3CN.*

Nous nous sommes ensuite intéressés à la synthèse de récepteurs moléculaires. En raison de sa simplicité par rapport aux autres architectures de récepteurs (macrocycle, cryptand, cage), une pince moléculaire (**39·PF$_6$**) a d'abord été envisagée. En utilisant la même procédure générale que celle suivie pour **33·PF$_6$** et **35·2PF$_6$**, un formyl phényl acridinium fonctionnalisé par une chaîne N-décényle (**37·PF$_6$**) a été utilisé pour le conjugué mono(N -décényl)acridinium porphyrine **38·PF$_6$** dans des conditions de Lindsey. Le composé **38·PF$_6$** a ensuite été utilisé pour synthétiser la pince moléculaire **39·2PF$_6$** par métathèse d'oléfine avec un rendement de 77% après purification (Figure 17).

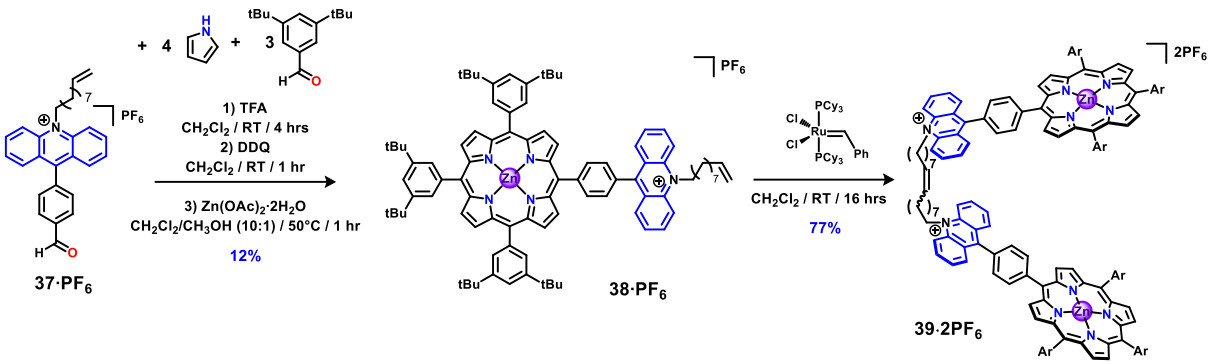

Figure 17. *Synthèse de la pince moléculaire* ***39·2PF₆*** *à partir du synthon acridinium benzaldéhyde* ***37·PF₆****.*

La coordination du composé **39·2PF₆** par des ligands ditopiques (DABCO et la 4,4'-bipyridine (**biPy**)) a ensuite été étudiée. La formation des complexes 1:1 correspondant a été observé par spectroscopie RMN 1D et 2D (Figure 18). Les dosages UV/Vis ont permis la détermiantion des constantes de liaison de 2,0 (± 0,3) × 10^6 M^{-1} et 1,8 (± 0,1) × 10^5 M^{-1} dans CH_2Cl_2 pour les complexes macrocycliques **DABCO@39·2PF₆** et **biPy@39·2PF₆**. Ces valeurs représentent une augmentation de l'affinité d'un facteur 20 et 47 fois supérieures par rapport aux valeurs obtenues avec le modèle analogue **33·PF₆**.

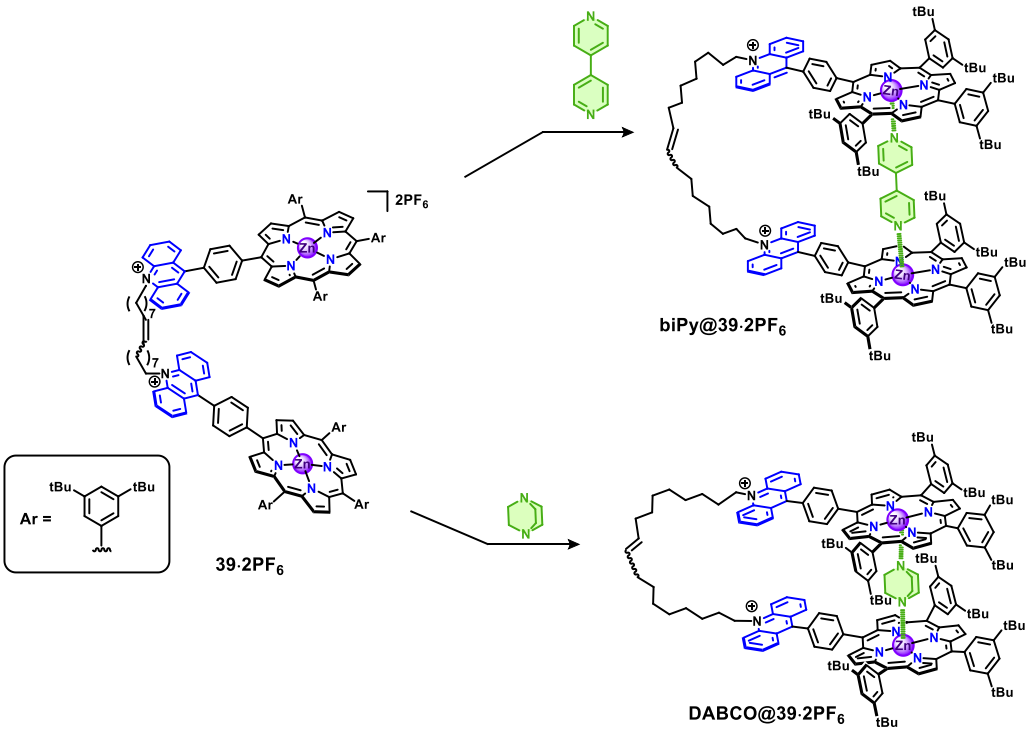

Figure 18. *Complexes formés entre la pince* ***39·2PF₆*** *en présence d'un équivalent de DABCO (****DABCO@39·2PF₆****) ou biPy (****biPy@39·2PF₆****).*

Le complexe **DABCO@39·2PF$_6$** a été évalué pour la complexation de molécules poly-aromatiques (le pyrène et le pérylène). Peu de changements dans les spectres RMN ^{1}H ont été observés suggérant qu'il n'y a pas d'interactions fortes entre le site d'acridinium et le pyrène. Cette observation a été rationalisée par l'existence d'une gêne stérique en les groupements di-tert-butyles. Cette interaction stérique empêche le récepteur d'adopter une conformation éclipsée mais favorise une conformation décalée. En conséquence, les unités acridiniums ne peuvent complexer les invités (Figure 19) comme démontré par des études de dynamiques moléculaires (Dr Dylan Serillon et Prof. Xavier Barril).

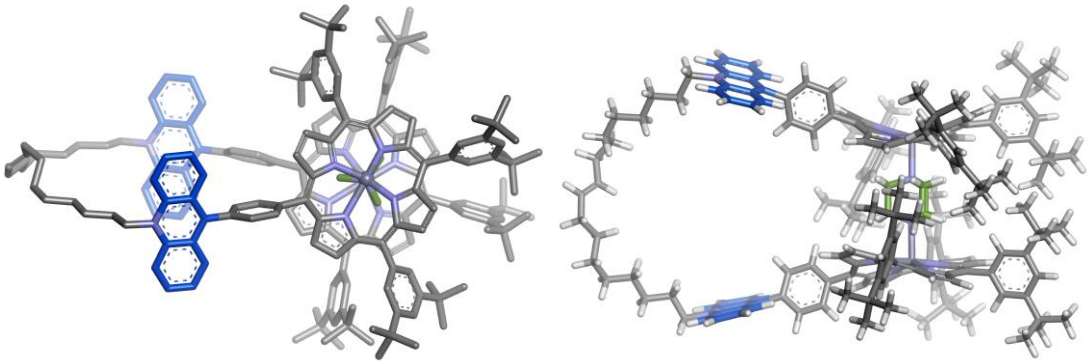

*Figure 19. Structure du complexe **DABCO@39·2PF$_6$** montrant le décalage des deux faces du récepteur.*

Afin de minimiser les gênes stériques, la bipy a été envisagée pour jouer le rôle d'effecteur. Dans ce cas, des aromatiques plus grands tels que le ferrocène ou deux molécules polyaromatiques planes jouerait le rôle d'invités (Figure 20). Aucune association n'a été observée entre le complexe **biPy@39·2PF$_6$** et le ferrocène. Cependant, l'ajout de quantités croissantes de pyrène (jusqu'à 360 équivalents) a conduit des modifications significatives dans le spectre RMN ^{1}H du complexe. Une constante d'association (K_{12}) a été estimée à 25 M^{-2} selon un modèle 1:2 avec une association spontanée (K_{11} supposée 0).

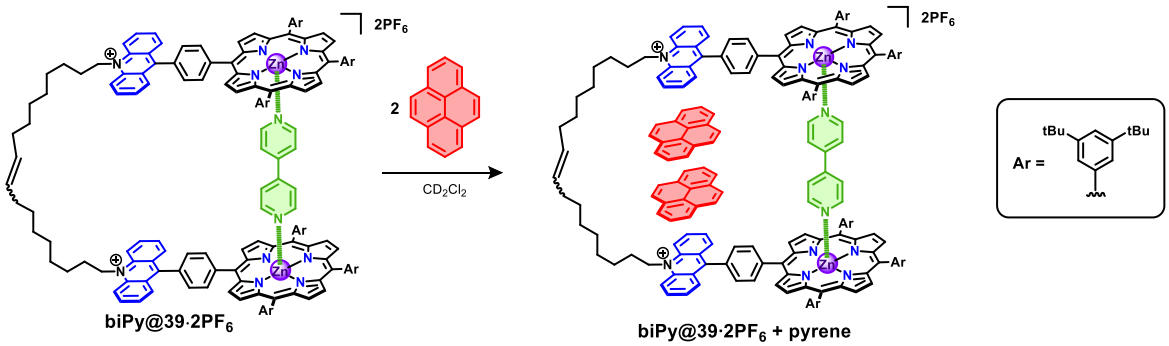

Figure 20. *Complexes formés par* ***39·2PF 6*** *dans CD_2Cl_2 lors de l'ajout de biPy (**biPy@39·2PF6**) et celui attendu suite à l'ajout de deux équivalents de pyrène (**biPy@39·2PF 6 + pyrène**).*

Les effets de stimuli chimiques ont également été exploités. L'ajout de TBAOH a conduit à la désaromatisation des unités acridiniums formant l'espèce neutre acridanol-porphyrine **40** (Figure 21). Ce processus a été suivi par spectroscopies RMN (^{1}H, ^{13}C), UV/Vis, de fluorescence. La forme de la pince moléculaire permet de complexer la bipy et les dosages suivi par spectroscopie UV/Vis ont montré une constante d'association de 1,4 (± 0,3) × 10^5 M^{-1} pour la formation du complexe 1:1 **biPy@39·2PF$_6$**.

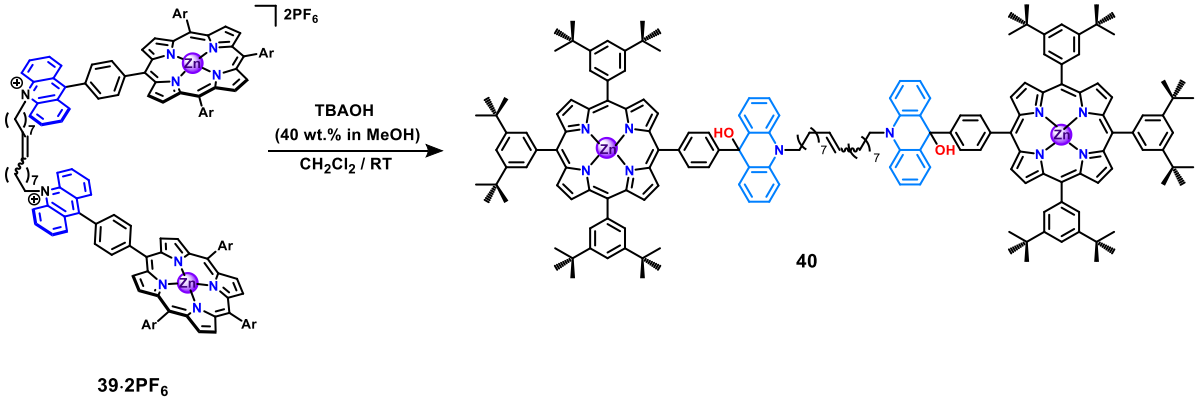

Figure 21. *Structure chimique de la pince moléculaire acridanol-porphyrine* ***40****.*

En plus du stimulus chimique, le stimulus électrochimique a été utilisé pour moduler la constante d'association entre les récepteurs **39·2PF$_6$** et **40**. Par exemple, la formation du complexe **biPy@39·2PF$_6$** s'oxyde plus facilement que le récepteur isolé **39·2PF 6** ($\Delta E_{1/2}$ = –57 mV). Une constante d'association de 2,1 × 10^3 M^{-1} a été estimée entre le récepteur oxydé et la bipy (diminuée d'un facteur 90 par rapport à la forme non oxydée). Dans le cas de la pince acridanol **40**, une constante d'association 4 fois plus petite a été trouvée pour sa forme oxydée (K_a = 3,1 × 10^4 M^{-1} correspondant à une variation de

potentiel ($\Delta E_{1/2}$) de −19 mV). L'ensemble de ces études a conduit à la caractérisation de huit états pour ce récepteur qui peuvent être représentés sous la forme d'un schéma cubique (Figure 22).

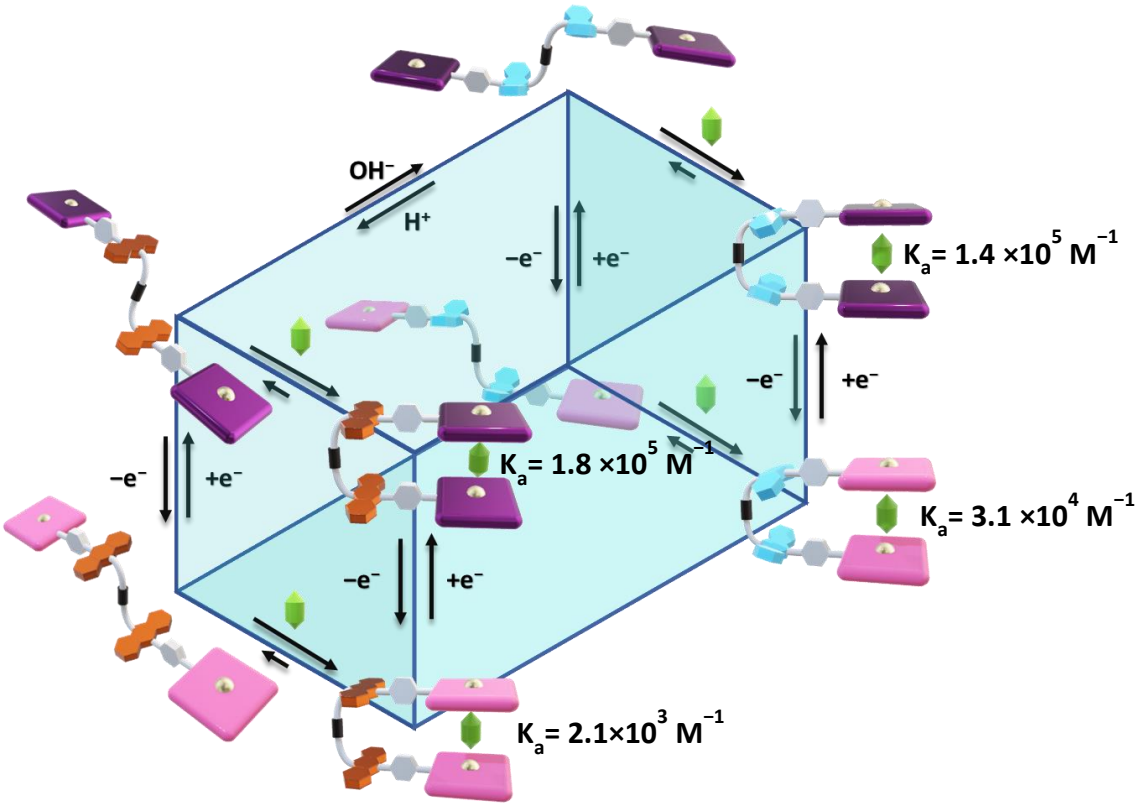

Figure 22. *Schéma cubique représentant les huit états de la pince moléculaire.*

Nous nous sommes ensuite intéressés à la synthèse d'une cage porphyrine-acridinium. Elle comporte huit sites de reconnaissance acridinium reliés entre eux par quatre espaceurs. Comme précédemment le composé **37·PF$_6$** a été utilisé dans des conditions de Lindsey afin de former la porphyrine A$_4$ **41·4PF$_6$** (Figure 23). La structure aux rayons X de ce composé a montré une coplanarité générale entre les unités acridiniums et les unités porphyrines. Les phényles pontant présentent quant à eux un angle moyen de 60° par rapport à ces unités. La superstructure est stabilisée par des interactions π-π entre la porphyrine d'une molécule **41·4PF$_6$** et un acridinium d'une autre molécule **41·4PF$_6$** adjacentes (distance de 3,5 Å).

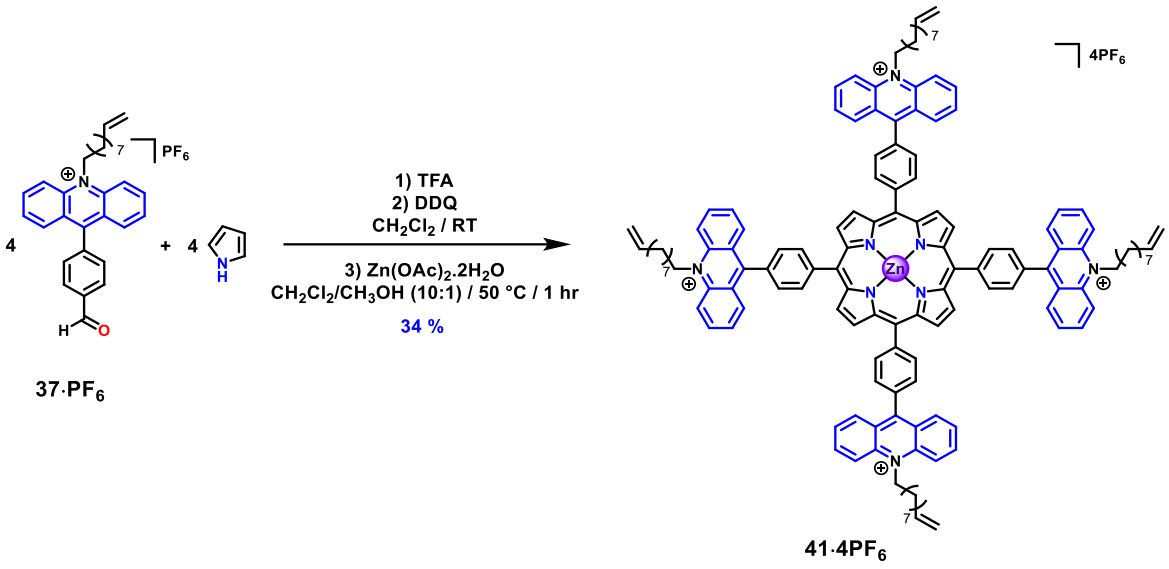

Figure 23. *Synthèse du précurseur de cage* ***41.4PF$_6$.***

Afin d'obtenir des rendements appréciables de la cage, un template a été utilisé afin de préorganiser deux molécules **41·4PF$_6$** en une structure en sandwich pour l'étape de macrocyclisation. En conséquence, une métathèse d'oléfine intramoléculaire serait favorisée par rapport à une métathèse intermoléculaire et la formation d'oligomères serait ainsi minimisée. L'efficacité des ligands ditopiques DABCO et biPy pour jouer le rôle de template ont été évaluées.

Bien que le composé **41·4PF$_6$** soit soluble dans le CH_2Cl_2, il a été constaté que des agrégats insolubles se formaient en présence de DABCO (0,5 équivalent). En revanche, l'ajout de bipy (0,5 équivalent) ne conduit à aucun précipité. Le spectre RMN ^{1}H de la solution a montré des décalages significatifs des pics pyrroliques de la porphyrine, ainsi que des pics larges qui pourraient être associés au biPy complexé ditopiquement. Ces observations indiquent la formation du complexe sandwich **biPy@(41·4PF$_6$)$_2$** (Figure 24). A partir du complexe **biPy@(41·4PF$_6$)$_2$**, la synthèse de la cage **42.8PF$_6$** a été réalisée **avec un** rendement de 49% (Figure 24).

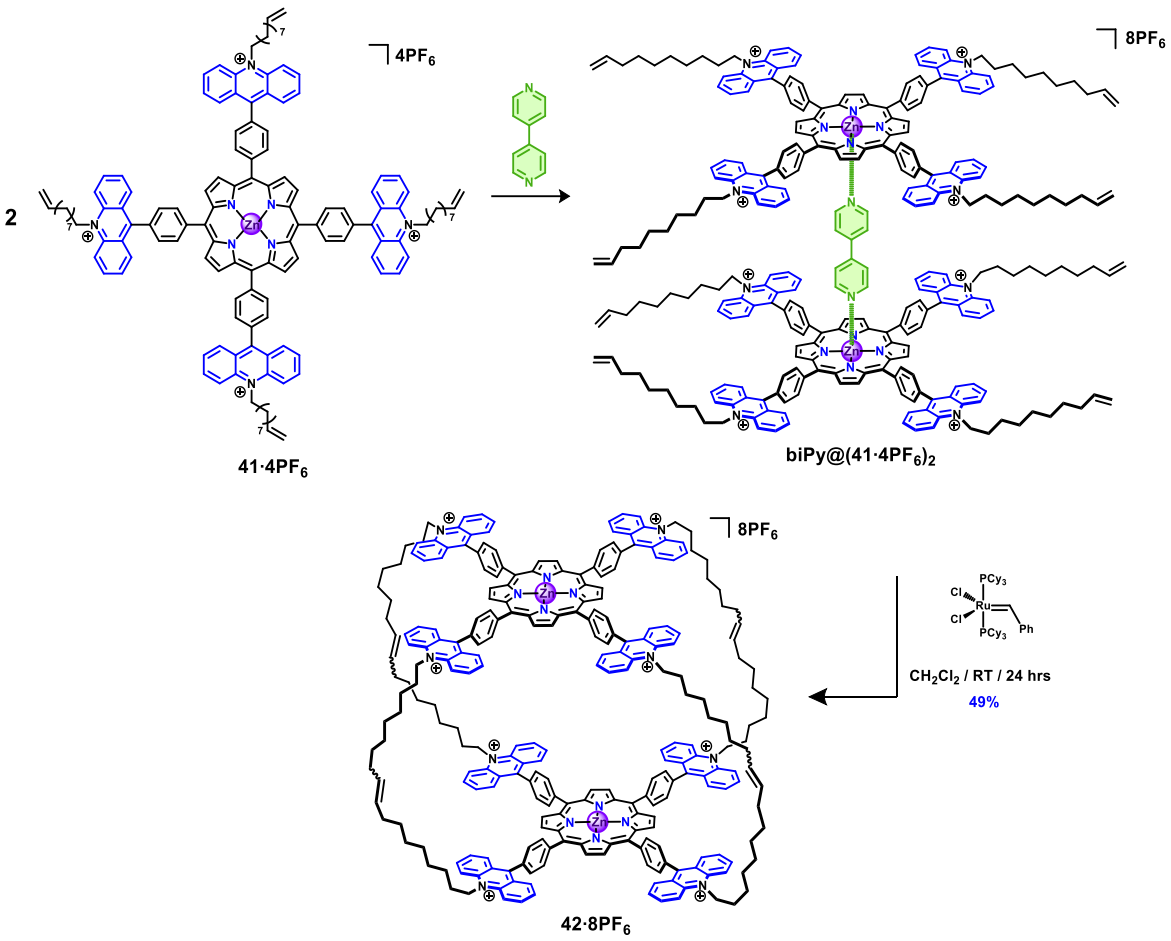

Figure 24. *Synthèse du récepteur cage* ***42·8PF₆*** *à partir du complexe* ***biPy@(41·4PF₆)₂*** *par métathèse d'oléfine.*

La cage **42·8PF₆** a montré une solubilité significativement réduite dans le CH_2Cl_2 par rapport à son précurseur. Les spectres RMN ^1H dans ce solvant sont larges et mal résolus.

La comparaison des spectres UV/Vis de la cage avec **41·4PF₆** dans le CH_2Cl_2 a révélé des déplacements bathochromes et hypochromes de la bande de Soret de **42·8PF₆**. De plus, aucun changement significatif dans des transitions π-π* centrées sur l'acridinium n'a été observé. Ces résultats suggèrent que des agrégats de type J entre porphyrines au sein de la cage existent et qu'aucune interaction intramoléculaire entre les unités acridinium et porphyrine ne sont présents.

Après addition de bipy, le spectre RMN ^1H correspondant au complexe **biPy@42·8PF₆** devient bien résolu (Figure 25). Ce spectre RMN présente les caractéristiques de la complexation interne ditopique (fort blindage des signaux biPy). De plus, les analyses

DOSY ont montré que les signaux biPy et **42·8PF $_6$** diffusent avec le même coefficient de diffusion témoignant d'un complexe d'inclusion. Le complexe a ensuite été caractérisé par spectroscopie UV/Vis. Une constante d'association moyenne de 4,2 (± 0,7) × 10^6 M^{-1} (dans CH_2Cl_2, 0,1% CH_3CN) a pu être déterminée par dosage.

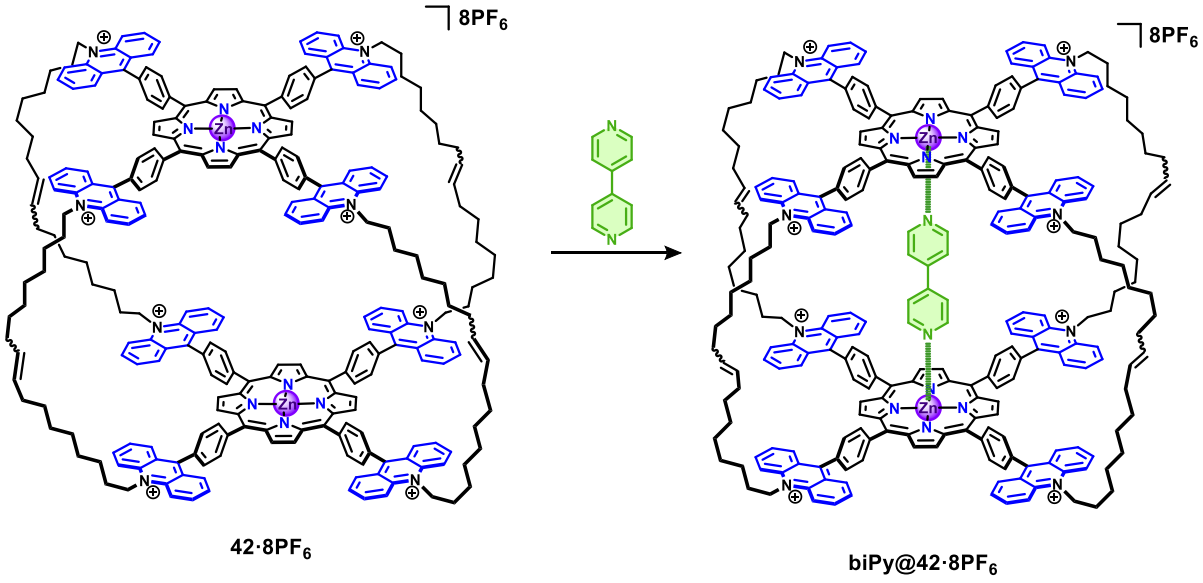

Figure 25. *Structure du complexe* ***biPy@42·8PF$_6$.***

Comme pour biPy, l'ajout de DABCO à une solution de **42·8PF$_6$** a conduit à un affinement des signaux en RMN ^{1}H (Figure 26). Les titrages UV-Vis effectués entre le DABCO et **42·8PF$_6$** dans CH_3CN ont démontré la formation du complexe 1 :1 **DABCO@42·8PF$_6$** (Ka = 4,5 (± 0,2) × 10^5 M^{-1}).

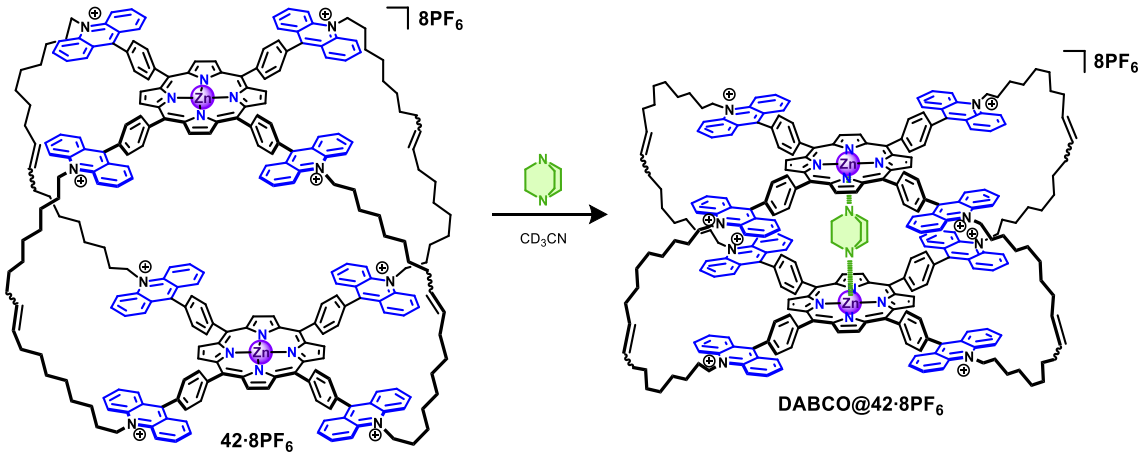

Figure 26*. Structure du complexe* ***DABCO@42·8PF$_6$.***

Le complexe **DABCO@42·8PF$_6$** a été mis en présence d'invité polyaromatique, pyrène ou de pérylène (Figure 27). L'ajout de cinq équivalents entraîne des changements significatifs dans les spectres RMN ^{1}H. Des déplacements vers les champs forts des protons d'acridinium (< 0,1 ppm) indique l'association de l'invité aromatique. Cependant, la faible solubilité du **DABCO@42·8PF$_6$** dans les solvants chlorés n'a pas permis la détermination d'une constante d'association.

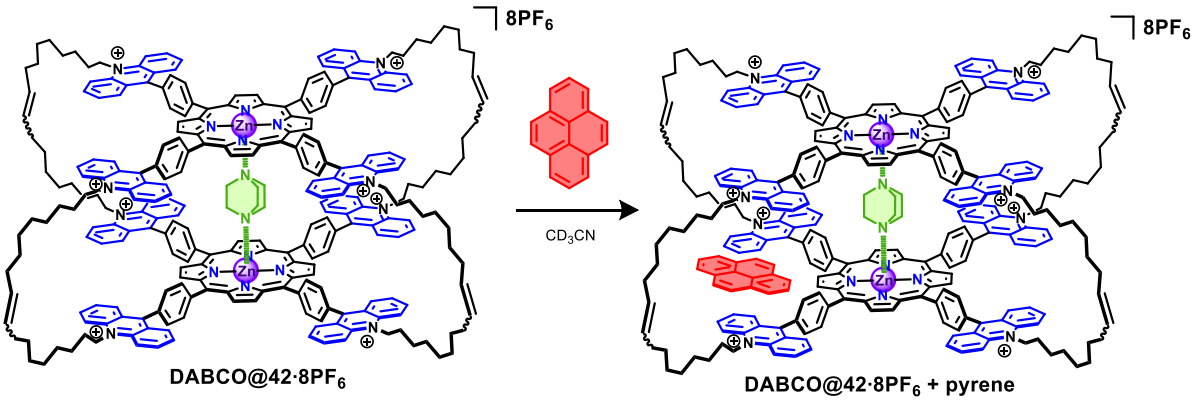

Figure 27. *Complexe formé par **42·8PF$_6$** dans CD_3CN lors de l'ajout de DABCO (**DABCO@42·8PF$_6$**) suivi de pyrène (**DABCO@42·8PF$_6$ + pyrène**).*

Pour permettre une plus grande solubilité dans le CH_2Cl_2, le contre-anion de la cage a été remplacé par du BArF. La cage **42·8BArF** montre une solubilité fortement accrue dans le CH_2Cl_2 (Figure 28). De plus, le spectre UV/Vis semble indiquer l'absence d'agrégats pour **42·8PF$_6$**. Lorsque les spectres RMN ^{1}H des composés **42·8BArF**, **41·4BArF** et NaBArF sont comparés, un déplacement des signaux vers les champs forts sont observés pour les protons du BArF de **42·8BArF**. Ceci suggère une interaction entre la cage et les ions BArF. Cela a été confirmé par la RMN ^{1}H DOSY, qui a montré que les contre-ions BArF de **42·8BArF** diffusent plus lentement que pour NaBArF.

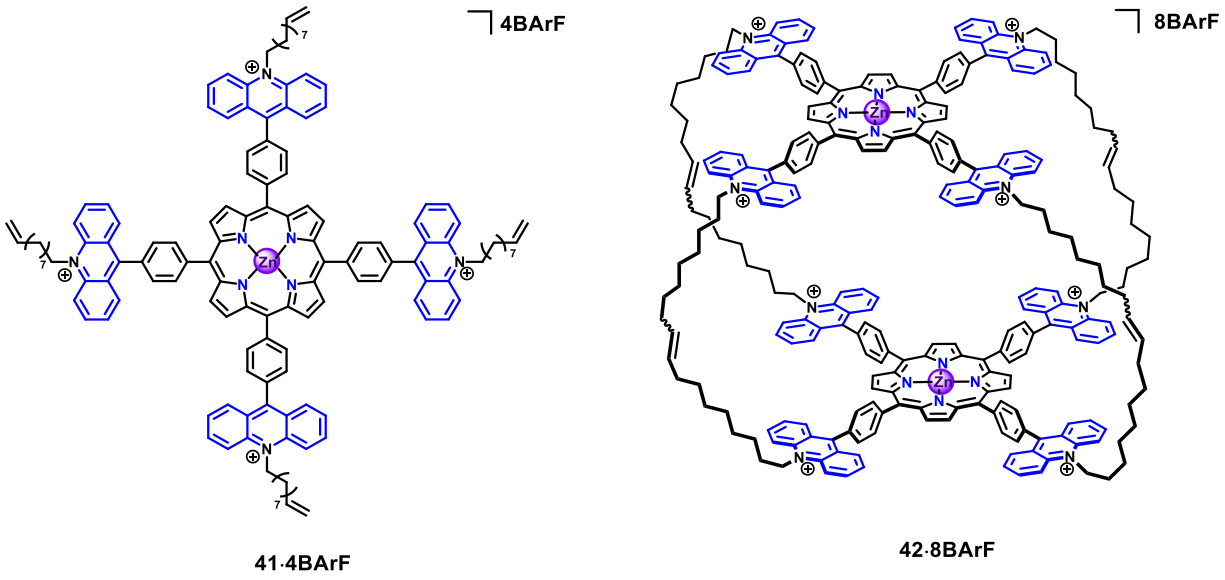

Figure 28. *Structures des deux composés* ***41·4BArF*** *et* ***42·8BArF****.*

Comme pour le composé **42·8PF$_6$**, le sel **42·8BArF** complexe des ligands ditopique (Figure 29). Par spectroscopie RMN 1D, 2D, UV/Vis, il a été constaté qu'il formait des espèces 1:1 avec biPy et DABCO. Les expériences DOSY confirment que les ligands ditopiques diffusent avec le même coefficient de diffusion que la cage dans les deux cas. De plus, les dosages UV/Vis ont donné des constantes d'association similaires de l'ordre de 1,2 × 10^7 M^{-1}.

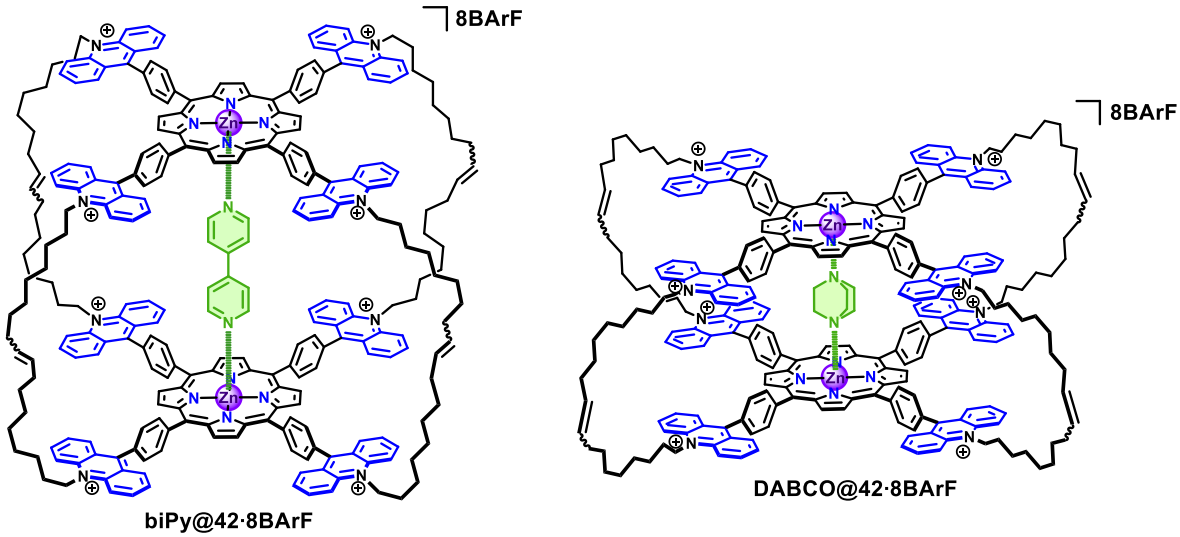

Figure 29. *Structures des complexes* ***biPy@42·8BArF*** *et* ***DABCO@42·8BArF****.*

Profitant de la solubilité accrue dans le CH_2Cl_2, des dosages suivis par RMN ^1H ont été effectués entre le complexe **DABCO@42·8BArF** et du pyrène. Un décalage significatif

vers les champs forts pour les pics associés à l'acridinium a été observé en présence d'invité. Après dosage, l'ajustement des données obtenues s'est avéré difficile et la stoechiométrie hôte:invité n'a pu être déterminée avec précision.

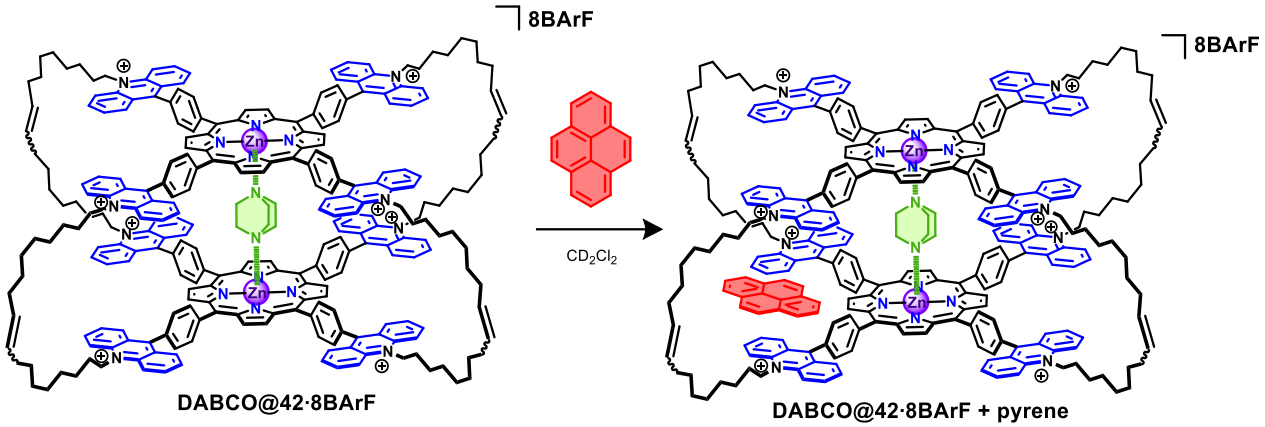

Figure 30. *Structure du complexe formé lors de l'addition d'un équivalent de pyrène à une solution de* ***DABCO@42·8BArF****.*

Les effets du stimulus chimique ont été étudiés par ajout de KOH ou de TBAOH. La cage **42·8PF$_6$** a été convertie en sa forme octaacridane **43** (Figure 31). A l'instar des pinces moléculaires **39·2PF$_6$** et **40**, la conversion a été suivie par spectroscopies RMN et UV/Vis. Ce processus est réversible par ajout de TFA. Des études de fatigue ont montré que la molécule est robuste jusqu'à 9 cycles puisque seule la formation des espèces acridinium et acridane a été observée.

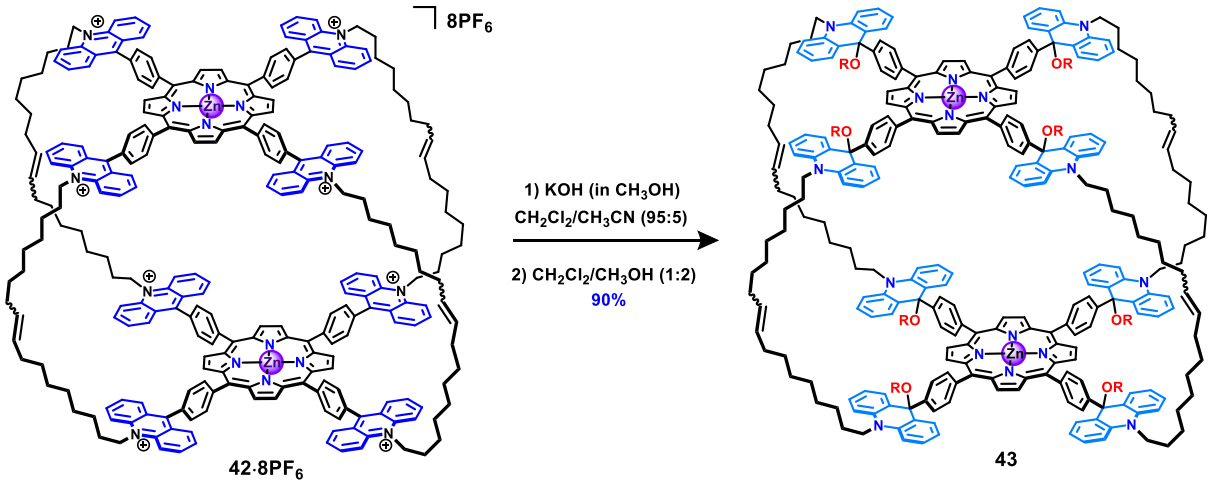

Figure 31. *Structure de la cage* ***43*** *formée lors de l'addition de KOH à une solution de* ***42.8PF$_6$****.*

Suivi par spectroscopie UV/Vis, des dosages entre la cage 43 et la bipy ont révélé une constante d'association (K_a = 1 × 10^6 M^{-1}) diminuée d'un facteur 13 par rapport à sa forme acridinium. Ainsi, l'association entre les porphyrines de la cage et un ligand ditopique a été démontrée.

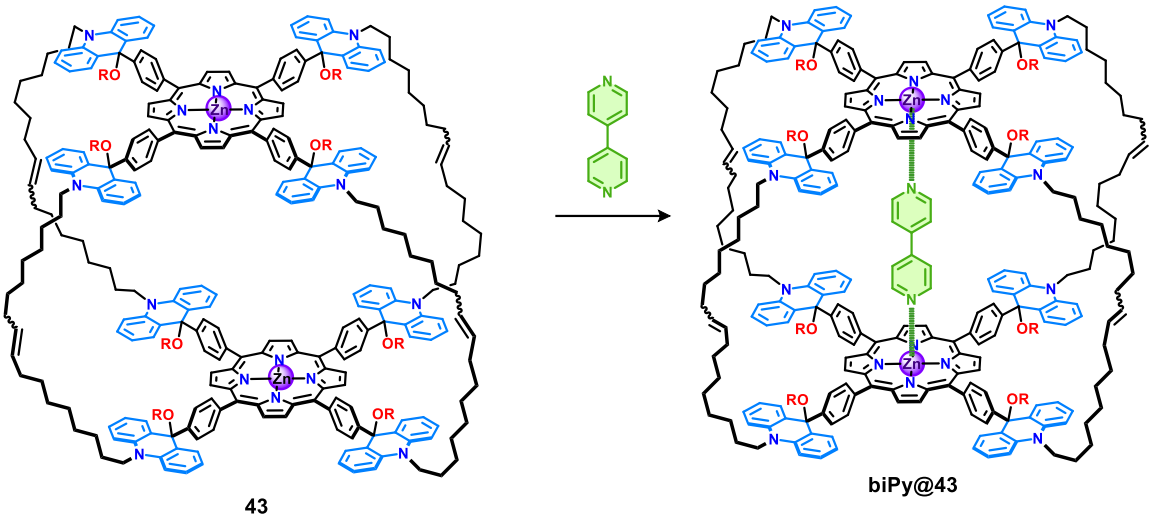

Figure 32. *Structure formée lors de l'ajout de biPy à une solution de* ***43****.*

En conclusion, nous avons réussi à synthétiser plusieurs conjugués acridinium-porphyrine par condensation de Lindsey (porphyrine de type A_3B et A_4). Les dérivés phénylacridinium sont les intermédiaires clés de ces synthèses et lorsqu'ils sont fonctionnalisé par un alcène, la formation des récepteurs moléculaires (pince et cage) a pu être réalisée. De plus, l'encapsulation par coordination de ligands ditopiques sur les sites porphyriniques des récepteurs ou de molécules polyaromatiques a été explorée. Enfin, l'association avec un ligand ditopique peut être contrôlée par ajout d'un stimulus chimique et électrochimique. Nous avons ainsi réussi à synthétiser des récepteurs allostériques multi-réponse.

Références

(1) Muraoka, T.; Kinbara, K.; Aida, T. Mechanical Twisting of a Guest by a Photoresponsive Host. *Nature* **2006**, *440* (7083), 512–515.

(2) Gilissen, P. J.; Vanthuyne, N.; Feringa, B. L.; A W Elemans, J. A.; M Nolte, R. J.; Johannes A A W Elemans, C. A. Light-Gated Binding in Double-Motorized Porphyrin Cages. *Nat Sci. 2*(1), **2022**.

(3) Iordache, A.; Retegan, M.; Thomas, F.; Royal, G.; Saint-Aman, E.; Bucher, C. Redox-Responsive Porphyrin-Based Molecular Tweezers. *Chem. Eur. J.* **2012**, *18* (25), 7648–7653.

(4) Jokic, D.; Boudon, C.; Pognon, G.; Bonin, M.; Schenk, K. J.; Gross, M.; Weiss, J. Structural and Binding Features of Cofacial Bis-Porphyrins with Calixarene Spacers: Pac-Man Porphyrins That Can Chew. *Chem. Eur. J.* **2005**, *11* (14), 4199–4209.

(5) Mansoor, I. F.; Dutton, K. G.; Rothschild, D. A.; Remsing, R. C.; Lipke, M. C. Uptake, Trapping, and Release of Organometallic Cations by Redox-Active Cationic Hosts. *J. Am. Chem. Soc.* **2021**, *143* (41), 16993–17003.

(6) Endo, K.; Ube, H.; Shionoya, M. Multi-Stimuli-Responsive Interconversion between Bowl- And Capsule-Shaped Self-Assembled Zinc(II) Complexes. *J. Am. Chem. Soc.* **2020**, *142* (1), 407–416.

(7) Rebek, J.; Trend, J. E.; Wattley, R. v.; Chakravorti, S. Allosteric Effects in Organic Chemistry. Site-Specific Binding. *J. Am. Chem. Soc.* **1979**, *101* (15), 4333–4337.

(8) Kawaguchi, M.; Ikeda, A.; Shinkai, S. A Novel Porphyrin-Homooxacalix[3]Arene Conjugate Which Creates a C 3-Symmetrical Capsular Space. *Tetrahedron Lett.* **2001**, *42* (22), 3725–3728.

(9) Ballester, P.; Oliva, A. I.; Costa, A.; Deyà, P. M.; Frontera, A.; Gomila, R. M.; Hunter, C. A. DABCO-Induced Self-Assembly of a Trisporphyrin Double-Decker Cage: Thermodynamic Characterization and Guest Recognition. *J. Am. Chem. Soc.* **2006**, *128* (16), 5560–5569.

(10) Lee, C.-H.; Yoon, H.; Jang, W.-D. Biindole-Bridged Porphyrin Dimer as Allosteric Molecular Tweezers. *Chem. Eur. J.* **2009**, *15* (39), 9972–9976.

(11) Lee, C. H.; Yoon, H.; Kim, P.; Cho, S.; Kim, D.; Jang, W. D. An Indolocarbazole-Bridged Macrocyclic Porphyrin Dimer Having Homotropic Allosterism with Inhibitory Control. *Chem. Commun.* **2011**, *47* (14), 4246–4248.

(12) Takeuchi, M.; Imada, T.; Shinkai, S. A Strong Positive Allosteric Effect in the Molecular Recognition of Dicarboxylic Acids by a Cerium(IV) Bis[Tetrakis(4-Pyridyl)Porphyrinate] Double Decker. *Angew. Chem. Int. Ed.* **1998**, *37* (15), 2096–2099.

(13) Ikeda, T.; Shinkai, S.; Sada, K.; Takeuchi, M. A Preliminary Step toward Molecular Spring Driven by Cooperative Guest Binding. *Tetrahedron Lett.* **2009**, *50* (17), 2006–2009.

(14) Djemili, R.; Kocher, L.; Durot, S.; Peuronen, A.; Rissanen, K.; Heitz, V. Positive Allosteric Control of Guests Encapsulation by Metal Binding to Covalent Porphyrin Cages. *Chem. Eur. J.* **2019**, *25* (6), 1481–1487.

(15) Zanetti-Polzi, L.; Djemili, R.; Durot, S.; Heitz, V.; Daidone, I.; Ventura, B. Allosteric Control of Naphthalene Diimide Encapsulation and Electron Transfer in Porphyrin Containers: Photophysical Studies and Molecular Dynamics Simulation. *Chem. Eur. J.* **2020**, *26* (72), 17514–17524.

(16) Oliveri, C. G.; Gianneschi, N. C.; Nguyen, S. T.; Mirkin, C. A.; Stern, C. L.; Wawrzak, Z.; Pink, M. Supramolecular Allosteric Cofacial Porphyrin Complexes. *J. Am. Chem. Soc.* **2006**, *128* (50), 16286–16296.

(17) Schmittel, M.; Pramanik, S.; De, S. A Reversible Nanoswitch as an ON–OFF Photocatalyst. *Chem. Commun.* **2012**, *48* (96), 11730.

(18) Claude, S.; Lehn, J.-M.; Schmidt, F.; Vigneron, J.-P. Binding of Nucleosides, Nucleotides and Anionic Planar Substrates by Bis-Intercaland Receptor Molecules. *J. Chem. Soc., Chem. Commun.* **1991**, *17*, 1182–1185.

(19) Hu, J.; Ward, J. S.; Chaumont, A.; Rissanen, K.; Vincent, J.; Heitz, V.; Jacquot de Rouville, H.-P. A Bis-Acridinium Macrocycle as Multi-Responsive Receptor and Selective Phase-Transfer Agent of Perylene. *Angew. Chem. Int. Ed.* **2020**, *59* (51), 23206–23212.

(20) Kurihara, K.; Yazaki, K.; Akita, M.; Yoshizawa, M. A Switchable Open/Closed Polyaromatic Macrocycle That Shows Reversible Binding of Long Hydrophilic Molecules. *Angew. Chem. Int. Ed.* **2017**, *56* (38), 11360–11364.

(21) Chaudhary, A.; Rath, S. P. Encapsulation of TCNQ and the Acridinium Ion within a Bisporphyrin Cavity: Synthesis, Structure, and Photophysical and HOMO-LUMO-Gap-Mediated Electron-Transfer Properties. *Chem. Eur. J.* **2012**, *18* (24), 7404–7417.

(22) Tanaka, M.; Ohkubo, K.; Gros, C. P.; Guilard, R.; Fukuzumi, S. Persistent Electron-Transfer State of a π-Complex of Acridinium Ion Inserted between Porphyrin Rings of Cofacial Bisporphyrins. *J. Am. Chem. Soc.* **2006**, *128* (45), 14625–14633.

(23) Kotani, H.; Ohkubo, K.; Crossley, M. J.; Fukuzumi, S. An Efficient Fluorescence Sensor for Superoxide with an Acridinium Ion-Linked Porphyrin Triad. *J. Am. Chem. Soc.* **2011**, *133* (29), 11092–11095.

(24) Edo-Osagie, A.; Sánchez-Resa, D.; Serillon, D.; Bandini, E.; Gourlaouen, C.; Jacquot de Rouville, H.-P.; Ventura, B.; Heitz, V. Synthesis, Electronic and Photophysical Properties of a Bisacridinium-Zn(II) Porphyrin Conjugate. *C. R. Chim.* **2021**, *24* (S3), 47–55.

Amy EDO-OSAGIE

Conception, synthèse et propriétés de récepteurs incorporant des unités acridiniums et porphyrines

Résumé

Les travaux de cette thèse portent sur la conception, la synthèse et l'étude de nouveaux récepteurs incorporant des conjugués acridinium-porphyrines. Les effets du couplage des deux motifs sur les propriétés électrochimiques et photochimiques des molécules et sur leur comportement de reconnaissance ont été explorés.

Deux voies de synthèse pour coupler les motifs acridinium et porphyrine ont été mises au point et ont conduit à différentes porphyrines méso-substituées par des acridiniums. Elles ont permis d'entreprendre la synthèse de récepteurs moléculaires, en utilisant la métathèse d'oléfines pour lier de manière covalente plusieurs conjugués acridinium-porphyrine. Grâce à cette réaction, une pince moléculaire et une cage acridinium-porphyrine ont été synthétisées avec succès. Les propriétés de reconnaissance de ces deux récepteurs ont été étudiées vis à vis de ligands ditopiques (DABCO et 4,4'-bipyridine) et d'hydrocarbures polyaromatiques. De plus, la présence/absence de coopérativité entre les sites de reconnaissance porphyrine et acridinium a été étudiée. Enfin, la réponse multiple suite à différents stimuli (chimiques et/ou redox) a été mise en évidence ainsi que le contrôle à distance de l'affinité de ces récepteurs pour les ligands ditopiques.

Mots-clés : pince moléculaire, cage moléculaire, récepteur à réponse multiple, reconnaissance moléculaire, acridinium, porphyrine.

Résumé en anglais

The work of this thesis has focused on the design, synthesis and study of new receptors incorporating acridinium-porphyrin conjugates. The effects of pairing the two motifs on the electro- and photo-chemical properties of the molecules and on their recognition behaviour were explored.

Two synthetic methodologies for coupling acridinium and porphyrin motifs were found allowing the synthesis of different meso-substituted acridinium-porphyrins. This was then extended into the synthesis of molecular receptors, using olefin metathesis as a means of covalently linking acridinium-porphyrin conjugates. Via this method, both a porphyrin-acridinium tweezer and cage were successfully synthesised. The binding abilities of the two receptors were investigated with respect to ditopic ligands (DABCO and 4,4'-bipyridine) and polyaromatic hydrocarbons. Furthermore, the presence/absence of cooperativity between the porphyrin and acridinium binding sites was investigated. Finally, the multi-switching behaviour based on different stimuli (chemical and/or redox) was studied and the remote-controlled tuning of the binding affinity for ditopic ligands evidenced.

Keywords: tweezer, cage, multi-switching receptor, host-guest chemistry, acridinium, porphyrin